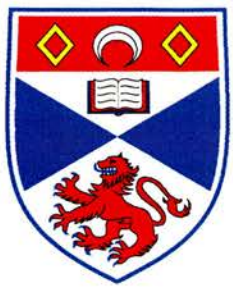

Receptors for the Broad Spectrum Acceleration of Chemical Reactions

A Comparison of Polar and Non-Polar Reactivity

by

Heidi Rowe

A Thesis Presented for the Degree of

Doctor of Philosophy

in the

School of Chemistry

University of St Andrews

St Andrews **December 2001**

(i) I, Heidi Rowe, hereby certify that this thesis, which is approximately 50 000 words in length, has been written by me, that it is the record of work carried out by me and that it has not been submitted in any previous application for a higher degree.

Signature of candidate ..... Date ..6/3/02.....

(ii) I was admitted as a research student in September 2000, and as a candidate for the degree of Doctor of Philosophy in September 2000; the higher study for which this is a record was carried out in the University of St Andrews between 2000 and 2001.

Signature of candida ..... Date ..6/3/02.....

(iii) I hereby certify that the candidate has fulfilled the conditions of the Resolution and Regulations appropriate for the degree of Doctor of Philosophy in the University of St Andrews and that the candidate is qualified to submit this thesis in application for that degree.

Signature of supervisor ..... Date 6/3/2002.....

In submitting this thesis to the University of St Andrews I understand that I am giving permission for it to be made available for use in accordance with the regulations of the University Library for the time being in force, subject to any copyright vested in the work not being affected thereby. I also understand that the title and abstract will be published, and that a copy of the work may be made and supplied to any *bona fide* library or research worker.

Signature of candic ..... Date ..6/3/02.....

Table of Contents

Acknowledgements

First of all I would like to thank my family, for all the practical and emotional help; my parents, Gavin and Evelyn and my sisters and their families Lisa, Carl, Emma and Kirsty and Julia and Allister.

I would like to thank Dr Douglas Philp for his supervision over the past three years and for all the proof reading of this thesis. Thank you to the Philp group past and present for the invaluable help with the chemistry stuff. I would particularly like to thank Dr Sarah (Skoog, Kindword) Howell, (Dr) Julie (Chins) Quayle, Dr Lyndsey Greig, Dr (Sticky) Vikki Allen, P.C. Sam Rigby, Dr Andy (blouse) Sinclair, Dr Raf Bennes, Dr Paul Comina, Dr Patrizia Calcagno, Dr Jim (Flash) Robinson, (Dr) Rachel Hopper, (Dr) Russell Pearson, (Dr) Rosalynn Cowie, (Dr) Mairead Minto, and (Dr) Eleftherios Kassianidis. Particular thanks have to go to the long suffering NMR specialists; Dr Neil Spencer, Mr Malcolm Tolley and Mrs Melanja Smith, without who this PhD would have been impossible to complete. Thank you especially to Melanja who taught me the intricacies of operating Oscar so I could run my own kinetic experiments.

Thank you to all the people in chemistry outside the Philp group who have kept me sane, particularly Dr Pete Barnes, Dr Howard (Lord) Easterfield, Dr Trevor Rutherford and all the people from the tea room in Birmingham for the banter.

Particular thanks have to go to Joe Pittaway and Karen Goodyer for being gorgeous, glamorous businesswomen and being my best friends and the best dancers in the West Midlands.

At the beginning of my final year I relocated from Birmingham to St Andrews. I'd like to thank Angela Tawse, (Dr) Sandra Jeffers, Tom Whalley, Kateri Wilson, (Dr) Veronica Poland, (Dr) David (Jif) Lemon and Mark Cox for making me feel at home here. Life would have been a lot harder without you all. Particular thanks to Kateri for making me laugh and buying me a Barbie ("every girl *needs* a Barbie"), Sandra for her barbeque skills ("do you think we have enough meat?") and Angela for the cookies, the "bog standard tea" and for listening to me whinge. Loads of thanks have to go to Mark for rescuing a "damsel in distress". Good luck with the bionic cat.

I would like to thank all of my fantastic friends from West Kirby and Calday who despite being scattered around the country, still feel like staying in touch with me. I'd particularly like to thank the bloody marvellous Martin Lockey (for saving my sanity at the expense of his), Johanna Bishop, Adam Todd, Helen Criddle, (Dr) Rebecca Elliott, Dr Rachel Wells, Raymond Wells, Rory Cullen and Chris Wylie.

I'd really like to thank Chris Weston, for all the chemistry and cricket wisdom. I wanted to miss out page 111 but I thought that would only confuse people.

Many of the people mentioned in these acknowledgements will realise how many problems I have had to face outside chemistry in the last four years and will realise the significance of the time of year I submitted this thesis for examination. I cannot put into words how proud I am to have got through the past few years and have achieved this much. I couldn't have managed this however, without the help of a lot of people, so this thesis is dedicated to all my family and friends who helped me through the difficult times.

Abbreviations

AMP	-	Adenosine monophosphate
Ar	-	Aryl
Bu	-	Butyl
DEAD	-	Diethyl azodicarboxylate
DMF	-	Dimethylformamide
DNA	-	Deoxyribonucleic acid
E.A.	-	Elemental analysis
Eq	-	Equivalents
Et	-	Ethyl
HOMO	-	Highest Occupied Molecular Orbital
HRMS	-	High resolution mass spectrometry
IPr	-	Isopropyl
IR	-	Infra-red
Lit.	-	Literature
LUMO	-	Lowest Occupied Molecular Orbital
Me	-	Methyl
m.p.	-	Melting Point
Nu	-	Nucleophile
ORTEP	-	Oak Ridge Thermal Ellipsoid Plot
PEG	-	Polyethylene glycol
PMA	-	Phosphomolybdic acid
quat	-	Quaternary
RNA	-	Ribonucleic acid
r.t.	-	Room temperature
σ	-	Standard deviation
tBu	-	Tertiarybutyl
THF	-	Tetrahydrofuran
TS	-	Transition state
Ts	-	Tosyl
UV	-	Ultra-violet

1. Introduction

1.1 Preamble

Enzymes are seen as ideal catalysts and chemists look to them to design artificial analogues attempting to emulate their selectivity and efficiency. The design of synthetic catalysts is often *"based on the mimicry of biological catalysis"*,[1] however, enzymes fail to catalyse every type of reaction, despite the structural diversity of natural products that have been identified. Catalysis of some classes of reaction by natural enzymes is very uncommon, for example pericyclic reactions.[2] It is of note that little attention has been dedicated to explaining how biosynthetic strategies evolved, limiting the number of synthetic transformations adopted.

The discussion that follows is designed to provide a general review of enzyme and synthetic catalysis, including catalytic antibodies and supramolecular catalysis. Attention is largely focussed on how catalysis is realised with particular emphasis on the polarity of the reactions. This review is intended to establlish the requirement for further investigation into the potential for hydrogen bond mediated catalysis.

1.2 Polar *vs.* Non-Polar reactivity – A Definition

Polar reactions can be defined as reactions that possess transition states leading to intermediates possessing full positive or negative charges. Examples of polar reactions are nucleophilic additions to carbonyl groups or the addition of HBr to an alkene.

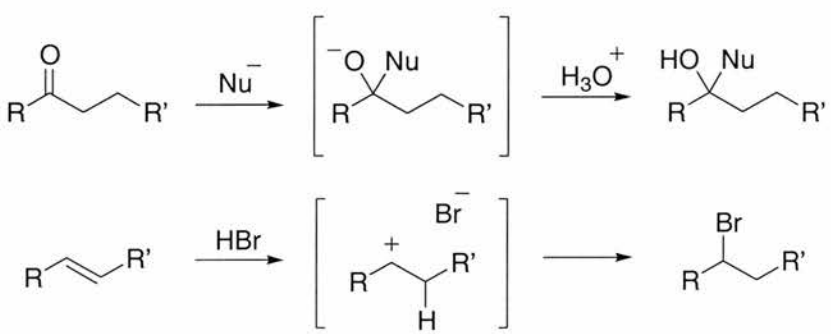

Figure 1.2.1 Examples of polar reactions, nucleophilic addition to a ketone and addition of HBr to an alkene. Both reactions have intermediates with a charge localised on a single atom.

Polar reactions will posses one or more charged intermediates in the reaction profile. In the case of the addition of HBr to an alkene, the carbocation resulting from the addition of the proton to the double bond forms a local minimum on the reaction coordinate.[3] The two transition states correspond to the initial addition of H^+ to the alkene and subsequent addition of Br^- to the intermediate. Although a carbocation localised on a single atom is only present in the intermediate, rather than the transition states of the addition, the reaction can be considered polar because highly localised charges are generated and destroyed in the two transition states.

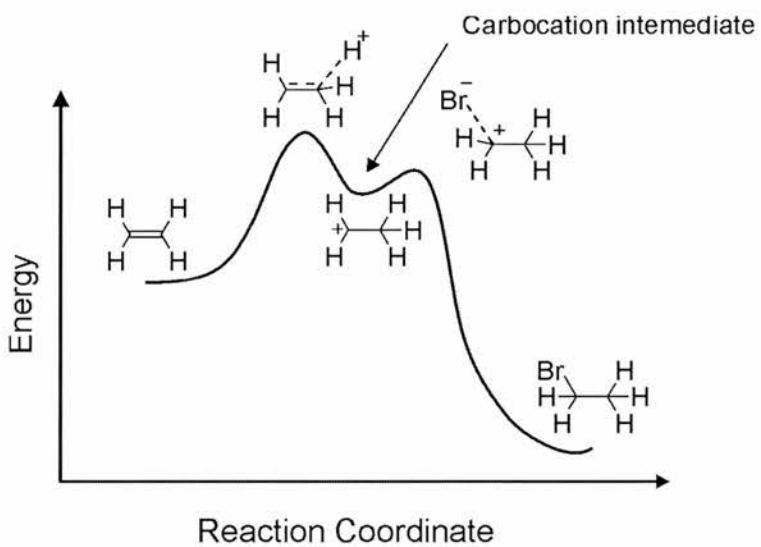

Figure 1.2.2 Schematic diagram of the reaction coordinate of the addition of HBr to an alkene.

The scope of polar reactions is extensive and includes all nucleophilic additions, eliminations and substitutions.

Reaction polarity however, is a sliding scale. It can be considered as being a function of the magnitude of the charge generated over the level of charge delocalisation at the transition state. Reactions in which charge is delocalised over several atoms are inherently less polar than the polar reactions discussed above. A reaction that could be considered in this category is the conjugate or "Michael" Addition. When a nucleophile reacts with an α, β-unsaturated ketone, two modes of addition can be observed, direct 1,2-addition to the carbonyl carbon and indirect 1,4-addition to the alkene carbon termed conjugate or Michael addition.

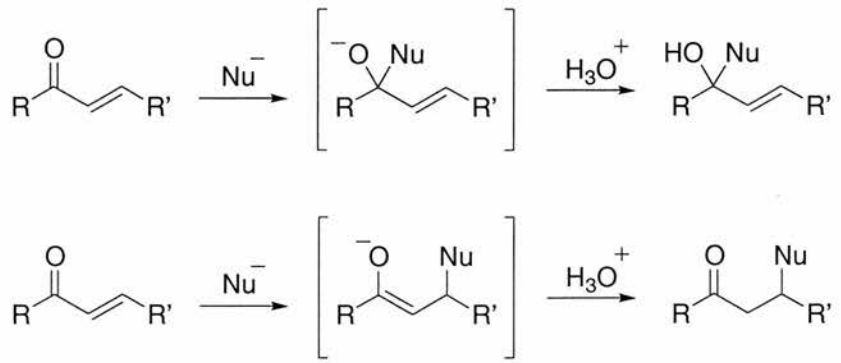

Figure 1.2.3 Direct and Michael additions onto an α, β-unsaturated ketone. The initial product formed in the Michael addition is an enol, which readily rearranges to the ketone.

The type of addition observed depends upon the nucleophile and the trend follows the hard soft theory.

Hard Soft Acid Base theory (HSAB) is based on several observations.[4] "Hard" bases bind electrons tightly for example, ^{-}OH whereas "soft" bases have more loosely bound valence electrons for instance $CH_2=CH_2$ and RSH. "Hard" acids are small and of high positive charge for example H^+, Li^+ whereas "soft" acids are large in size and of low positive charge. HSAB theory is commonly applied to reactions not normally considered to be acid / base in nature.[5] In this case it is sometimes more useful to term the base a "donor" and the acid an "acceptor" in terms of electrons. For example in the case of a carbonyl group, the carbon is a hard acceptor and the oxygen is a hard donor.

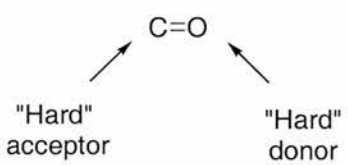

Figure 1.2.4 Illustration of the application of HSAB theory with a carbonyl group

Within a reactant, one reaction centre can be harder than another and this may affect the type of reaction that occurs. In enones the carbonyl carbon is significantly harder than the alkene and can be confirmed by considering a series of experiments conducted by Bottin and co-workers.[6] Bottin examined reductions of enones and revealed that the softer the reducing agent, the greater the preference for 1,4

reduction over 1,2 reduction, proceeding *via* initial addition of hydride in a direct or conjugate manner.

Bottin noted that as B^{3+} was softer than Al^{3+}, B-H must be more covalently bonded than Al-H. Because of this rationalisation, it was concluded that borohydrides must be softer reagents than aluminium hydrides. To test this hypothesis the reduction of a conjugated enone **1** was investigated.

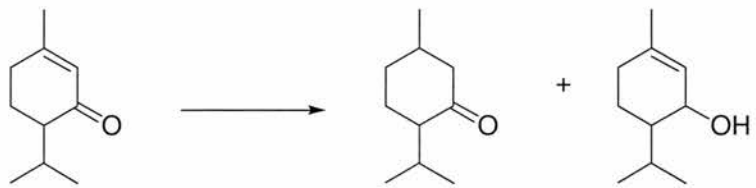

1 **2** **3**

i) $LiAlH_4$	0%	100%
ii) $LiBH_4$	28.5%	48.5%

Scheme 1.2.5 Comparison of the product distribution when an enone is reduced with $LiAlH_4$ or $LiBH_4$.

The harder aluminium hydride reagent causes reduction of the hard carbonyl group. With the softer borohydride reagent, some ketone product **2** is formed as well as the allylic alcohol **3**. It had been previously established that soft donors react with soft acceptors and so these results confirm that the C4 position of an enone is softer and will react with softer donors than the C2 position.

Extending these observations we can say qualitatively, hard, highly polarised nucleophiles such as organolithium species would react at the harder carbonyl carbon, soft nucleophiles for example enolates would react at the alkene.

If the transition state of the addition is examined for the conjugate addition, it is apparent how it is less polar than direct additions. It was previously stated that transition state polarity can be considered to be a function of the charge generated over the degree of charge delocalisation. In the initial addition of a nucleophile, Nu^- to an enone a charge of –1 is present in each transition state. In the case of conjugate addition, this charge is delocalised over five atoms whereas in direct addition the negative charge is delocalised over three atoms. If the charge is

delocalised evenly, it is apparent how direct addition generates a more compact, polar transition state than conjugate or Michael addition.

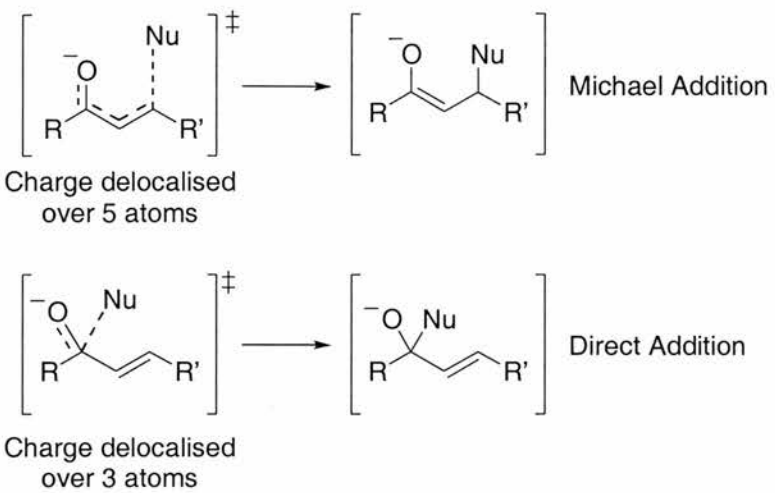

Figure 1.2.6 A representation of the transition states of direct and Michael additions. In the Michael addition the charge resulting from addition is delocalised over 5 atoms rather than 3.

As noted previously, reaction polarity is a sliding scale and many reaction transition states are considerably less polar. Pericyclic reactions involve no charged intermediates or radicals, but generate carbon carbon bonds by the rearrangement of π electrons. The cycloaddition is concerted and so both σ bonds are created at the same time leading to a high level of selectivity relative to stepwise cyclisations; *cis* and *trans* relationships in the starting materials are maintained in the product. The size of the 4π component in the pericyclic reaction allows a subdivision in the classification. [3+2] Dipolar cycloadditions have a 3-atom 4π electron component whereas in Diels-Alder reactions, traditionally the 4π electrons are distributed over 4 atoms.

Some pericyclic reactions containing heteroatoms can be considered to possess charge in the ground state but the charge is small and delocalised over several atoms, [3+2] dipolar cycloadditions can be considered in this category, although the ground state charges are lost during the cycloaddition.

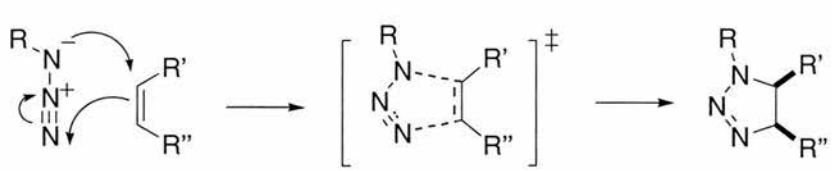

Figure 1.2.7 The mechanism of a [3+2] dipolar cycloaddition between an azide and an alkene, *syn* stereochemical relationships in the starting alkene are conserved in the product.

Formally, the dipole in the [3+2] dipolar cycloaddition carries full positive and negative charges, however, several canonical forms can be written delocalising the charges over the three constituent atoms. The formal charges are lost in the process of conversion from starting material to transition state to product. The orbital coefficients of the dipole are considered reminiscent of the allyl anion, however, as can be observed by the two significant resonance forms of benzyl azide, the molecule is zwitterionic.

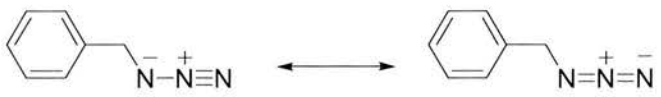

Figure 1.2.8 Two of the resonance forms of benzyl azide

[3+2] Dipolar cycloadditions are generally considered to proceed *via* a concerted mechanism[7,8] but can exhibit lower regiospecificity than Diels-Alder reactions. In terms of frontier molecular orbital theory, [3+2] dipolar cycloadditions can be HOMO or LUMO dipole controlled and it is this trait which can affect product regiochemistry.

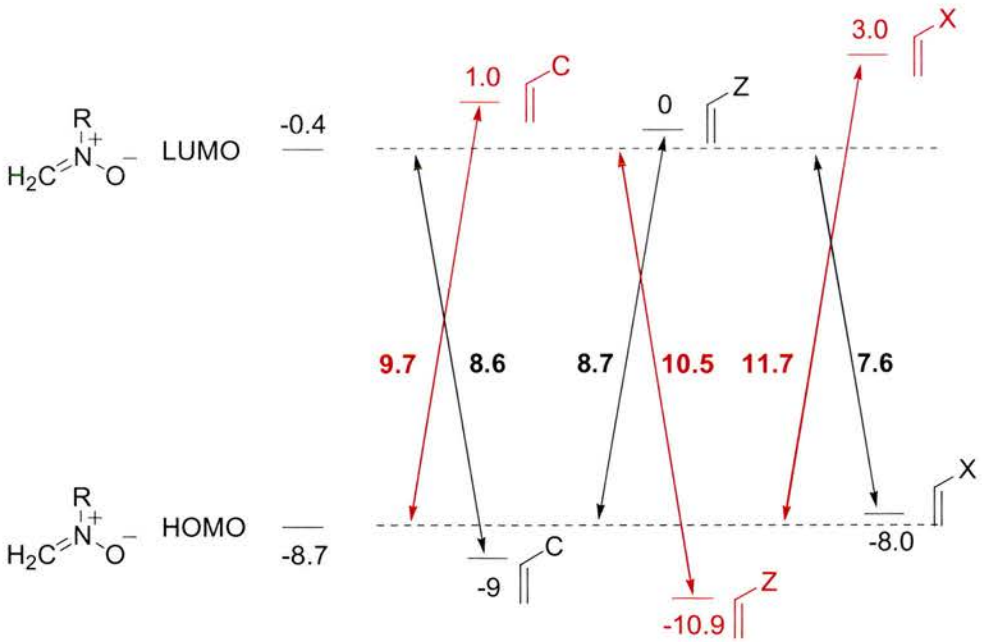

Figure 1.2.9 Representation of the HOMO LUMO energy gaps observed in the [3+2] dipolar cycloaddition between a nitrone and an alkene. The reaction is HOMO dipole controlled with an electron deficient alkene (Z) and LUMO dipole controlled with electron rich alkenes (X) or alkenes containing electronically neutral groups (C). All energies are measured in electron volts (eV). The energetically favoured interactions are in black; the less favoured interactions are red.

Diels-Alder reactions are fastest with electron deficient Z substituted alkenes and normally react through the HOMO of the diene (4π component) and the LUMO of the dienophile (2π component). If reacted with electron deficient alkenes, [3+2] dipolar cycloadditions follow this trend.

In the nitrone example of a cycloaddition depicted in **Figure 1.2.9,** the reaction is HOMO dipole controlled by 1.8 eV when reacted with a Z substituted alkene. With C or Z substituted alkenes, the trend is reversed.[9]

There are also reactions that create no formal charge in the transition state or the charge is fully delocalised. Simple examples of non-polar reactions are Diels-Alder reactions.[10]

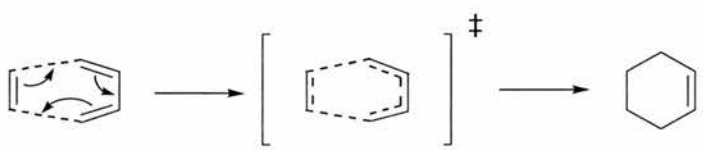

Figure 1.2.10 The Diels-Alder cycloaddition, an example of a non-polar reaction

The Diels-Alder reaction tends to possess a late, product like transition state. No intermediates are formed in the reaction profile as the reaction is concerted.

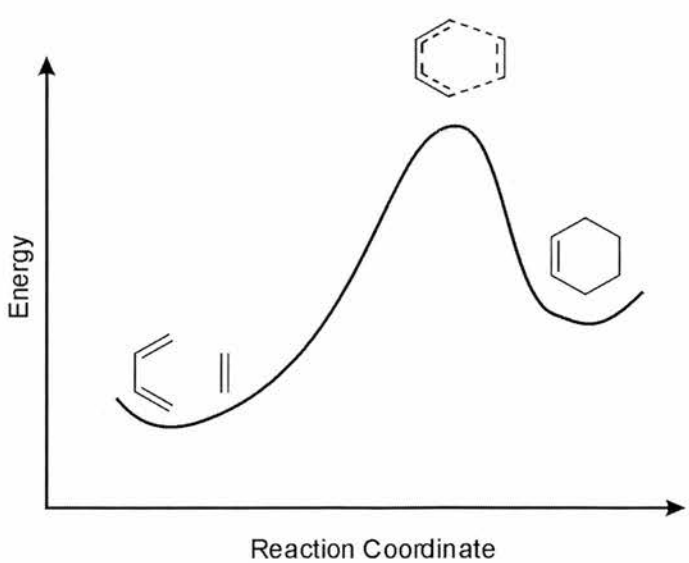

Figure 1.2.11 A schematic diagram of the energy profile of a Diels-Alder reaction. No charges and no intermediates are formed during the progress of the reaction.

The Diels-Alder reaction is generally rationalised in terms of frontier molecular orbital theory. In most Diels-Alder cycloadditions, the HOMO of the diene interacts with the LUMO of the dienophile (normal electron demand). Overlap of electrons leads to a six-centre transition state.

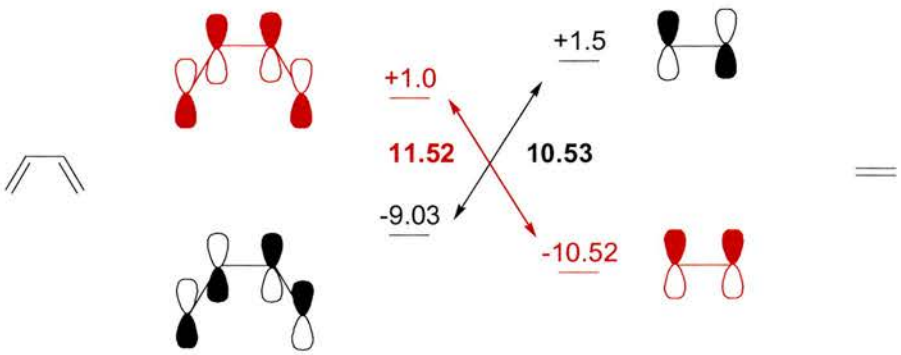

Figure1.2.12 A representation of the frontier orbitals in the cycloaddition of butadiene with alkene with the interaction between the $HOMO_{butadiene}$ $LUMO_{ethane}$ labelled. Adapted from *Organic Synthesis.*[11] All energies are measured in eV. The red interaction represents the less favoured orbital overlap on energetic grounds.

Diels-Alder cycloadditions are synthetically useful reactions and they are not restricted to the synthesis of carbocyclic rings. The diene or dienophile can include carbonyl moieties or occasionally imines.

Diels-Alder reactions take two simple components and can create several new stereogenic centres in one synthetic step. The concerted nature of the reaction can make relative control of the new stereogenic centres facile.

1.3 Investigating Non-Polar Enzyme Catalysis

Investigating the means of catalysis observed in natural and synthetic systems may further our knowledge of enzyme catalysis and the mechanism whereby rate enhancements are achieved. This advancement in knowledge may, in turn, assist synthetic catalyst design and affect the choice of reactions for enzyme catalysis.

Pericyclic reactions in natural systems are rare,[12] Silverman[2] noted, when considering enzyme mediated reactions, *"There are very few examples of these [pericyclic] reactions, unless catalytic antibodies are included."*

1.3.1 Chorismate Mutase

Chorismate mutases catalyse an intramolecular rearrangement from chorismate **4** to prephenate **5**. *In vitro* the reaction proceeds *via* a concerted asynchronous Claisen type rearrangement, which is analogous to a Diels-Alder reaction and so can be considered relatively non-polar.

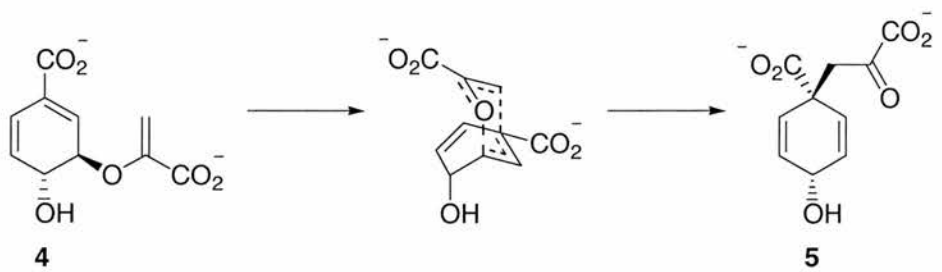

4 **5**

Figure 1.3.1.1 The rearrangement of (-)-chorismate to prephenate *via* a chair like transition state.

It has been stated[13] that the rate acceleration in the enzyme and catalytic antibodies arises from pre-organisation of the substrate by the enzyme, constraining the substrate in the correct conformation for reaction, which is described as an "Entropy trap". Visual analysis of the transition state however, shows that the ground state possesses a ring inversion, which converts the substrate between the non-reactive and reactive conformations. It was suggested by Edwards and Jackman[14] that chorismate mutase catalyses the reaction by orientating the reactant in the less favoured pseudo axial conformer.

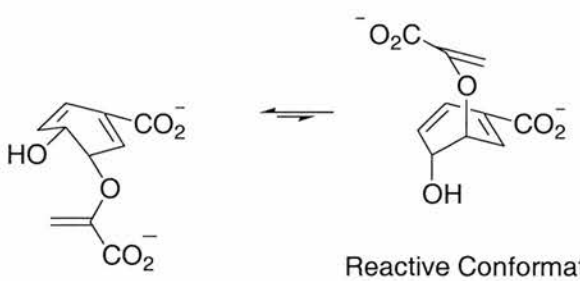

Reactive Conformation

Figure 1.3.1.2 Diagrammatic representation of the ring inversion from the pseudo equatorial to the reactive pseudo axial conformation.

Analysis of the pseudo axial conformer suggests that the only two fully rotateable bonds in the starting material would strongly influence the conformation of the reactant once in the pseudo axial conformer. If the enzyme restricted the rotors prior

to the transition state of the rearrangement, it may not account fully for the rate increase observed.[15]

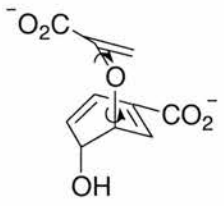

Figure 1.3.1.3 The rotateable bonds affecting transition state geometry in the axial conformer.

It had been previously established *via* kinetic isotope effects[16] that the transition state of the rearrangement of chorismate to prephenate *in vivo* is more dissociative; specifically the C-O ether linkage is more broken in the enzyme-catalysed reaction than *in vitro*. Additionally, analysis of crystal structures of wild type *Bacillus subtilis* chorismate mutase has established that the arginine at position 90 forms a hydrogen bonding interaction with the ether and carbonyl oxygens.[17]

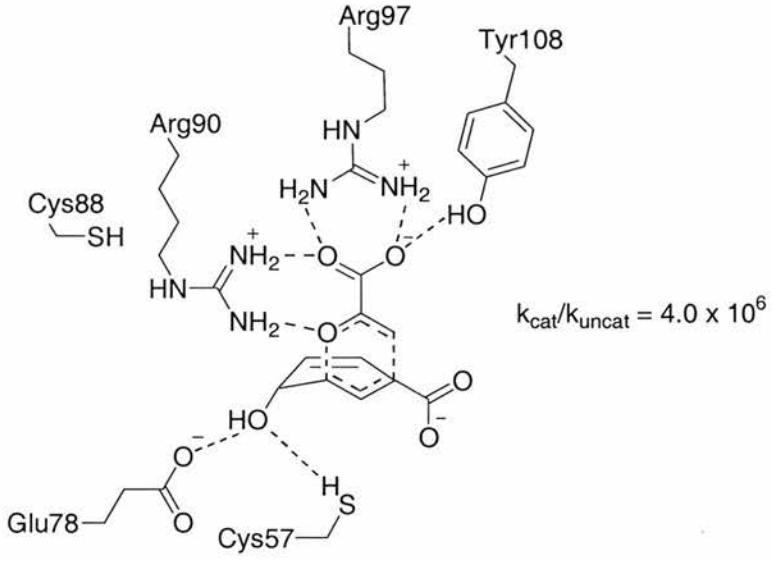

Figure 1.3.1.4 Representation of the active site of *Bacillus subtilis* chorismate mutase with the arginine residue hydrogen-bonded to the ether and acid groups of the transition state.

Key residues in the protein sequence were randomised and the resulting mutants were tested for survival. The only surviving mutants possessed a positively charged group in the region of the ether oxygen of chorismate.

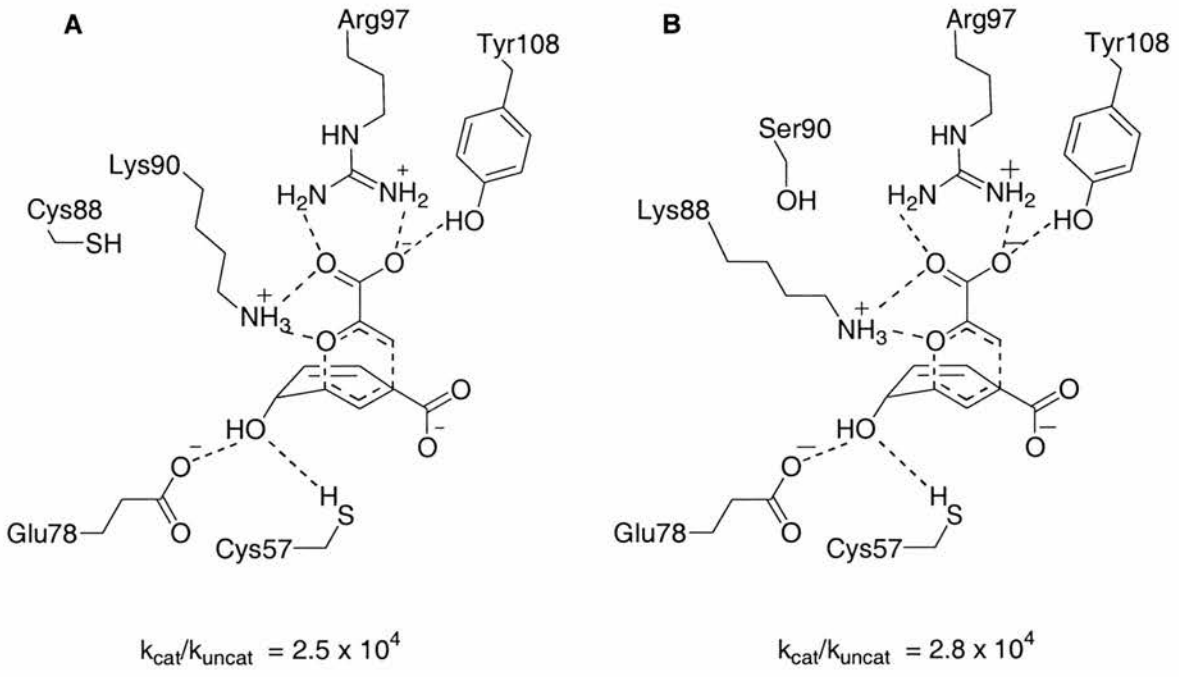

Figure 1.3.1.5 **A** variant C88S/R90K, **B** variant C88K/R90S displaying catalysis approximately 10^2 times less than the wild type enzyme but 10^3 times more than the R90G variant lacking a positively charged residue.

Investigation of a mutant possessing a glycine residue at position 90 revealed it had dramatically reduced activity than the wild type enzyme, $k_{cat}/k_{uncat} = 23$. Mutants with positively charged residues in position 88 possessed only slightly reduced activity than the wild-type enzyme. Although the arginine containing wild type enzyme was more efficient than those containing lysine, the dramatically reduced catalysis in the absence of a positively charged residue indicated a strong hydrogen bond donor is vital for catalysis. This suggests that negative charge is accumulating on the ether oxygen in the transition state because of the largely broken C-O bond. The partial negative charge can be stabilised electrostatically by charge-reinforced hydrogen bonding to the arginine 90 residue in the wild type enzyme. This hypothesis of charge stabilisation is reinforced by partial resumption of catalysis for mutants with lysine residues in the 88 or 90 positions.

Marti *et al*[18] studied the *Bacillus subtilis* chorismate mutase rearrangement using computational methods. They concluded that the enzyme preferentially binds the reactive pseudoaxial conformer of the substrate but also they calculated that the activation energy of the reaction was reduced by *"providing an environment which preferentially stabilises the transition state."*

Bacillus subtilis chorismate mutase therefore performs a relatively non-polar rearrangement and effects acceleration by altering the transition state to make the rearrangement more polar *in vivo* than *in vitro*.

1.3.2 Intermolecular Diels-Alder Reactions

It has been suggested that the formation of a few natural products may proceed *via* intermolecular Diels-Alder reactions although little evidence has been presented to support this. The biosynthesis of the sesterterpenoid Heliocide H_2 **6** may proceed *via* an intermolecular Diels-Alder reaction of hemiglossypolone **7** with myrcene **8** but no enzyme has been isolated to date.[19]

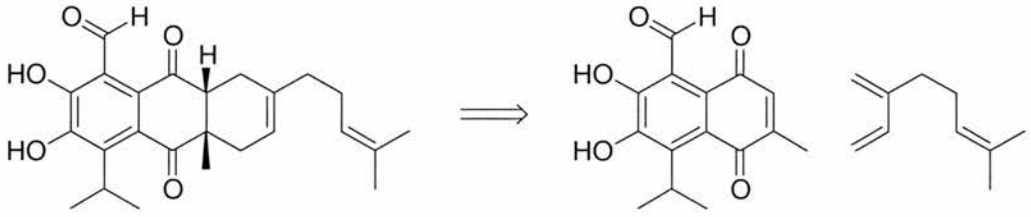

6 **7** **8**

Figure 1.3.2.1 The postulated Diels-Alder reaction to form Heliocide H_2.

In vitro, the cycloaddition between myrcene and hemiglossypolone proceeds uncatalysed at room temperature to form Heliocide H_2 regioselectively. Stipanovic and co-workers stated that hemiglossypolone is found in the pigment glands in young buds and leaves of Upland cotton (*Glossypium hirsutum*) but is replaced by heliocides as the leaves age. Myrcene constitutes 8% of the essential oil of glanded flower buds of the cotton plant. From the observations indicating the accessibility of the starting materials, the authors conclude that an enzyme catalysed Diels-Alder cycloaddition was employed *in vivo,* however as no other evidence was provided, it cannot be assumed that the presence of the starting materials for a Diels Alder reaction proves the existence of an enzyme to catalyse the cycloaddition. The two starting materials implicated by Stipanovic and co workers are isoprenoids which are widespread naturally occurring compounds.

1.3.3 Brevianamides

Brevianamides are examples of mycotoxins and it has been hypothesised that the biosynthesis occurs *via* a key [4+2] cycloaddition.[20,21]

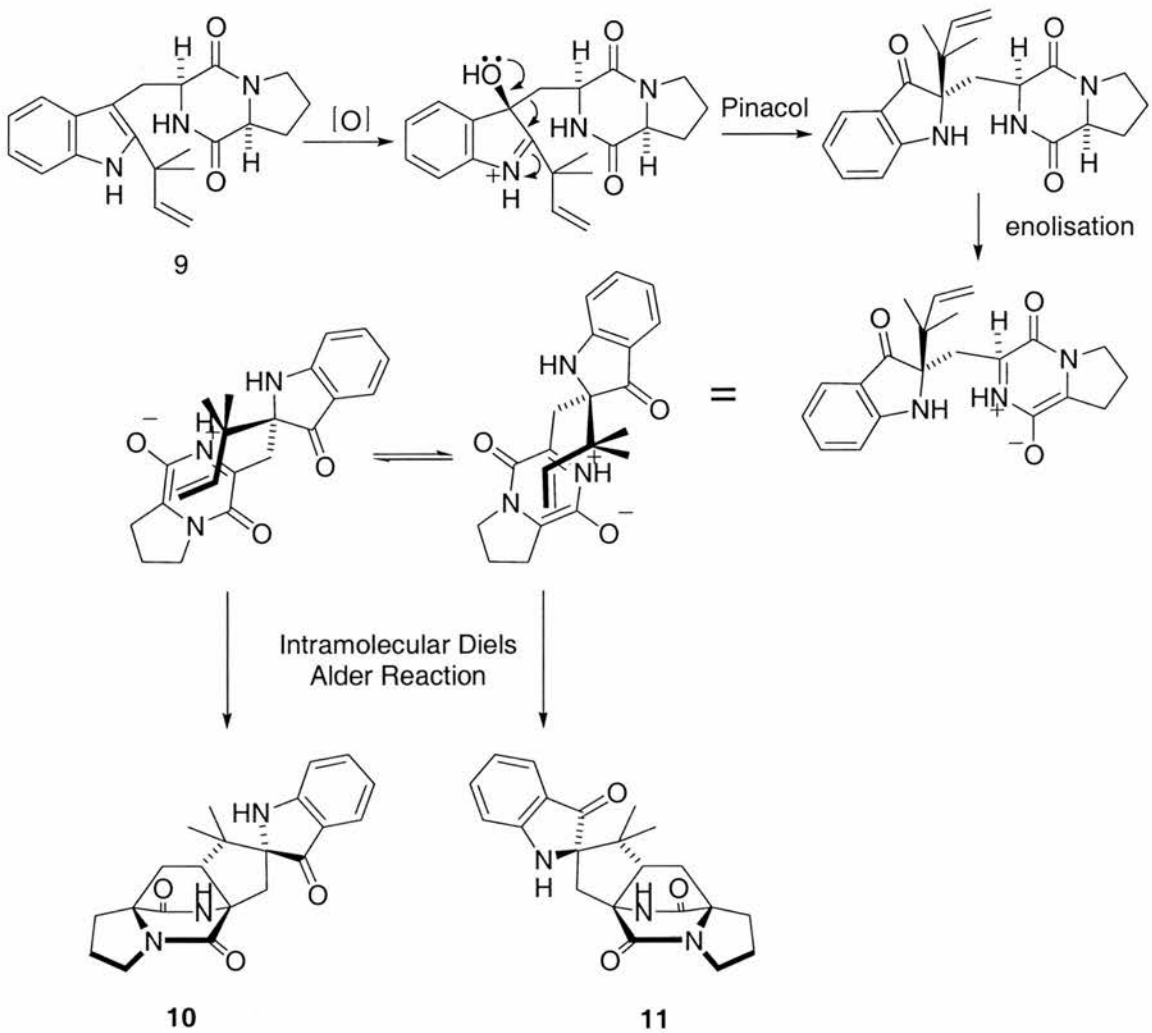

Scheme 1.3.3.1 The suggested biosynthetic pathway for the formation of Brevianamides A and B.

Sanz-Cervera and co-workers performed feeding experiments with deoxybrevianamide E **9**, labelled with tritium in the methylene position. They observed 7.8% incorporation into Brevianamide A **11** and 0.93% incorporation into Brevianamide B **10** indicating that deoxybrevianamide E was a synthetic precursor. From these observations the scheme indicated in **Figure 1.3.3.1** was hypothesised, however there is no further evidence to confirm the presence of the Diels-Alder reaction postulated.

1.3.4 Solanapyrone synthase

One of the few enzymes catalysing a Diels-Alder reaction that has been identified is Solanapyrone synthase in *Alternaria solani* extracts, which catalyses an intramolecular Diels-Alder reaction of prosolanapyrone III **12**. [22-26] Depending on the orientation of the transition state, Solanapyrone A **13** or Solanapyrone D **14** are formed.

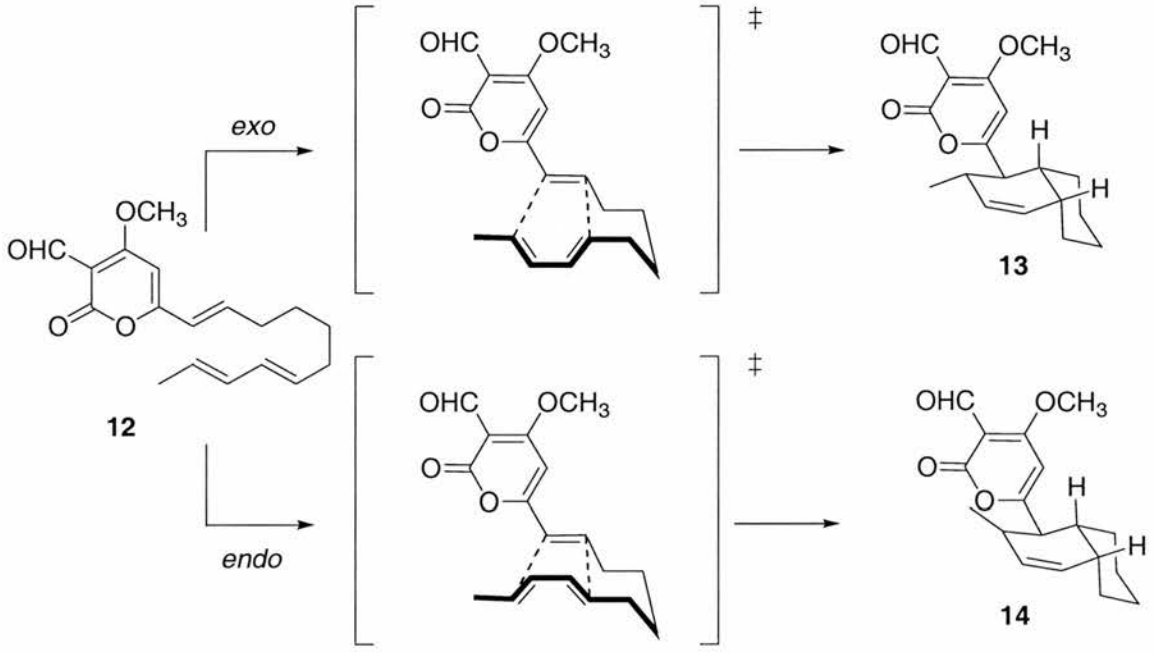

Scheme 1.3.4.1 The proposed chemical action of Solanapyrone Synthase derived from toxins from potato blight. The enzyme molecular weight is 40–60 kDa, however the structure is unknown.

A cell free extract of *Alternaria solani* containing the Solanapyrone Synthase enzyme changed the regioselectivity of this reaction to afford and *endo*:*exo* ratio of 53:47. The reaction *in vitro* favours the *endo* transition state in a ratio of 97:3. This would suggest the Solanapyrone synthase enzyme contained in the extract is capable of lowering the transition state energy of the *exo* cyclisation. The enzyme responsible however, has not been isolated.

Other research groups have proposed Diels-Alder reactions in biosynthesis, however, they also arrive at this conclusion without identification and isolation of the proposed enzyme.[27-31]

1.4 Natural Product Synthesis

It is interesting to compare the synthetic routes adopted by nature with those *in vitro* in natural product synthesis. Synthesis of natural products is not restricted to the use of enzyme reactions alone. Reactions are chosen because they are the most efficient available to the researchers. Several natural product syntheses have utilised the Diels-Alder reaction as a means to introduce increased complexity into the substrate in a specific and selective manner. For example, in the total synthesis of the female sex hormone estrone **20** by Vollhardt and co-workers an intermolecular cobalt catalysed cyclisation is utilised in one step followed by an intramolecular Diels-Alder reaction of **18** later in the synthesis.[32]

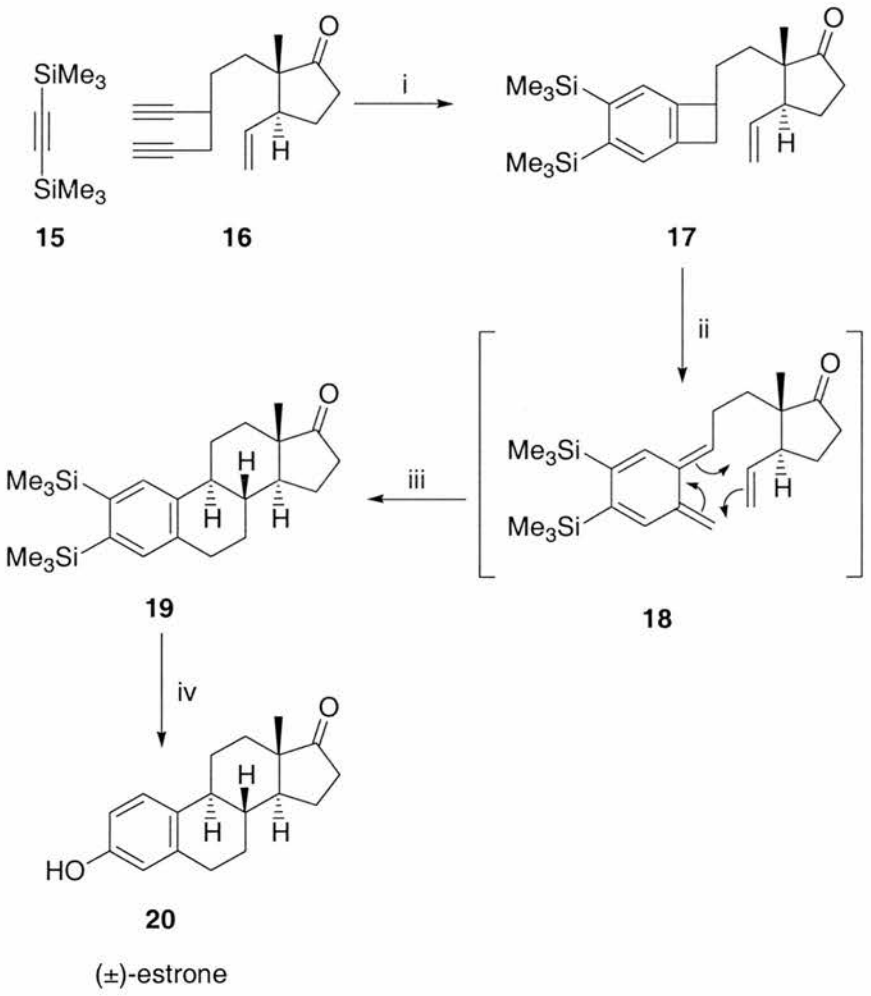

Scheme 1.4.1 Part of the recemic total synthesis of the natural product, estrone. i) $CpCo(CO)_2$ (5 mol %). Intermolecular cobalt catalysed cyclisation. ii) Decane, reflux. iii) Intramolecular Diels-Alder. iv) 1. TFA, CCl_4, 2. $Pb(OCOCF_3)$. Deprotection and oxidative cleavage.

The cyclisation proceeds diastereoselectively to the desired estrone product *via* an intramolecular Diels-Alder cycloaddition and subsequent deprotection.

The Diels-Alder reaction has also been used as a method to generate precursors for natural product synthesis. In Corey and co-workers Prostaglandin synthesis[33] a method of generating the bicyclic Corey Lactone **26** was developed using a copper catalysed Diels-Alder reaction of **22** in the second step.

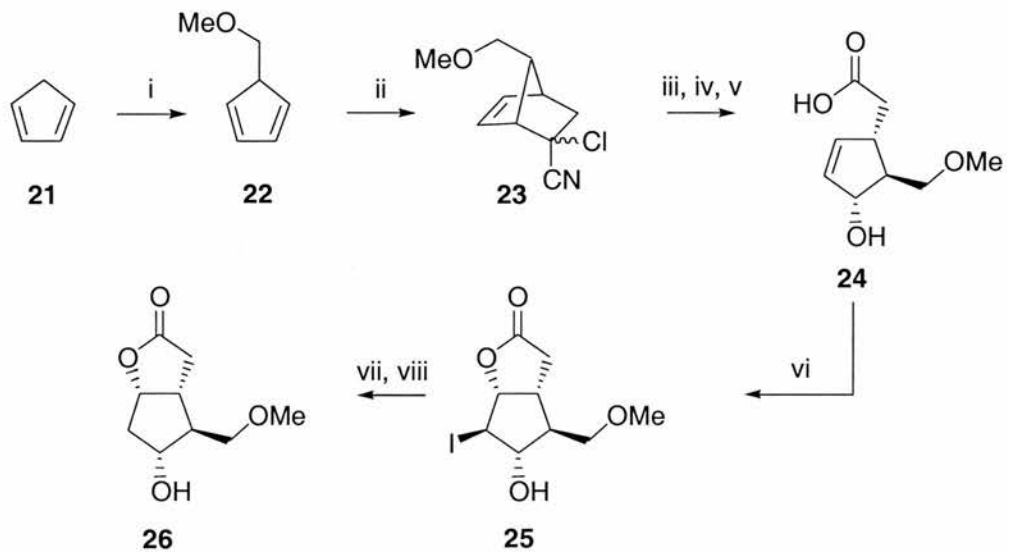

Scheme 1.4.2 Synthesis of the Corey Lactone. i) NaH, THF, $MeOCH_2Cl$, THF, -55°C, ii) $Cl(CN)CCH_2$, $Cu(BF_4)_2$, 0°C, iii) KOH, H_2O/DMSO , iv) mCPBA, $NaHCO_3$, CH_2Cl_2, v) NaOH, H_2O, 0°C then CO_2, vi)KI_3, $NaHCO_3$, H_20, 0°C Ac_2O, pyr, viii) n-Bu_3SnH, AIBN, PhH, Δ

Other examples of natural product synthesis utilising pericyclic reaction methodology are common. These represent only a few examples of the utilisation of cycloaddition methodology in natural product synthesis to introduce stereogenic centres in a controlled, specific manner.[34-40]

Hetero Diels-Alder reactions are a useful method to synthesise pyrans, commonly found in natural products. Several examples of hetero Diels-Alder reactions, can be found.[41-43] Oxygen containing hetero Diels-Alder cycloadditions are a useful means of accessing substituted pyrans.

Figure 1.4.3 Cycloaddition of butadienes with aldehyde or ketones allows access to pyrans.

Guillam *et al*[44] developed a double cycloaddition onto a bis-diene **26** to afford a highly oxygenated bis-pyran **27**. The product was formed slowly but in high yield and under mild conditions.

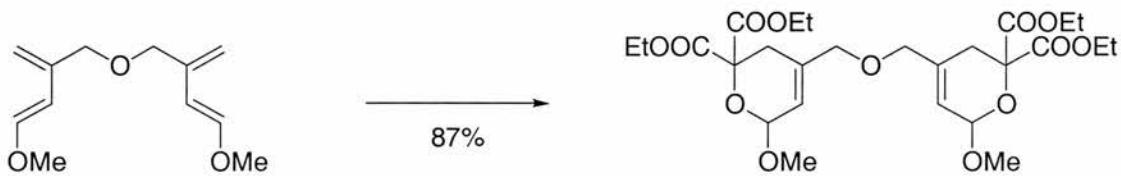

26 **27**

Scheme 1.4.4 Double Diels-Alder reaction of a ketone onto a bisdiene. i) $CO(COOEt)_2$, Et_2O, r.t, 3 days

The low incidence of non-polar reactions in nature is not because of the lack of availability of suitable synthetic precursors; dienes based on an isoprenoid structure could be envisaged. The presence of the isoprenoid Diels-Alder starting materials myrcene and hemiglossypolone led researchers to believe natural synthesis of Heliocide H_2 proceeded *via* an enzyme-mediated cycloaddition.[19] Small numbers of pericyclic reactions are implicated in nature but chorismate mutase, the only enzyme to achieve this that has been extensively studied, has been shown to alter the reaction to render the process more dissociative and thus more polar *in vivo*. Even if the few examples of enzyme catalysed non-polar reactions are confirmed to proceed without alteration of the reaction mechanism, there are far fewer non-polar than polar reactions in nature, however, non-polar reactions like cycloadditions are very common in natural product synthesis. Presented with the same synthetic target, synthetic chemists commonly choose unnatural non-polar reactions to synthesise the target compound in an efficient manner. Cycloaddition reactions are capable of generating five and six membered rings cleanly, creating up to four new stereogenic centres in one synthetic step. If synthetic chemists have identified these routes as a specific and high yielding method of increasing complexity, why has nature rejected them?

1.5 Catalytic Antibodies

In the adaptive immune response, antibodies are proteins expressed by the immune system of a vertebrate in response to the presence of foreign substances or organisms to bind and remove the offending material. One of the properties of immunoglobulins is the ability to distinguish between self and non-self, this property allows recognition and removal of foreign material. Recognition is normally effected by specific and tight binding of molecules specific to the foreign organisms usually antigens on the surface of a cell membrane. All the immunoglobulins have a similar structure and it has been proposed that all immunoglobulins, the T cell receptor and the molecules of the major histocompatibility complex arise from a common ancestral precursor.

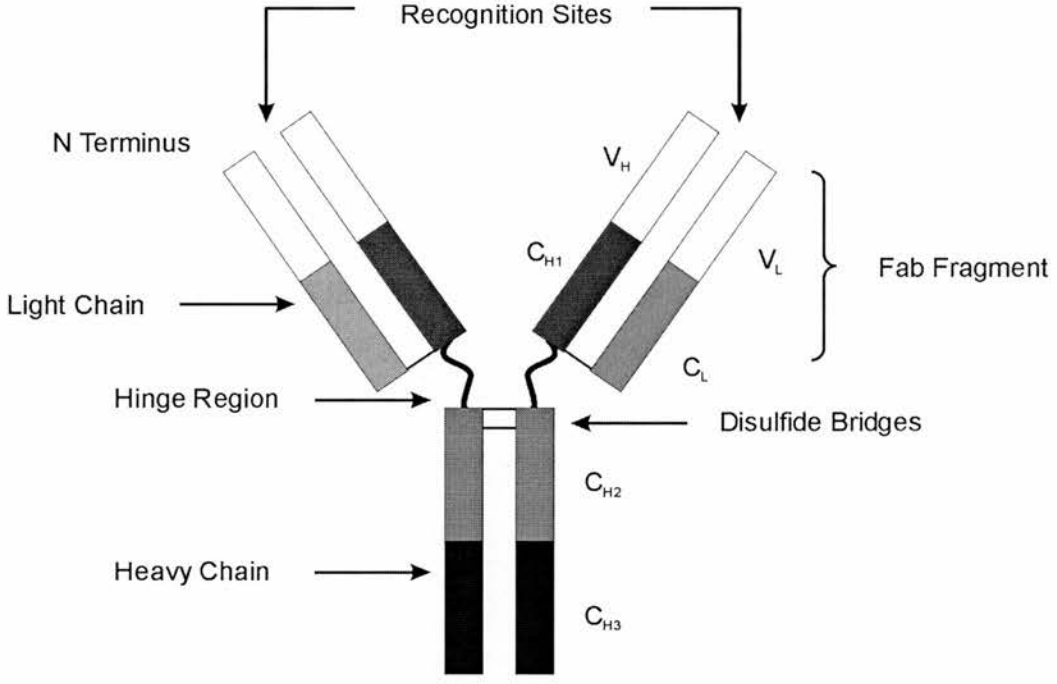

Figure 1.5.1 A schematic representation of the structure of an IgG molecule.

The IgG structure depicted in **Figure 1.5.1** is a simple diagrammatic representation of an immunoglobulin. A monomeric IgG molecule consists of two identical light and two identical heavy chains connected by disulfide bridges. The light chains contain two domains, a constant domain C_L that is the same in all IgG molecules and a variable domain V_L, which is altered to suit the antigen. The heavy chain is divided into three constant domains C_{H1}, C_{H2} and C_{H3} and one variable V_H. The variable

domains of the molecule are the binding sites in the antibodies. Only the Fab fragment is required for recognition.

Antibodies possess similarities to enzymes, they are composed of proteins that bind molecules with high specificity; however, antibodies bind molecules in their ground state whereas it has been postulated that enzymes effect catalysis by the binding and stabilising of transition states.[13] Antibodies can be raised against artificial haptens, small molecules bound to a protein that elicit antibody production. The adaptability of the immune response can be exploited by synthesising haptens containing transition state analogues (TSAs) and therefore develop antibody-derived catalysts with shape and charge complimentarily to ground state TSAs. Once the catalytic antibody is exposed to the parent reaction the transition state should be recognised by the variable domain of the immunoglobulin. Recognition may be used to stabilise the transition state, lowering the energy and increasing the rate of the reaction.

Catalytic antibodies can be thought of as enzyme analogues because the constituent units in both systems are similar, both are synthesised from naturally occurring amino acids. Interestingly, very few catalytic antibodies catalyse pericyclic reactions; there could be various hypotheses as to why this is be the case. One argument is that researchers have tried to emulate enzyme efficiency and so have attempted to create catalytic antibodies that catalyse reactions normally performed by enzymes. Other considerations are the ease of identification of a transition state and ease of design and synthesis of an analogue. For example, a phosphate readily models the tetrahedral intermediate in hydrolysis of an ester. If a Diels-Alder reaction is considered as a target for catalysis, a transition state analogue is difficult to design. The transition state is late and so according to the Hammond Postulate will be inherently "product like", transition states are difficult to devise and synthesise unless the product is used resulting in low reaction turnover.

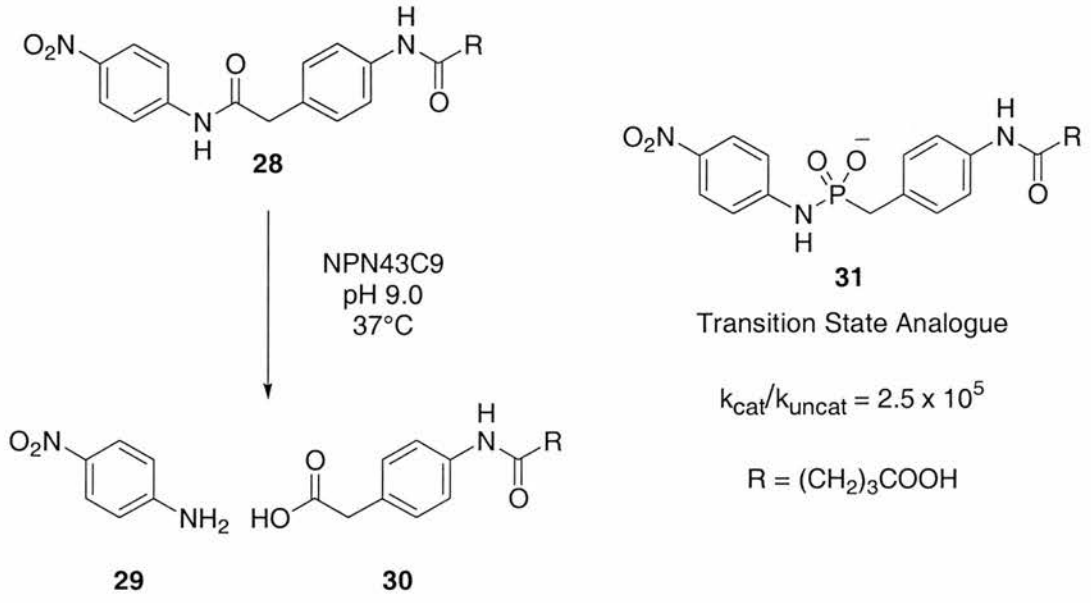

Scheme 1.5.3 Hydrolysis of an amide modelled by a phosphonoamidate transition state analogue.

A typical antibody catalysed reaction is presented in **Figure 1.5.3**.[45] A phosphonate **31** is utilised to model the hydrolysis of a synthetic amide **28**. The reaction is analogous to enzyme catalysed peptide hydrolysis and the rate acceleration achieved is very high.

Catalytic antibodies have been designed to catalyse some non-polar reactions, for example the catalysis of a Diels-Alder reaction shown in **Figure 1.5.4**, the antibody also catalyses a pH dependent hydrolysis of the ester **34**, to alcohol **35** however only the k_{cat}/k_{uncat} values for the cycloaddition were reported.[46]

The rate increase achieved by H11 is typical for catalytic antibodies catalysing a Diels-Alder reaction and is 10000 times less efficient than in **Scheme 1.5.3**, for a polar reaction.

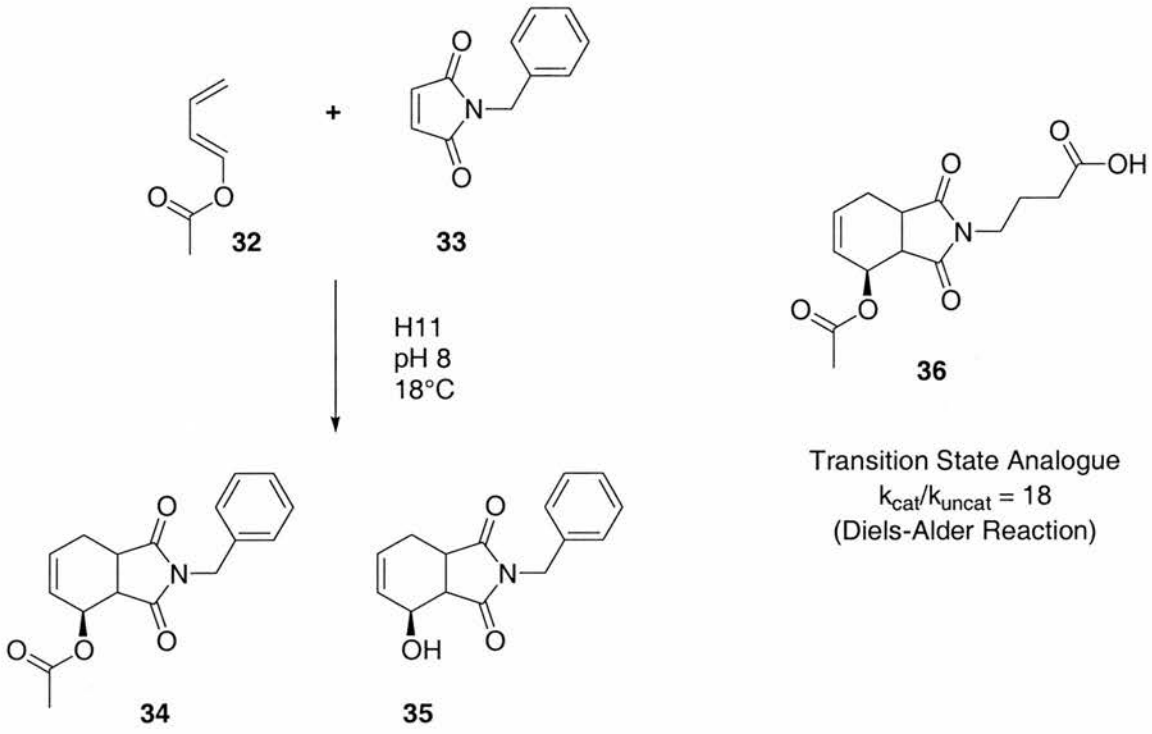

Scheme 1.5.4 The antibody catalysed Diels-Alder reaction as designed by Suckling and co-workers.

Interestingly, Hilvert and co-workers[47] have improved on the typical values observed by coupling a cycloaddition to fast extrusion of SO_2.

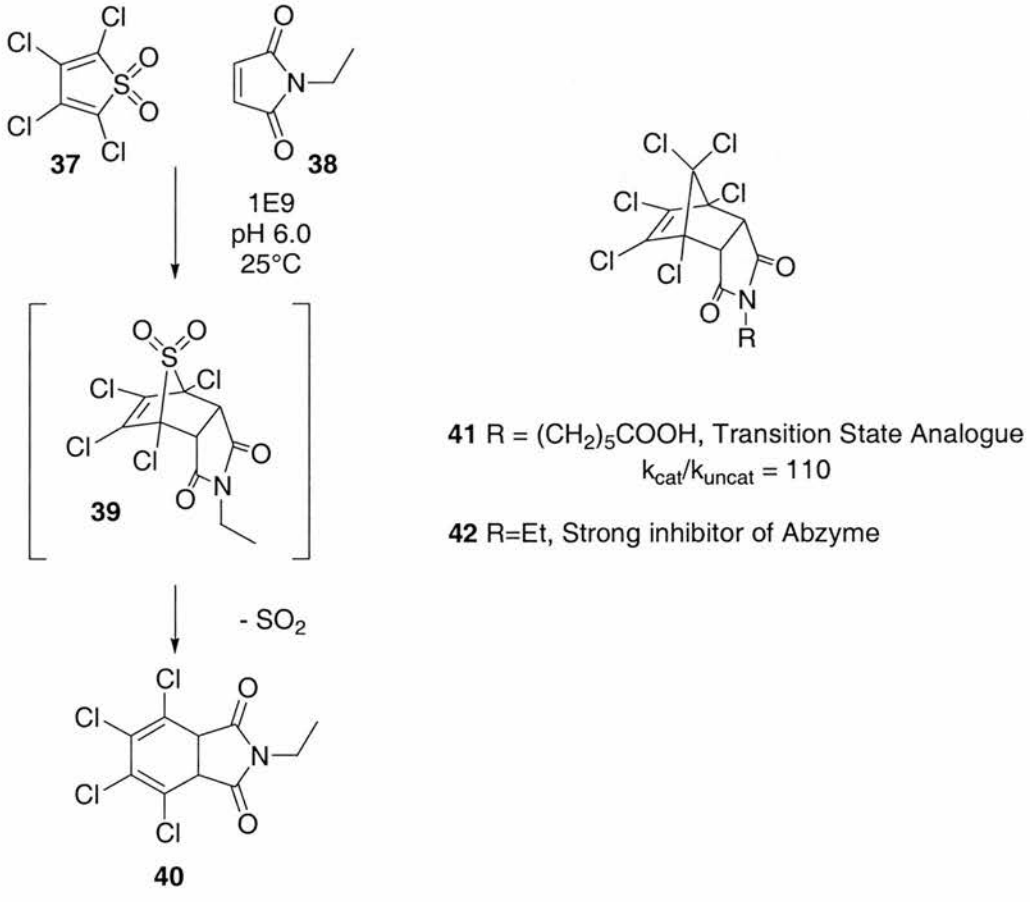

Scheme 1.5.5 Catalysis of a modified Diels-Alder reaction extruding sulphur dioxide to prevent product inhibition of the catalyst.

The Diels-Alder reaction is promoted in excess of a hundredfold. Multiple turnovers were observed (>50) and the reaction is strongly inhibited by **41** where R=Et. The improved rate increase lends weight to the argument that the poor catalytic rates normally observed for Diels-Alder reactions are as a result of product inhibition, however, although the value for k_{cat}/k_{uncat} is improved, it is far from the typical rate increases observed for polar reactions, indicating that product inhibition is not the entire problem in Diels-Alder catalysis.

Rearrangements have also been catalysed by catalytic antibodies, e.g. chorismate mutase mimics[48,49] and to catalyse an Oxy-Cope rearrangement.[50,51] The advantage with rearrangements is the product is acyclic and as a result the ground states differ widely from the transition state of the reaction, enabling turnover. The Oxy Cope reaction also results in the formation of an enol which rapidly tautomerises to the aldehyde product.

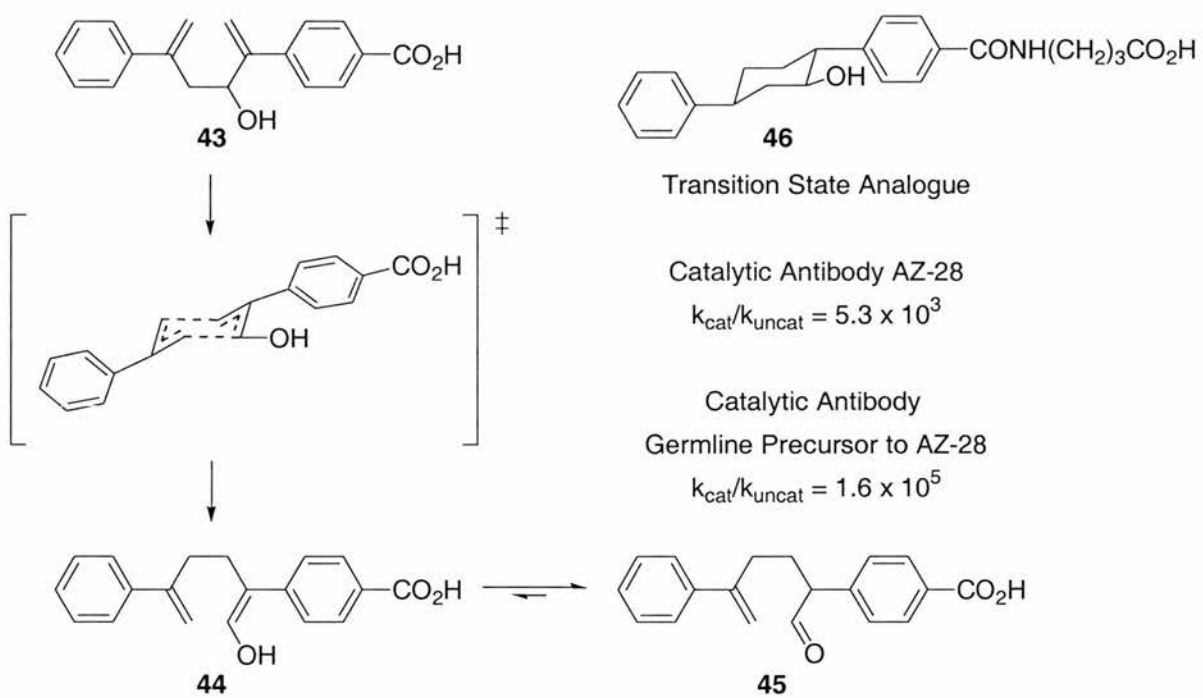

Scheme 1.5.6 An Oxy Cope rearrangement which is catalysed by a catalytic antibody developed by Mundorff and co-workers.

Impressive rate accelerations are achieved with this more recent example of a catalytic antibody catalysing a non-polar reaction although again interesting questions about the origin of catalysis should be posed. As the original reaction is

unimolecular, acceleration can only be obtained by orientating the reactant **43** in a reactive conformation and some subsequent stabilisation of the transition state. The authors state that when the mutations were investigated in isolation between the two antibodies they discovered that only one mutation had a significant effect upon catalysis and the germline antibody had a lower binding affinity for the transition state analogue. The substitution of a serine residue possessing an alcohol sidechain for an asparagine residue containing a primary amide sidechain increases the rate of reaction thirty-fold. The authors suggest[52] that the difference is as a result of rigidifying the active site, however, they fail to explain the reasons behind the reduced affinity for the transition state analogue **46**. The increased catalysis yet reduced association constant for the analogue suggests the transition state analogue is not a correct approximation of the transition state, however, further work will have to be performed to elucidate the origins of this dramatic rate difference.

Collating catalytic antibody data from Blackburn and co-workers' extensive review[13] reveals some interesting trends (**Figure 1.5.7**). Comparing Diels-Alder reactions (graph D) with hydrolysis experiments (graphs A to C) reveals clear relationships in the overall trends. Even data compression as a result of plotting the k_{cat}/k_{uncat} values on a logarithmic scale reveals large differences.

The first point of note is the lower incidences of antibody catalysed Diels-Alder reactions (graph D) when compared with the more polar reactions (A, B and C). Although the data set for Diels-Alder reactions is small, the $\log(k_{cat}/k_{uncat})$ values lie to the left of the graph, indicating low levels of catalysis. With the polar reactions (A, B and C), the mode lies further to the right hand side indicating more efficient catalysis. It is interesting to compare the three polar reactions, as the distribution of rate increases is analogous. It could be suggested that these trends arise from a small data set of inefficient catalysis as Diels-Alder catalysis is still in its infancy, the data set presented only contains Diels-Alder catalysts from 1989 - 1998, however the reported literature for polar reactions encompasses a similar time-span (1986 - 1998).

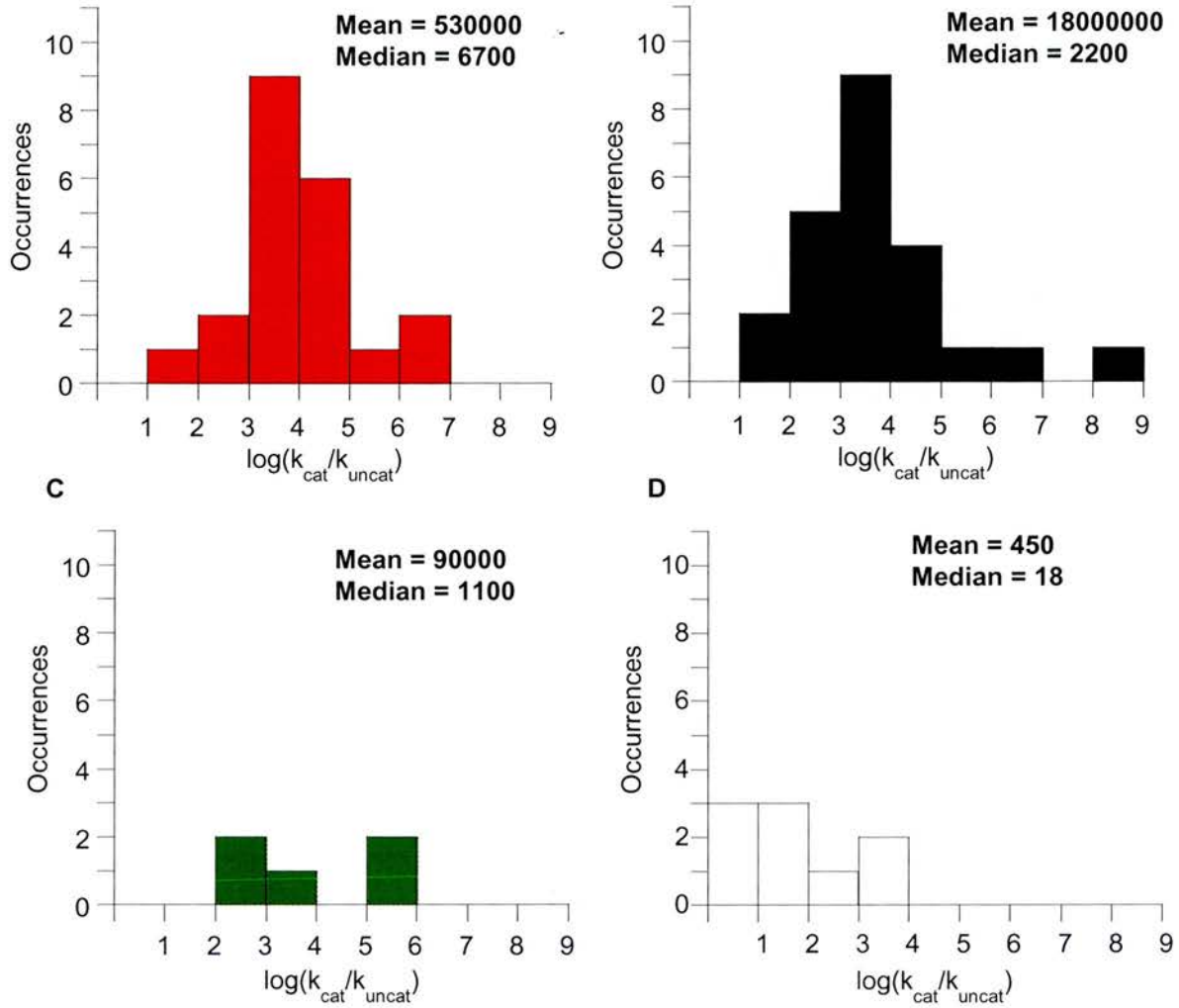

Figure 1.5.7 Representation of the distribution of kcat/kuncat values. Data is collated from Blackburn and co-workers and is depicted using logarithmic scales on the x-axes. Graph A – Aromatic Ester Hydrolysis, Graph B – Aliphatic Ester Hydrolysis, Graph C – Amide Hydrolysis, Graph D – Diels Alder Reaction

Comparing the statistics of the four reaction classes provides no information for the basis of the differing values but the trends suggest further investigation is necessary.

Hilvert has recently reviewed catalysis by antibodies and compared them with enzyme catalysis.[53] He assessed the catalytic efficiency of natural enzymes and compared them with catalytic antibodies. Interestingly, Hilvert showed that transition state binding in the systems he investigated was proportional to catalysis confirming Pauling's intuitive prediction.[54] Hilvert compiled these observations into a graph also detailing the type of reaction performed by each catalyst.

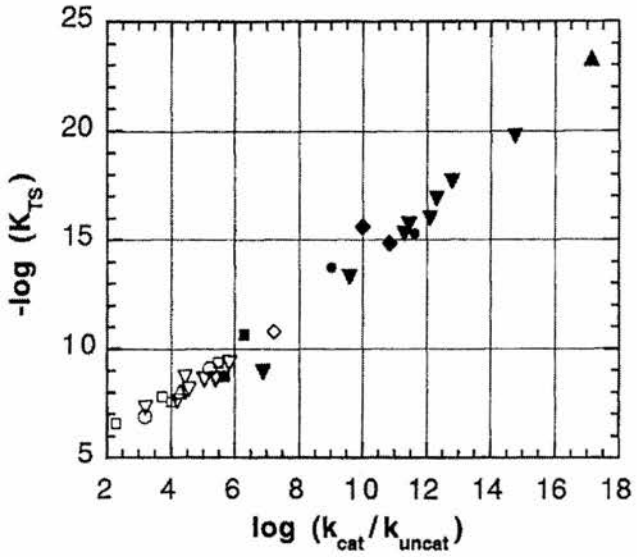

Figure 1.5.8 The correlations between - log K_{TS} and log k_{cat} / k_{uncat} for enzymes and catalytic antibodies as observed by Hilvert (taken from Ref. 53). Open symbols represent catalytic antibodies, closed systems represent reactions catalysed by enzymes. Squares represent non-polar rearrangement reactions, all other symbols represent polar reactions.

The first observation to make from **Figure 1.5.8** is that enzymes (closed symbols) are generally faster than the catalytic antibody counterparts. The second point of note is that the enzyme examples are almost exclusively polar reactions such as hydrolyses or decarboxylations. The only non-polar enzyme reactions are rearrangements, both examples possessing the lowest value of k_{cat} / k_{uncat} of all the enzymes featured. The polar reactions of the catalytic antibodies are also generally faster than the rearrangement reactions.

1.6 RNA Catalysis

Recent research has shown that RNA is capable of molecular recognition and subsequent accelaration of chemical transformations.[55] Wiegand and co-workers[56] adopted a strategy to develop RNA amide synthases by synthesising an RNA library attached to a primary amine *via* a polyethylene glycol (PEG) linker. The PEG linker was utilised to enable the amine to resemble a free substrate as it was highly mobile and heavily solvated.

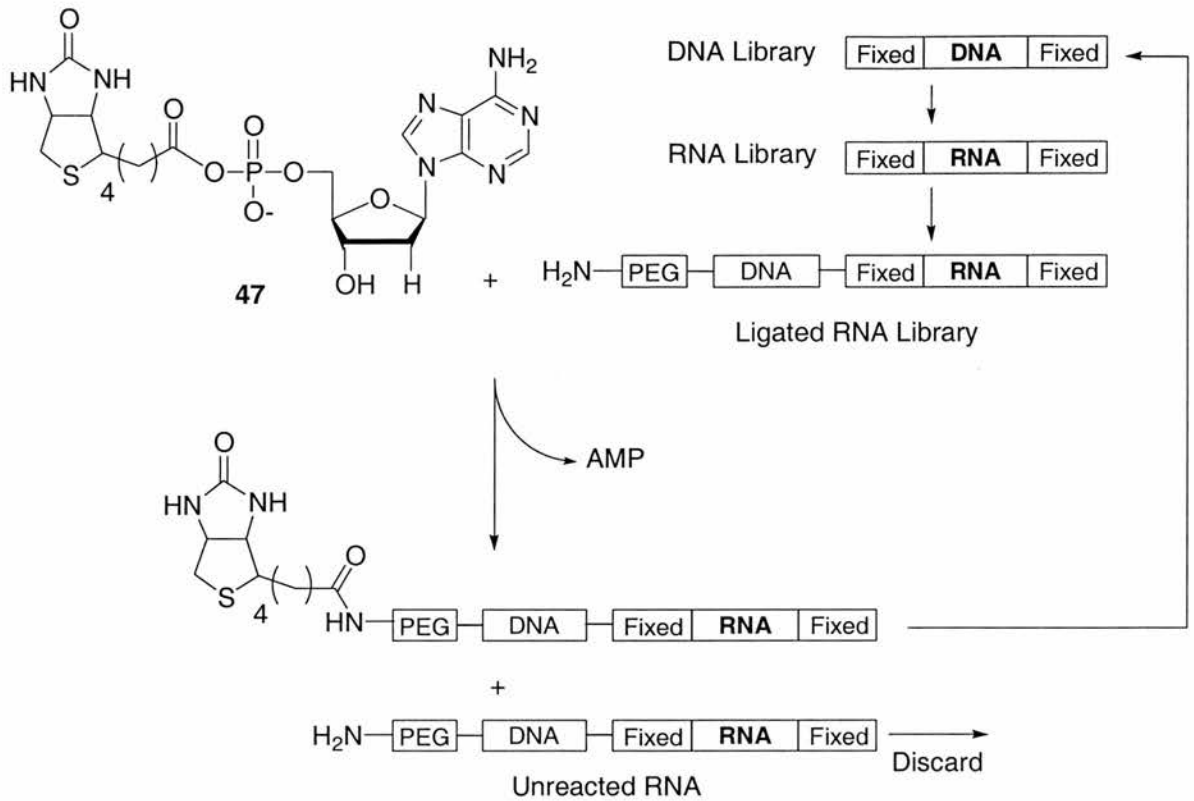

Figure 1.6.1 The procedure described by Wiegand *et al* for the isolation of RNA amide synthases. PEG represents polyethylene glycol. DNA is a fixed DNA 10-mer, fixed represents fixed nucleotide sequences of 5 and 3 residues respectively. **DNA** and **RNA** in bold type represent variable nucleic acid sequences.

The modified RNA sequences were exposed to AMP-biotin **47** and the sequences which reacted were reserved. After reverse transcription and amplification of the DNA template (polymerase chain reaction – PCR) the RNA was reattached to the DNA-PEG-primary amine sequence. This process was repeated increasing the harshness of the reaction conditions by lowering substrate concentration and shortening reaction time until the RNA catalysed amidation reached a maximum. This led the researchers to identify sixteen unique sequences which catalysed the amide formation.

The fastest amide synthase identified AS25, was shown to possess moderate dependence for containing a Cu^{2+} ion. The rates of reaction were similar, in the presence of the cation, $k_{cat} = 6.6 \pm 0.2 \times 10^{-4}\ s^{-1}$, compared with $6.9 \pm 0.6 \times 10^{-4}\ s^{-1}$ in the absence of the cupric ion.

$$RE_{AS25} = \left(\frac{k_{cat}}{K_m}\right)\left(\frac{1}{k_{uncat}}\right)$$

Figure 1.6.2 Equation relating rate enhancement (RE) with K_m, k_{cat} and k_{uncat}.

Michaelis Menten kinetics were calculated for the reaction which established a rate enhancement of 1.1 x 10^5 (**Figure 1.6.2**). Interestingly in the presence of the Cu^{2+} ion, the Michaelis Menten constant, K_m is reduced tenfold. As K_m is inversely a measure of how efficiently the receptor and substrate bind, the cupric ion must assist ground state binding rather than specifically assisting transition state binding.

Tarasow and co-workers[57-59] adopted a similar approach for their catalysis of a Diels-Alder reaction by RNA and their approach is displayed in **Figure 1.6.3**.

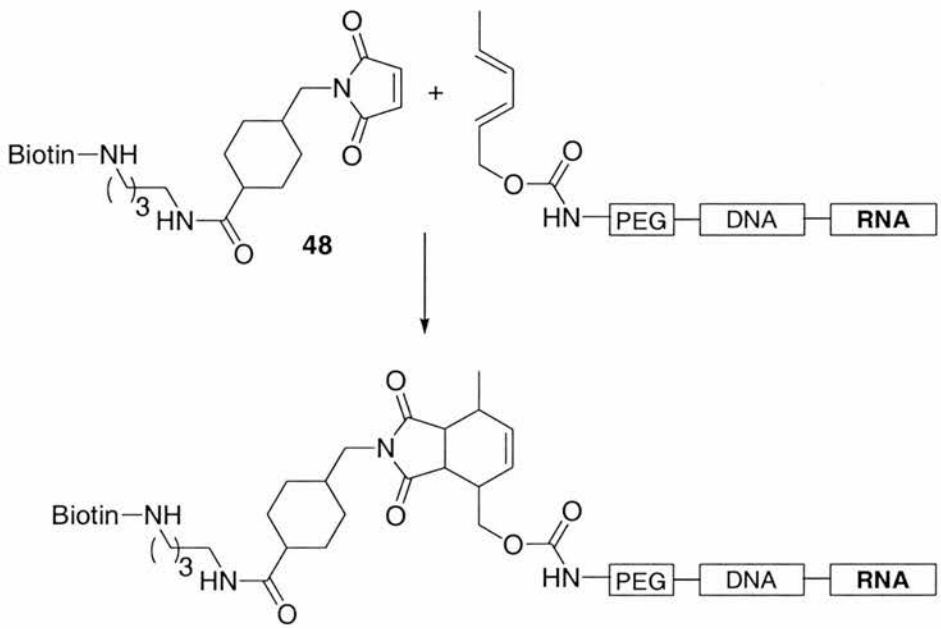

Figure 1.6.3 Formation of a RNA Diels-Alderase as described by Tarasow *et al.*[58]

The RNA Diels-Alderase displayed a 800 fold acceleration of the reaction over the spontaneous reaction rate. Although found to possess good substrate specificity, the RNA Diels-Alderase was absolutely dependent on the presence of a cupric ion. It is well known that Diels-Alder reactions can be catalysed by Lewis acids so it appears that in this example of a "Diels-Alderase", the RNA backbone is merely providing ligands for metal coordination and also providing some binding to account for the observed substrate specificity.

Seelig and Jaschke have also reported an RNA Diels-Alderase.[60] It is dependent upon the presence of Mg^{2+}, however, other metal cations can be substituted. The origin of acceleration is, however, likely to arise from Lewis acid catalysis.

1.7 Molecular Imprinting

Molecular imprinting could be seen as a synthetic derivative of catalytic antibodies because polymers are generated to bind to specific ground state guests. Monomers containing recognition sites can be exposed to a substrate and subsequently polymerised to create a complimentary recognition site within the polymer in a similar manner to raising an antibody to a hapten. One of the methods that can be employed is recognition *via* hydrogen bonding. The resulting cavity should contain an appropriate array of donors and acceptors to form a host-guest interaction.

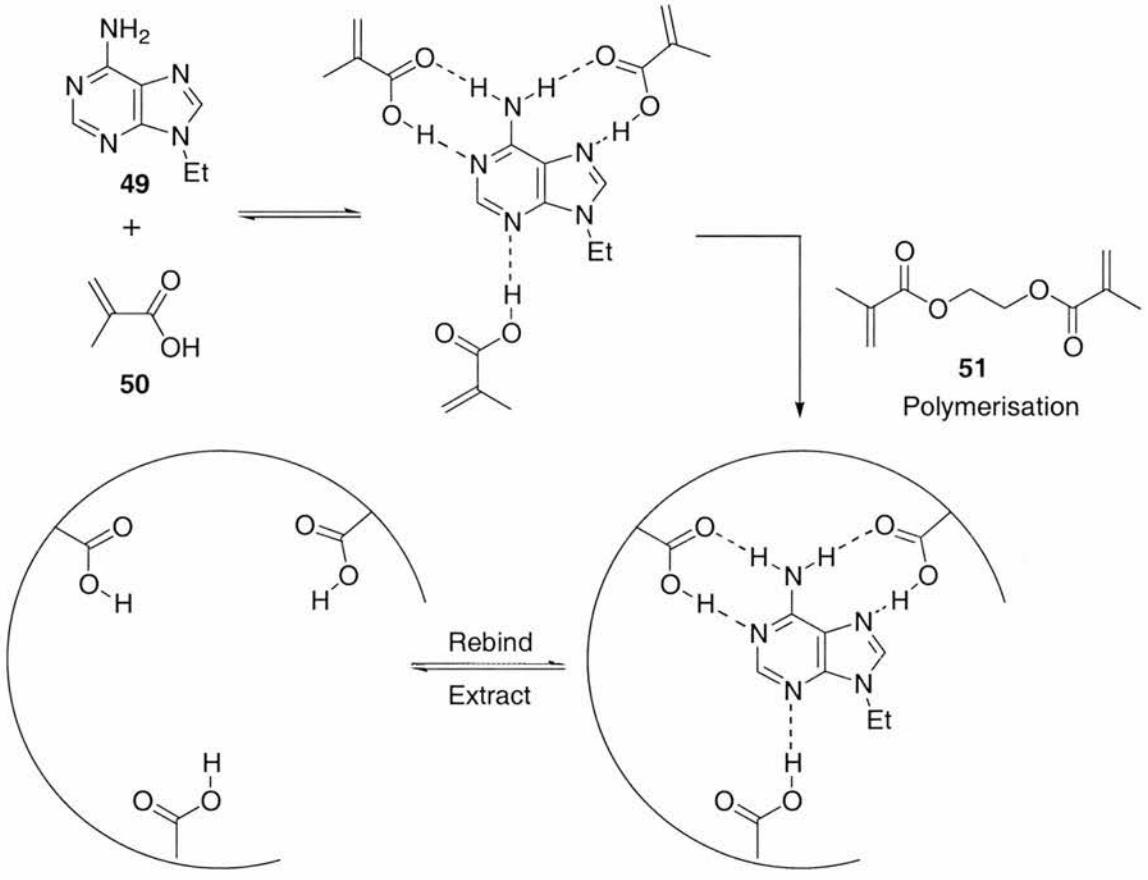

Figure 1.7.1 Molecular imprinting using hydrogen bond mediated recognition. Removal of the template leaves a cavity that is complimentary to the guest in shape and hydrogen bonding motifs.

Spivak and co-workers[61] designed an imprinted polymer specific to 9-ethyladenine **49**, which was formed by hydrogen bonding between the guest and the host monomers **50** prior to polymerisation with **51**.

In the same manner that antibodies recognise ground states, the resulting polymer will be specific for the ground state of the guest, however an extension could be envisaged by imprinting polymers for transition state analogues analogous to generating catalytic antibodies. The resulting polymer has the advantage of transition state recognition with improved stability under more varied reaction conditions than catalytic antibodies. Sellergren and co-workers[62] have adopted this procedure in their enantioselective ester hydrolysis. A combination of hydrogen bonding interactions and covalent bonds were used to develop "active sites" in the polymer specific for a transition state analogue.

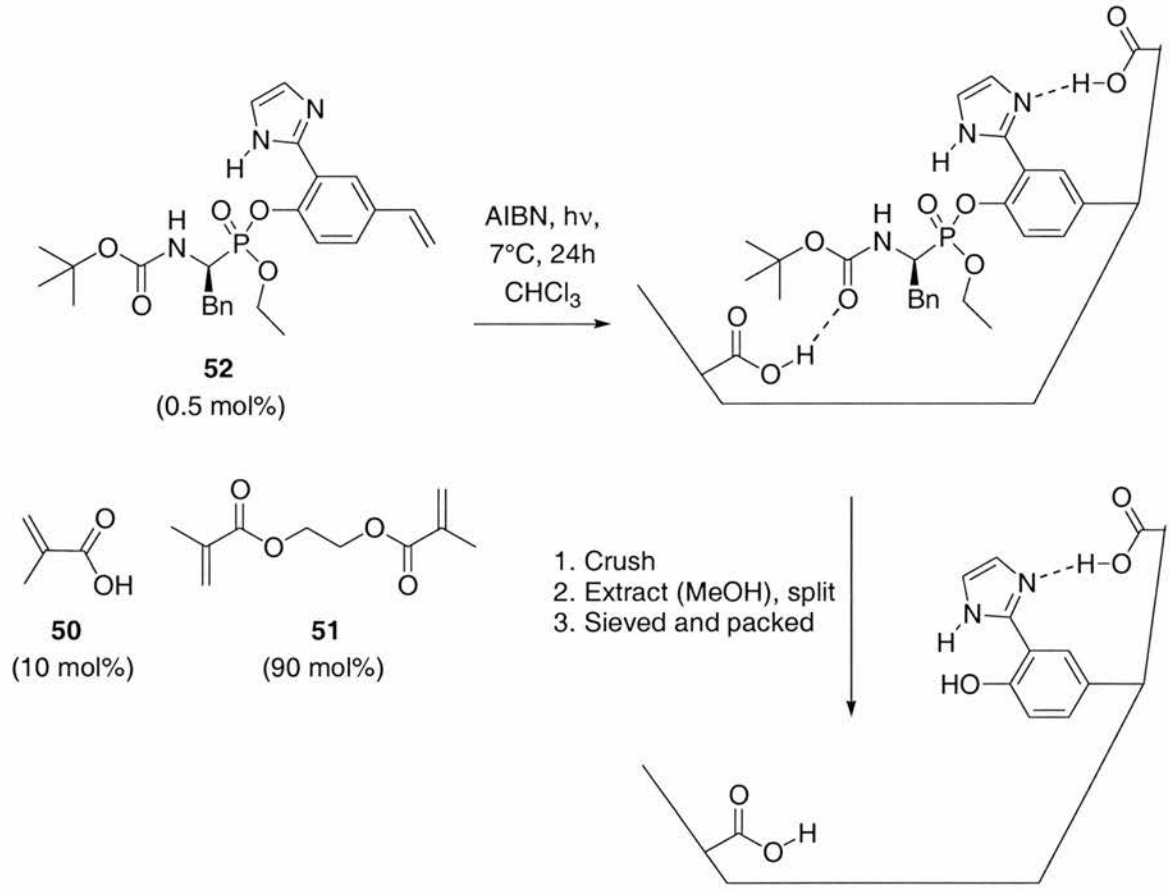

Figure 1.7.2 Schematic representation of the formation of a polymer template to catalyse the degradation of an ester.

The polymeric receptor catalyses the nucleophilic degradation of an ester *via* a tetrahedral intermediate. A phosphonate models the transition state accurately as previously observed for the catalytic antibody systems.

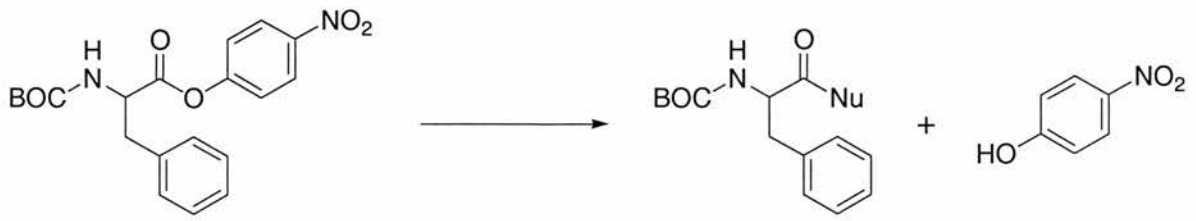

53 **54** **55**

BOC-D(L)-PheONP

Scheme 1.7.3 The reaction catalysed by the imprinted polymer

In the presence of aqueous sodium hydroxide, the reaction proceeds with a rate of $k = 1.02 \times 10^2$ min^{-1} for the D enantiomer. In the presence of the imidazole monomer shown in **Figure 1.6.4**, the reaction only proceeds with a rate of 14 min^{-1}, an increase of seven-fold.

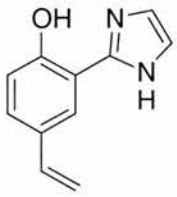

56

Figure 1.7.4 The imidazole monomer, used as a control compound for comparison with the imprinted polymer developed by Sellergren and co-workers.

It is important to question, however, whether the imidazole monomer **56** depicted in **Figure 1.7.4** is a fair control. The reaction under consideration is an ester hydrolysis which can be acid catalysed, so performing the reaction in the presence of the imidazole monomer but the absence of the acid monomer may result in an artificially slow calculated background rate.

The imprinted polymer depicted in **Figure 1.7.2** also preferentially catalyses the hydrolysis of the D ester as $k_D/k_L = 1.6$ indicating the recognition sites formed in the polymer displayed a small degree of specificity for the D transition state in preference to the L.

An imprinted polymer catalysing the Diels Alder reaction has also been prepared,[63] although the polymer relies on Lewis acid catalysis by a high concentration of titanium (IV) complexes contained within the structure. The obsevation of catalysis in

this example is not surprising. A [3+2] dipolar cycloaddition has been shown since to be catalysed by a chiral non-imprinted polymer containing aluminium cations generating excellent enantiomeric excesses.[64]

A difficulty with imprinted polymers, is that they can prove to be difficult to analyse. Several different active sites can be formed in the polymer with differing accessibility to solvent. The effective catalyst concentration and the specific interactions catalysing the reaction can therefore be difficult to assess.

1.8 Supramolecular Catalysis

Supramolecular chemistry is concerned with the development of systems containing non-covalent bonding interactions. Much of the focus of supramolecular chemistry has been the development of ordered structures from simple structural motifs[65-69] or the specific binding[70-73] of ground state molecules. Ground state binding has frequently been applied[74-76] to the binding of natural products. Indeed, in some examples[77-79] very high association constants have been detected.

Several catalysts have been developed using synthetic systems and non-covalent interactions, which can be broadly classed as "Supramolecular Catalysts". In comparison with enzymes and biological systems, synthetic catalysts have potentially the advantage of being simpler than natural systems and more open to chemical modification to adjust the binding and reaction properties. Any possible catalysis may be exploited through these systems and reactivity is not limited to enzyme-like reactions.

The strategies employed are discussed with appropriate examples of each class of catalysis, acceleration or facilitation.

1.8.1 AB Methodology

Enzyme catalysed reactions are often as efficient as truly intramolecular reactions. Kirby stated in his Review of Enzyme Models and Mimics, *"The only simple reactions that can rival their enzyme-catalysed counterparts in rate are intramolecular reactions*

such as cyclisations."[80] Catalysis cannot be achieved by an intramolecular system, however acceleration of a particular type of reaction may be attained.

The increase in rate observed by rendering a reaction intramolecular could be exploited by forming a temporary complex rendering a reaction process pseudointramolecular. The greater the preorganisation of the starting material to bind a guest and subsequently react, the greater the acceleration or "kinetic effective molarity".

Examples of polar reactions accelerated by pseudointramolecularity include reactions adopting "AB" methodology. Although not catalytic, their mode of action involves hydrogen bonding and acceleration or facilitation.

The starting materials **A** and **B** have complimentary recognition sites with reaction centres that are capable of orientating themselves in a suitable position for reaction within the **[A•B]** complex. A schematic representation of this process can be seen in **Figure 1.8.1.1**.

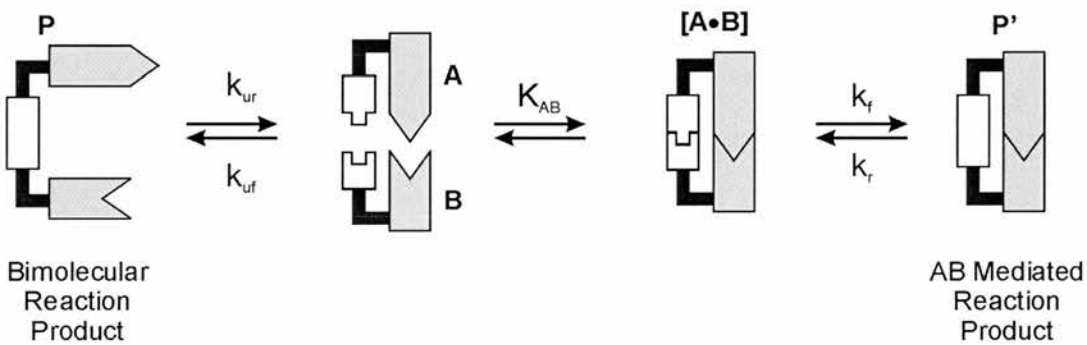

Figure 1.8.1.1 A schematic representation of an AB system. The grey shaded figures represent the recognition sites and the white shapes are the reaction sites. K_{AB} represents the association constant and k_f and k_r are the forward and reverse rate constants of reaction, k_{uf} and k_{ur} are the equivalent uncatalysed rates.

Unlike truly catalytic systems, no turnover can be observed because the host is altered by the reaction. Although k_{cat}/k_{uncat} is meaningless for this type of system, a measure termed kinetic "effective molarity" can be invoked, calculated from k_f/k_{uf}, which describes the efficiency of the system in terms of the molarity of the bimolecular reactants lacking the ability for recognition required to achieve the same reaction rate.

Hamilton and Tecilla[81] designed a receptor for barbiturates with appended functionality capable of accelerating a nucleophilic substitution relative to the intermolecular reaction. The receptor was irreparably altered by the reaction and so the process cannot be termed catalysis but is an example of acceleration by pseudointramolecularity.

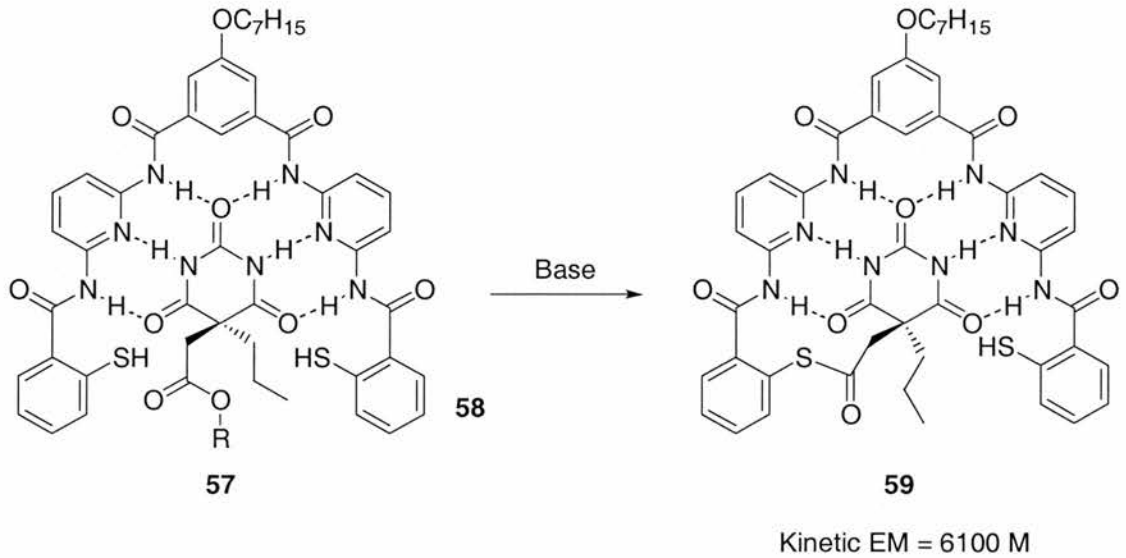

Scheme 1.8.1.2 Increasing the rate of a nucleophilic substitution by rendering the reaction pseudointramolecular. The kinetic effective molarity reported is for 2.5 equivalents of receptor **58**. R =

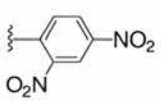

In the presence of 10 equivalents of thiol **58**, the nucleophilic substitution depicted in **Figure 1.8.1.2** proceeded with an observed[82] rate of 6.82 x 10^{-2} s^{-1}. In the presence of 20 equivalents of a control compound **60** the rate constant was observed to be 5.78 x 10^{-5} s^{-1}, nine times faster than the rate in the absence of any hosts or controls.

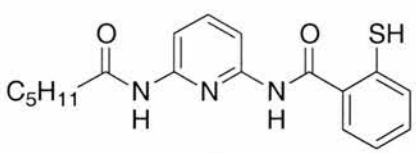

60

Figure 1.8.1.3 Control compound developed to assess the efficiency of **58**.

Lower concentrations of the thiol receptor **58** still yielded impressive rates, in the presence of two and a half equivalents of **58**, the reaction rate constant calculated was of a similar order of magnitude, 3.95 x 10^{-2} s^{-1}. Unfortunately, the real efficiency

and thus effective molarity of the system cannot be assessed because results for lower stoichiometries were not reported.

Bennes and Philp[83] have also employed AB methodology for the facilitation of Diels-Alder reactions. In this example, the increase in product is attributed to hydrogen bonding which is maintained in the product, lowering the product ground state energy rather than acceleration alone. This effect is termed "facilitation" and arises from altering the position of the equilibrium of the reaction.

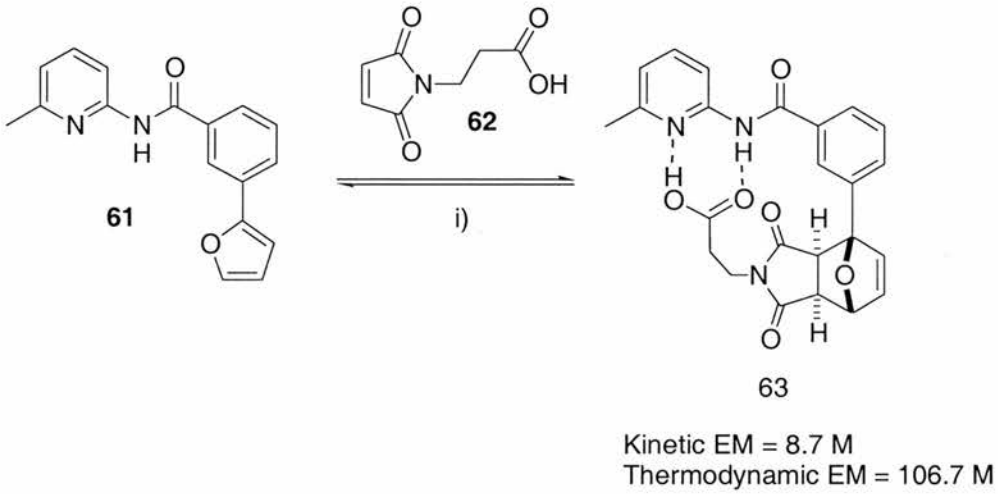

Scheme 1.8.1.4 The facilitation of a Diels-Alder reaction by the acid amidopicoline recognition motif. i) $CDCl_3$, 50°C

In the absence of the recognition sites, the reaction only proceeds to 1% completion. In the presence of the recognition sites the *exo* product **63** is produced exclusively in 40% yield. The reaction is readily reversible under the observed conditions and in the absence of the recognition sites the equilibrium is heavily in favour of the starting materials. Conjugation of the furan with the benzene ring adds resonance stability to the starting material **61** that is not retained in the product. In the presence of the recognition sites, however, hydrogen bonding persists in the *exo* product enabling some thermodynamic compensation for the loss of conjugation. Thermodynamic effective molarity is more informative for this type of reaction, which is the ratio of the equilibrium constants for the reaction against a suitable control lacking recognition sites.

[3+2] Dipolar cycloadditions have also been subject to AB reactivity.[84] Azides can undergo cycloadditions with maleimides in analogous systems to the Diels-Alder reaction reported previously.

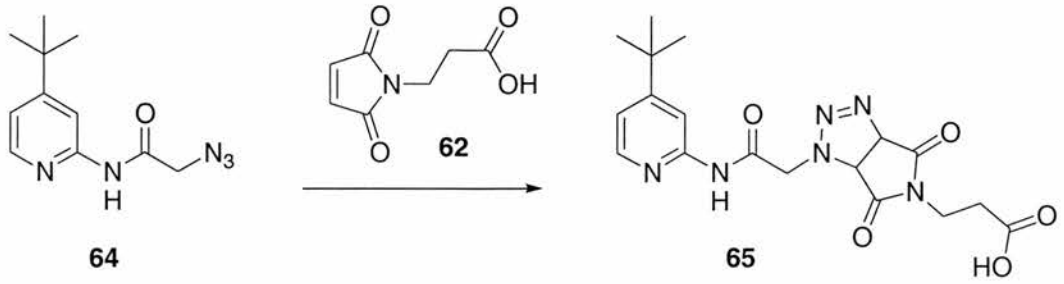

Scheme 1.8.1.5 A simple two-component system capable of exploiting AB reactivity.

In contrast to the previous system, the rate acceleration observed is largely kinetic in origin, indicating the reaction is assisted by a reduction in the activation energy rather than increased product stability, several other examples of this reactivity have been reported often inducing regio or diastereocontrol on a cycloaddition reaction.[85-88]

The AB methodology can be adapted to obtain true catalytic turnover. An example of how the process can be modified is depicted in **Figure 1.8.1.6**.

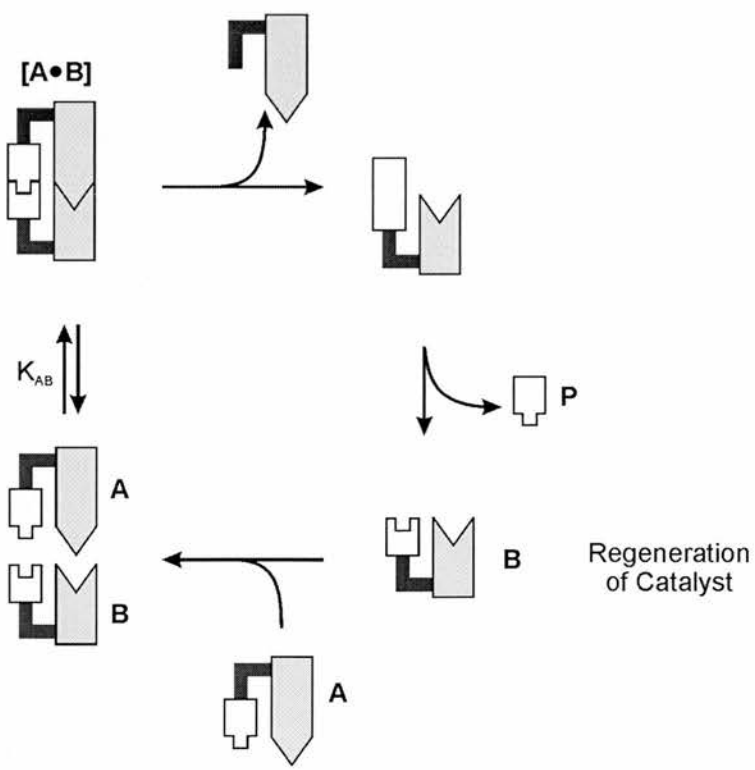

Figure 1.8.1.6 Modification of the AB methodology to obtain true catalytic turnover. The recognition site is lost in the initial reaction and the resulting reaction site is regenerated by hydrolysis.

In the initial reaction, after binding of host **B** to guest **A** to form a complex **[A•B]**, the recognition site of guest **A** is removed and a modified receptor is generated. Hydrolysis of this intermediate to yield the product **P** however, returns the catalyst **B** to the reaction mixture rendering the reaction truly catalytic.

Lehn and co-workers have employed appended functional groups in this manner in the elegantly designed cryptand **66** shown in **Figure 1.8.1.7**.

Use of the cryptand receptor as a catalyst is simple yet effective because at pH 7, four of the ring nitrogens are protonated and two are not. This enables two of the ring nitrogens to retain their nucleophilicity. Lehn and co-workers used this receptor to accelerate the fragmentation of ATP to ADP.[89-92] Binding is promoted by charge-reinforced hydrogen bonding of the phosphate groups to the ammonium protons for efficient acceleration of phosphate cleavage from ATP.

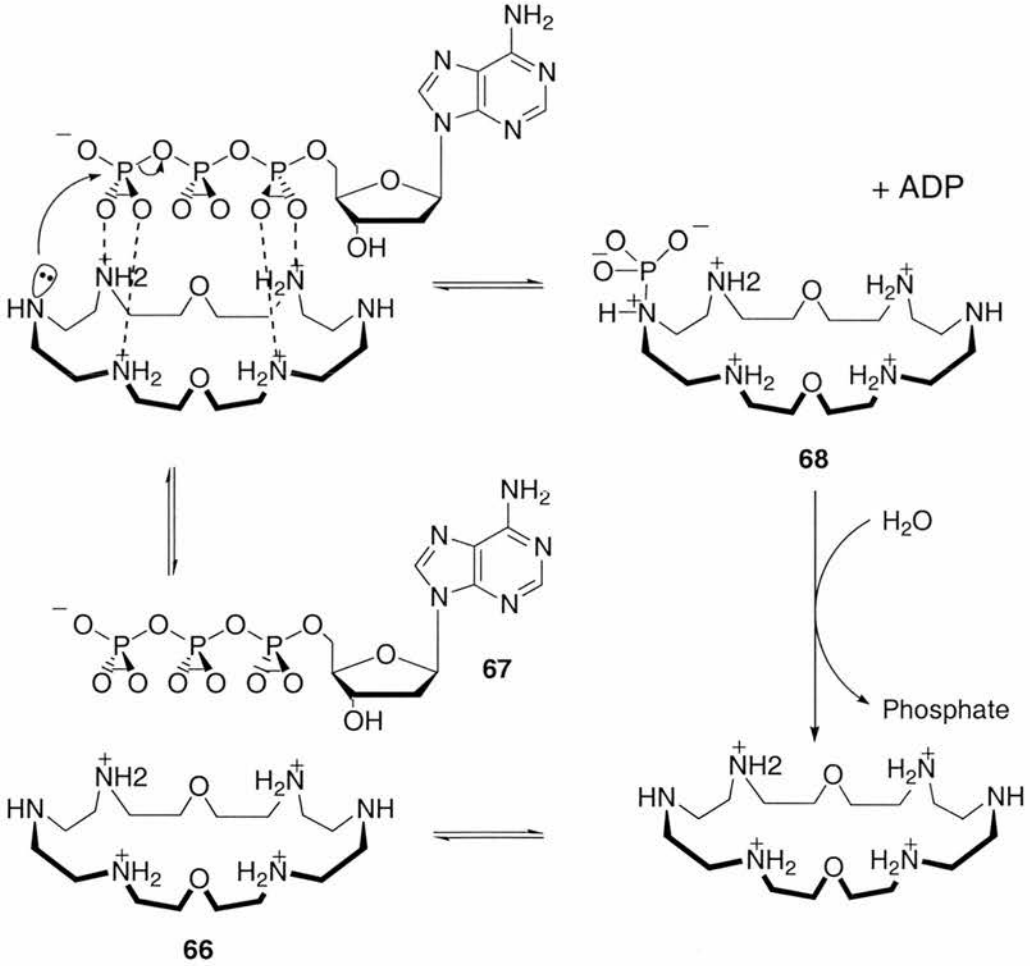

Scheme 1.8.1.7 Binding of ATP to a cryptand to accelerate the degradation of ATP to ADP.

At pH 7.5 in the presence of an equivalent of the macrocyclic substrate the rate of hydrolysis was 7.9 x 10^4 min^{-1}. In the absence of the host at pH 7.7, the rate constant fell to 2.6 x 10^2 min^{-1}. Although AB reactivity is initially implied, the phosphoramidate **68** is cleaved *in situ* to regenerate the free host **66**, enabling turnover and rendering the reaction truly catalytic. Assuming initial nucleophilic substitution is rate determining and not subsequent hydrolysis provides a value of $k_{cat}/k_{uncat} \approx 300$. Unfortunately the authors fail to conduct the reaction with lower stoichiometries and as a result fail to confirm the catalytic mechanism proposed.

1.8.2 Bisubstrate Reaction Templates

We have previously established that intramolecular reactions are faster than bimolecular reactions. If a bimolecular reaction process can be rendered pseudointramolecular by non-covalent bonding, it has been shown that the reaction process would be accelerated. If a three component system is employed to accelerate a bimolecular reaction, this process can be termed "templating" as the product formed is complimentary to the starting material and is effectively a "negative image". This process is represented by a schematic diagram in **Figure 1.8.2.1.**

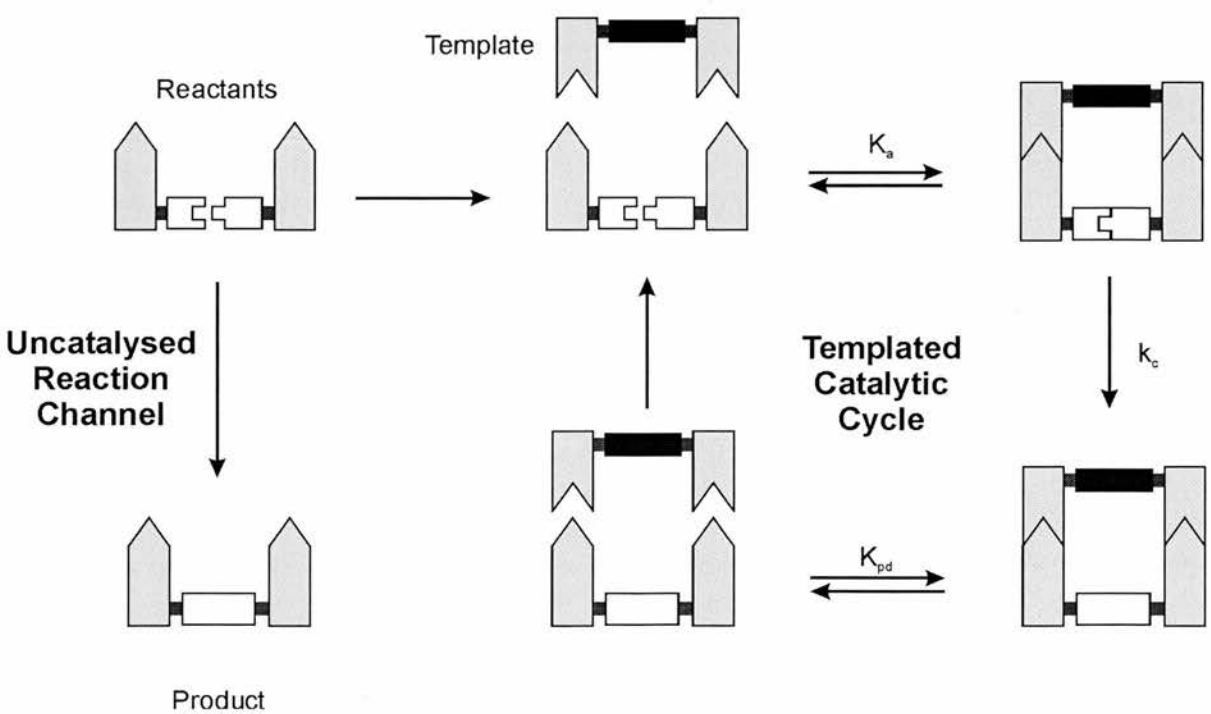

Figure 1.8.2.1 Schematic diagram representing a templated process rendering a bimolecular reaction pseudointramolecular. The grey shapes represent the recognition motifs, the black represents the spacer on the template and the white blocks represent the reaction components and product. K_a represents the association constants to form the ternary complex, kc is the catalysed rate constant and K_{pd} is the dissociation constant of the product template complex.

Simple reaction templates have been used to catalyse polar reactions[93] for example Kelly and co-workers bisubstrate reaction template.[94] Templates require temporary binding of ground state substrates and resulting reaction followed by dissociation of reactants.

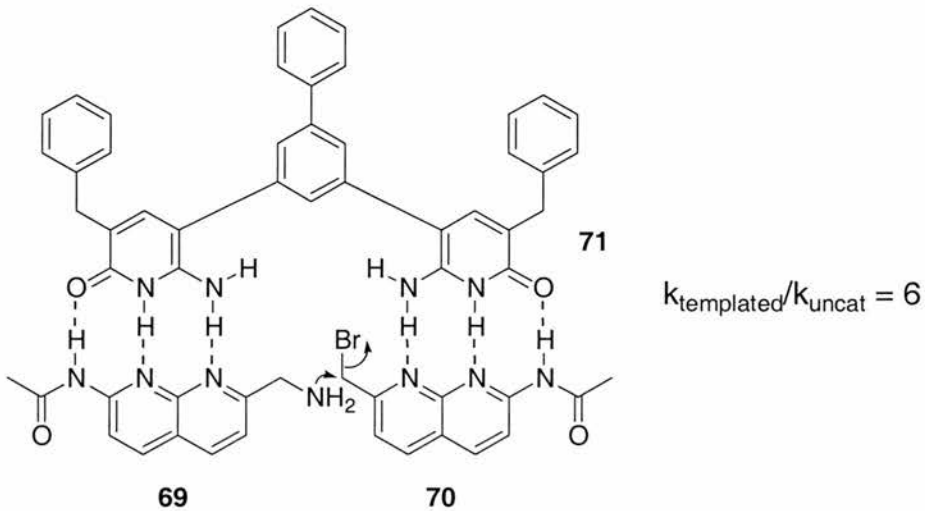

Figure 1.8.2.2 A bisubstrate reaction template catalysing a pseudointramolecular S_N2 reaction. The catalyst is present in 100 mol%.

The bimolecular reaction is accelerated 6 fold despite strong binding ($K_a \approx 10^4\ M^{-1}$ for the binding of each substrate) and product inhibition is unlikely as a result of using one equivalent of host and the product precipitating as an HBr salt. The report of this templated reaction however, raises an interesting issue. Kelly *et al* acknowledge that their receptor fails to stabilise the transition state of the reaction but merely associates the reactants in close proximity for reaction to occur, this moves the entropic cost of the reactants meeting in solution to earlier in the reaction sequence.

The recognition sites in the reaction need not be identical, indeed this might be a non-ideal situation as the rate of exchange of the two starting materials will have to be significantly faster than the rate of reaction to avoid competitive inhibition. Kelly extended their existing system developing a receptor with non-identical recognition sites.[95] Although the rate of reaction was improved relative to the original system, the acceleration observed was only 24 fold relative to the background rate.

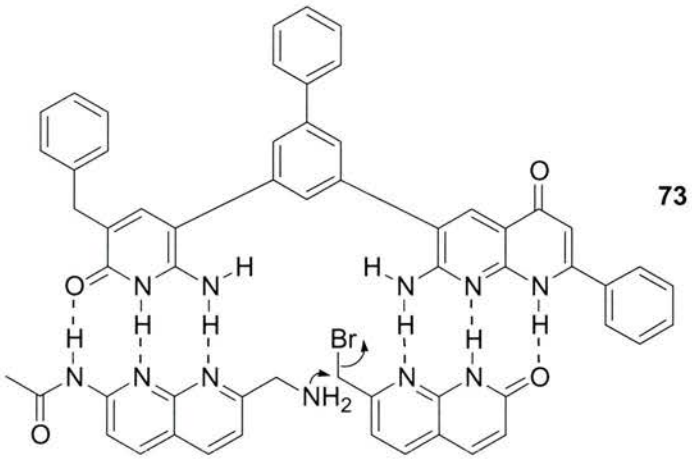

Figure 1.8.2.3 The adapted bisubstrate reaction template designed by Kelly and co-workers to prevent non-productive binding.

The aldol reaction has also been accelerated by the formation of sandwich complexes between a metal ion and crown ethers. Termed an ABC reaction where C represents a cofactor, the cofactor could also be considered to be a primitive template.[96]

Appending binding sites on to functional groups is also a method of binding and organising transition states. Mock et al have employed this in the catalysis of a [3+2] cycloaddition of an azide with an alkyne in the cavity of cucurbituril. Ammonium functionalities on the two reactants bind to the carbonyl oxygens making the reaction faster and more regiospecific.[97]

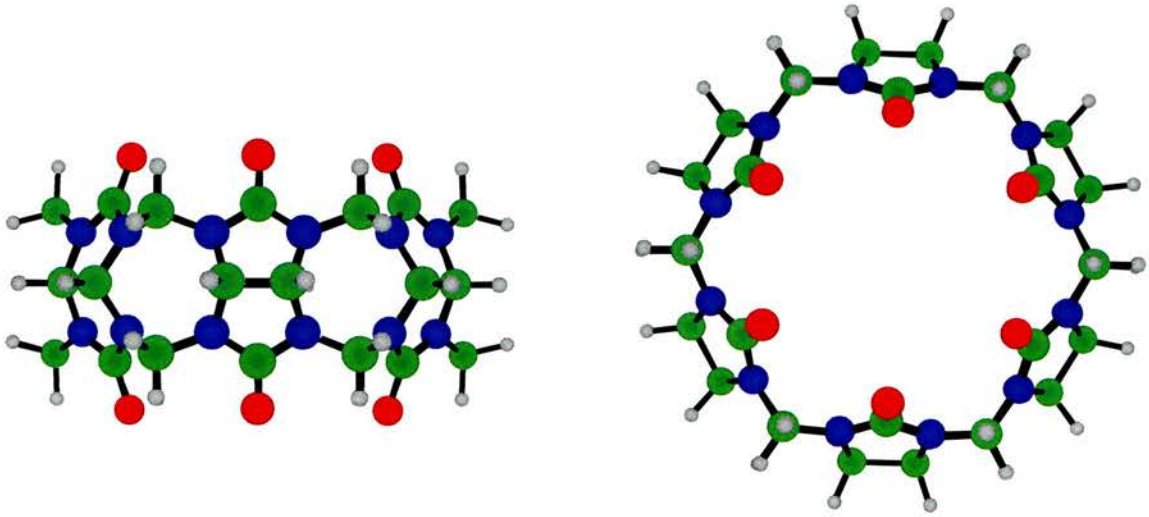

Figure 1.8.2.4 Ball and stick representation of the top-view and side-view of cucurbituril generated using Macromodel. Carbon is green, oxygen red; nitrogen blue and hydrogen atoms are white.

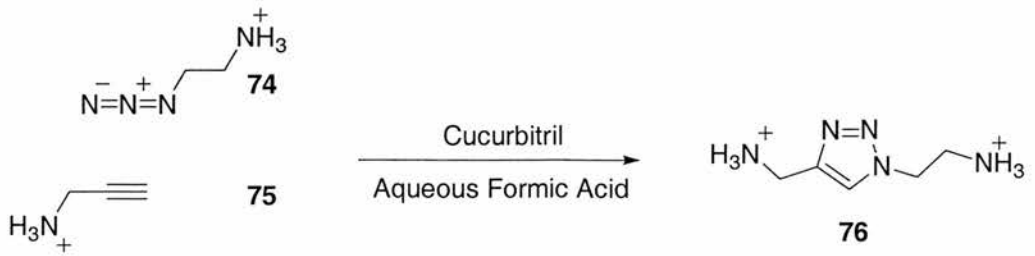

Scheme 1.8.2.5 Cucurbituril as a template for a [3+2] dipolar cycloaddition

A dipolar cycloaddition is catalysed by one equivalent of the cucurbituril host. Mock and co-workers suggest that acceleration is not only because of templating the reaction but also achieved by specific binding of the transition state. Unfortunately, they were unable to substantiate specific forces that are present in the transition state but absent in the substrate or product complexes. The rate data is also confusing, suggesting acceleration of 5.5×10^4 and 4.9×10^2 by different criteria.

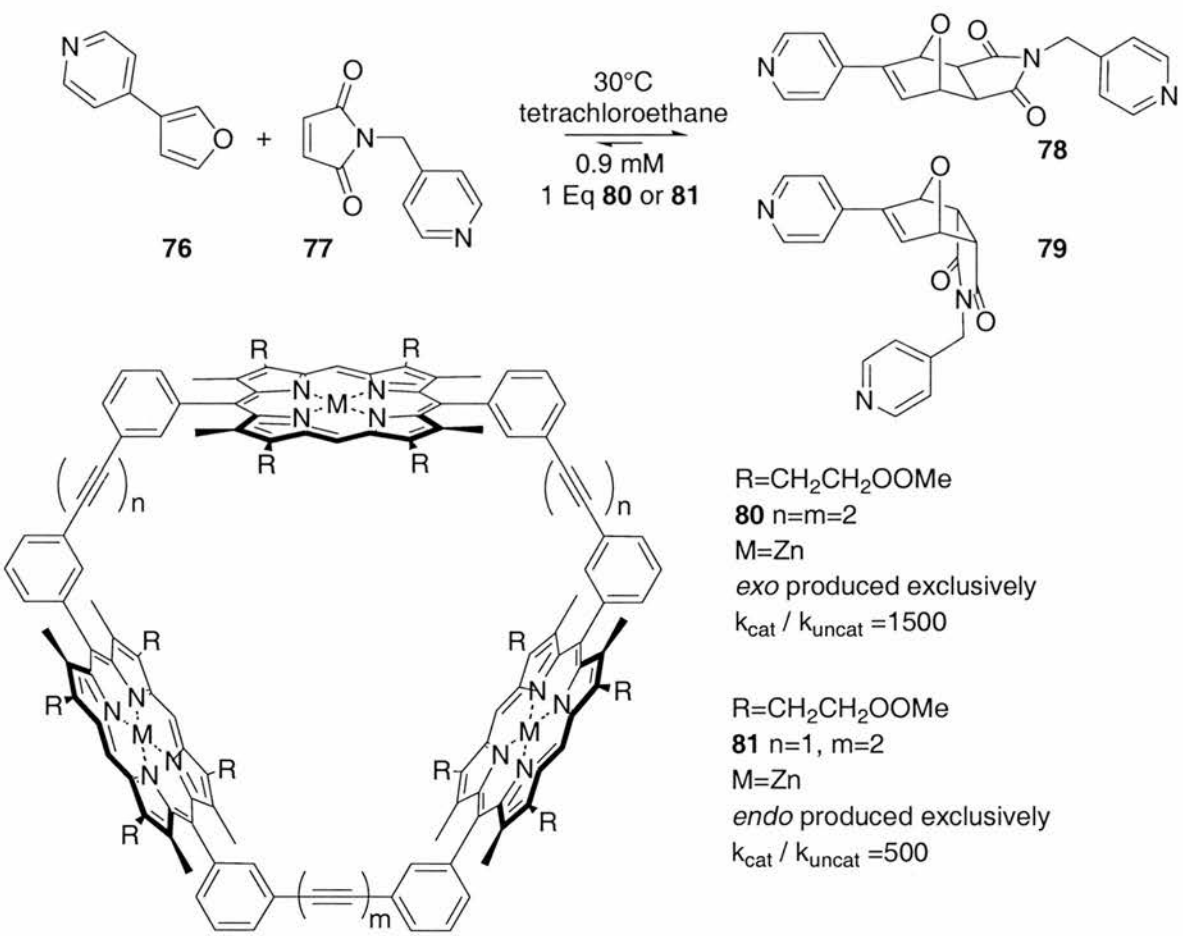

Scheme 1.8.2.6 Selected results from the Sanders porphyrin trimer data.

Templating a non-polar reaction has also been achieved by binding pyridyl functionalised diene and dieneophiles to the Sanders and co-workers porphyrin trimer has effected control and acceleration.[98]

The receptor **80** where n = m = 2 catalyses the formation of the *exo* cycloadduct exclusively. The second receptor, **81**, n = 1, m = 2 catalyses the *endo* cycloaddition exclusively. The rationalisation for the observed reactivity is shown pictorially in **Figure 1.8.2.7**.

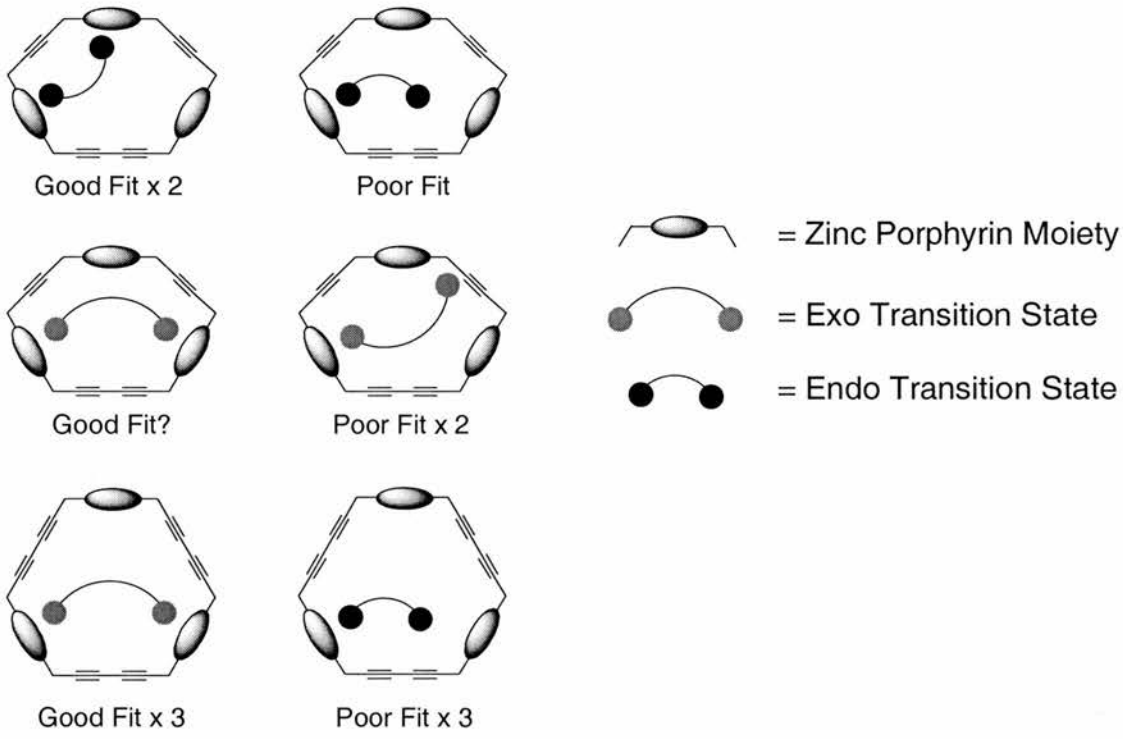

Figure 1.8.2.7 Rationalisation provided for the results observed for the catalysed Diels-Alder reaction between a functionalised furan and a functionalised maleimide

The results are rationalised as a series of good or bad "fits". The *exo* transition state is deemed long enough to form a two point binding interaction with two of the porphyrin rings in the **80** and can form three degenerate interactions. The *endo* transition state is assumed to only be able to reach the metal centres if spaced by one alkyne group. This results in two "good" *endo* binding interactions for the smaller cavity **81** and only one "good fit" for the *exo* transition states. Other than the one good fit observed for the *exo* transition state with the smaller cavity, all other associations would invoke severe steric hindrance and be deleterious to catalysis. From this, the explanation for the exclusive acceleration of the *endo* reaction was explained.

1.8.3 Self-Replication

A situation can be envisaged whereby the reaction template in **Figure 1.8.2.1** is the product of the reaction being catalysed, if this is the case, the reaction is termed to be "self-replicating". Careful design of the reactants results in the formation of another template molecule on reaction. A similar schematic diagram to the bisubstrate reaction template **Figure 1.8.2.1** can be invoked for this process, **Figure 1.8.3.1**, the difference is that, similar to a palindromic nucleic acid sequence, the "negative image" is identical to the template, so the template catalyses its own formation.

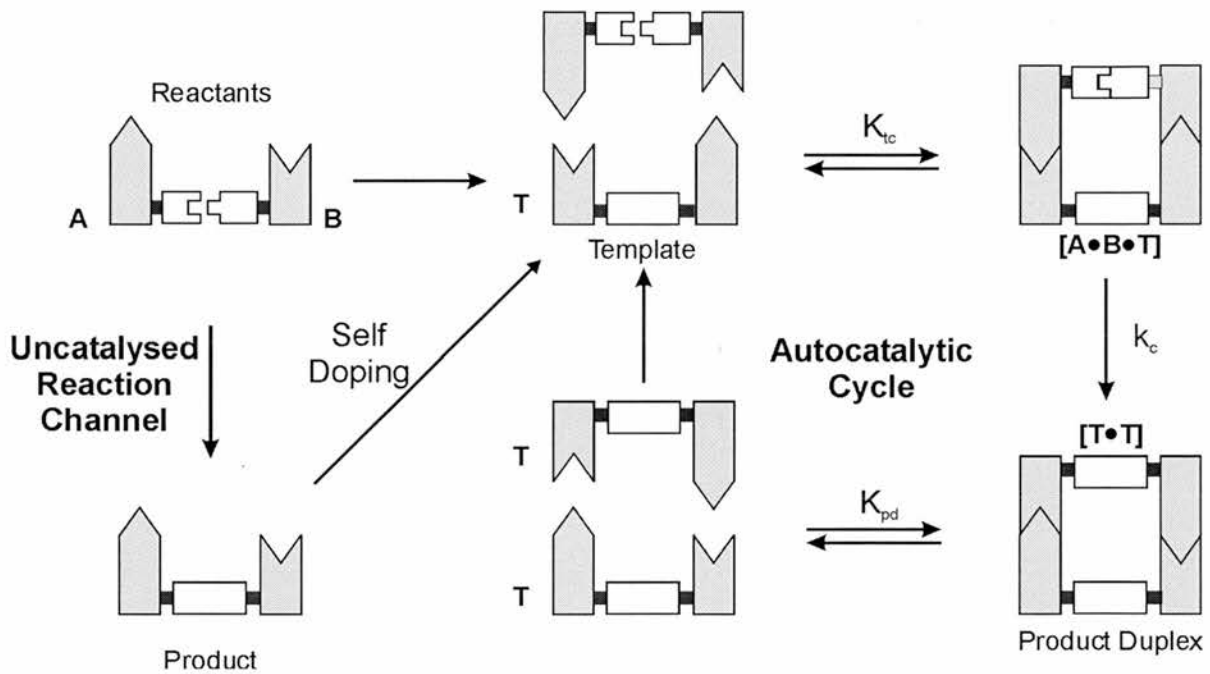

Figure 1.8.3.1 Model of a minimal self-replicating system. Reactants A and B initially react in a bimolecular fashion to afford template T which through non-covalent interactions catalyses its own formation. K_{tc} association constant for the ternary complex, k_c catalysed pseudointramolecular rate constant, K_{pd} dissociation constant for the duplex

Self-replication is often portrayed as a primitive precursor to life. Although non-enzyme replication may have played an important role in pre-biotic life forms, in chemical terms a self-replicating molecule possesses many similarities with a templated reaction. The only difference between a templated reaction and a self-replicating reaction is the template is added externally to the former. The elegance of not requiring reaction doping with preformed template is attractive from an intellectual perspective, indeed the slow bimolecular reaction performs a self-doping of the self-

replication reaction mixture before autocatalysis can proceed. This self-doping mechanism confirms self-replication as a class of templated reactions.

A strictly self-replicating system will result in the formation of a sigmoidal growth curve for the formation of the product template.

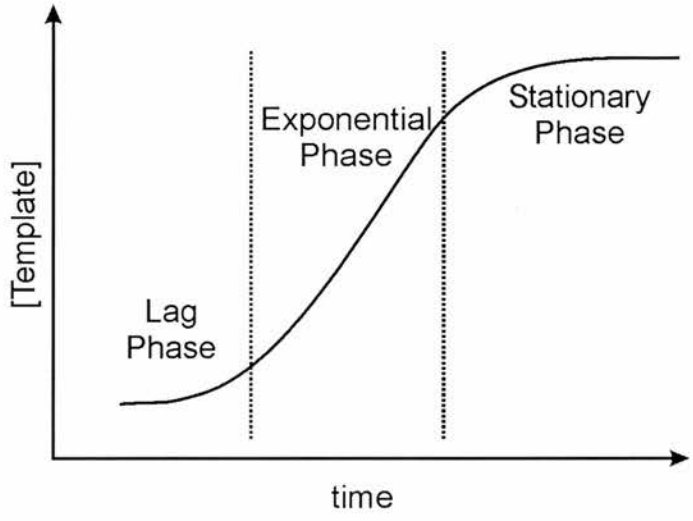

Figure 1.8.3.2 Graph indicating the expected sigmoidal curve for the appearance of template in a true self-replicating system.

Initially the rate of reaction is slow, the lag phase, as only a small quantity of the template is present in solution as formed by bimolecular reaction. Once a critical template concentration is reached, catalysis *via* the ternary complex **[A•B•T]** predominates. A final stationary phase is reached once reactant concentration has diminished.

An ideal self-replicating molecule is truly catalytic unlike AB reactions, however these systems have a tendency to exhibit product inhibition because of strong binding in the product duplex. Natural and synthetic examples of polar reactions that have been catalysed in this manner are known.[99,100]

Rebek and co-workers have used this methodology in amide formation templated by a Kemps triacid-based receptor.[101-105]

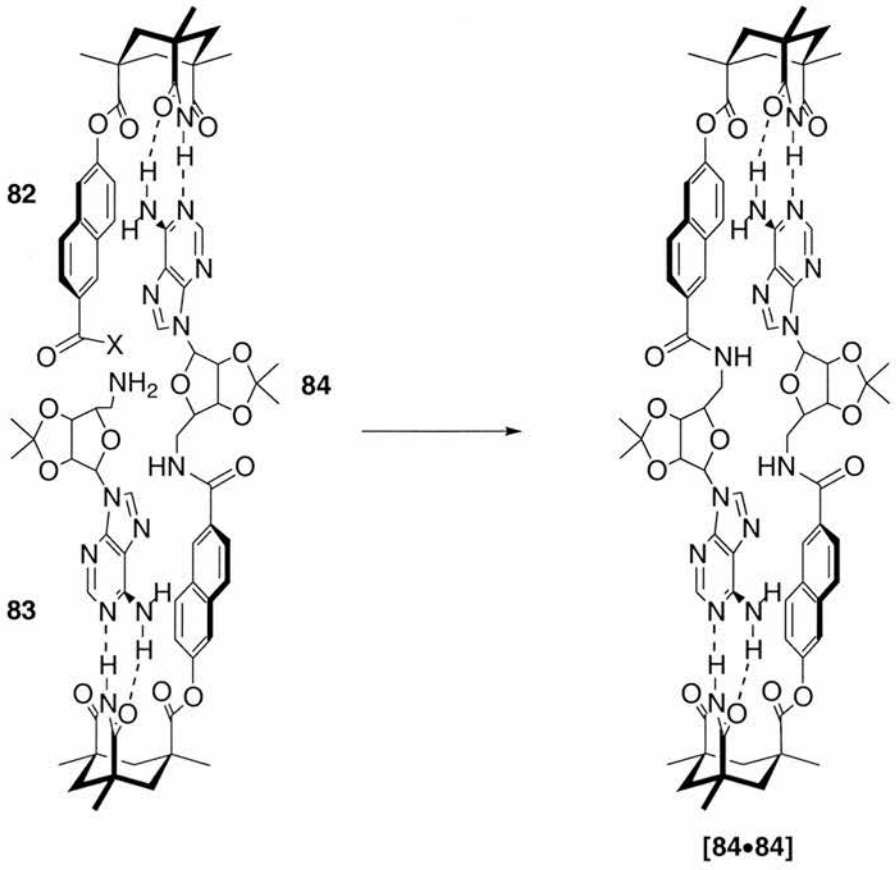

Scheme 1.8.3.3 The product templated pathway of reaction in the replication of an amide molecule *via* a hydrogen bonding assembly. The ternary complex **[82•83•84]** (X=OC_6F_5) reacts to form the product duplex **[84•84].**

Template **84** which was a modification of a previously synthesised more flexible system was shown to be produced in a sigmoidal manner, indicative of autocatalytic self-replication. The origin of the self replication was later disputed by Menger *et al,* who postulated that catalysis of the amide formation may have arisen by internal stabilisation of the tetrahedral intermediate.[106,107] Reinhoudt later proved that both of the suggested hypotheses contribute towards the rate acceleration but also AB reactivity is significant.[108] Rebek and co-workers however, continued their studies with further examples of molecules developed from their initial design.[109]

Imine formation has been catalysed by von Kiedrowski's receptor with guanidinium and carboxylate recognition motifs **87**. Charge reinforced hydrogen bonding holds the reactants **85** and **86** tightly in the appropriate reaction conformation, however, the product duplex, containing two hydrogen-bonded motifs is bound more strongly than the reactants leading to product inhibition. Self-replicators are frequently described as following a "Square Root Law" which takes account of strong duplex binding,

using this hypothesis a value of autocatalytic efficiency of $\varepsilon = 16.4 \pm 4.4 M^{-1/2}$ is observed.

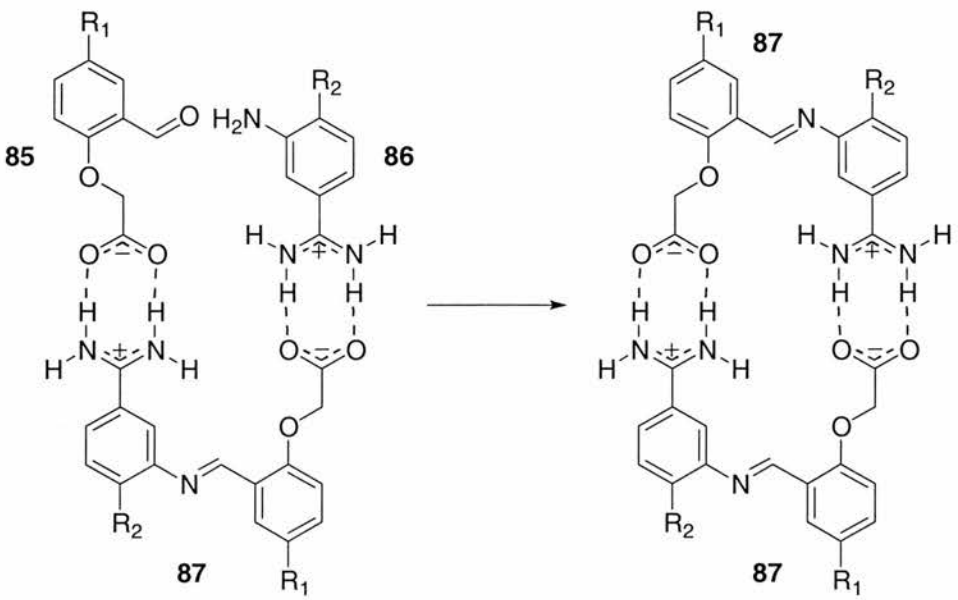

Scheme 1.8.3.4 Self-replication of an imine-based system. Strong product binding inhibits true autocatalysis.

Autocatalytic efficiency ε derives from a pair of equations as follows:

$$A + B + 0.5\,T \xrightarrow{k_1} 1.5T$$

$$A + B \xrightarrow{k_2} T$$

$$\varepsilon = \frac{k_1}{k_2}$$

Figure 1.8.3.5 The equations derived to describe the efficiency of autocatalysis.

Sutherland and Wang[110] reported a Diels-Alder self-replication system, which specifically generated the *endo* adduct. Importantly a sigmoidal curve was observed in this system. Importantly, on the addition of 5 and 10% of template, the lag period disappeared. Disappointingly, the authors fail to fully identify the template and the stereochemical assignment as *endo* is only "assumed". The diene also possesses a chiral centre so two possible diastereoisomeric *endo* products are possible, however, despite differentiation of the respective NMR resonances being possible, the authors state that the product "may consist of one or both of the two possible diastereoisomers".

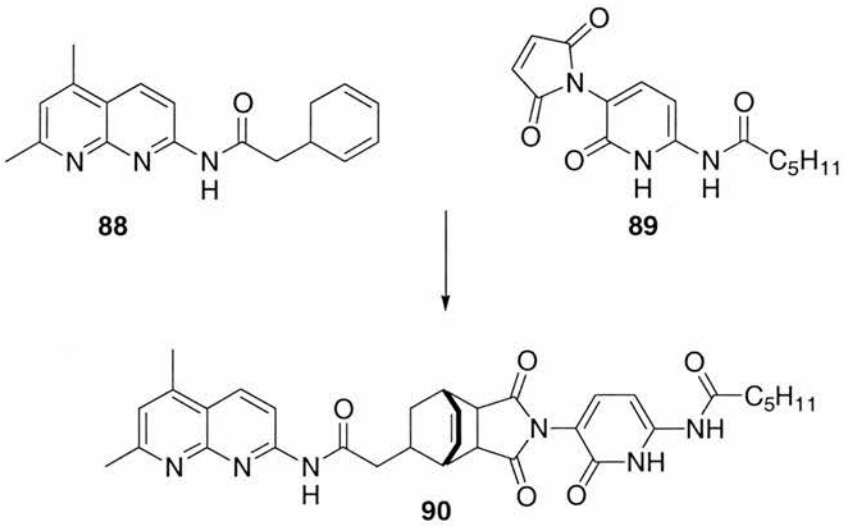

Scheme 1.8.3.6 Sutherland's self replicating system accelerating the Diels Alder reaction between **88** and **89**.

Philp and Allen[111] have developed the AB methodology further and transformed it into a self-replicating system with structural similarities to the systems developed by Philp and Bennes. The recognition motifs are identical, however, the orientation of the reacting species enables the self-replication pathway to dominate.

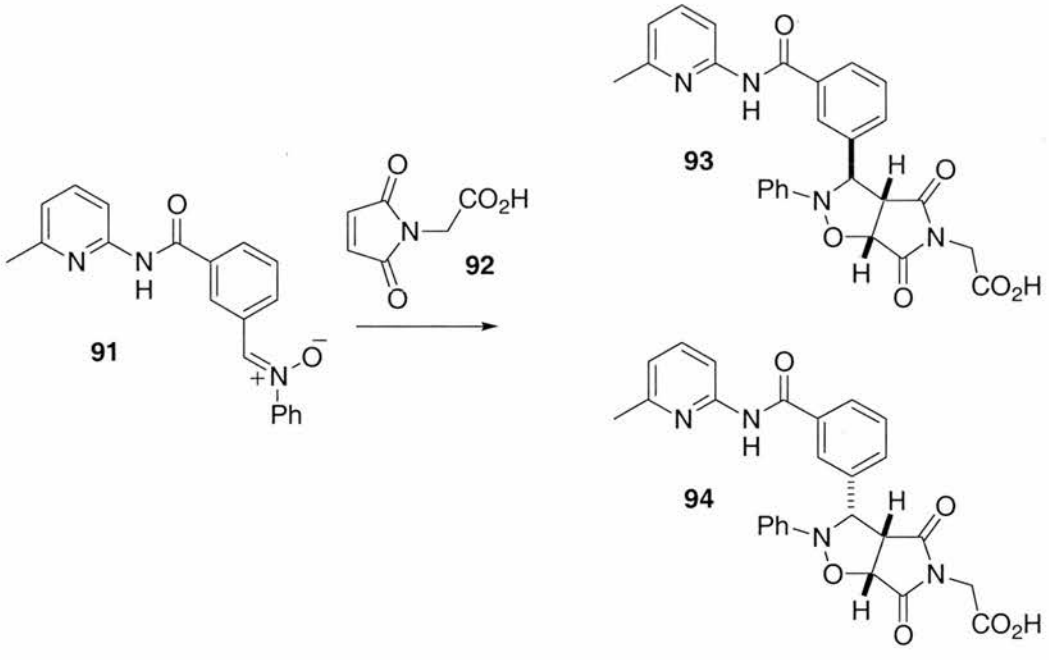

Scheme 1.8.3.7 Philp and Allen's self replicating system accelerating the [3+2] dipolar cycloaddition between a nitrone and a functionalised maleimide.

The system is selective for the *endo* stereoisomer **93**. The reaction is truly self-replicating as is indicated by the sigmoidal graph. A conformational change during

reaction results in unexpectedly low duplex association constants and hence, low levels of product inhibition.

The analogy of self-replication with the early development of life[112-114] may, however, be flawed. These arguments arise from comparison with DNA replication, which is rarely palindromic in natural systems. A strictly palindromic sequence would fail to allow adaptation to environmental conditions that would be deleterious to the organism as a whole. To allow a wide range of synthetic products, palindromic sequences would be unsatisfactory. Replication must also be capable of "making mistakes" to enable evolution.

Self-replication intuitively appears to reinforce early life hypotheses however, because if reaction completion against time is observed for a self-replicating system, a graph of the data will possess a particular sigmoidal shape reminiscent natural systems.[115] In an idealised logistic population growth curve, the initial lag phase arises because few mature members of a species are capable of reproduction, comparable with low template concentration. A population then undergoes exponential growth because of plentiful resources until limiting factors such as food or space cause the growth to stabilise. The population fluctuates around the upper limit termed the "carrying capacity". The similarities between population growth and self-replication are, however, an academic curiousity rather than evidence that self-replication performed a role in prebiotic chemistry.

1.8.4 Solvophobicity

Traditional hydrophobic receptors[116-118] were designed to bind polyaromatic hydrocarbons (PAHs). One of the series of receptor used was the family of cyclodextrins.[119-121]

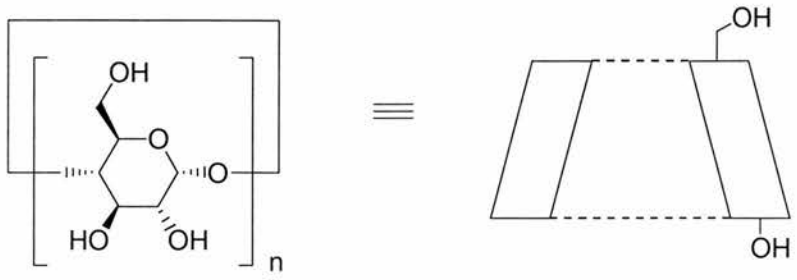

α-Cyclodextrin n=6 **95**
β-Cyclodextrin n=7 **96**
γ-Cyclodextrin n=8 **97**

Figure 1.8.4.1 Representations of cyclodextrins.

A non-polar guest that is poorly solvated in water is more suited to the non-polar environment in the cyclodextrin cavity. Binding of the non-polar guest into a cavity also releases highly organised poorly hydrogen bonded solvent (usually water) from the non-polar cavity by the non-polar guest. The release of solvent coupled with the removal of the poorly solvated guest from the bulk solution renders the process thermodynamically and entropically favourable.

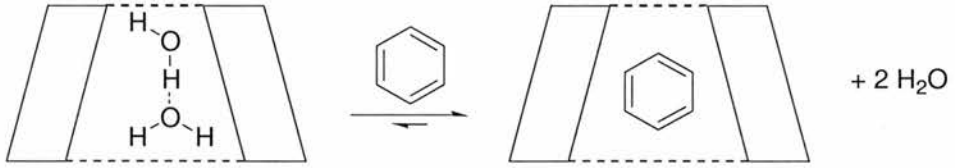

Figure 1.8.4.2 Binding of neutral non-polar molecules in a hydrophobic cavity by the release of "High Energy Water"

In the same way that ground state structures can be bound releasing "high energy water" from a cavity, binding of substrates, transition states or products of non-polar reactions can achieve the same result. β-Cyclodextrin **96** can catalyse a Diels-Alder reaction between cyclopentadiene **21** and acrylonitrile **98** by the displacement of water from the cavity on binding of the two substrates.[122,123] A functionalised β-cyclodextrin has also been shown to reverse the stereochemistry of a cycloaddition by hydrophobic binding of an aryl sidearm into the hydrophobic cavity.[124]

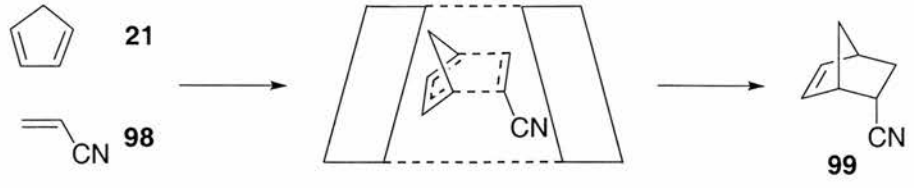

Scheme 1.8.4.3 Cyclodextrin catalysis of a Diels-Alder reaction

When amphiphiles are added to water, organised structures can result to minimise the deleterious interactions between the amphiphile and the bulk solvent. Highly fluid elliptical or rod like structures called micelles can form as shown in **Figure 1.8.4.4**. In this way, the system can maximise the hydrophilic interactions with water and maximise the lipid – lipid interactions.

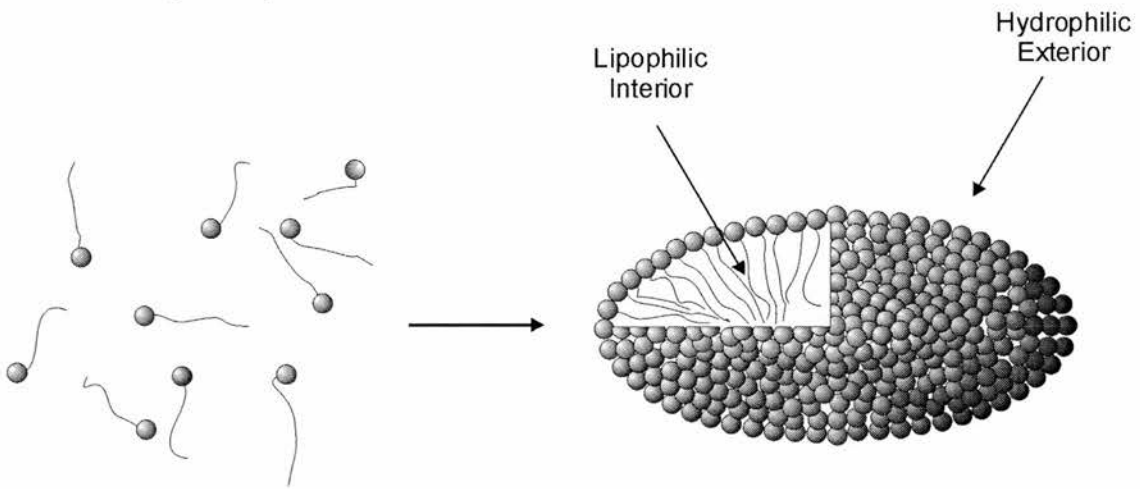

Figure 1.8.4.4 Representation of the formation of an elliptical micelle. The interior of the cell is a more lipophilic environment than the exterior.

Micellar catalysis can be seen as an extension to this hydrophobic cavity theory. Catalysis is as a result of bringing together the reacting species in a micellar phase that has very different properties to bulk solvent. For example, reactions between non-polar molecules could be accelerated by the incorporation into a non-polar surfactant micelle.

A 1939 patent reports the use of detergents as a method of increasing yields in Diels Alder reactions.[125] Braun and co-workers[126] also observed this phenomenon in the cycloaddition between cyclopentadiene and an allylic ester. In dioxane, the reaction proceeded slowly and with low product specificity. In a solution containing sodium dodecylsulfate, the reaction was accelerated by in excess of a hundred fold and the product specificity was improved.

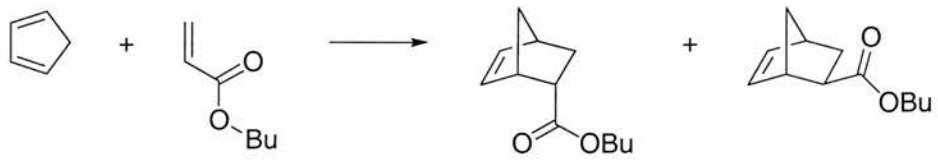

21 **100** **101** **102**

Dioxane	75.1	:	24.9
With SDS	89.9	:	10.1

Scheme 1.8.4.5 In the presence of SDS (sodium dodecylsulfate) the Diels Alder reaction between cyclopentadiene and ester **100** is accelerated and made more diastereoselective.

Alongside reaction acceleration, a modest but significant increase in *endo* product from approximately 3:1 to 9:1 is observed.

Interestingly Grieco *et al* observed[127] that acceleration is observed for Diels Alder reactions performed in water without the presence of a surfactant. The authors still term this effect "Micellar Catalysis" as it is assumed that unreacted starting materials and product aggregate to form micellar structures in solution, as product ratio was heavily dependent on concentration. Breslow and co-workers[128] made comparisons between solutions containing surfactant and purely aqueous solutions of diene and dienophile and observed that there was no rate or selectivity advantage to be gained by including surfactant molecules into the aqueous reaction mixture. This is not to dispute the action of surfactants in accelerating the Diels Alder reaction. Indeed the mode of acceleration in water by either technique is assumed to arise by aggregation to minimise contact between bulk solvent and hydrophobic stating materials and products.

Micellar catalysis is an interesting phenomenon because a common misconception when discussing enzyme catalysis is that enzymes catalyse aqueous reactions. The active site microenvironment of a given enzyme may possess different conditions to the bulk cytoplasm. In the same manner, micelles, create a different microenvironment for reactions.

1.8.5 Transition State Stabilisation and Polarisation

In 1948, Linus Pauling proposed the origin of enzyme catalysis.[54]

"I think that enzymes are molecules that are complementary to the activated complexes that they catalyse...The attraction of the enzyme molecule for the activated complex would thus lead to a decrease in its energy, and hence to a decrease in the energy of activation of the reaction, and an increase in rate of the reaction."

Pauling arrived at this conclusion with little hard evidence to support his theory. Since this statement, acceleration by non-covalent bond mediated catalysts has been developed to exploit this property. In this way, the charged nature of the polar reaction has sometimes been used as a means of binding and stabilising the transition state in supramolecular catalysis.

Molecular clefts and receptors synthesised by Moran and co-workers[129] have been shown to accelerate Michael Addition reactions for example a guanidinium receptor **103** that exploits charge reinforced hydrogen bonding between the receptor and the intermediate.

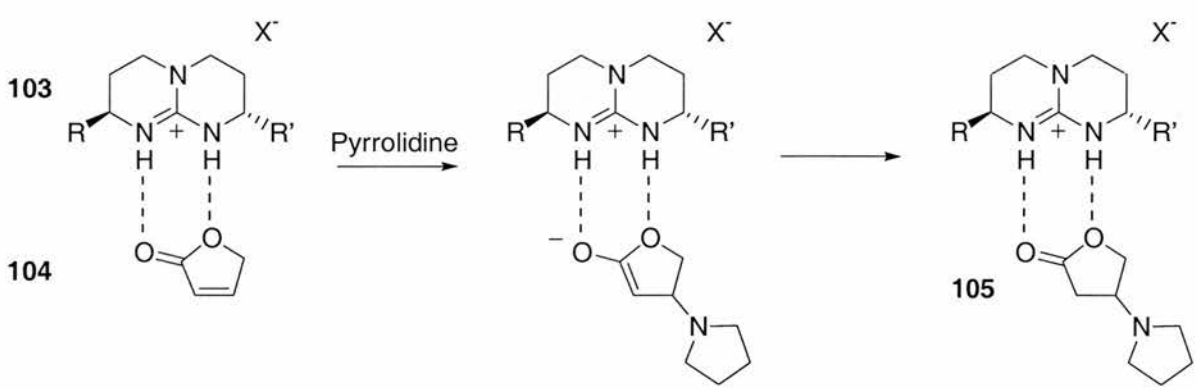

Scheme1.8.5.1 Guanidinium receptor to catalyse Michael Addition to unsaturated lactones

Addition of a nucleophile in the 4 position results in an enolate-like intermediate, which is protonated resulting in a non-charged Michael Adduct. In this manner, binding energies to the substrate and product were minimised while maximising the association with the high energy charged species. Product inhibition was minimised and catalytic efficiency maximised. Unfortunately no further kinetic data wer supplied to study the catalysis further.

Charge stabilisation has also been utilised in a Michael Addition reaction in a molecular cleft binding furanone.[130]

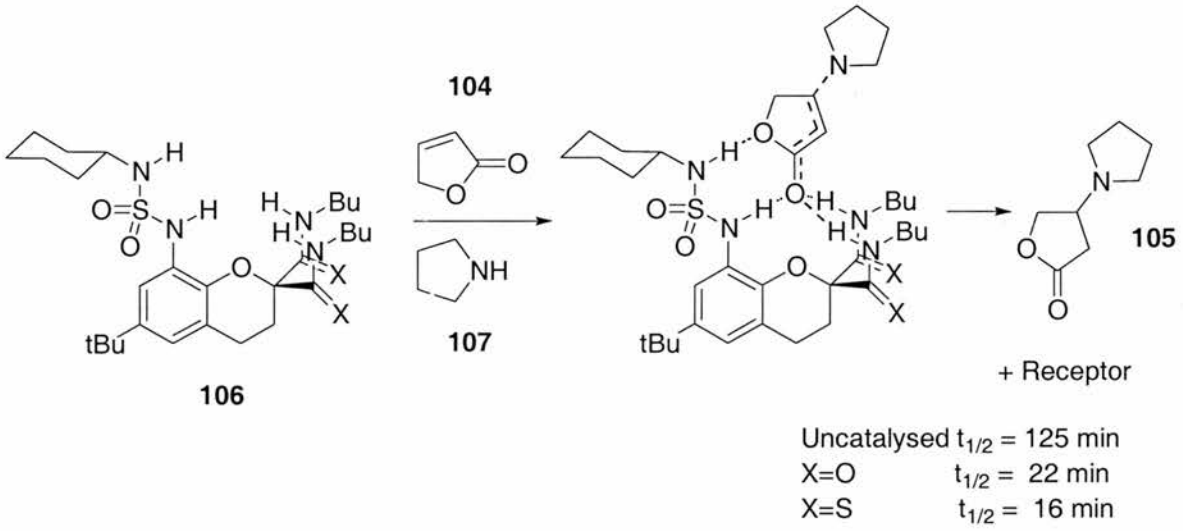

Scheme 1.8.5.2 Molecular cleft catalysis of a conjugate addition

As previously, the enolate-like intermediate is bound by the cleft and the transition state is stabilised as a result. Addition of 0.1 equivalent of the amide and thioamide receptors in deuterated benzene resulted in the half-life of the reaction falling from 125 minutes to 22 and 16 minutes respectively. Again, no further kinetic data were provided by the authors making more detailed analysis impossible. This design was developed further by the authors forming new receptors capable of performing a similar transformation.[131,132] and a decarboxylation [133]

Phosphorylations of alcohols have also been catalysed by transition state stablisation. Prepared alongside a pseudocatalytic AB complex, Muche and Gobel[134] discovered that a simple cationic host lacking the alcohol nucleophile accelerated a bimolecular phosphorylation reaction by a factor of 5000 even though the reaction was still intermolecular.

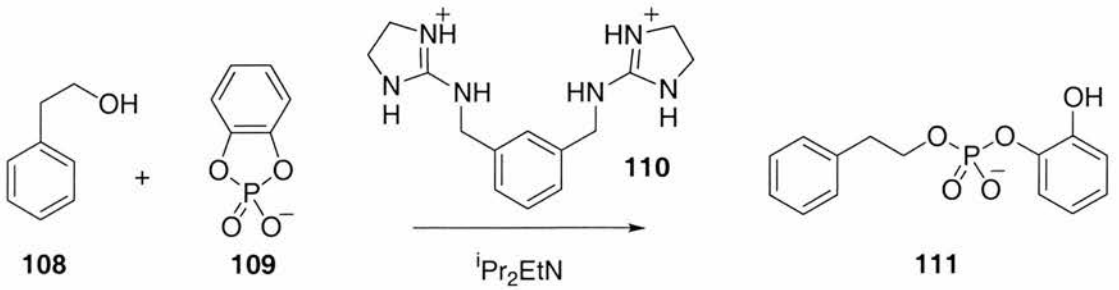

Scheme 1.8.5.3 Acceleration of a phosphorylation reaction by stabilisation of transition state charge.

The authors found that the receptor bound to the transition state anion 21 kJmol^{-1} more strongly that the ground state anion as a result of the increase in negative charge on the phosphate group during the nucleophilic addition and the resulting strong charge reinforced hydrogen bonding. The corresponding AB receptor possessing an alcohol functionality positioned between the two recognition sites displays a corrected rate acceleration of 380000 relative to the uncatalysed bimolecular rate. Although impressive, it is important to note that this value only represents a 76-fold increase on the bimolecular rate catalysed by the bis(guanidinium) receptor **110** indicating transition state binding in this example was much more important to catalysis than intramolecularity.

Jubian and co-workers used a similar receptor[135] to catalyse the intramolecular nucleophilic addition of an alcohol onto a phosphate. It is significant that any catalysis can only arise from stabilisation of the transition state, as the reaction is intramolecular in both cases.

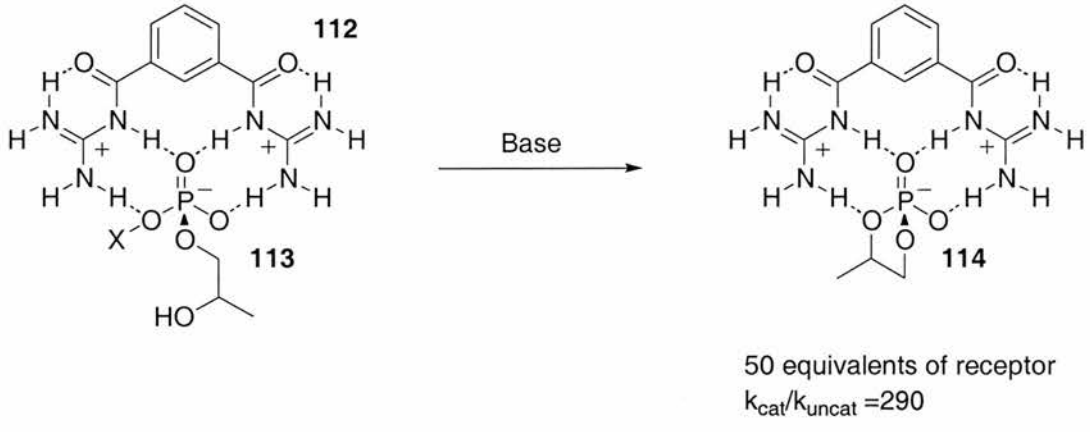

Scheme 1.8.5.4 Acceleration of an intramolecular addition of an alcohol to a phosphate.

Rate enhancements of 700 fold are observed but on investigation of the data, this rate acceleration is only achieved in the presence of 300 equivalents of receptor in acetonitrile solvent. Although acetonitrile is a polar reaction medium, it would be expected that catalysis should be observed with lower stoichiometries of the receptor. The host is highly preorganised to the guest possessing only two freely rotateable bonds and binds the ground state using charge-reinforced hydrogen bonding. On progression along the reaction co-ordinate to the transition state, the negative charge on the phosphate would be increased so reporting "catalysis" in the presence of 300 equivalents of receptor appears to be unsound.

The aminolysis of 6-chloropurine **116** has been investigated by Tominaga and co-workers[136]; the results found lend credence to Pauling's theory on catalysis. Tominaga observed that 1-hexadecyluracil **115** accelerated the aminolysis by a factor of 11.7 (see **Figure 1.8.5.5**).

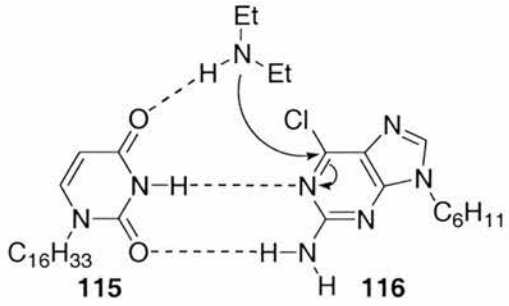

$k_{obs}/k_{uncat} = 11.7$

Scheme 1.8.5.5 Aminolysis of 6-chloropurine as catalysed by 1-hexadecyluracil

Rankin and co-workers[137] have extended the investigation using computational methods to the structurally analogous 6-chloropyrimidine systems. Binding functional groups to the pyrimidine was found to significantly lower the barrier to aminolysis, specifically binding of proton acceptors to the incoming amine.

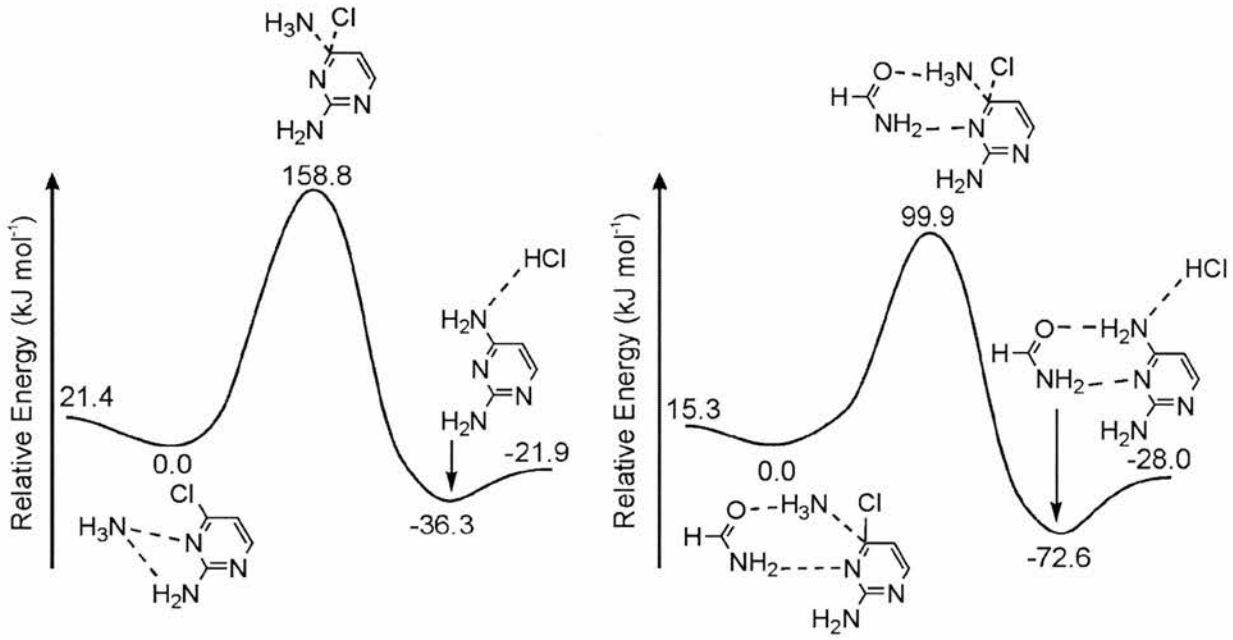

Figure 1.8.5.6 Schematic representation of the aminolysis of 6-chloropyrimidine in the absence and presence of an amide.

The computational calculations confirm the lowering of the transition state by the two point binding to an amide. This suggests that hydrogen bonding to the attacking amine in the transition state assists in the stabilisation of charge and hence, accelerates the reaction.

Exploiting transition state charge has also been used to change the regioselectivity of a reaction. Calcagno and co-workers[138] have shown that an unselective addition reaction can be made more selective by the addition of a bis(phosphine oxide).

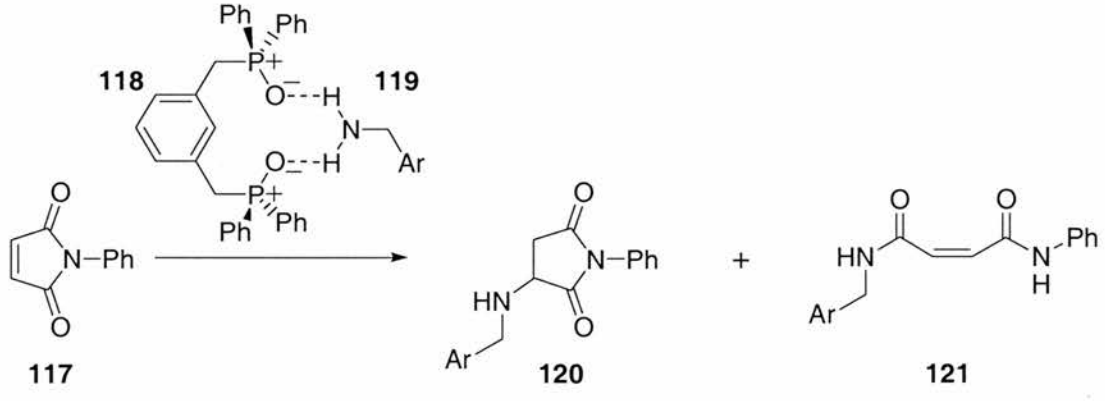

117 120 121

Scheme 1.8.5.7 The Conjugate and Direct additions catalysed by receptor **118**. Ar = 4-fluorophenyl.

If product formation is observed, it can be seen that the receptor not only catalyses the reaction but induces some product selectivity.

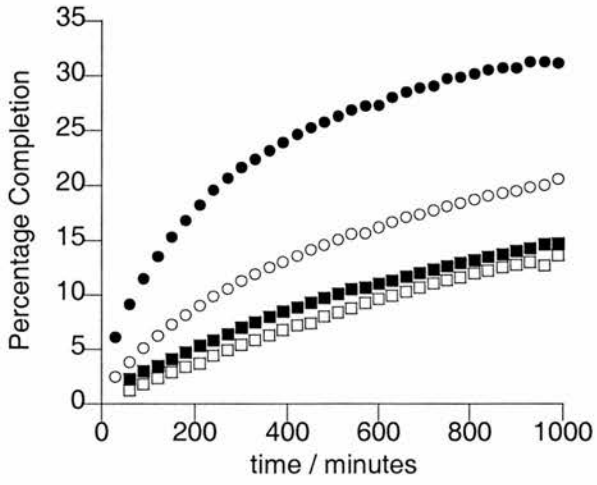

Figure 1.8.5.8 The Conjugate and Direct addition reactions catalysed by receptor **118**. The closed shapes represent the direct addition product; the open shapes represent the conjugate addition product. The squares are the uncatalysed reaction; the circles represent the catalysed reaction.

Both conjugate and direct addition are catalysed by the receptor, however, from the **Figure 1.8.5.8** it is apparent that the receptor catalyses the direct addition more readily than the conjugate addition. The ratio of products after 1000 minutes changes from approximately 1:1 to 3:2 in favour of the direct addition. In **Figure 1.2.6**, it was observed that reaction polarity is a sliding scale. Not only does direct addition possess more polarised transition states but also the carbonyl of a maleimide is a hard electrophile and binding of the amine to receptor **118** renders the amine a harder nucleophile. As mentioned in **Section 1.2**, hard electrophiles react with hard nucleophiles and soft nucleophiles react with soft electrophiles. This tendency may also lie at the cause for the differentiation by receptor **118** between direct and conjugate addition.

Kelly and co-workers[139] adopted a more novel approach to catalyst design in the phenolic receptor for enones. The action of the receptor is more analogous to Lewis acid catalysis of cycloadditions.

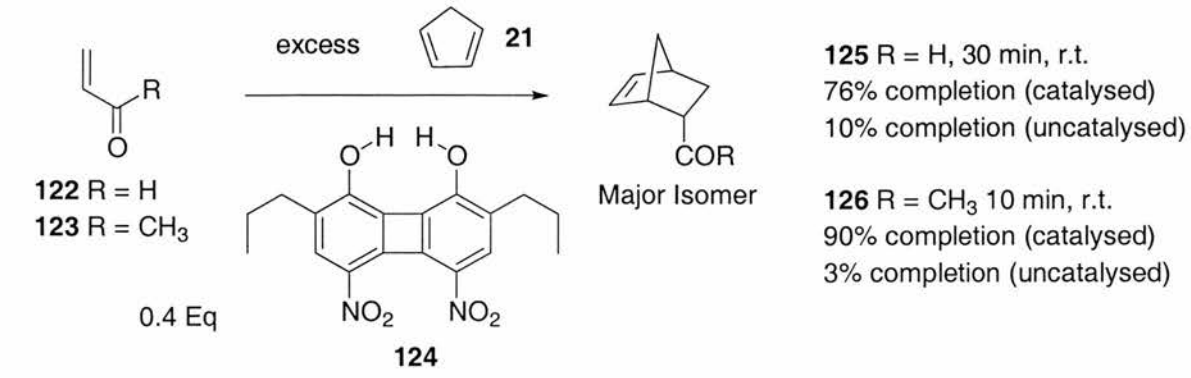

Scheme 1.8.5.10 Selected results from the Kelly receptor.

Binding of the Kelly receptor to an enone results in removal of electron density from the conjugated system and hence, lowering of the LUMO of the dienophile. The altering of the electronic distribution in a complex by hydrogen bonding has been termed "polarisation" and can also be observed in crystal structures.[140]

Amidinium salts have been used in a similar manner to catalyse the formation of Diels-Alder products. Schuster and co-workers have utilised this in two different systems to synthesise molecules with a steroidal four-ring backbone.[141]

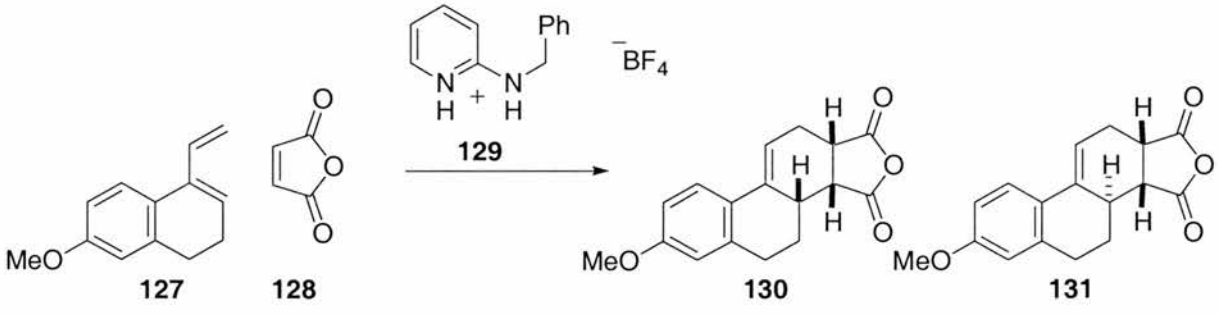

Scheme 1.8.5.11 Catalysis of a Diels-Alder reaction by an amidinium salt.

The reaction was accelerated by 2.6 times in the presence of one equivalent of the amidinium salt rising to 3.9-fold with two equivalents. Interestingly, just as Lewis acid catalysis can enhance selectivity, the ratio of **130:131** increased from 6:1 in the uncatalysed case to 17:1 in the presence of 2 equivalents of the salt although this only represents an 8% increase in specificity.

The research was extended to a diketone substrate **132**, which had a measurable association constant with the amidinium salt of 70 M^{-1}.

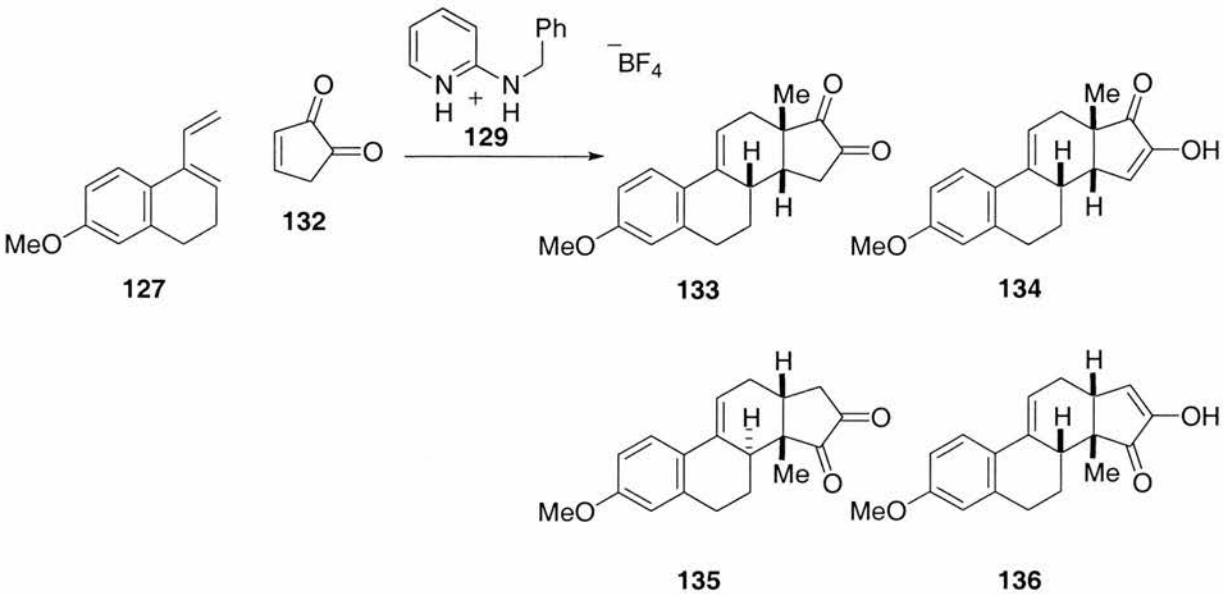

Scheme 1.8.5.12 Catalysis of a Diels-Alder reaction with a diketone dienophile.

The Diels-Alder reaction is complicated by the existence of constitutional isomers and the slow reaction to form enol tautomers. The cycloaddition was however, accelerated 125 fold by the addition of 0.25 equivalents of catalyst providing a 3.5:1 ratio of products in favour of the **134**.

1.9 Aims and Objectives

The demand for non-polar reactivity has been established by displaying its use *in vitro* and illustrating that non-polar catalysis is rare and inefficient *in vivo* and in catalytic antibodies. On reviewing catalysis by non-covalently bonded systems, few patterns emerge. Polar and non-polar catalysis have been used in a wide variety on receptors with few clear trends apparent in the results achieved. Indeed in the case of the non-polar self-replicator based upon a [3+2] dipolar cycloaddition, autocatalysis is more efficient than has been observed in polar systems.

The difficulty inherent on reviewing the data to date is that no research has been performed on utilising the same receptor and the same substrate across classes of reaction.

On considering the biological data, we hypothesise that the main contributing factor to the problems associated with catalysing non-polar reactions may be the lack of charge in the transition state and the associated reduction in association constant on

binding, which extending to Pauling's theory would lead to a reduction in efficiency. To prove this hypothesis it is necessary to investigate catalysis as observed in simple, well-understood systems. This will be investigated by subjecting substrates to polar and non-polar reactions in the presence and absence of broad-spectrum hydrogen bonded catalysts.

1.10 Design of Suitable Guests and Reactions

Receptor design has to take into account the reactivity we intend to investigate. It was decided that for each host under investigation the guest should remain the same to enable accurate comparisons to be drawn. An enone-based substrate was deemed a suitable substrate for broad-spectrum reactivity, as several reaction paths are possible. The four we will investigate in further detail are a Diels-Alder Reaction, a dipolar cycloaddition, direct nucleophilic addition and a Michael addition.

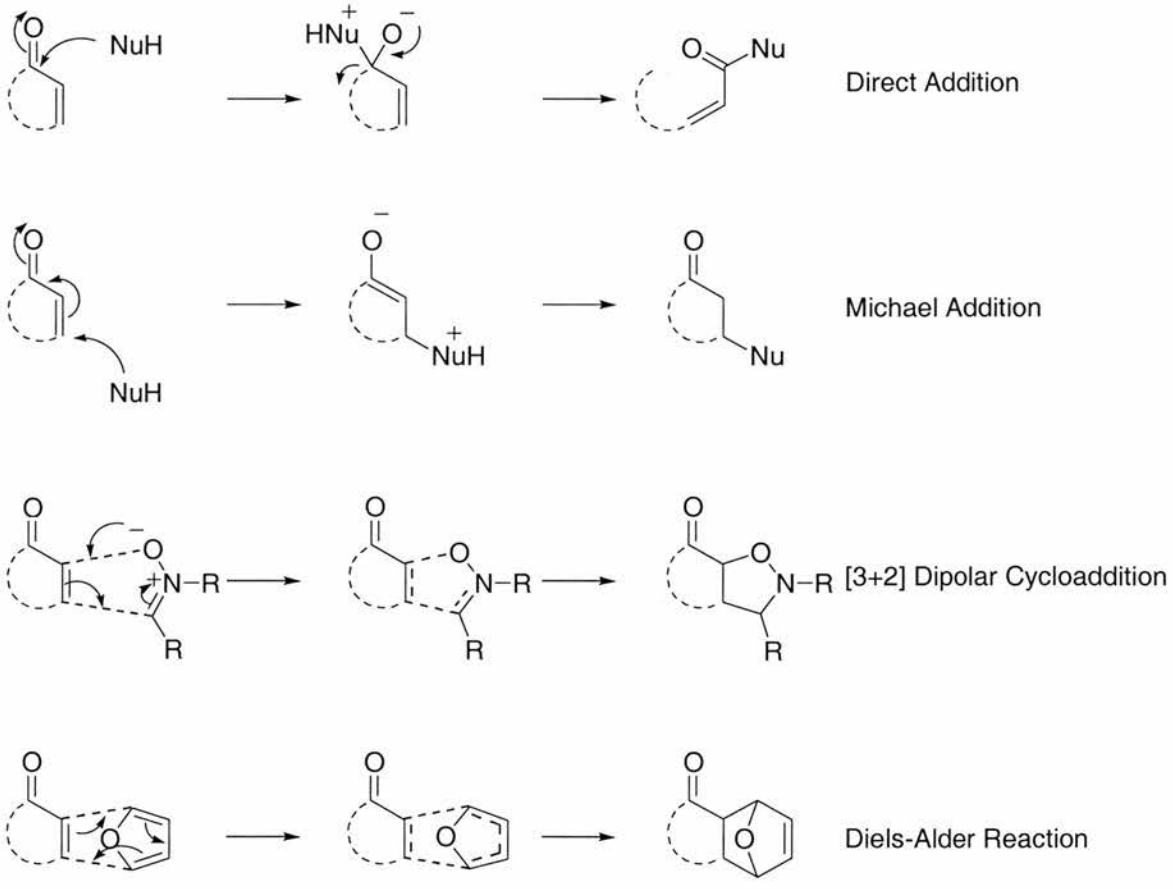

Figure 1.10.1 The proposed reactions to be investigated

The structure of the enone provides a potential site for binding to the receptor and the conjugation to the π system provides communication to the site of reaction. In

this manner, it is suggested that it will enable comparisons to be drawn between polar and non-polar reactivity.

The ultimate aim of our research is to explain the tendency of enzymes to catalyse polar reactions by investigating a series of synthetic receptors. Ideally, the objective is to not only reach qualitative conclusions but also attempt a quantitative summary of the polarity of reactions related to catalysis.

If we consider reaction polarity related to the level of catalysis we can imagine several potential relations between the two sets of data. Considering the reactions in **Figure 1.10.1**, they are listed in order of decreasing transition state polarity. If these transition states are represented numerically and plotted against a term reflecting the rate increase on addition of a catalyst, for example k_{cat}/k_{uncat}, it would be interesting to observe the mathematical relationship between the two sets of data.

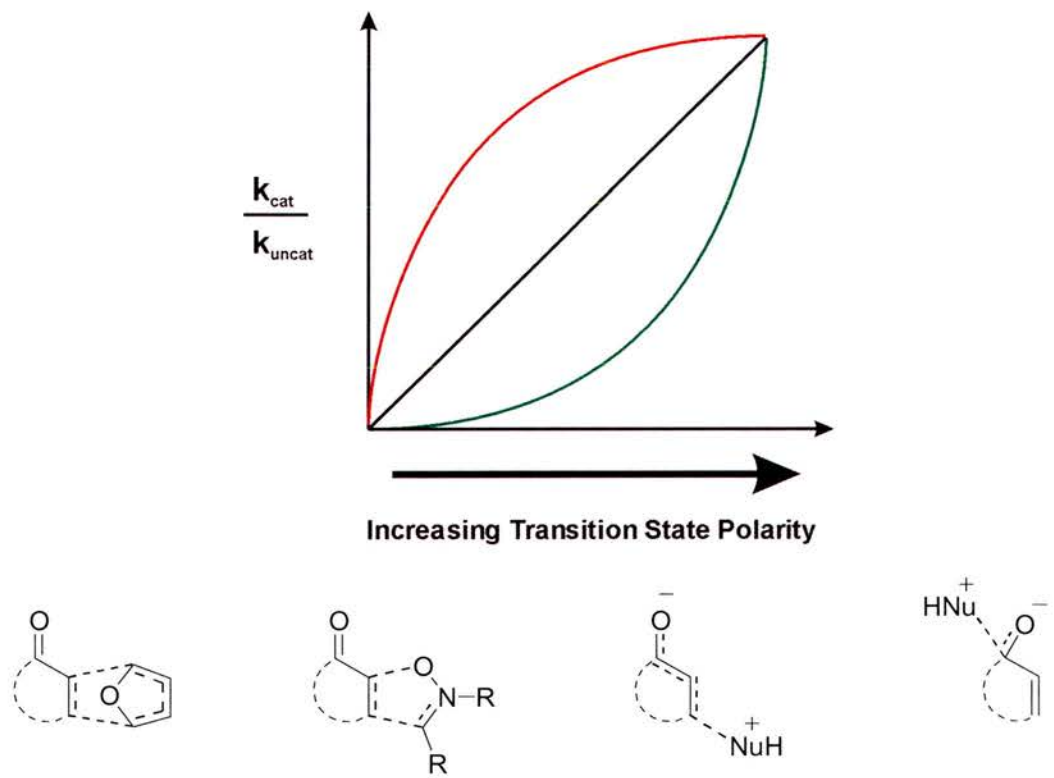

Figure 1.10.2 A graph to predict three potential associations between transition state polarity and kcat/kuncat.

If, as we expect, there is a function relating transition state charge and reaction acceleration for a given receptor, three extreme cases could be imagined (**Figure 1.10.2**). The catalysis may be directly proportional to transition state charge so an increase in charge relates to a proportional increase in catalysis (solid line). The

correlation between the data may be more similar to the dashed line, where a small increase in charge would result in a disproportionately large increase in catalysis. The third possibility is represented by the dotted line where a large charge increase would be needed for the rate to increase by any significant amount.

Different receptors and catalysts could eventually be compared using this method to investigate whether any trends present are universal. If this is the case, it would not only contribute to our understanding of enzyme catalysis but may also assist with synthetic catalyst design in the future.

2. Acceleration by a Simple Receptor

2.1 Designing a Receptor to Bind an Enone

In **Section 1.8**, it was hypothesised that polar reactions[129-138] are more readily catalysed than non-polar reactions by hydrogen-bonded receptors.[140,141] The existence of only a few examples of enzymes confirmed to catalyse non-polar pericyclic reactions may be analogous to the difficulty in catalysing similar reactions *in vitro* with solely hydrogen bonded systems. We also observed that there are no examples to date of hydrogen-bond mediated, broad-spectrum catalysts. Our aims were to develop these catalysts to accelerate different types of reactions and to use them to investigate our hypotheses concerning enzymic processes. To achieve these aims, we designed a simple system to catalyse reactions with a wide range of transition state polarity. It was considered desirable to synthesise a simple receptor initially as comparisons between reaction accelerations was sought rather than individually impressive rate enhancements.

It was decided to develop a receptor substrate complex that could be represented schematically in **Figure 2.1.1**. The receptor **R** and guest **G** should possess complimentary recognition sites. Binding the guest, **G** to the receptor should then effect a change in the electronics in the bound substrate, withdrawing electron density; this is termed "Ground State Polarisation". On reaction of the guest, the transition state should be bound tightly by the receptor leading to "Transition State Stabilisation". The resulting receptor product complex **[R•P]** can then dissociate to regenerate the receptor and the free product.

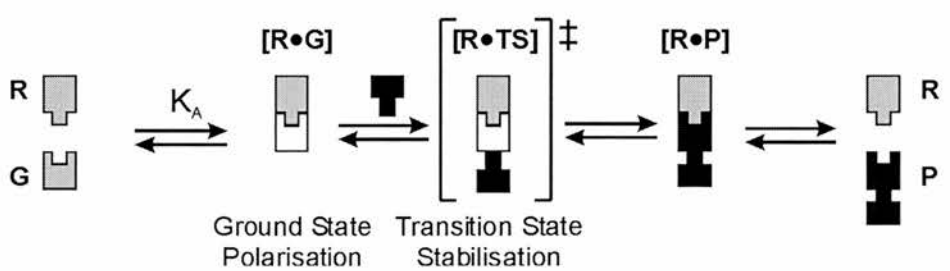

Figure 2.1.1 A schematic diagram representing the receptor designed to accelerate polar and non-polar reactions. Communication with the ground state and transition state of the reaction is through the reaction substrate only. The reactive partner may be altered, changing the polarity of the reaction.

The processes represented schematically in **Figure 2.1.1** can be represented by reaction coordinates or frontier molecular orbital diagrams. If we initially consider a

polar reaction of the addition of a nucleophile to a substrate, we have previously established that the intermediate and transition states could be stabilised.

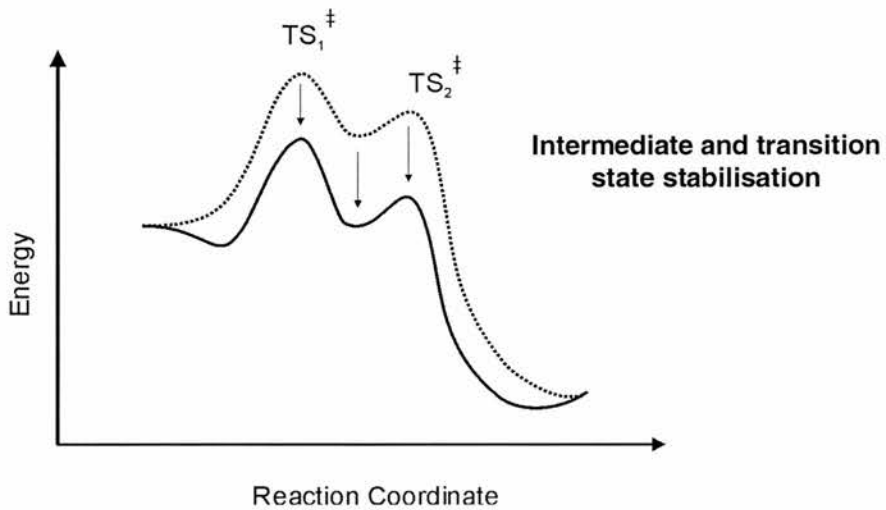

Figure 2.1.2 Diagrammatic representation of the stabilisation of the intermediate and transition states in a polar reaction on addition of a catalyst capable of stabilising negative charge.

Figure 2.1.2 demonstrates the expected reduction in intermediate and transition states energies on addition of a hydrogen bonded receptor. The diagram assumes that both transition states would be stabilised, however depending on the complex produced, this isn't necessarily the case, one transition state may be stabilised preferentially depending upon the specific interactions between the substrate and the receptor.

Relating this schematic diagram, to the Arrhenius equation, we would expect the rate constant and hence the observed reaction rate to increase

$$\ln k = \ln A - \frac{E_a}{RT}$$

Equation 2.1.3 The Arrhenius equation relates rate constant, k, and activation energy, E_a. A is a pre-exponential factor.

Equation 2.1.3 demonstrates that as the activation energy E_a decreases, ln k and hence k, the rate constant increases.

Figure 2.1.1 also indicates that ground state polarisation can also be effected by a receptor of this type. It is expected that this property would accelerate cycloaddition reactions by lowering the LUMO of the 2π component.[142] Pictorially this can be

readily visualised by inspecting the frontier molecular orbitals of a Diels-Alder cycloaddition.

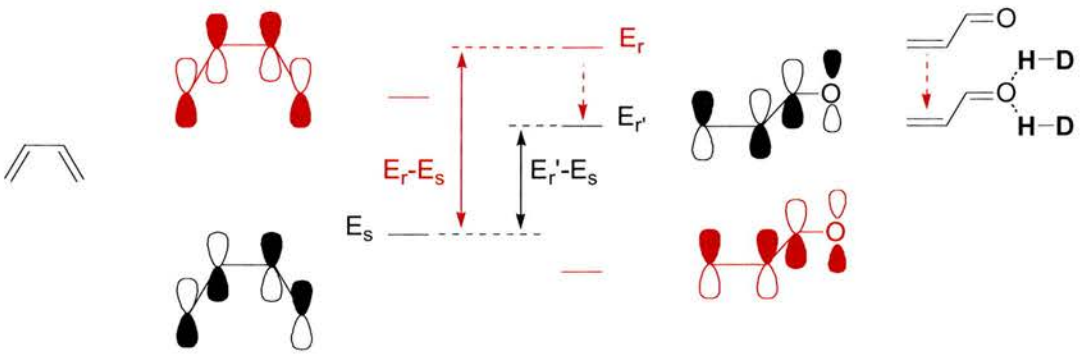

Figure 2.1.4 A schematic diagram displaying the lowering of the enone LUMO by hydrogen bonding to a suitable receptor. As the difference in energy between the HOMO and LUMO closes, the rate of reaction increases. E_r and E_s relate to the relative energies of the frontier orbitals, see **Equation 2.1.5**.

The frontier molecular orbital diagram in **Figure 2.1.4** demonstrates the closing of the HOMO LUMO energy gap on addition of a suitable hydrogen bonding receptor.

Frontier Molecular Orbital theory (FMO)[142, 143] states that when two reactants approach each other there are three terms that account for the mutual perturbation in the two reactants.

1. Closed shell repulsion. The filled orbitals in each reactant repel each other.
2. Coulombic forces including attractive Van der Waals interactions and coulombic repulsions.
3. Second order perturbation term. This accounts for all attractive interactions between occupied and unoccupied molecular orbitals of the reactants possessing appropriate symmetry.

The repulsive interactions in these three terms exceed the attractive ones leading to the existence of activation energy. Mathematically we can relate the energy difference of the occupied and unoccupied orbitals with the energy gain from interacting the orbitals.

$$\Delta E = \sum_{r}^{occ} \sum_{s}^{unocc} - \sum_{s}^{occ} \sum_{r}^{unocc} \frac{2\left(\Sigma_{ab} c_{ra} c_{sb} \beta_{ab}\right)}{E_r - E_s}$$

Equation 2.1.5 Equation relating the energy gain in the second order perturbation term with difference in orbital energy. The two reacting molecules are denoted r and s, the reaction centres on r are termed a, on s they are termed b. $c_{ra}c_{sb}$ represents the overlap of atomic orbitals and converts the efficiency of overlap to an energy term

The information contained in **Equation 2.1.5** connects the energy gain ΔE for the second order perturbation with the energy difference of the molecular orbitals E_r-E_s see **Figure 2.1.4**. Frontier molecular orbital theory states that the HOMOs and LUMOs of the two reactants possess the lowest separation and so are the greatest contributors to the energy difference term. As E_r-E_s is reduced by binding to the receptor, ΔE increases, which increases the favourable interactions between the HOMO and LUMO and hence lowers the activation energy, increasing the rate of the reaction.

In summary, as the energy gap between the reactants closes, the overlap of the orbitals can increase and the rate of reaction is accelerated. Sustman and co-workers[144] collated experimental results correlating HOMO-LUMO energy separation and rate of reaction.

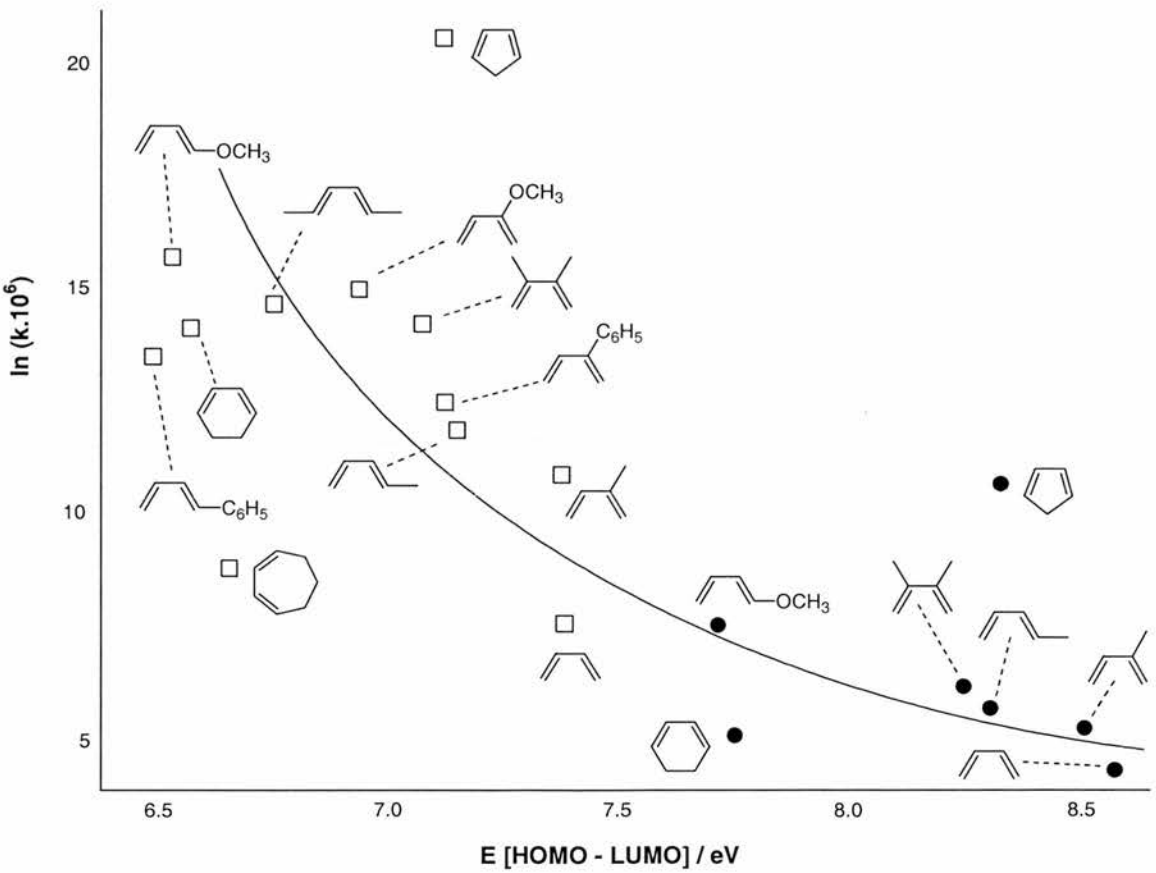

Figure 2.1.6 Graph displaying the correlation between HOMO LUMO energy separation and rate of reaction, adapted from Sustmann and co-workers

□ Reactions with TCNE (tetracyanoethylene)

● Reactions with maleic anhydride

Deviations from the best-fit line drawn were explained by errors in theoretical data or increased reactivity of cyclopentadiene by preorganisation in the *cisoid* conformation.

Enones were identified in **Section 1.8** as suitable substrates for a range of reactions. The initial design aimed to form two hydrogen-bonding interactions with an enone. *N*-Phenylmaleimide was chosen for its solubility, symmetry and commercial availability.

A hydrogen-bonding interaction could bind to the two lone pairs on one of the carbonyl groups, which can act as two hydrogen bond acceptors.

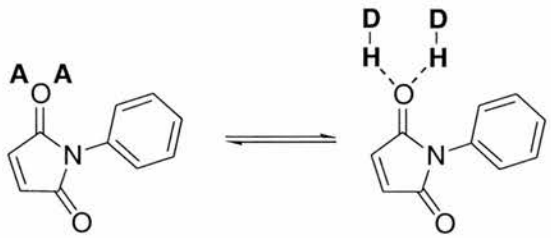

117 **117**

Figure 2.1.7 A two-point hydrogen-bonding interaction can be employed to bind to *N*-phenylmaleimide *via* one of the carbonyl moieties.

Depending upon the receptor, the symmetry of *N*-phenylmaleimide would also allow simultaneous binding to both carbonyl groups.

117 **117**

Figure 2.1.8 An alternative binding orientation that may be adopted by *N*-phenylmaleimide. Electron density can be withdrawn from both carbonyl groups.

Either of the binding orientations in **Figures 2.1.7** and **2.1.8** may be adopted. The more favoured binding orientation is determined by multiple factors. The "bite angle" of the tweezer receptor will exert an influence as will any additional stabilisation afforded by the interactions between other groups on the hosts and guests.

A simple receptor which would bind in one of the modes depicted in **Figures 2.1.7** and **2.1.8** would be a bis-sulfonamide connected by a 1,3-phenyl spacer.

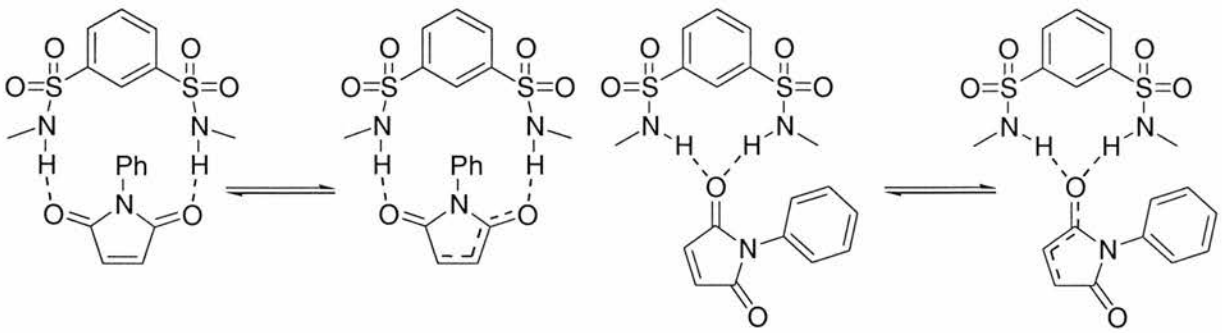

Figure 2.1.9 The manner in which a bis-sulfonamide could bind and withdraw electron density from *N*-phenylmaleimide in either of the suggested binding orientations from **Figure 2.1.7** or **2.1.8**

It is envisaged that binding to the carbonyl lone pairs would remove electron density from the ground state lowering LUMO energy and would stabilise negative charge in an intermediate or transition state as described previously. In this way, receptor **138** is predicted to be capable of becoming a broad-spectrum catalyst.

2.2 Synthesis

2.2.1 Synthesis of the Receptor

The sulfonamide receptor **138** was chosen as a means of binding with *N*-phenylmaleimide. The appended butyl groups were intended to lend the receptor solubility in deuterated chloroform.

The bis-sulfonamide **138** was readily synthesised in one step from the bissulfonyl chloride **137** precursor. Reacted in excess butylamine, the bis-sulfonamide was isolated in high yield.

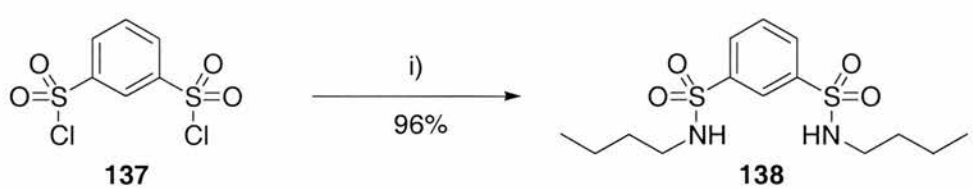

137 **138**

Scheme 2.2.1.1 i) Butylamine, CH_2Cl_2, 0 °C - r.t., 16hrs

Most of the reactants were commercially available, however, *N*-benzylidene-aniline *N*-oxide **141** was synthesised *via* a two step reaction, first synthesising the crude hydroxylamine by careful reduction of nitrobenzene by a zinc / aqueous ammonium chloride mixture. It was essential to optimise the reaction time

for the reduction as nitrobenzene is readily reduced to aniline under these reaction conditions. The *N*-benzylidene-aniline *N*-oxide synthesis was completed by the addition of crude β-phenyl hydroxylamine to benzaldehyde and subsequent crystallisation from EtOH.

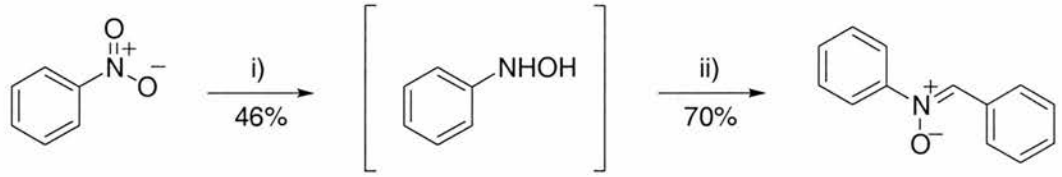

139 **140** **141**

Scheme 2.2.1.2 i) Zn, $NH_4Cl_{(aq)}$, r.t., 20 min, ii) Benzaldehyde, EtOH, r.t. 16 hrs

2.2.2 Characterisation of Reaction Products

The adducts were synthesised independently for characterisation purposes. *N*-Phenylmaleimide was stirred with one equivalent of 4-fluorobenzylamine in dichloromethane solvent and the resulting adducts were isolated *via* gradient elution column chromatography in poor yield. The poor yield arose from poor conversion to product and difficulty in subsequent separation of reactants.

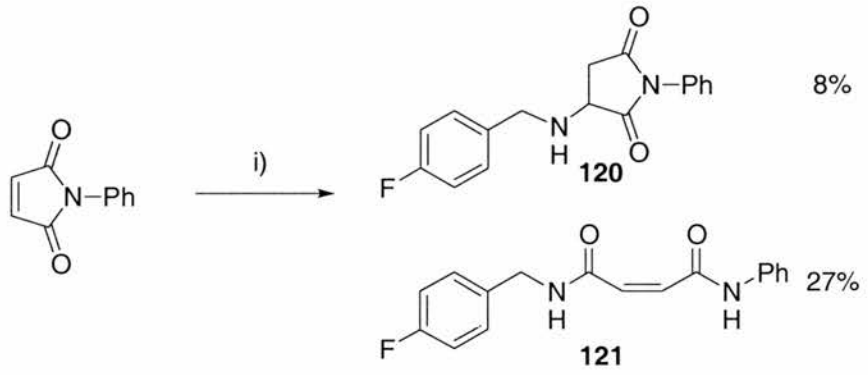

Scheme 2.2.2.1 i) 4-fluorobenzylamine, CH_2Cl_2, r.t. 3 days.

N-Benzylidene-aniline *N*-oxide was stirred with a stoichiometric quantity of *N*-phenylmaleimide to yield the diastereoisomeric products in poor yield. The poor yield was as a result of incomplete reaction of starting materials and difficulties in separating the products.

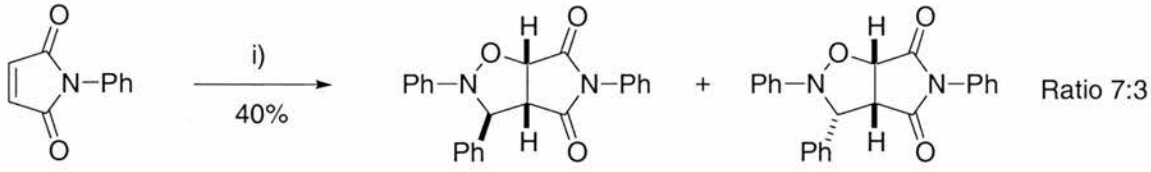

117 **142** **143**

Scheme 2.2.2.2 i) *N*-benzylidene-aniline *N*-oxide, CH_2Cl_2, r.t. 5 d

A 1:1 mixture of furan and *N*-phenylmaleimide in dichloromethane was stirred at room temperature and the resulting cycloadducts were purified *via* recrystallisation. Only the *exo* cycloadduct could be isolated.

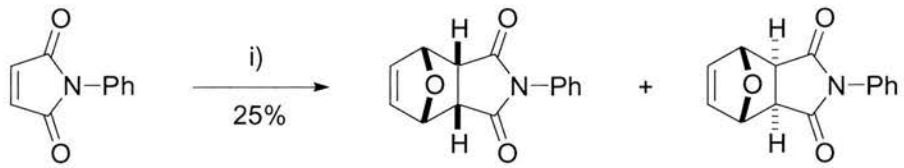

117 **144** **145**

Scheme 2.2.2.3 i) furan, CH_2Cl_2, r.t. 5 d. Only the *exo* cycloadduct was isolated from the reaction mixture.

2.3 Computational Investigations

Molecular modelling was undertaken using the Macromodel program and the AMBER* forcefield simulated in chloroform solution.[145] After initial minimisation, a Monte-Carlo conformational search technique was employed to find the lowest energy conformations in the system. It was hoped that in this manner it would be possible to find the lowest energy coconfirmations and assess the number of hydrogen bonds present.

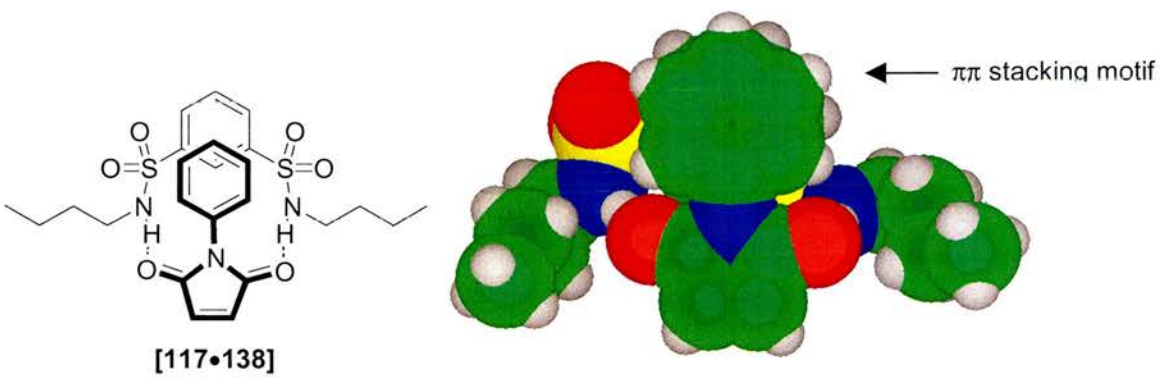

[117•138]

Figure 2.3.1 A simplified two-dimensional representation of the binding between the bis-sulfonamide **138** and *N*-phenylmaleimide **117** with a space filling representation of the complex.

It was observed that the lowest energy confirmations possessed two hydrogen bonds, binding to both carbonyl groups rather than one. The phenyl group then lends extra stability in a π-π stacking arrangement with the receptor.[146] A simplified diagram of this arrangement is depicted in **Figure 2.3.1** with the corresponding space filling representation of the lowest energy structure.

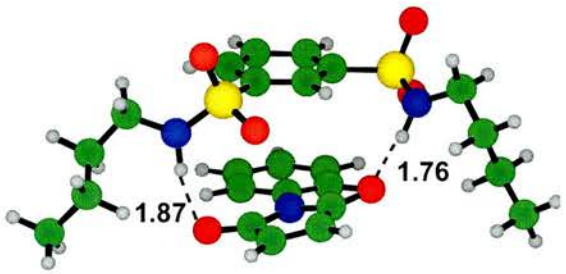

Global Minimum Energy Structure

Figure 2.3.2 A computer generated energy minimised structure of receptor **138** bound to *N*-phenylmaleimide using the AMBER* forcefield. Carbons are shown in green, hydrogen atoms in grey, oxygen in red, nitrogen blue and sulphur is yellow. The hydrogen bond distances are measured in Å. The complex is also stabilised by π-π stacking of the aromatic rings.

A ball and stick representation of the complex is depicted in **Figure 2.3.2** displaying the two hydrogen bonds between the NH protons and the carbonyl groups. The N-H···O angles were measured to be 170° and 164°, which is a departure from the idealised 180° geometry.[147]

The data obtained by the Monte Carlo conformational search was analysed in greater detail to evaluate all the accessible solution binding coconformations. The scatter plot in **Figure 2.3.3** shows the intermolecular distances in the lowest energy structures. Contact distances between hydrogen bond donors and acceptors of less than 2.5 Å are considered to be hydrogen bonds.

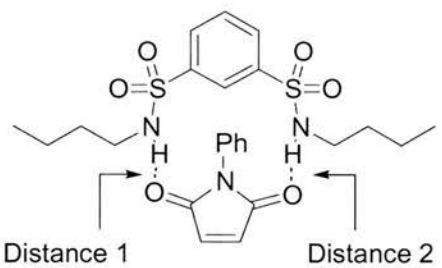

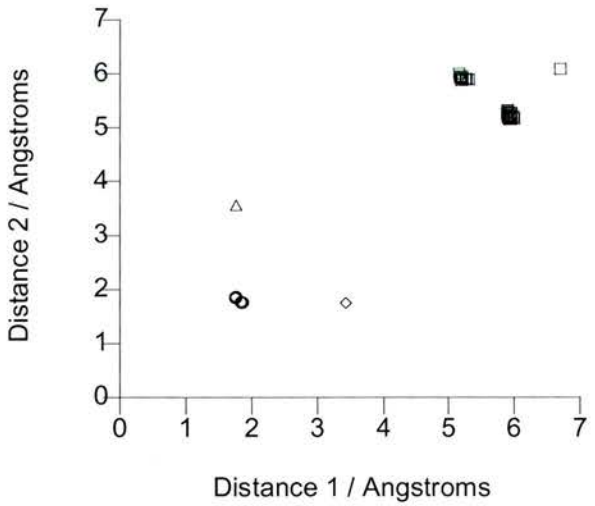

Figure 2.3.3 Scatter plot of the distances between the carbonyl groups and sulfonamide protons in the structures with energies + 10kJ mol^{-1} relative to the Global minimum. Circles represent coconformations possessing both hydrogen bonds, triangles and diamonds possess one hydrogen bond and squares represent structures with no hydrogen bonding present.

A few of the lower energy coconformations possess two hydrogen-bonding interactions (represented as circles in **Figure 2.3.3**) but many contain neither. This

suggests that only a small amount of substrate is bound at any one time by the receptor.

Expanding the data set including all structures up to 20 $kJmol^{-1}$ higher in energy than the lowest energy coconformation reveals that many accessible structures possess one hydrogen bond.

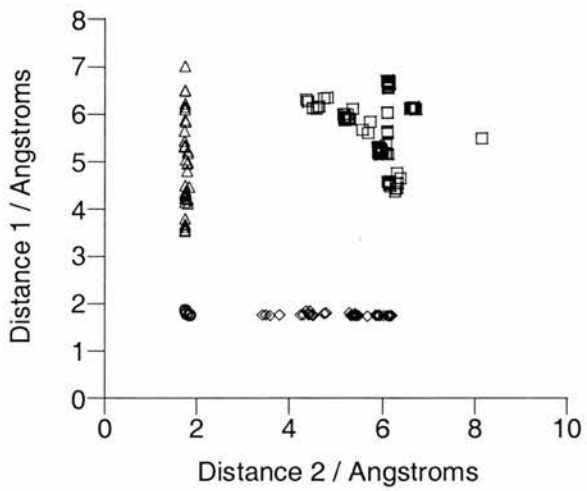

Figure 2.3.4 Scatter plot of the distances between the carbonyl groups and sulfonamide protons in the structures with energies + 20kJ mol^{-1} relative to the Global minimum. Circles represent coconformations possessing both hydrogen bonds, triangles and diamonds possess one hydrogen bond and squares represent structures with no hydrogen bonding present.

Figure 2.3.4 clearly shows that the coconformations are divided into four regions. One region the interatomic distances are too large to be arising from hydrogen bonds and are represented as squares in **Figure 2.3.4**. Two of the other regions, represented by triangles and diamonds have one short contact (about 2 Å) attributable to a hydrogen bond and one non-hydrogen bonding interaction. One small scatter of coconformations shown as circles represents the coconformations with two short contacts. Although small in number, these coconformations are some of the lowest in energy.

Modelling the lowest energy coconformation using electronic structure methods can provide additional data concerning the electron distribution in the guest before and during the binding event. An initial electronic structure was calculated, subsequently an approximate solution of the Schrodinger equation by semi-empirical methods (AM1) yielded information concerning the electron density, calculated as a series of

charges, which can then be mapped to a van der Waals surface. The charges can then be colour coded and displayed as a spectrum for visual analysis.

Figure 2.3.5 shows the calculated structures for the guest and [host•guest] complex as space-filling models. Alongside each model is the calculated electrostatic potential mapped onto the van der Waals surfaces. The charge on the surfaces is modelled as thus, blue areas represent positively charged portions of the molecule; red areas represent negatively charged portions of the molecule or complex.

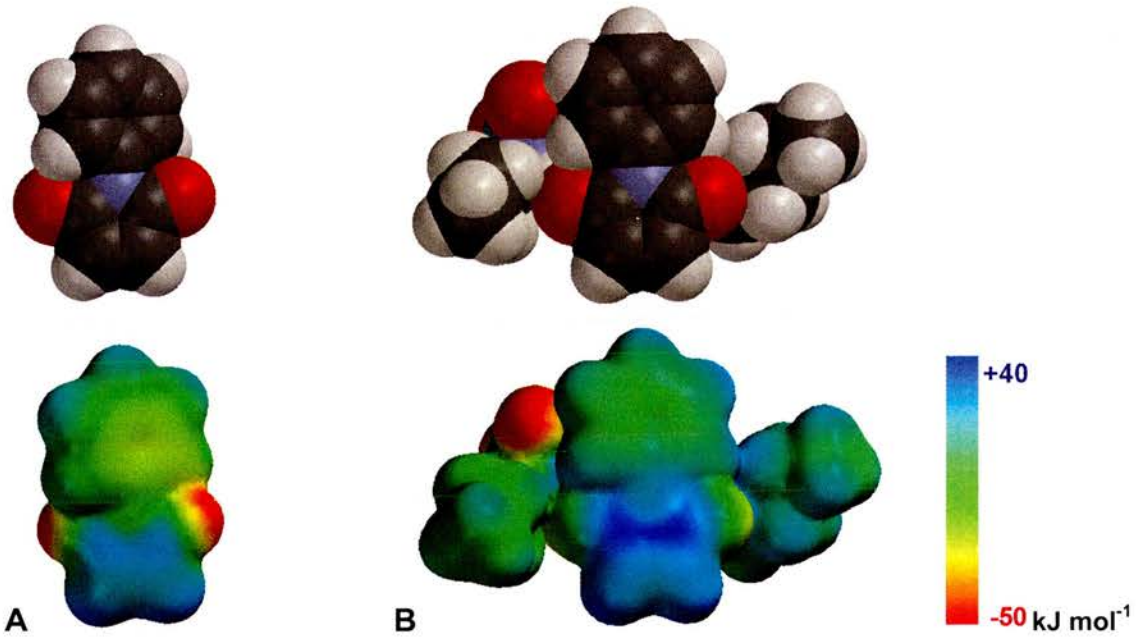

Figure 2.3.5 Representation of the electrostatic potential of *N*-phenylmaleimide in the bound (**B**) and unbound (**A**) states. Areas of positive charge are coloured towards the blue end of the spectrum and areas of negative charge are red. Above each structure is the corresponding space-filling model in the same orientation.

As can be seen in **Figure 2.3.5**, on binding the receptor, all four carbonyl and alkene carbons tend towards the blue end of the spectrum. This indicates an increase in the δ+ charge of the four atoms. This confirms the trend intuitively predicted in **Figure 2.1.7** that electron density would be withdrawn from the *N*-phenylmaleimide by binding to the receptor.

2.4 Binding Investigations

Binding constants are a measure of the efficiency of binding a host and guest. One of the most accurate methods for assessing binding constants is by

NMR spectroscopic titration.[148] For small to moderate association constants, the equilibrium in **Equation 2.4.1** is faster than the NMR timescale.

$$RH + S \underset{}{\overset{K_a}{\rightleftharpoons}} RH::S$$

Equation 2.4.1 Representation of the equilibrium between a receptor (RH) and a substrate (S) and a receptor substrate complex (RH::S). This equilibrium is represented by a constant K_a, the association constant.

The NMR of a dynamic complex appears as a time-averaged spectrum with chemical shift corresponding to a weighted average of the proportion of bound and unbound species.

NMR spectroscopic titrations were performed for the *N*-phenylmaleimide **117**, bis-sulfonamide **138** complex. However, the chemical shift changes were seen to be linear over the available concentration range, indicating a very low K_a for the complex. This confirms the conclusion drawn in **Section 2.3** from the computational investigations that only a small proportion of substrate is bound at any one time by the receptor. Chemical shift changes are observed in the host resonances. As the host concentration is held constant over the titration, the chemical shift changes must arise through complexation.

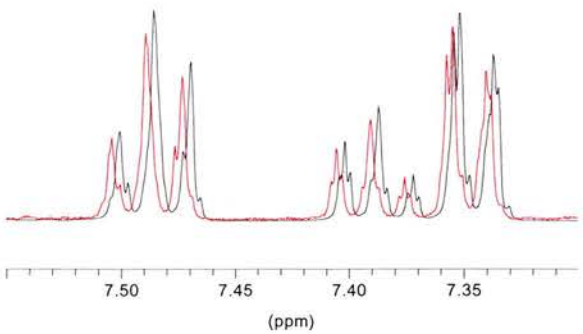

Figure 2.4.2 Partial 500 MHz ^{1}H NMR spectra showing the changes in chemical shift on the aromatic receptor resonances on the addition of *N*-phenylmaleimide guest. The red spectrum arises from a solution containing 25 mM of receptor **138** and 5 mM of *N*-phenylmaleimide. The black spectrum was recorded using a solution containing 25 mM of receptor **138** and 160 mM of *N*-phenylmaleimide. Both spectra were recorded at 283 K in $CDCl_3$ and are presented on the same scale.

Small chemical shift changes were observed in the aromatic resonances of the receptor as shown in **Figure 2.4.2**, suggesting the predicted low energy coconformation containing π-π stacking is observed in solution.

For kinetic analysis purposes, an estimated figure of 5 M^{-1} was taken as the association constant. This would be a very low value for K_a and so is a valid estimate. Assignment of a value for the association constant will enable the calculation of k_{cat}/k_{uncat} and subsequent comparison of reactions.

2.5 Nucleophilic Reactions

2.5.1 Reactivity

It was previously established that binding of a transition state to receptor **138** might stabilise the limiting transition state of any nucleophilic addition reaction. The receptors designed by Moran and co-workers[130-133] use transition state charge stabilisation to catalyse a reaction process. These receptors however, are often synthetically complex and so it was decided to investigate if similar catalytic effects can be induced with a smaller, more synthetically accessible receptor such as bis-sulfonamide **138**.

Polar and non-polar reactions were tested on a small scale in deuterated solvent with and without the receptor. Two solutions were prepared for each reaction containing the two reactants; one of the solutions also contained an equivalent of the receptor. Reaction completion was evaluated by 300 MHz ^{1}H NMR spectroscopy after 16 hours. Where reaction was observed, the conversion to product was assessed by deconvolution procedures and noted.

Deconvolution is a method used for both initial reaction evaluation and for following the kinetics of each reaction. All spectra were evaluated using WinNMR and were processed in the normal manner.

Deconvolution fits the area of each ^{1}H NMR resonance to an idealised Lorenzian curve. This is particularly similar to the resonance shapes observed on the collection of the full kinetic data as all were collected using non-spinning

500 MHz ^{1}H NMR spectroscopy and resonances arising from non-spinning samples are known to more closely resemble Lorenzian than Gaussian curves.

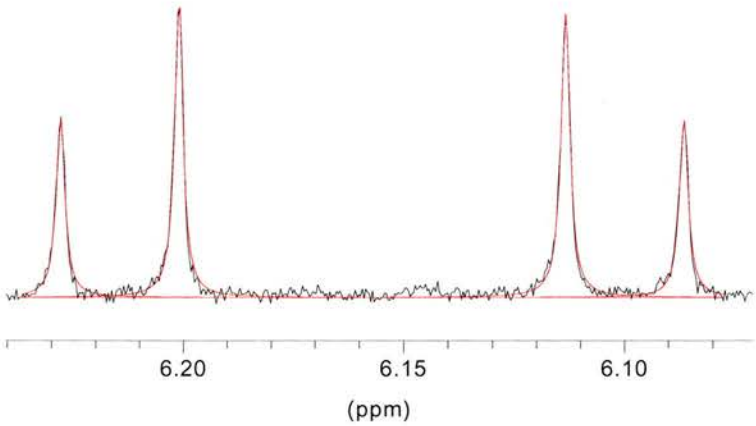

Figure 2.5.1.1 A partial 500 MHz ^{1}H NMR spectrum with the calculated deconvoluted curves in red. The relative areas of the curves fitted to the proton resonances are then calculated.

A partial sample spectrum is displayed in **Figure 2.5.1.1** with the best fit found from deconvoluting the two product resonances. The area of the curves is then calculated and compared with the area of a resonance relating to the starting material. Deconvolution methodology was employed as it has been found to be more accurate, faster and less subjective than integration.

Initially, nucleophilic additions to the *N*-phenylmaleimide were investigated.

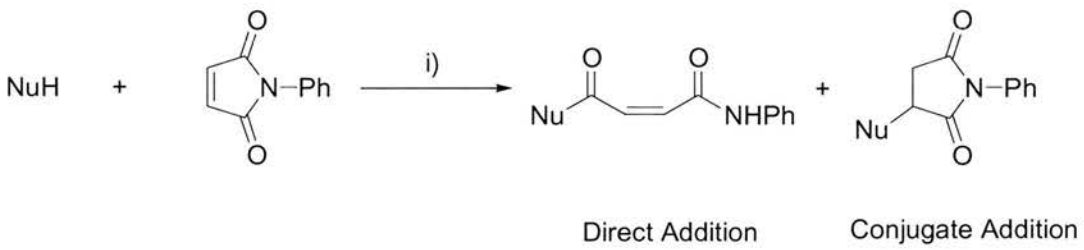

Scheme 2.5.1.2 The two possible products arising from nucleophilic addition to *N*-phenylmaleimide. i) $CDCl_3$,

Reactions were performed in deuterated chloroform on a 1:1 ratio of *N*-phenylmaleimide to nucleophile in the presence and absence of an equivalent of host. Percentage completions were assessed after a fixed time period by 300MHz ^{1}H NMR spectroscopy, deconvoluting methylene or alkene product

resonances against the starting material. This initial assessment was utilised to select suitable experiments for further investigation.

Table 2.5.1.3 A table showing the initial assessments of reaction of *N*-phenylmaleimide with various nucleophiles. Percentage completions were assessed by 300 MHz ^{1}H NMR spectroscopy and subsequent deconvolution after 16 hours.

		% Completion With **138**		% Completion Without **138**	
Nucleophile	Temperature	Direct	Michael	Direct	Michael
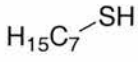	0	0	0	0	0
	50	0	0	0	0
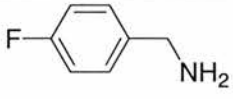	10	10	8	4	4

Although no reaction was observed with heptane thiol, this is not an indication that the receptor is incapable of accelerating polar reactions. This conclusion can only be inferred if a background rate is observed which is not accelerated by the presence of the receptor. The initial results suggested that the amine addition is accelerated and indicated that some selectivity may be observed.

Investigation of the amine addition to *N*-phenylmaleimide was conducted by 500 MHz ^{1}H NMR spectroscopy. The kinetic experiments were only conducted once to minimise the time using the NMR apparatus, however the similarity between the kinetic results and those obtained for the small-scale reactions in **Table 2.5.1.3** confirmed the reproducibility of the experiment.

One ^{1}H NMR spectrum was recorded of the non-spinning reaction sample every 30 minutes for 16 hours and the appearance of the two products was noted. **Figure 2.5.1.4** shows the emergence of product as observed over the initial, sixteenth and thirty second spectra.

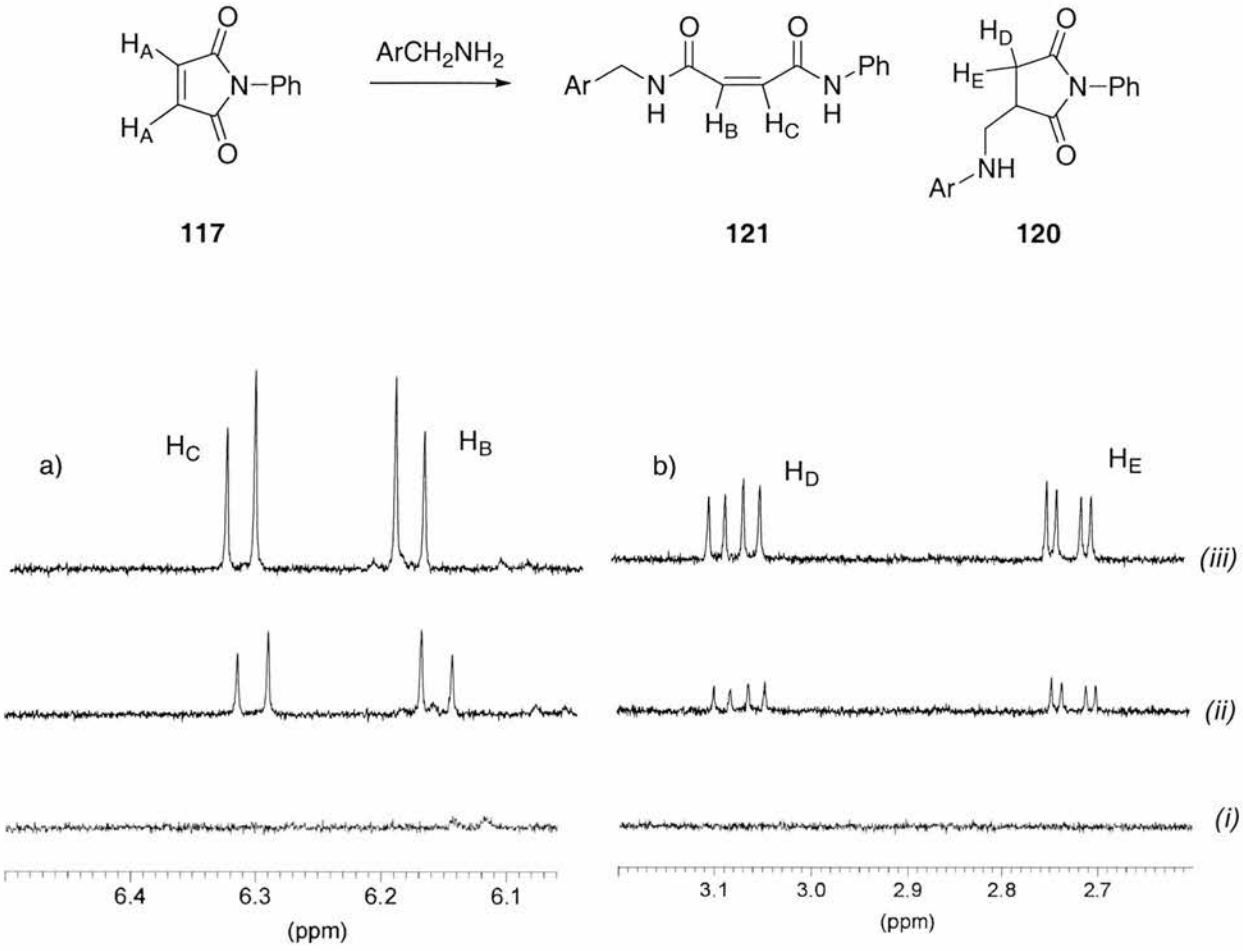

Figure 2.5.1.4 Partial 500 MHz ^{1}H NMR spectra recorded as solutions in $CDCl_3$ at 10 °C, displaying the appearance of resonances arising from the alkene protons from the a) direct product and b) conjugate methylene resonances over *(i)* 0, *(ii)* 510, *(iii)* 990 min. All spectra are displayed on the same scale. Protons A to E were deconvoluted to obtain the measurements in **Figure 2.5.1.5**. Ar represents FC_6H_4.

Figure 2.5.1.5 shows the total conversion to product calculated from the 500 MHz ^{1}H NMR resonances arising from the alkene *N*-phenylmaleimide protons and the alkene and methylene product resonances shown as protons H_A to H_E in **Figure 2.5.1.5**.

The initial reaction data in the absence of the receptor **138** is omitted as a result of the inaccuracy of the initial deconvolution of the eight peaks relating to the four product resonances.

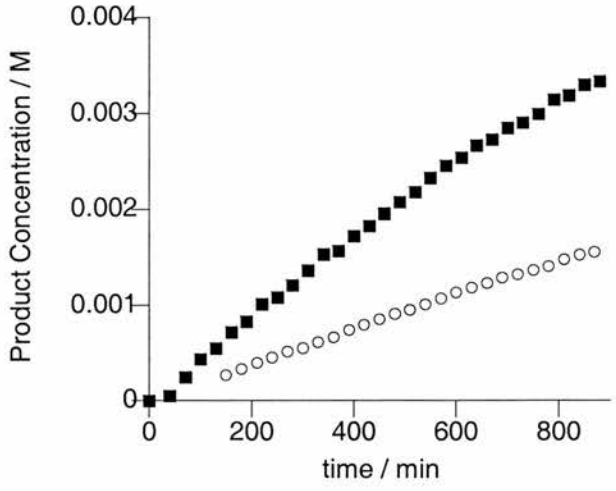

Figure 2.5.1.5 Kinetic data of the total formation of product in the presence (filled squares) and absence (unfilled circles) of receptor **138**. Protons A to E were deconvoluted to obtain the measurements in the graph. Ar represents FC_6H_4.

It may be informative to extract the data for the conjugate and direct addition to investigate whether any selectivity is observed.

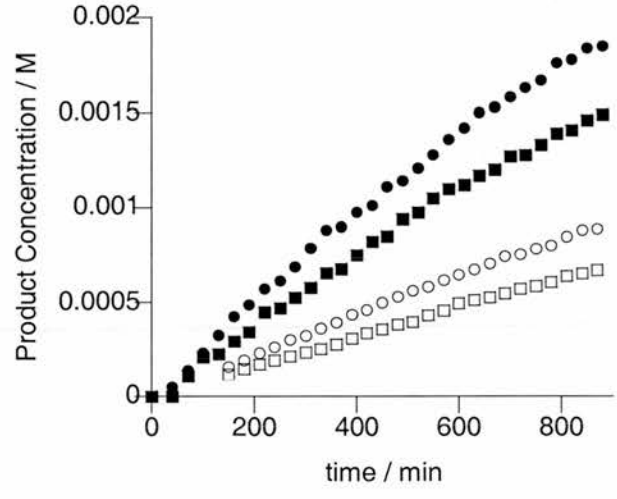

Figure 2.5.1.6 Kinetic data of the reaction between *N*-Phenylmalemide and 4-Fluorobenzylamine. The filled shapes represent the reaction in the presence of receptor **138** and the unfilled shapes represent the control background reaction. Conjugate addition is represented by the squares; direct addition is represented by circles.

Initial rates of reaction were estimated by linear regression of the first 250 minutes of reaction data. The relative initial rates of the direct and Michael additions are displayed in **Figure 2.5.1.7**.

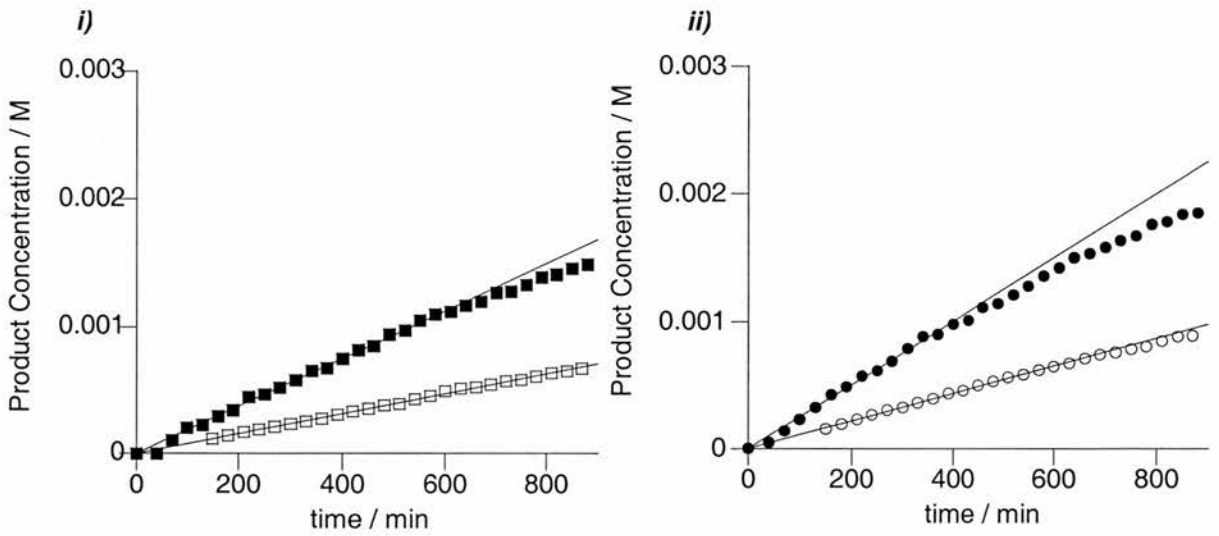

Figure 2.5.1.7 Graphs displaying the projection of the initial rates of *i)* direct and *ii)* Michael addition as calculated by linear regression analysis of product concentration in the initial reaction.

From **Figure 2.5.1.7** displaying an extrapolation of the initial reaction rates, it is apparent that both types of addition are accelerated and that the direct and Michael additions are accelerated by a similar magnitude. The characteristic parabolic appearance of product in the presence of the receptor is also evident.

It might be expected, however, that the receptor would strongly accelerate the direct addition in preference to the conjugate addition. The effect of the removal of electron density is more strongly felt in the 2 position of the enone than the 4 position. This can be observed by inspecting orbital coefficients on protonated and deprotonated acrolein that would serve as an extreme example of a hydrogen bonded enone.

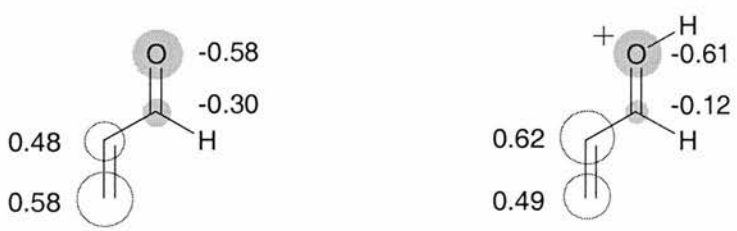

Figure 2.5.1.8 Acrolein and protonated acrolein with the associated orbital coefficients. The electron density is directly proportional to the square of the orbital coefficient.[149]

The protonation of acrolein causes several electronic changes in the molecule. The orbital coefficients of the oxygen and C4 carbon aren't altered by any significant amount. The main changes occur at the C2 and C3 carbons. The square of orbital coefficients is directly proportional to electron density, it is apparent from

Figure 2.5.1.8 that the electron density of the C2 carbon is significantly reduced. This change may have a significant effect on the reactivity in both polar and non-polar reactions. It could be predicted that the carbonyl group is more electrophilic than the alkene and would be made even more so by binding to a hydrogen binding receptor, the amine, however, shows borderline reactivity and may react at either the hard carbonyl carbon or the softer enone.[138] Increasing the hardness of the carbonyl carbon may hinder the reaction. With this factor working against acceleration of the direct addition, the direct addition appears to be accelerated by a greater degree than the conjugate addition reaction. This suggests that the receptor is displaying partial selectivity for the compact, polar transition state over the more dissociated transition state of the Michael Addition reaction.

2.5.2 Fitting *N*-Phenylmaleimide 4-Fluorobenzylamine Reaction Data

The kinetic data recorded was fitted to the kinetic model presented in **Figure 2.5.2.1.** It was previously observed that the ground state association constant was too small to be accurately measured over the available concentration range. It was seen in **Section 2.4** that chemical shift changes were observed. It is not unreasonable to assume therefore, that if greater concentrations were available, the saturated chemical shift change would be observed, relating to the presence of a high concentration of the receptor **138** *N*-phenylmaleimide **117** complex.

Unfortunately, we cannot measure transition state or intermediate binding directly. Ignoring ground state binding from the kinetic model will therefore result in the formation of rate constants that cannot be compared to the background reaction. It was stated in **Section 2.4** that a reasonable estimate of the association constant would be 5 M^{-1} and this figure was adopted in the kinetic modelling.

The kinetic model presented in **Figure 2.5.2.1** is a simplification of the kinetic processes in the reaction. **Section 2.1** discussed the nature of polar and non-polar reactions and observed that polar reactions tended to possess two transition states and an intermediate. The nucleophilic addition reactions of *N*-phenylmaleimide follow this trend shown in **Figure 2.1.2**. The initial transition state corresponds to the bimolecular addition of the nucleophile to the substrate, a local minimum on the energy profile is then formed corresponding with the tetrahedral intermediate or

enone like intermediate which would undergo rapid decomposition and protonation or protonation and tautomerisation to form the direct and conjugate products respectively.

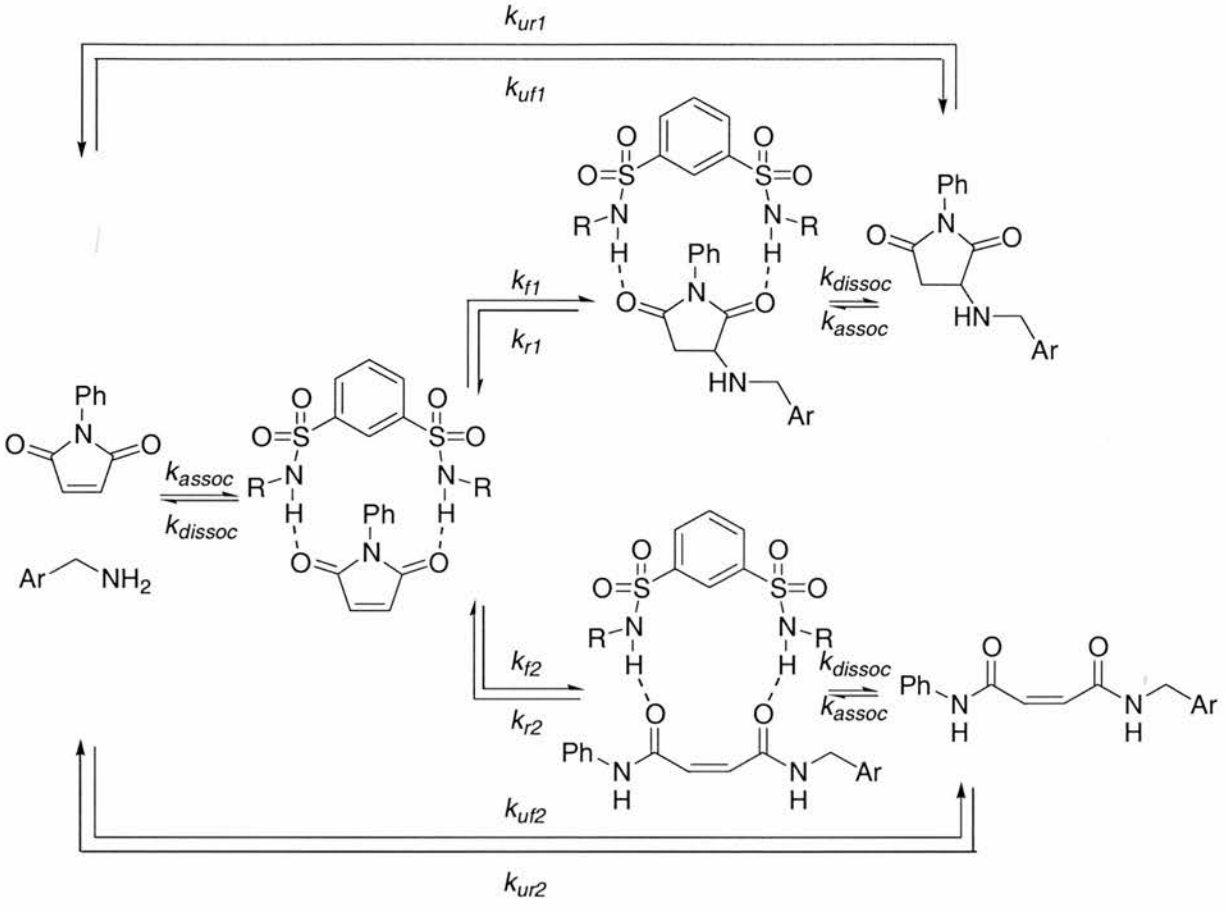

Figure 2.5.2.1 Representation of all the kinetic processes in the reaction between diphenylmaleimide and *N*-Phenylmaleimide in the presence and absence of receptor **138**. R = $(CH_2)_3CH_3$, k_{assoc}, k_{dissoc} = Association rate constants, $K_a=k_{assoc}/k_{dissoc}$, k_{f1}= forward rate constant of the Michael Addition, k_{r1} = reverse rate constant of the Michael Addition, k_{f2}= forward rate constant of the Direct Addition, k_{r2} = reverse rate constant of the Direct Addition, k_{uf1} = forward background rate constant of the Michael Addition, k_{ur1} reverse background rate constant of the Michael addition k_{uf2} = forward background rate constant of the Direct Addition, k_{ur2} reverse background rate constant of the direct addition.

A term to account for the binding of the receptor **138** to the reaction intermediate cannot be included into the kinetic model as only the rate constants associated with the formation of the first transition state can be calculated. We can assume that if binding to the intermediate occurs, the transition states will be lowered in energy as a transition state will most closely resemble the nearest local minimum energy on a reaction profile however, we cannot quantify this effect into the model. Association to the starting material is therefore assumed as described previously. Association to the direct addition product is assumed to be retained as the carbonyl groups would still be capable of hydrogen bonding.

The background rate was established initially for comparison and to enable calculation of k_r and k_f, the rate constants for the reaction in the presence of receptor **138**. It is assumed that the background rate of reaction will be identical in the presence and absence of the receptor.

The Background Kinetic Model ⇨

NPM + Amine $\xrightarrow{k_{uf1}}$ Conjugate

Conjugate $\xrightarrow{k_{ur1}}$ NPM + Amine

NPM + Amine $\xrightarrow{k_{uf2}}$ Direct

Direct $\xrightarrow{k_{ur2}}$ NPM + Amine

Figure 2.5.2.2 Model of the addition reaction between *N*-phenylmaleimide and 4-fluorobenzylamine. NPM represents *N*-phenylmaleimide, amine represents 4-fluorobenzylamine, direct represents the direct adduct, conjugate represents the conjugate adduct.

The kinetic parameters for the reaction in the presence of sulfonamide receptor **138** were calculated from the following kinetic model.

The Kinetic Model ⇨

NPM + Amine $\xrightarrow{k_{uf1}}$ Michael

Michael $\xrightarrow{k_{ur1}}$ NPM + Amine

NPM + Amine $\xrightarrow{k_{uf2}}$ Direct

Direct $\xrightarrow{k_{ur2}}$ NPM + Amine

NPM + R $\xrightarrow{k_{assoc}}$ [NPM•R]

[NPM•R] $\xrightarrow{k_{dissoc}}$ NPM + R

[NPM•R] + Amine $\xrightarrow{k_{f1}}$ [Michael•R]

[Michael•R] $\xrightarrow{k_{r1}}$ [NPM•R] + Amine

[Michael•R] $\xrightarrow{k_{dissoc}}$ Michael + R

Michael + R $\xrightarrow{k_{assoc}}$ [Michael•R]

[NPM•R] + Amine $\xrightarrow{k_{f2}}$ [Direct•R]

[Direct•R] $\xrightarrow{k_{r2}}$ [NPM•R] + Amine

[Direct•R] $\xrightarrow{k_{dissoc}}$ Direct + R

Direct + R $\xrightarrow{k_{assoc}}$ [Direct•R]

Figure 2.5.2.3 The seven equilibria representing the reaction between *N*-phenylmaleimide and 4-fluorobenzylamine in the presence of receptor **138**. NPM represents *N*-phenylmaleimide, amine represents 4-fluorobenzylamine, direct represents the direct adduct, conjugate represents the conjugate adduct, and R represents sulfonamide receptor **138**.

The kinetic data recorded can only provide information about the rate limiting process. Therefore, the only rate constant for which meaningful data can be extracted will be the initial addition step. Therefore it is essentially meaningless to calculate energy profiles for the polar addition reactions, a comparison of relative initial reaction rates is more informative.

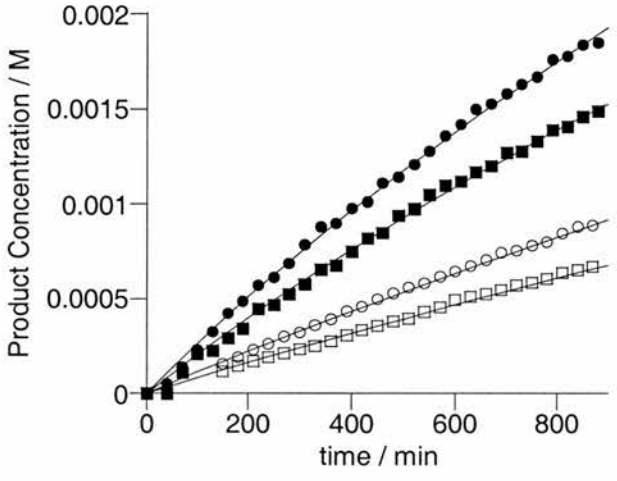

Figure 2.5.2.4 Kinetic data fitted to the reaction model for the direct and conjugate and direct additions to *N*-phenylmaleimide. Closed shapes represent the reaction in the presence of the receptor. Circles represent the direct addition, squares represent the conjugate addition.

The fitting applied to the kinetic data is displayed in **Figure 2.5.2.4**. From the fitted data, it was possible to calculate the rate constants for the formation of the first transition states of the reaction.

Table 2.5.2.5 Rate constants derived for the direct addition of 4-flourobenzylamine to *N*-phenylmaleimide.

Background Reaction		**With Receptor 138**	
k_{uf} / M^{-1} min^{-1}	k_{ur} / M^{-1} min^{-1}	k_f / M^{-1} min^{-1}	k_r / M^{-1} min^{-1}
4.74 (± 0.05) x 10^{-5}	8 (± 5) x 10^{-7}	8.27 (± 0.04) x 10^{-4}	3.3 (± 0.4) x 10^{-5}

Tables 2.5.2.5 and **2.5.2.6** display the kinetic parameters of the direct and conjugate additions respectively.

Table 2.5.2.6 Rate constants derived for the conjugate addition of 4-flourobenzylamine to *N*-Phenylmaleimide.

Background Reaction		With Receptor 138	
k_{uf} / M^{-1} min^{-1}	k_{ur} / M^{-1} min^{-1}	k_f / M^{-1} min^{-1}	k_r / M^{-1} min^{-1}
3.45 (± 0.05) x 10^{-5}	2 (± 6) x 10^{-5}	7.63 (± 0.04) x 10^{-4}	8 (± 2) x 10^{-7}

The data in **Table 2.5.2.5** and **Table 2.5.2.6** provides k_{cat}/k_{uncat} = 17.4 ± 0.3, k_{cat}/k_{uncat} = 22.1 ± 0.4 for the direct and conjugate additions respectively. The conjugate addition of the amine is accelerated more than the direct addition, however the difference is small and may arise from the arguments about hard and soft nucleophiles presented previously. The important conclusion, which should be drawn from this data, is that the both additions are accelerated by the receptor despite the low level of ground state binding in the system.

2.6 Cycloaddition Reactions

2.6.1 Reactivity

In **Section 1.8.5** we observed that a method of accelerating a truly bimolecular cycloaddition reaction with a hydrogen bonded receptor is by polarisation, analogous to Lewis acid catalysis. This method utilises hydrogen bonding to remove electron density from an enone.

The bis-sulfonamide receptor **138** has been used to bind to *N*-phenylmaleimide **117** to stabilise the negative charge formation on addition of a nucleophile. The same receptor could however, be used to bind to *N*-phenylmaleimide to withdraw electron density by polarisation. In this manner, the same receptor could be used to attempt catalysis of less polar cycloaddition reactions.

As previously, small-scale reactions were tested in deuterated solvent. One equivalent of the dipole or diene was added to the *N*-phenylmaleimide in each case, in the presence or absence of receptor **138** and total product formation observed.

Table 2.6.1.1 Initial percentage completion results for some cycloaddition reactions of *N*-phenylmaleimide. Percentage completions were assessed by NMR spectroscopy and subsequent deconvolution after 16 hours.

Nucleophile	Temperature °C	With Receptor % Completion	Without Receptor % Completion
	0	0	0
	50	0	0
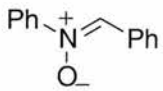	10	45	49
	40	10	10

2.6.2 [3+2] Dipolar Cycloaddition

The *N*-benzylidene-aniline *N*-oxide, *N*-Phenylmaleimide cycloaddition was investigated in greater detail by 500 MHz ^{1}H NMR spectroscopy. The appearance of the product was observed in spectra recorded every 30 minutes over 16 hours.

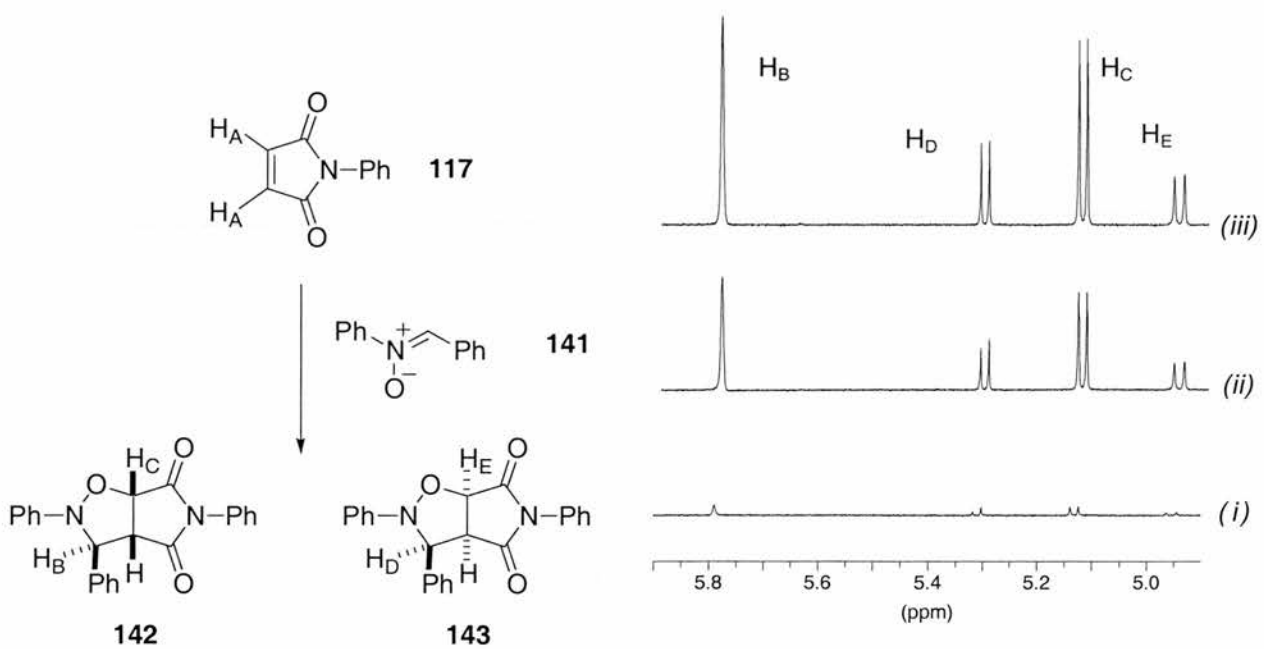

Figure 2.6.2.1 Partial 500 MHz ^{1}H NMR spectra recorded as solutions in $CDCl_3$ at 10 °C, displaying the appearance of resonances arising from cycloadduct over *(i)* 30, *(ii)* 540, *(iii)* 1020 min. All spectra are displayed on the same scale. Protons A to E were deconvoluted to obtain the measurements in **Figure 2.6.2.2**.

The appearance of the proton resonances on the fused 5,5 *exo* and *endo* ring systems is displayed in **Figure 2.6.2.1**. Deconvolution of these resonances and comparison with resonances arising from the starting material allows percentage conversion to product to be calculated.

The initial rate of reaction was observed to be as follows. The total conversion to product is presented in **Figure 2.6.2.1** rather than the data arising from the separate *endo* and *exo* resonances.

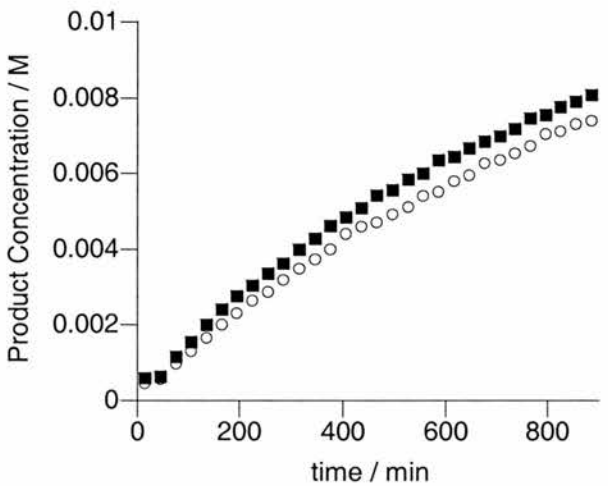

Figure 2.6.2.2 Kinetic data of the reaction between *N*-phenylmalemide and *N*-benzylidene-aniline *N*-oxide. Open circles represent the background reaction, closed squares represent the reaction in the presence of one equivalent of receptor **138**.

Initial rates were extrapolated from the preliminary reaction data and the extrapolation is depicted in **Figure 2.6.2.3** alongside the experimental data points.

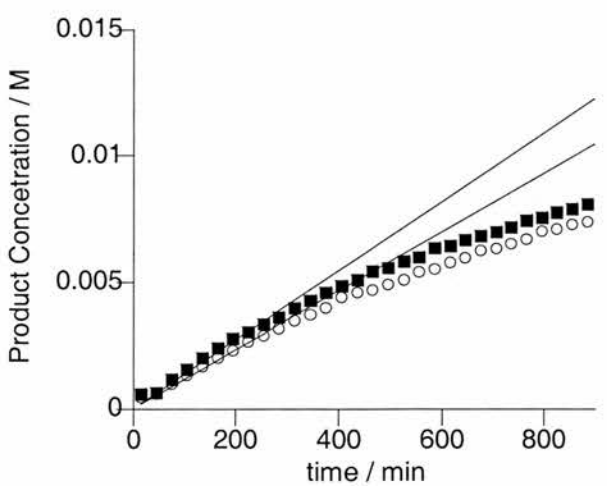

Figure 2.6.2.3 Graph displaying the projection of the initial rates of the cycloaddition between *N*-phenylmaleimide and *N*-benzylidene-aniline *N*-oxide as calculated by linear regression analysis of product concentration in the initial reaction.

Figure 2.6.2.3 shows the initial rates alongside the reaction data deconvoluted. It can be observed that there is a small initial rate acceleration indicated by the divergence of the tangential lines and this will be investigated in greater detail by fitting the data to a kinetic model.

2.6.3 Fitting the *N*-Benzylidene-aniline *N*-oxide *N*-Phenylmaleimide Cycloaddition

The reaction processes involved in the formation of the cycloadduct between *N*-phenylmaleimide and *N*-benzylidene-aniline *N*-oxide in the presence of receptor **138** are presented in **Figure 2.6.3.1.**

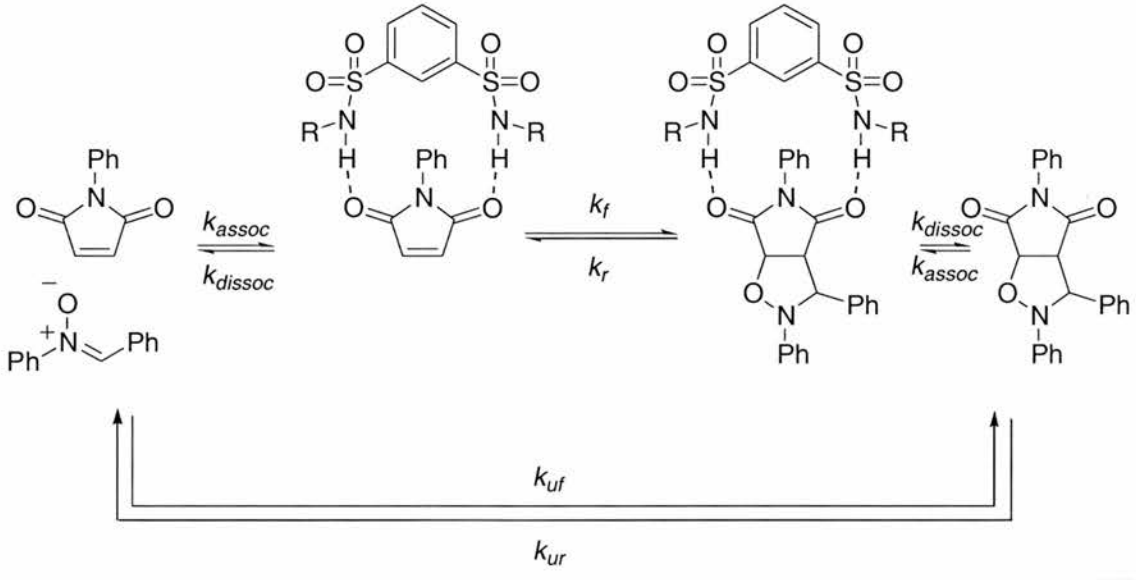

Figure 2.6.3.1 Representation of all the kinetic processes in the reaction between diphenylmaleimide and *N*-Phenylmaleimide in the presence and absence of receptor **138**. R = $(CH_2)_3CH_3$, k_f = forward rate constant, k_r = reverse rate constant, k_{uf} = forward background rate constant, k_{ur} reverse background rate constant K_d = Dissociation constant of the product.

The cycloaddition between *N*-phenylmaleimide and *N*-benzylidene-aniline *N*-oxide is simplified to the model presented in **Figure 2.6.3.1**. Two diastereoisomeric products can be formed in the [3+2] dipolar cycloaddition between the reactants, however as the receptor is achiral it is assumed that there is no basis for discrimination between the two transition states as both are capable of transition state binding and would possess similar transition state association constants. The kinetic model is therefore simplified.

The Background Kinetic Model ⇨

NPM + Dipole $\xrightarrow{k_{uf}}$ Adduct

Adduct $\xrightarrow{k_{ur}}$ NPM + Dipole

Figure 2.6.3.2 Model of the [3+2] dipolar cycloaddition reaction between *N*-benzylidene-aniline *N*-oxide and *N*-phenylmaleimide. NPM represents *N*-phenylmaleimide, dipole represents *N*-benzylidene-aniline *N*-oxide, adduct represents the combined *endo* and *exo* adducts.

The Kinetic Model ⇨

NPM + Dipole $\xrightarrow{k_{uf}}$ Adduct

Adduct $\xrightarrow{k_{ur}}$ NPM + Dipole

NPM + R $\xrightarrow{k_{assoc}}$ [NPM•R]

[NPM•R] $\xrightarrow{k_{dissoc}}$ NPM + R

[NPM•R] + Dipole $\xrightarrow{k_f}$ [Adduct•R]

[Adduct•R] $\xrightarrow{k_r}$ [NPM•R] + Dipole

[Adduct•R] $\xrightarrow{k_{dissoc}}$ Adduct + R

Adduct + R $\xrightarrow{k_{assoc}}$ [Adduct•R]

Figure 2.6.3.3 Kinetic model employed for the calculation of the composite rate constants, k_f and k_r. k_{uf} and k_{ur} are previously determined by the background reaction, k_{assoc} and k_{dissoc} are determined by K_a. NPM represents *N*-phenylmaleimide, dipole represents *N*-benzylidene-aniline *N*-oxide, adduct represents the combined *endo* and *exo* adducts, R represents receptor **138**.

The two equilibria are described in **Figure 2.6.3.3**, these were modelled using non-linear curve fitting methodology in SimFit. The background reaction was assumed to proceed at the same rate in the reaction mixture containing the receptor **138**.

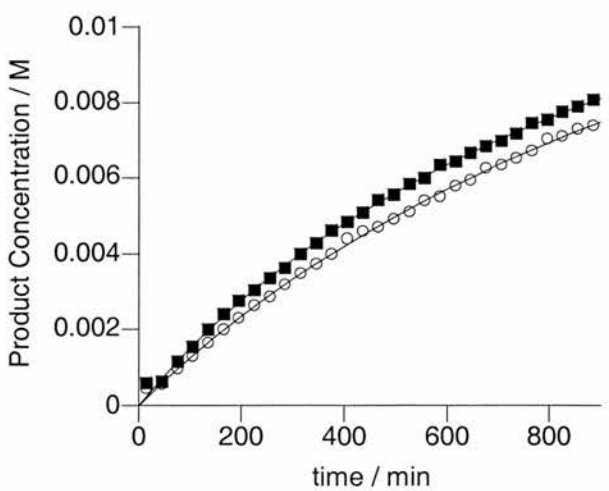

Figure 2.6.3.4 Kinetic data fitted to the reaction model for the cycloaddition of *N*-benzylidene-aniline *N*-oxide to *N*-phenylmaleimide. Closed squares represent the reaction in the presence of the receptor, open circles represent the background reaction.

The data collected alongside the calculated curves fitting the reaction data are displayed in **Figure 2.6.3.4.**

Table 2.6.3.5 Rate constants calculated for the cycloaddition reaction between *N*-benzylidene-aniline *N*-oxide and *N*-phenylmaleimide.

Background Reaction		**With Receptor 138**	
k_{uf} / M^{-1} min^{-1}	k_{ur} / M^{-1} min^{-1}	k_f / M^{-1} min^{-1}	k_r / M^{-1} min^{-1}
5.59 (± 0.02) x 10^{-4}	7 (± 0.3) x 10^{-10}	2.82 (± 0.03) x 10^{-3}	1.3 (± 0.3) x 10^{-6}

Table 2.6.3.5 provides a value of k_{cat}/k_{uncat} = 5.04 ± 0.08 for the reaction, this indicated that the reaction is accelerated by the receptor. This is not clearly observed in the reaction data however, as a result of the low association constant with receptor **138**.

2.6.4 Diels Alder Reaction

Diels-Alder cycloadditions were established to be non-polar in **Section 1.2** as no charged transition states form in the reaction coordinate. The cycloaddition is concerted and involves the rearrangement of π electrons to form two new σ bonds.

It had been previously established in **Table 2.6.1.1** that the cycloaddition reaction with cyclopentadiene did not proceed under the reaction conditions available, however, the cycloaddition between furan and *N*-phenylmaleimide **117** proceeded smoothly in the presence and absence of the receptor **138**.

The appearance of resonances attributable to the *endo* and *exo* cycloadducts is visible over the spectra recorded.

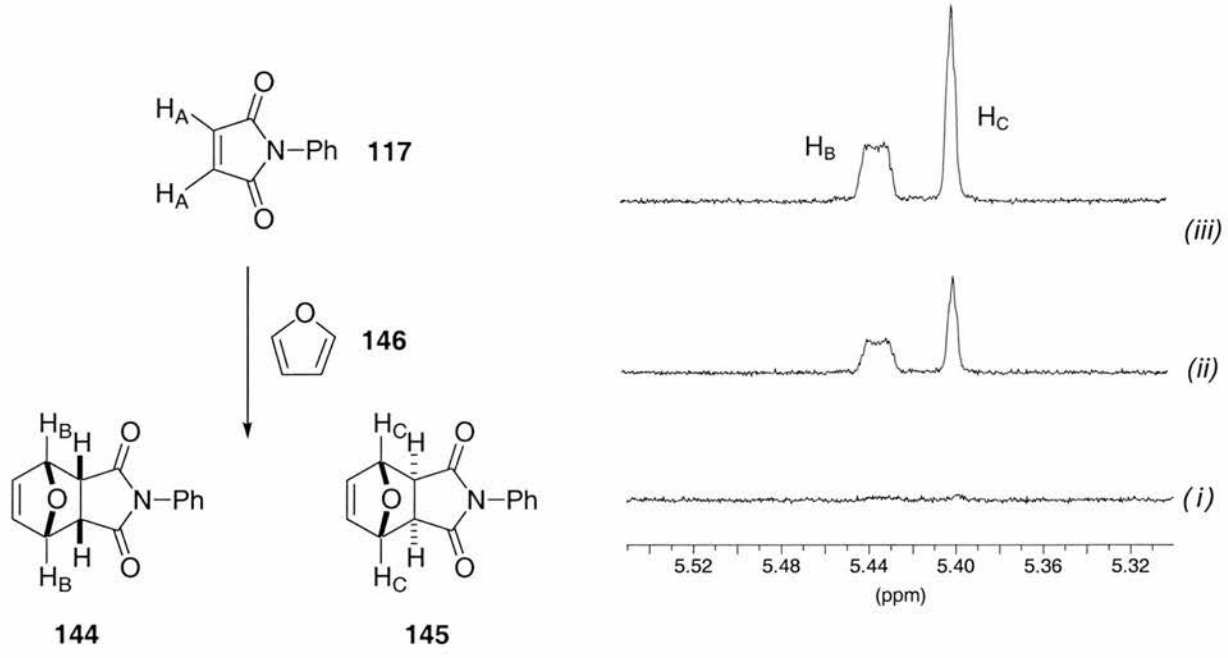

Figure 2.6.4.1 Partial 500 MHz ^{1}H NMR spectra recorded as solutions in $CDCl_3$ at 10 °C, displaying the appearance of resonances arising from cycloadducts over *(i)* 0, *(ii)* 510, *(iii)* 990 min. All spectra are displayed on the same scale. Protons A to E were deconvoluted to obtain the measurements in **Figure 2.6.4.2**.

Full experimental data were gathered on the reaction to investigate the process further. The resonances attributable to the maleimide protons were deconvoluted against appropriate resonances arising from the endo and exo cycloadducts. The relative areas were assessed as a percentage and the percentage completion was extracted.

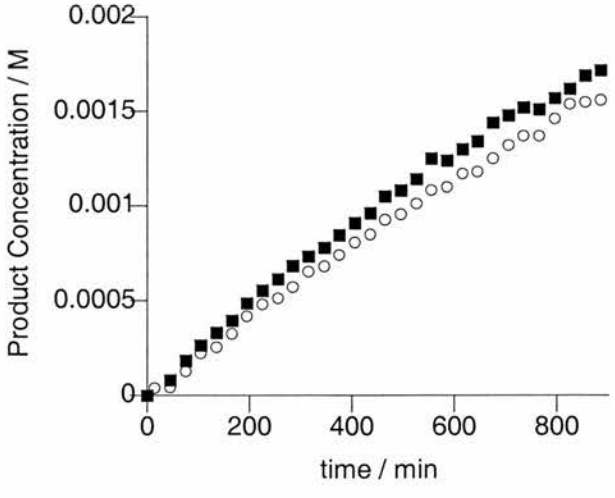

Figure 2.6.4.2 Kinetic data of the reaction between *N*-Phenylmalemide and furan. Open circles represent the background reaction, closed squares represent the reaction in the presence of one equivalent of receptor **138**.

Figure 2.6.4.2 shows the very low level of rate enhancement of the Diels-Alder reaction between furan and *N*-phenylmaleimide in the presence of receptor **138**.

The initial rates of reaction were again estimated for qualitative investigation by linear regression of the initial reaction data.

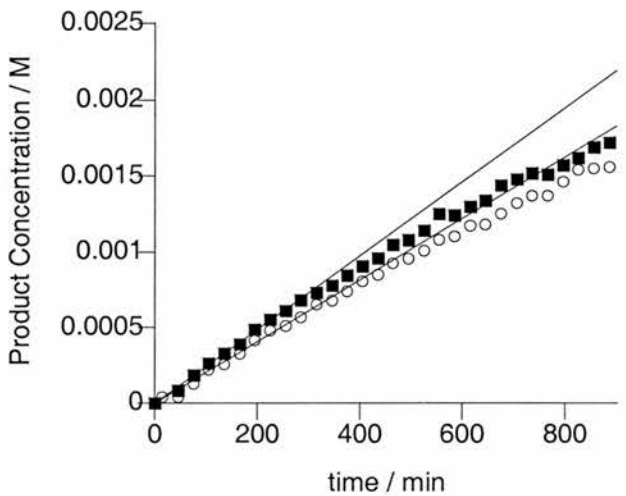

Figure 2.6.4.3 Graph displaying the projection of the initial rates of the cycloaddition between *N*-phenylmaleimide and furan as calculated by linear regression analysis of product concentration in the initial reaction.

Figure 2.6.4.3 shows the product concentration alongside the extrapolated initial rates calculated from linear regression of the initial reaction data. It is apparent that the tangential initial rate lines are divergent and so the rate may be accelerated by a greater degree than initially suggested by the reaction data. This will be investigated in greater detail by fitting of the kinetic data.

2.6.5 Fitting of Furan, *N*-Phenylmaleimide Diels Alder reaction

The reaction between furan and *N*-phenylmaleimide was fitted according to a model shown in **Figure 2.6.5.1**, similar to the model for the cycloaddition between *N*-phenylmaleimide and *N*-benzylidene-aniline *N*-oxide.

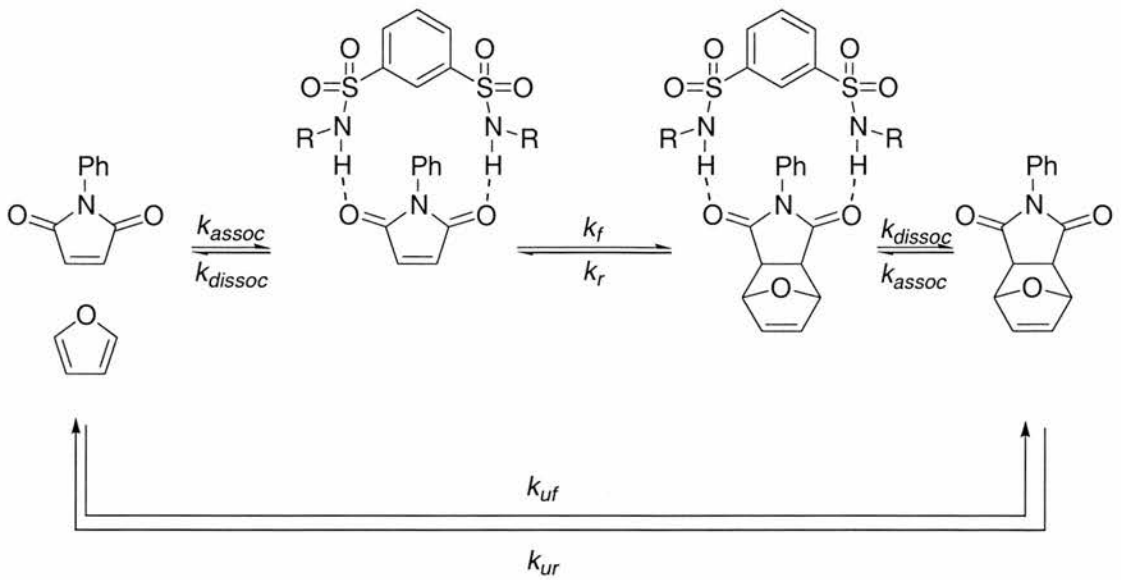

Figure 2.6.5.1 Representation of all the kinetic processes in the reaction between furan and *N*-Phenylmaleimide in the presence and absence of receptor **138**. R = $(CH_2)_3CH_3$, K_a = Association constant, k_f = forward rate constant, k_r = reverse rate constant, k_{uf} = forward background rate constant, k_{ur} reverse background rate constant K_d = Dissociation constant of the product.

A simple model was adopted for the furan maleimide Diels Alder reaction considering total product formation rather than the individual rates of *exo* and *endo* formation. The rate constants generated will therefore be a composite of the rates of formation of the *exo* and *endo* adducts.

Figure 2.6.5.2 Model of the [3+2] dipolar cycloaddition reaction between *N*-benzylidene-aniline *N*-oxide and *N*-phenylmaleimide. NPM represents *N*-phenylmaleimide, diene represents Furan, adduct represents the combined *endo* and *exo* adducts.

The rate constants calculated according to **Figure 2.6.5.2** were incorporated into the kinetic model in **Figure 2.6.5.3**. The association rate constants were set so $K_a = k_{assoc}/k_{dissoc}$ so only k_f and k_r were unknown rate constants in **Figure 2.6.5.3** and were calculated by non-linear curve fitting.

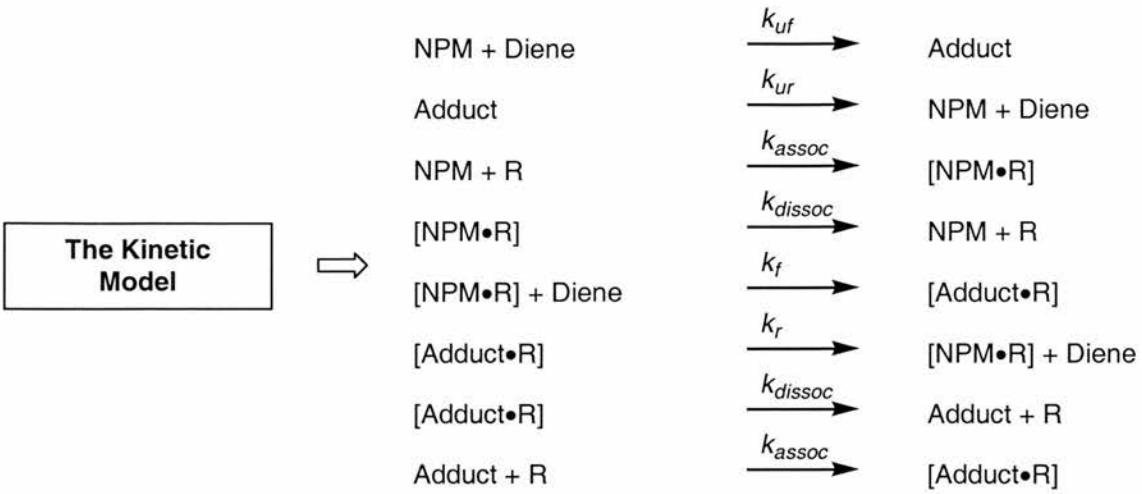

Figure 2.6.5.3 Kinetic model employed for the calculation of the composite rate constants, k_f and k_r. k_{uf} and k_{ur} are previously determined by the background reaction, k_{assoc} and k_{dissoc} are determined by K_a. NPM represents *N*-phenylmaleimide, Diene represents furan, adduct represents the combined *endo* and *exo* adducts, R represents receptor **138**.

The calculated fitted curves are depicted in **Figure 2.6.5.4** alongside the experimental reaction data.

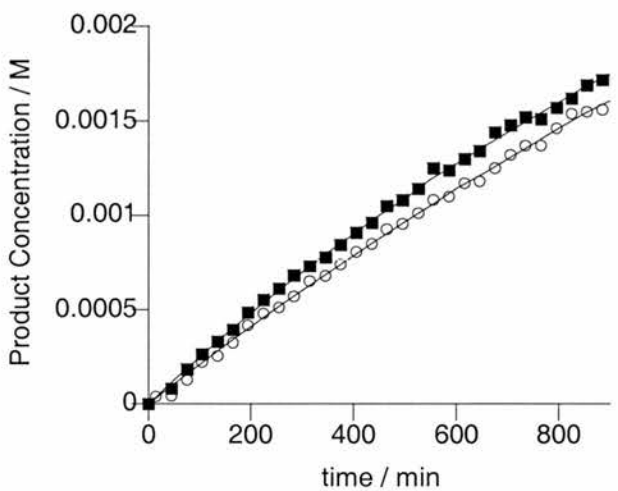

Figure 2.6.5.4 Kinetic data fitted to the reaction model for the cycloaddition of furan to *N*-phenylmaleimide. Closed squares represent the reaction in the presence of the receptor, open circles represent the background reaction.

The process of minimising the errors between the curve and the experimental data provided calculated solutions of k_f and k_r and these are listed in **Table 2.6.5.5** with the associated errors.

Table 2.6.5.5 Rate constants calculated for the Diels Alder reaction between furan and *N*-phenylmaleimide.

Background Reaction		With Receptor 138	
k_{uf} / M^{-1} min^{-1}	k_{ur} / M^{-1} min^{-1}	k_f / M^{-1} min^{-1}	k_r / M^{-1} min^{-1}
8.9 (± 0.1) x 10^{-5}	3.2 (± 0.5) x 10^{-6}	4.38 (± 0.08) x 10^{-4}	4.7 (± 0.3) x 10^{-5}

Table 2.6.5.5 provides a value of k_{cat}/k_{uncat} = 4.9 ± 0.2 for the reaction, this indicated that the reaction is accelerated by the receptor to a small degree. This isn't clearly observed in the reaction data however, as a result of the low association constant with receptor **138**.

2.7 Kavallieratos Receptor

Since the development of the sulfonamide receptor, Kavallieratos and co-workers[150] developed a receptor for the catalysis of imine formation possessing phenyl rather than butyl R groups. Previous work within the research group[151] had shown the receptors affinity for anions and on this basis the receptor was utilised as a catalyst.

Imine formation is acid catalysed and the sulfonamide receptor has a pK_a of approximately 8.05. If 100 mol % of 2-chlorophenol (pK_a = 8.49) is added the reaction is accelerated relative to the background rate, reaching approximately 7% completion in twenty minutes in comparison with the catalysed reaction reaching approximately 36% completion. It is apparent that some of the acceleration arises from simple acid catalysis. A large excess of the control compound 2-chlorophenol is used, however, it is important to note the reduced acidity of the control compound with respect to the receptor.

A tetrahedral intermediate is formed in the initial addition step of imine formation. If the initial addition of the amine to the aldehyde is rate limiting, imine formation can be considered a polar reaction. Stabilisation of the tetrahedral intermediate will lower the energies of the intermediate and the transition states leading to the formation and destruction of the zwitterionic intermediate. Use of a receptor similar to **138** for this catalysis is confirmation of the ease of catalysis of polar systems by hydrogen bond mediated systems.

2.8 Conclusions

Table 2.8.1 shows a summary of the k_{cat}/k_{uncat} values, comparing them reveals some interesting trends.

Table 2.8.1 Comparison of the relative kcat/kuncat values from the kinetic data concerning the reaction between *N*-phenylmaleimide and a range of other reactants.

Direct Addition	Michael Addition	[3+2] Dipolar Cycloaddition	Diels Alder
17.6 ± 0.3	22.1 ± 0.7	5.04 ± 0.08	4.9 ± 0.2

All the values of k_{cat}/k_{uncat} are higher than expected from inspection of the reaction data alone. This arises from the fact that ground state binding is too weak to measure under appropriate conditions. Comparing the levels of acceleration however, is informative. Lower levels of acceleration are observed when *N*-phenylmaleimide is subjected to cycloadditions in comparison to polar reactions. This is a significant result and confirms that for this synthetic receptor, polar reactions are more readily catalysed than non-polar.

It is not surprising that some catalysis is observed for cycloaddition reactions. On comparison of the bis-sulfonamide receptor **138** with the receptor **124** designed by Kelly and co-workers[139] there are certain similarities, (**Section 1.7.5**) the bisnitrophenol receptor would have a pK_a of approximately 7, the pK_a of a sulfonamide is approximately 8. Hydrogen bond strength is approximately proportional to acidity.[76] The major differences are in the flexibility of the two receptors and the adoption of a different binding mode for receptor **138**. However, the sulfonamide receptor **138** appears to be much less efficient at accelerating cycloaddition reactions.

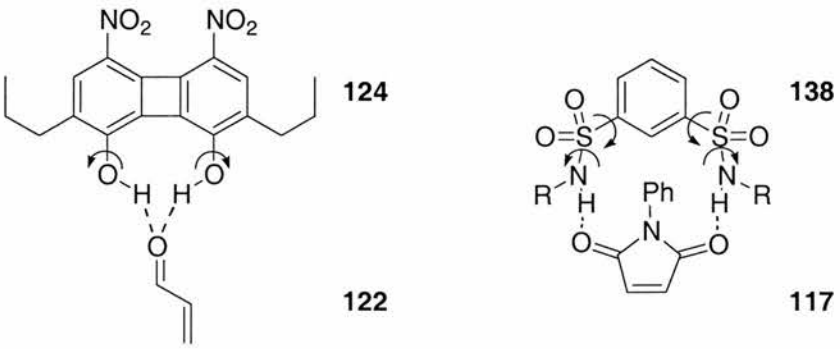

Figure 2.8.2 A comparison of Kelly's bis phenol receptor **124** with the bis-sulfonamide receptor **138**. Kelly's receptor requires the restriction of 2 rotors for binding, the bis-sulfonamide receptor requires the restriction of 4.

The greater the loss of entropy on binding, the lower the association constant. A receptor, which loses little entropy on binding, is termed "preorganised". In simple receptors, this can be readily assessed by observing the number of freely rotateable bonds (rotors) in the unbound receptor, which are restricted by binding.

Kelly's bisnitrophenol receptor **124** only possesses two rotors, which would significantly affect binding. The bis-sulfonamide receptor **138** has four. The resulting fall in association constant must prevent catalysis of non-polar reactions by this receptor. Indeed, no ground state binding could be observed. This suggests that if the association constant of the complex could be increased, our secondary aim of a truly broad-spectrum catalyst might be achievable.

It is important to note however, that Kelly and co-workers did not publish systematic kinetics of the appearance of cycloadducts as reported here. An unspecified excess of diene was used in each example, in some cases addition of the diene continued throughout the course of the reaction. Considering the reversibility of the Diels Alder reaction the calculated acceleration of the cycloaddition in **Table 2.6.5.5** may be more readily observed with an excess of furan in the reaction mixture. This is a consideration for the future should it be desired to utilise receptors of this type for synthetic catalytic means.

Despite the flexibility of the receptor, a definite difference is observed between the polar and less polar reactions. Significant rate acceleration is only observed for nucleophilic additions to the *N*-phenylmaleimide. This information provides evidence

towards the theory that polar reactions are more straightforward to catalyse than less polar cycloaddition reactions by hydrogen bonded systems.

3. Bisamide Receptor

3.1 The Design of a Receptor to Bind Maleimide

The initial receptor **138** designed in **Chapter 2** was calculated to bind to *N*-phenylmaleimide **117** in a two point hydrogen-bonding interaction to both carbonyl groups simultaneously but the association constant was too low to be measurable under standard conditions. It was decided to design a host guest complex, which would adopt a similar conformation, however, adopting a three point hydrogen-bonding interaction.

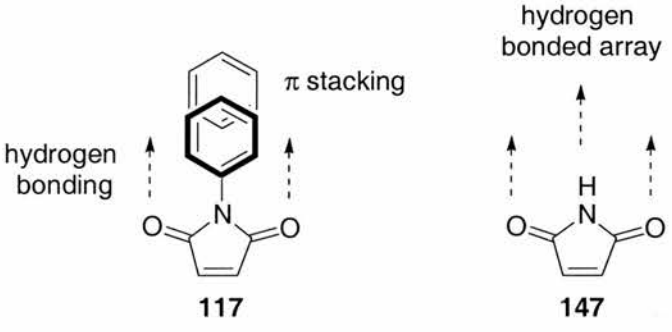

Figure 3.1.1 Development of the receptor design from a two point hydrogen bonding interaction with stabilisation by π stacking to a hydrogen bonded array.

Maleimide **147** was chosen as a suitable guest as it is capable of undergoing cycloadditions and polar addition reactions whilst avoiding problems with regioselectivity owing to its σ symmetry element. The structure of maleimide also possesses a convenient array of hydrogen bond donors and acceptors with which it can be bound.

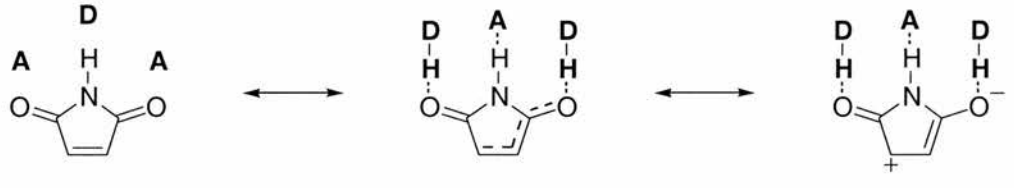

Figure 3.1.2 Maleimide has an array of three sites capable of hydrogen bonding in an acceptor (**A**), donor (**D**), acceptor (**A**) array. A **D A D** arrangement of groups capable of hydrogen bonding would be complimentary and would enable withdrawal of electron density or stabilisation of negative charges.

Binding of the acceptor, donor, acceptor pattern to a complimentary array would enable electron density to be withdrawn from maleimide or stabilisation of negative charges arising from addition reactions. This arrangement of hydrogen bond donors and acceptors is reminiscent of 2,6-diamidopyridines.

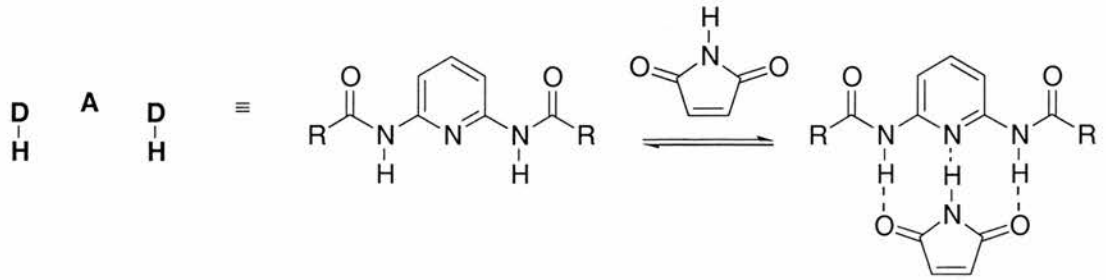

Figure 3.1.3 Representation of 2,6 diamidopyridines as receptors possessing a donor, acceptor, donor array of hydrogen bonding groups.

A simple bisamide receptor was therefore envisaged incorporating the simple hydrogen bonding design motif. Isovaleryl chloride was chosen as the activated acid starting material to incorporate solubilising groups to enable the receptor and receptor substrate complex to be soluble in common organic solvents.

3.2 Synthesis

3.2.1 Synthesis of Receptors and Controls

2,6-Diaminopyridine **147** was reacted with 2 equivalents of isovaleryl chloride in dry THF with dry Et_3N to yield the receptor **149** in 69% yield.

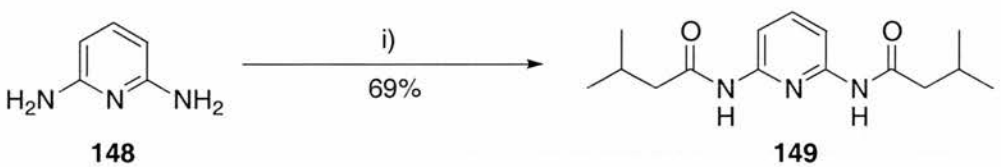

148 **149**

Scheme 3.2.1.1 i) Isovaleryl chloride, 2,6-diaminopyridine, Et_3N, dry THF

Control compounds were prepared by selective methylation. 2,6-Diaminopyridine **148** was reacted with paraformaldehyde in the presence of sodium methoxide. The bisimine was reduced *in situ* to produce **150** in 29% yield over the two synthetic steps. The methylated bisamine **150** was then reacted with isovaleryl chloride as before to form the first control **151** in a poor yield of 40%.

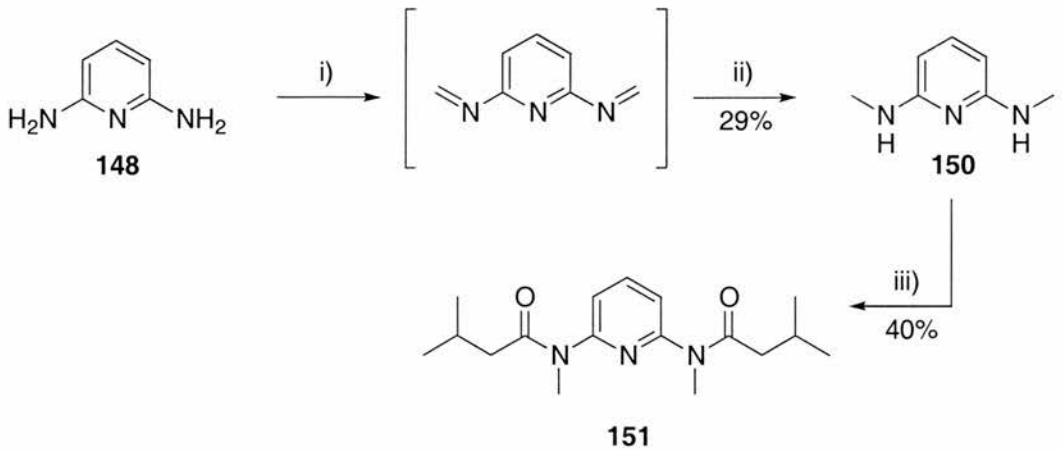

Scheme 3.2.1.2 i) Na, MeOH, paraformaldehyde 15h, r.t, 1h reflux, ii) $NaBH_4$, 1h, reflux, iii) 2 Eq Isovaleryl chloride, THF, Et_3N 15h, r.t.

A monomethylated control was also developed to cause a minor disturbance in the three-point hydrogen bonding interaction between maleimide and the host to investigate the effect upon the reactions investigated.

Three equivalents of 2,6 diaminopyridine were reacted with isovaleryl chloride to produce **152** efficiently in high yield. The product **152** was reacted with paraformaldehyde to produce the corresponding imine, which, once reduced *in situ*, yielded **153** in moderate yield, 59% over two synthetic steps. The resulting secondary amine was again reacted with isovaleryl chloride to produce **154** in high yield.

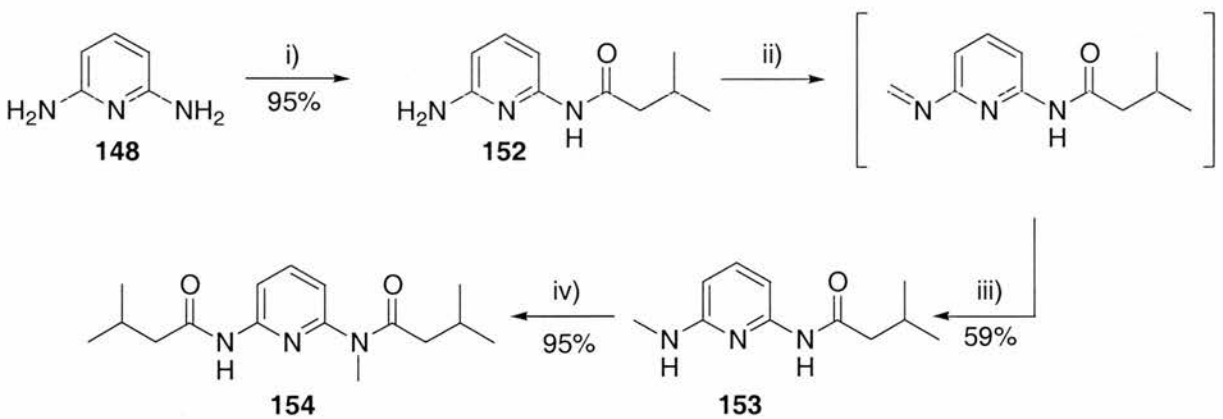

Scheme 3.2.1.3 i) 3 Eq 2,6 diaminopyridine, Isovaleryl chloride, THF, 15h, r.t., ii) Na, MeOH, paraformaldehyde 15h, r.t, 1h reflux, iii) $NaBH_4$, 1h,reflux, iv) Isovaleryl chloride, THF, Et_3N 15h, r.t.

3.2.2 Characterisation of Reaction Products

4-Fluorobenzylamine was added in stoichiometric quantities to maleimide in dichloromethane solvent and stirred at room temperature for seven days. The resulting adduct was isolated by column chromatography.

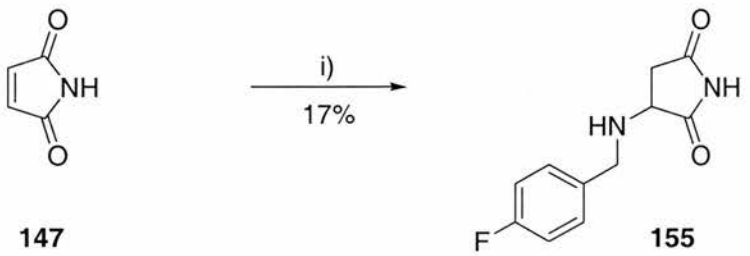

147 **155**

Scheme 3.2.2.1 i) 4-Fluorobenzylamine, CH_2Cl_2, r.t. 7 days.

N-Benzylidene-aniline *N*-oxide and maleimide were stirred at room temperature for 5 days, the diastereoisomeric products were isolated by column chromatography.

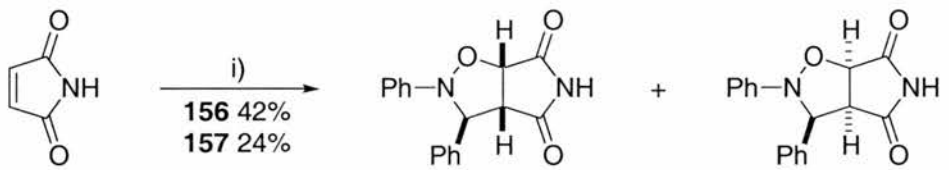

147 **156** **157**

Scheme 3.2.2.2 i) *N*-Benzylidene-aniline *N*-oxide, $CHCl_3$, r.t., 5 days.

Furan and maleimide were stirred at room temperature for 5 days until the reaction was judged to have reached maximum conversion.

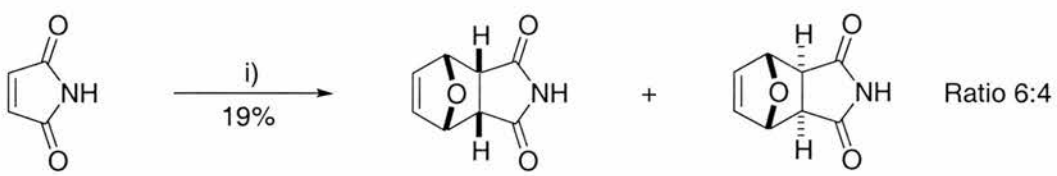

147 **158** **159**

Scheme 3.2.2.3 Furan, CH_2Cl_2, r.t., 48 hrs.

3.3 Solid State Structure

The conformation of the receptor was investigated in further detail by x-ray diffraction of a single crystal. Diamidopyridines possess a slight advantage over other systems as the dipoles created by the carbonyl groups are offset to a minor extent by the pyridine ring dipole. This renders the "closed" conformation in **Figure 3.3.1** highly unfavourable and decreases the energies of the "half open" and "open" conformations relative to a system lacking the central pyridine ring.

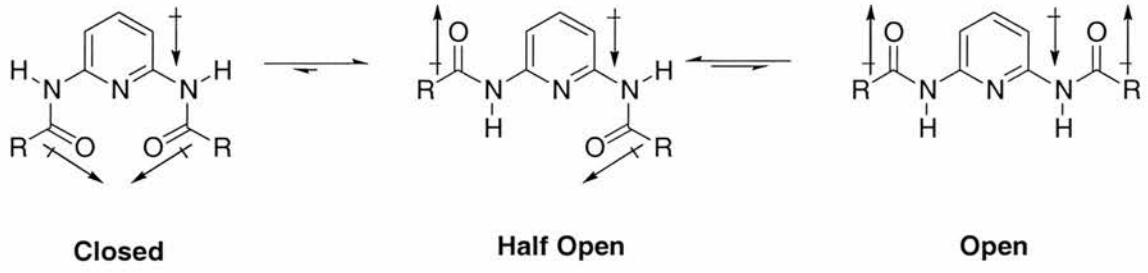

Figure 3.3.1 A representation of the conformational extremes possible for receptor **149**. The drive to avoid dipole alignment makes the "closed" conformation disfavoured.

Solid state and solution conformations may differ greatly from each other, however, solution of the crystal structure supported the argument that the open receptor conformation was of low enough energy to be accessible.

The crystal structure obtained is shown in **Figure 3.3.2** in an ORTEP representation.

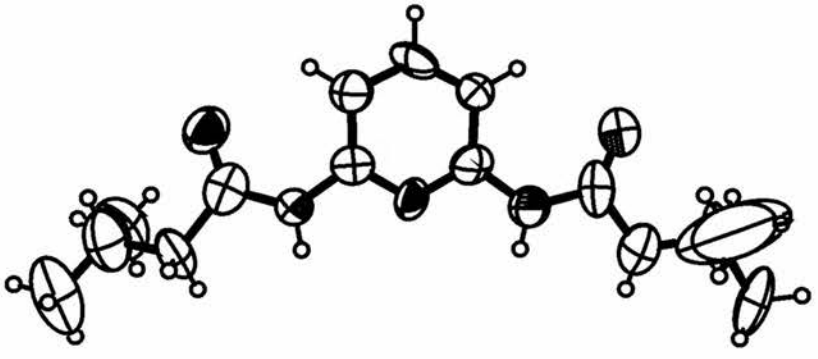

Figure 3.3.2 The crystal structure of receptor **149**, the structure is displayed as 50% thermal probability ellipsoids indicating the degree of disorder in the position of the atoms. As can be observed, the alkyl chains possess a high degree of disorder.

ORTEP diagrams display thermal motion in the crystal as ellipsoids. From **Figure 3.3.2**, it is clear that the alkyl chains are highly mobile, however, despite this

mobility the open amide – pyridine – amide motif is retained, ensuring the receptor is preorganised for binding with maleimide.

3.4 Computational Investigations

The binding modes of the complex were investigated using Macromodel simulations. The lowest energy structure calculated by Monte-Carlo technique with an AMBER* forcefield in simulated chloroform is depicted in **Figure 3.4.1**. Hydrogen bonds are present between each donor and acceptor group in the expected binding motif.

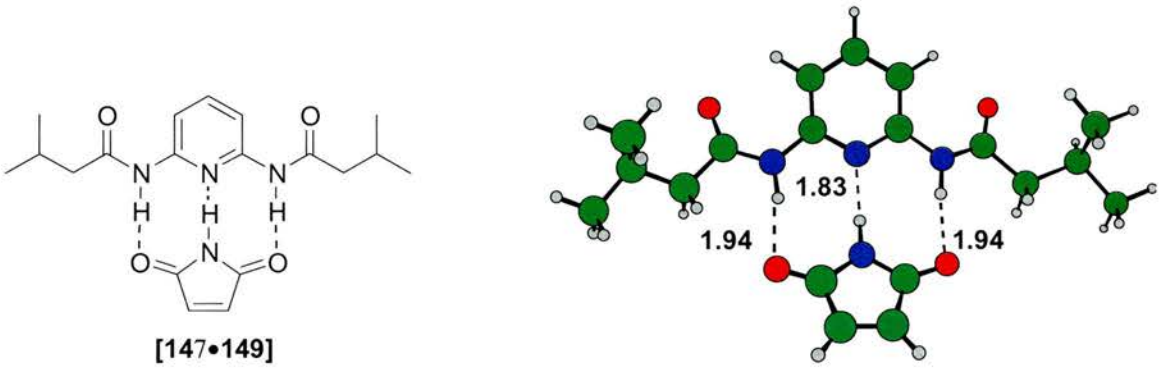

[147•149]

Figure 3.4.1 The lowest calculated energy structure for the complex between maleimide and receptor **149**. Structure was simulated in chloroform using the AMBER* forcefield. All intermolecular distances are in Å.

Other low energy structures were assessed and recorded using this technique. The resulting coconformations were filtered to include structures possessing energies less than 5 kJ mol^{-1} higher in energy than the global minimum.

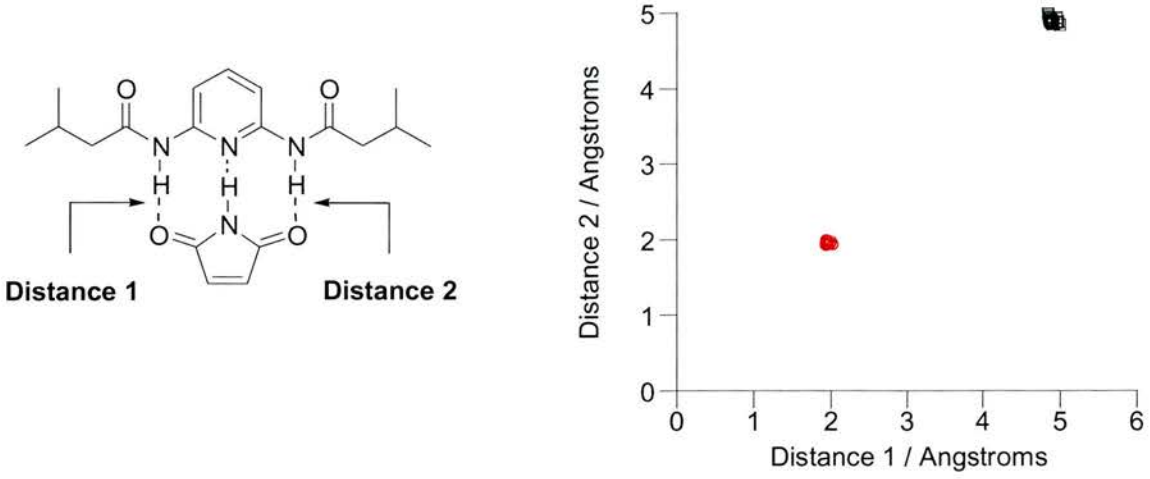

Figure 3.4.2 Scatter plot of the distances between the carbonyl groups and amide protons in the structures with energies + 5 kJ mol^{-1} relative to the Global minimum. All structures contain the central hydrogen bond. Red circles represent coconformations possessing both hydrogen bonds, and squares represent structures with no hydrogen bonding present.

All the structures observed had a short contact distance between the NH proton of the maleimide and the pyridyl nitrogen, the mean contact distance is 1.82 ± 0.01 Å (3 σ). The central hydrogen bond is conserved in all the structures and so only the other two hydrogen bonds are inspected in **Figure 3.4.2**.

From **Figure 3.4.2** it is apparent that there are two regions populated with structures, this indicates that two types of coconformation are populated in chloroform solution. In the first coconformation represented by red circles, all three hydrogen bonds are present; in the second type of coconformation, black squares, only one hydrogen bond is formed. By inspection, we would expect these two coconformations to readily interconvert.

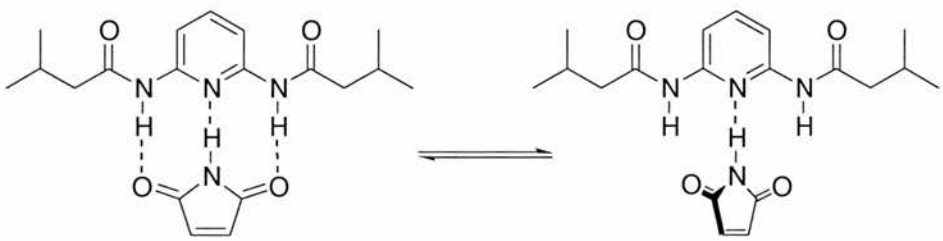

Figure 3.4.3 Representation of the ready interconversion of the two binding classes observed from the Monte-Carlo conformational search technique.

Including all coconformational structures with energies up to 20 kJ mol^{-1} higher than the most favoured coconformation provides additional data.

The 582 structures are represented in the scatter graph in **Figure 3.4.4**. This reveals that additional coconformations may be accessible under the reaction conditions.

A small number of the coconformations in this energy range have no central hydrogen bond however, most still possess this interaction. From **Figure 3.4.4** it is apparent that some coconformations exist with two hydrogen bonds in regions (triangles and diamonds) as well as the coconformations depicted in **Figure 3.4.3**, however, these are somewhat less stable.

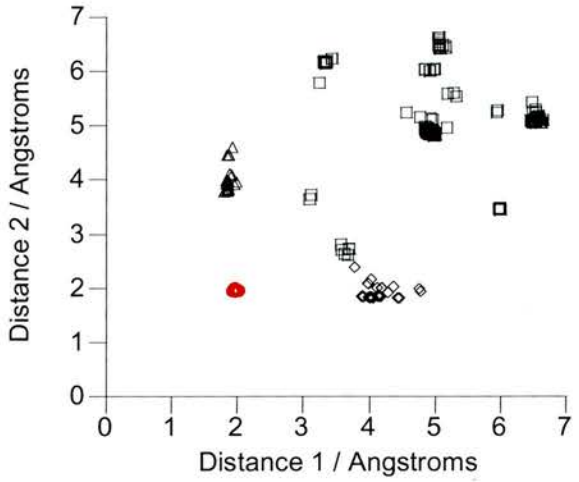

Figure 3.4.4 Scatter plot of the distances between the carbonyl groups and amide protons in the structures with energies + 20kJ mol^{-1} relative to the Global minimum. Most structures retain the central hydrogen bond Red circles represent coconformations possessing both hydrogen bonds, triangles and diamonds possess one hydrogen bond and squares represent structures with no hydrogen bonding present.

We predicted that binding to the receptor would have an effect on the ground state of the bound maleimide as well as potentially stabilising any negative charge in the transition state. Sustman and co-workers[144] have shown that a correlation exists between HOMO-LUMO separation and rate of reaction in Diels-Alder cycloadditions. Removing electron density from the dienophile will assist to lower the LUMO energy.

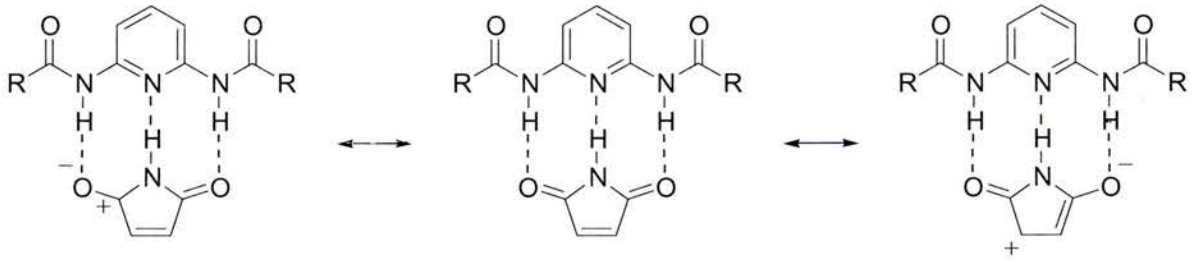

Figure 3.4.6 A representation of the resonance forms contributing to the overall structure. A mirror image of each zwitterionic resonance structure can also contribute to the overall electronic structure.

Binding to the receptor is expected to lower the LUMO energy by the promotion of two equivalent canonical forms with a positive charge at an alkene carbon and a negative charge located on the oxygen atom. These zwitterionic states would be more tightly bound to the receptor *via* charge reinforced hydrogen bonding. A more significant contribution of these resonance forms to the overall electronic structure will reduce the bond order of the alkene.

To quantitatively investigate the effects of binding a maleimide molecule **147** to receptor **149** the complex was modelled using electronic structure methods. The electron distribution on maleimide was modelled in the presence and absence of the receptor.

Electrostatic potential is portrayed in **Figure 3.4.7** as a spectrum. Areas at the blue end of the spectrum indicate region of partial positive charge. Areas with colouration from the red end of the spectrum have partial negative charges.

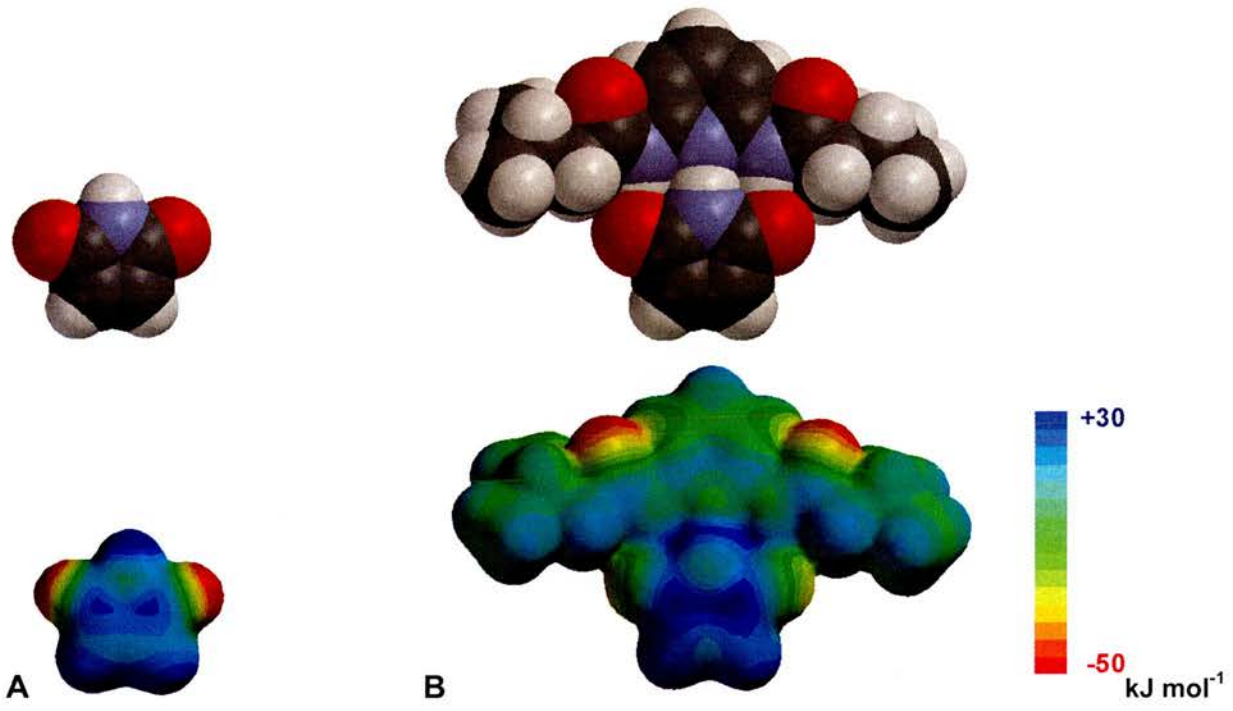

Figure 3.4.7 Electrostatic potential (ESP) diagrams. Blue areas indicate regions of δ+ charge, the red end of the spectrum represents δ- charge.

In the unbound state (**Figure 3.4.7, A**) the carbonyl groups are apparent by the dark blue colouration of the carbon and the red of the δ- oxygen atom. The alkene carbons are a pale blue. On binding to the receptor, all four carbon atoms are a darker blue colour indicating electron withdrawal on complexation. Removal of electron density from the alkene moiety would lower the LUMO energy, which would accelerate Diels Alder reactions and most [3+2] dipolar cycloadditions. Removal of electron density would also result in increased electrophilicity in all four carbon atoms, which may be reflected in reactivity.

3.5 Investigation of Association

As previously stated in **Section 2.4**, NMR spectroscopy has been frequently employed as a method to assess binding in supramolecular systems.[148] Initial assessments can be made by preparing equimolar solutions in an appropriate solvent and observing chemical shift changes.

Table 3.5.1 Initial investigation of association between maleimide and host **149** or controls **151** or **154**. The sign of the chemical shift change relates to the equation $\Delta\delta$ = [host•guest] - free (host or guest).

Receptor	$\Delta\delta$ NH Receptor	$\Delta\delta$ NH Maleimide
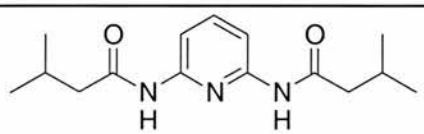 **149**	+ 0.47 ppm	+ 0.48 ppm
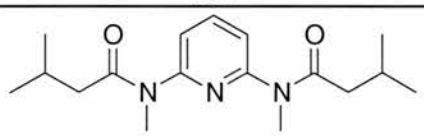 **151**	N.A.	+ 0.16 ppm
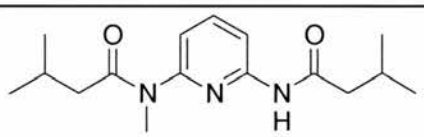 **154**	+ 0.05 ppm	+ 0.10 ppm

Solutions of each receptor and maleimide were prepared separately at 10 mM and in 1:1 ratios. Changes in the chemical shift of each of the NH resonances were noted and recorded in **Table 3.5.1**. In this manner, it was clear that hydrogen bonding was largely or completely absent from the control complexes and large chemical shift changes were observed for the host **149** maleimide **147** complex. Separate resonances for bound and unbound species were, however, not observed indicating the complex was in fast exchange between the bound and unbound species.

In the titration experiment the concentration of the receptor or the substrate in solution is held constant. The concentration of the other species is then varied over a wide concentration range. The resulting chemical shifts on the constant species are evaluated. Plotting the chemical shift change against concentration of the species, which was varied in the experiment and subsequent non-linear curve fitting, can be used to extract K_d and subsequently K_a. **Appendix 1**

Association constants are temperature dependent. Le Chatelier's principle states that a system at equilibrium, when subjected to a perturbation, responds in a way that tends to minimise its effect. Therefore, for all exergonic processes at equilibrium, increased temperature favours the reactants and as the temperature is raised, a hydrogen bond would be weakened. The effect on the association constant (an equilibrium constant) can be expressed mathematically by the following equation.

$$\ln K = -\frac{\Delta G}{RT}$$

Equation 3.5.2 The relation of equilibrium constant K to free energy G.

The **Equation 3.5.2** demonstrates that for favourable, exergonic processes (those where $\Delta G < 0$) lnK is positive but falls in value as the temperature T rises. This in turn results in a fall in equilibrium constant K and the equilibrium would favour the staring materials over products. In the same manner, an association constant will fall accordingly favouring the unbound species over the bound complex.

The association between receptor **149** and maleimide **147** was assessed by 500 MHz ^{1}H NMR spectroscopic titration.[148] The concentration of maleimide was held constant at 10 mM and the concentration of the host was varied from 5 mM to 200 mM. From this the association constant (K_a) and free energy of association (ΔG) at 10 °C and 50 °C may be calculated. The association constants were calculated for temperatures appropriate to the reactions followed by NMR spectroscopy in **Section 3.6**.

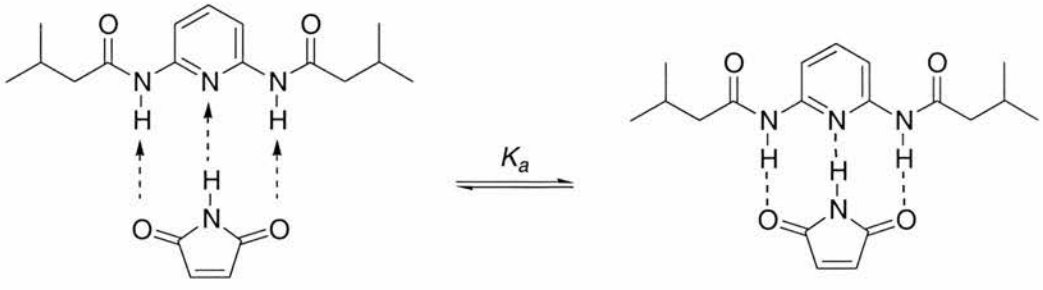

Figure 3.5.3 The equilibrium investigated to calculate the association constant.

The initial experiments examining a mixture of one equivalent of host and guest indicated the equilibrium between the complex and free species depicted in **Figure 3.5.3** was in fast exchange. The equilibrium between the free and bound species was faster than the NMR timescale. This was apparent by the absence of

two resonances relating to the bound and unbound species and the appearance of a resonance relating to a weighted average of the bound and unbound substrate resonances.

The maleimide NH resonance was chosen as a suitable probe to follow the association over both temperatures, this was chosen as a result of the large change in chemical shift observed on the addition of the host.

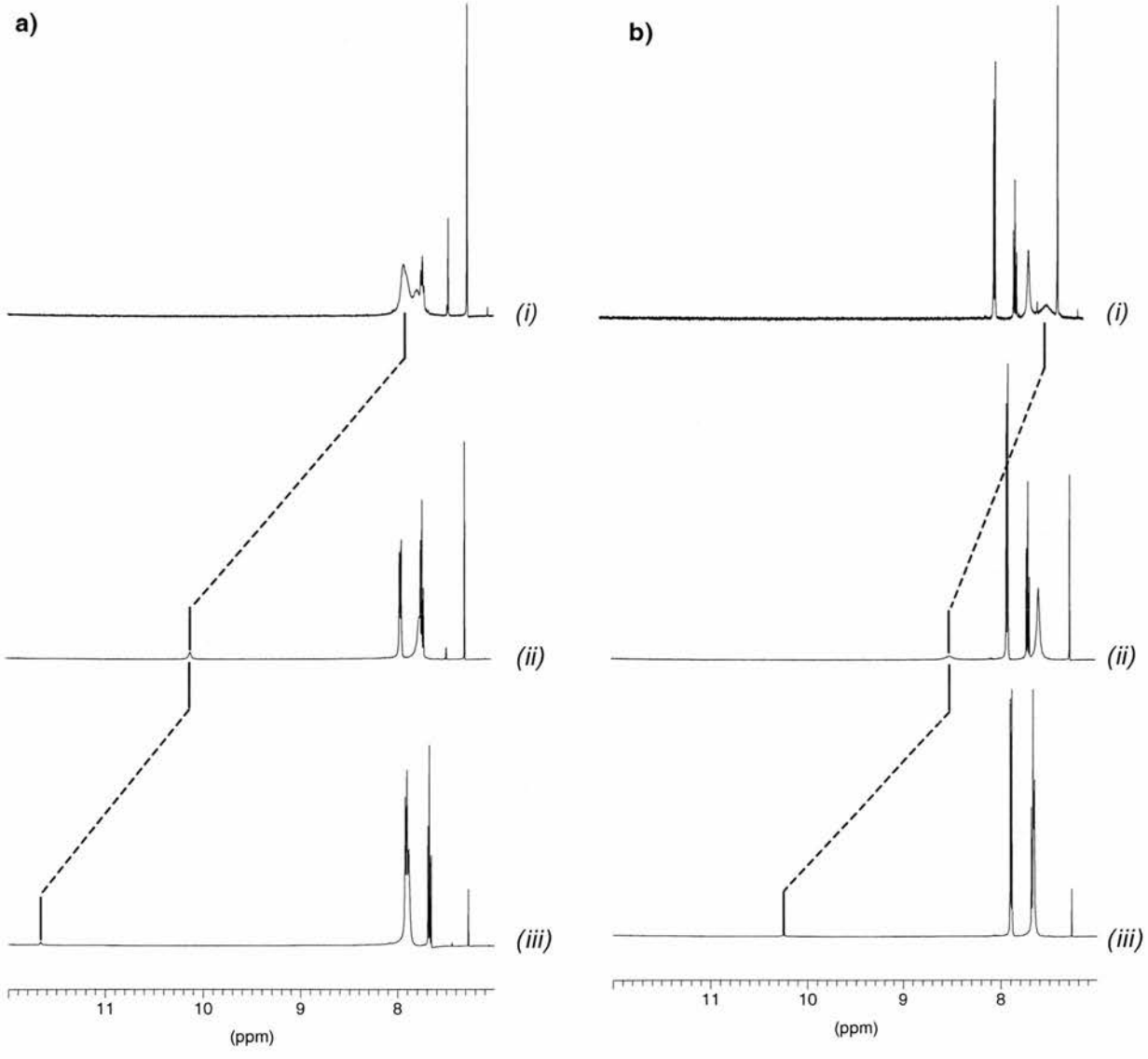

Figure 3.5.4 Partial 500MHz ^{1}H NMR spectra of the movement of the NH maleimide resonance with increasing host concentration, all samples contained 10mM maleimide solution. **a)** 10°C, **b)** 50°C, i) 5 mM receptor **149**, ii) 40 mM receptor **149**, iii) 200 mM receptor **149**.

Problems associated with the concentration dependence of chemical shifts for amides were avoided by adopting the titration methodology of calculating association constants and holding the maleimide concentration constant in all the measurements taken.

Partial 500 MHz ^{1}H NMR spectra are displayed in **Figure 3.5.4** showing the changes in the chemical shift of the maleimide NH resonance on the addition of host.

The data was initially recorded at 283 K and fitted using a non-linear curve fitting program, WineqnNMR.[152] The calculated fit was as follows.

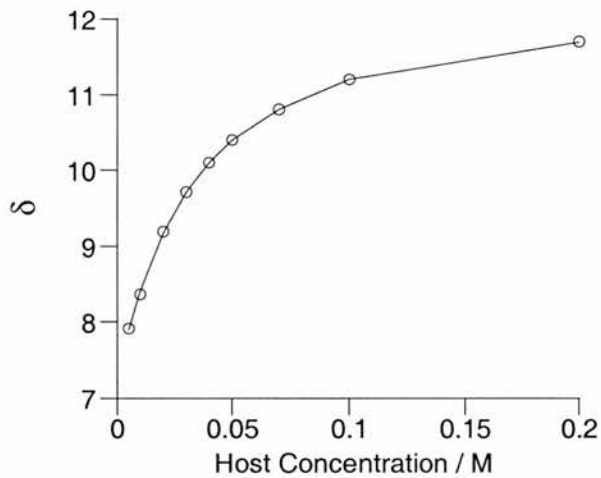

Figure 3.5.4 A graph of the chemical shift changes against host concentration for a series of solutions with varying host concentrations in $CDCl_3$ and 10 mM of maleimide with the calculated best fit. The experimental data is represented by open circles.

The calculated fit for the complex at 283K was 38 ± 1 M^{-1}. This corresponds to a free energy of association of –8.55 ± 0.06 kJ mol^{-1}.

The same process was completed for the receptor **149** maleimide complex at 323 K. The experimental data with the calculated fit are shown in **Figure 3.5.5**.

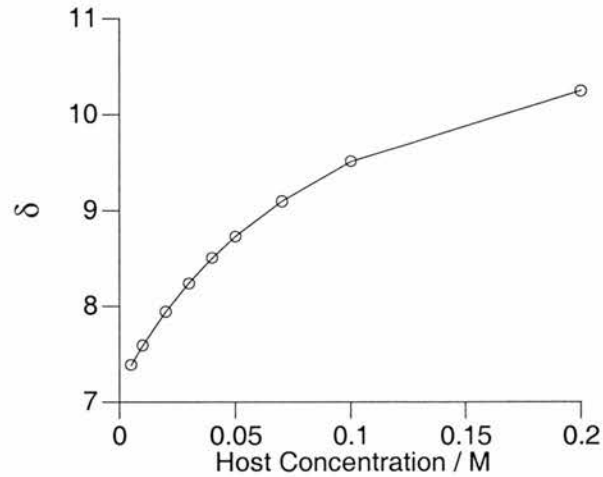

Figure 3.5.5 Data for the calculation of the equilibrium constant between maleimide and bisamide **149** at 50 °C with the calculated fitted curve. Open circles represent experimental data.

Fitting the data depicted in **Figure 3.5.5** indicated that the association constant at 323 K was 11.7 ± 0.1 M^{-1}. This relates to a free energy of association of -6.61 ± 0.03 kJ mol^{-1} at 323 K.

The association constant was found to be low at both temperatures, this however, is unsurprising.[153] The bisamide receptor **149** was designed with a complimentary array of recognition sites; however, it has been shown by Murray and co-workers that linear recognition sites are subject to "secondary hydrogen bonding interactions".[154]

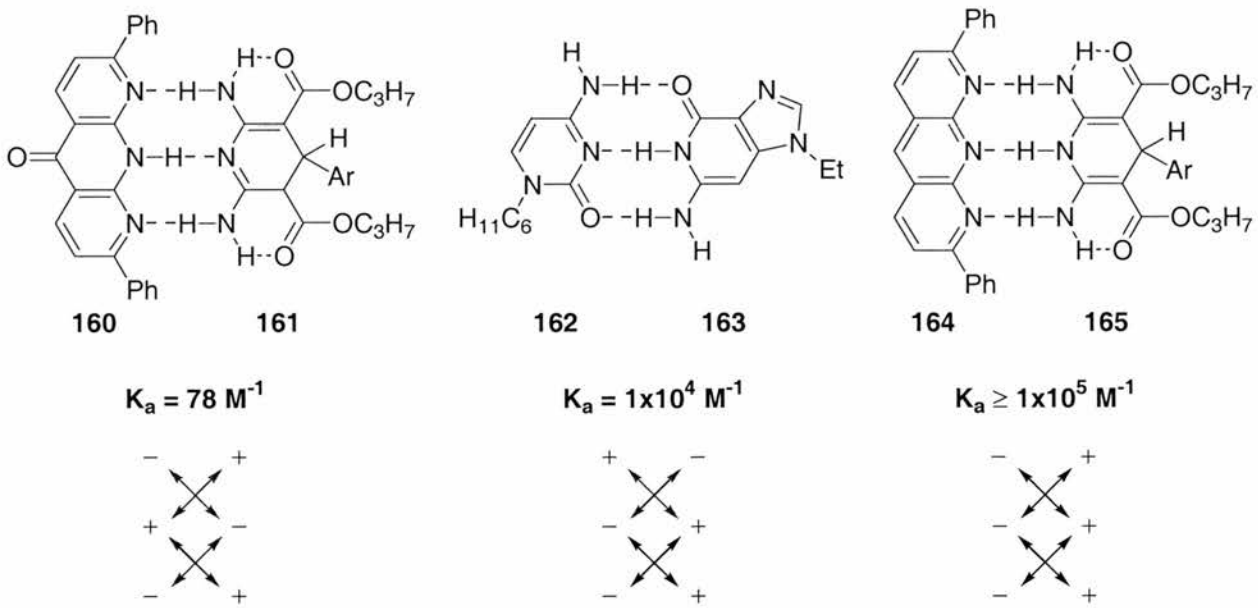

Figure3.5.6 Examples of the association between secondary hydrogen bonding interactions and binding constant. Hydrogen bond donors are represented as (+), hydrogen bond acceptors as (-). Red lines symbolise repulsive interactions, and black lines indicate attractive interactions.

If the donors and acceptors are considered as positive and negative charges respectively, diagonal attractive or repulsive interactions are present see **Figure 3.5.6**. Murray and co-workers observed that association constants were highest when these secondary interactions were attractive and lowest when the interactions would be deleterious. It was also displayed that the changes in the binding constants were significant. The difference between the association constants for the acceptor donor acceptor (ADA) and the AAA arrays is more than 1000 fold despite the similarity between the individual hydrogen bonding interactions, indeed the only significant difference which can be identified is the relative positioning of the donors and acceptors in the complexes.

Binding is also hampered by the shape of maleimide itself. Although sp^2 hybridised, the internal bond angles of maleimide are approximately 109°, constrained by the five-membered ring. This results in the carbonyl groups on the maleimide exterior splaying outwards from the perfect 120° geometry. As a result, any hydrogen bonds formed would depart from the idealised 180° geometry between the acceptor lone pair and the covalent bond to the donor hydrogen atom. Although only a small change would be observed, this will place strain on the weak hydrogen bonds.

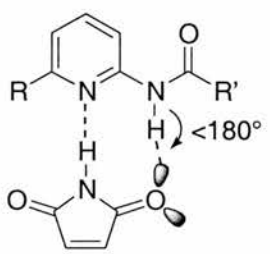

Figure 3.5.7 Representation of the hydrogen bonding between maleimide and one of the amide groups in the receptor. The internal angles in the maleimide force non-ideal hydrogen bonding.

Despite this difficulty, binding between receptor **149** and maleimide albeit weak, is confirmed by ^{1}H NMR spectroscopy.

3.6 Reaction Analysis

It was important to show that these receptors were not only capable of accelerating different polarities of reaction, but also use conditions in which fair comparisons could

be made between different reactions. It was decided that all reactions should be performed in deuterated chloroform, which is capable of dissolving a wide range of reactants and receptors. All reactions were performed with 1:1 ratio of reactants, each at 20 mM owing to the low solubility of maleimide in all but polar solvents. In reactions where a receptor was added, an arbitrary amount, 100 mol%, was always used. Prior to running full kinetics, conditions were evaluated by running small experiments in deuterated chloroform and assessing the percentage completion over a fixed time.

3.7 Assessing Polar Reactions

A number of polar reactions were attempted over sixteen hour periods.

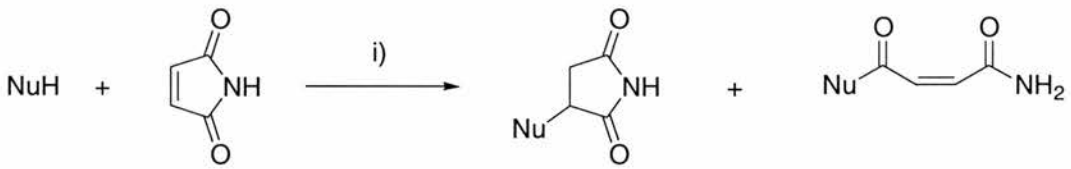

Scheme 3.7.1 i) Nucleophile and maleimide each at 20 mM concentration in $CDCl_3$ in the presence or absence of 20 mM of receptor **149**. Other conditions are as indicated in **Table 3.6.2.**

Table 3.7.2 A table of the percentage completion observed in each reaction by 300 MHz ^{1}H NMR spectroscopy of the crude mixture after 16 hours.

Nucleophile	Temperature	With Receptor % Completion		Without Receptor % Completion	
		Direct	Michael	Direct	Michael
$H_{15}C_7$–SH	0	0	0	0	0
	50	0	0	0	0
F–C$_6$H$_4$–CH$_2$NH$_2$	0	0	0	0	0
	50	0	4	0	8

As observed in **Table 3.6.2**, heptane thiol did not react with maleimide. It is irrelevant that the receptor **149** fails to accelerate this reactions because, with no background rate of adduct formation, there is no point of comparison. A catalyst can only accelerate a reaction towards equilibrium, in some cases, the background rate of reaction is so slow as to appear to be non-existent. Reaction with

4-fluorobenzylamine, the most nucleophilic reactant is evident, however, and this will be taken forward and investigated in further detail.

3.7.1 Assessing the Kinetics of the Addition of 4-Fluorobenzylamine to Maleimide

Full kinetic measurements were performed on this polar reaction and the appearance of the conjugate addition product was followed by 500 MHz ^{1}H NMR spectroscopy. Product concentration was evaluated from spectra recorded at half hourly intervals by deconvolution methodology. The percentage of conversion to product was calculated by comparing the areas of the starting material and product resonances.

Figure 3.7.1.1 shows the appearance of the conjugate adduct over the sixteen hours of spectra. No resonances arising from direct addition were observed.

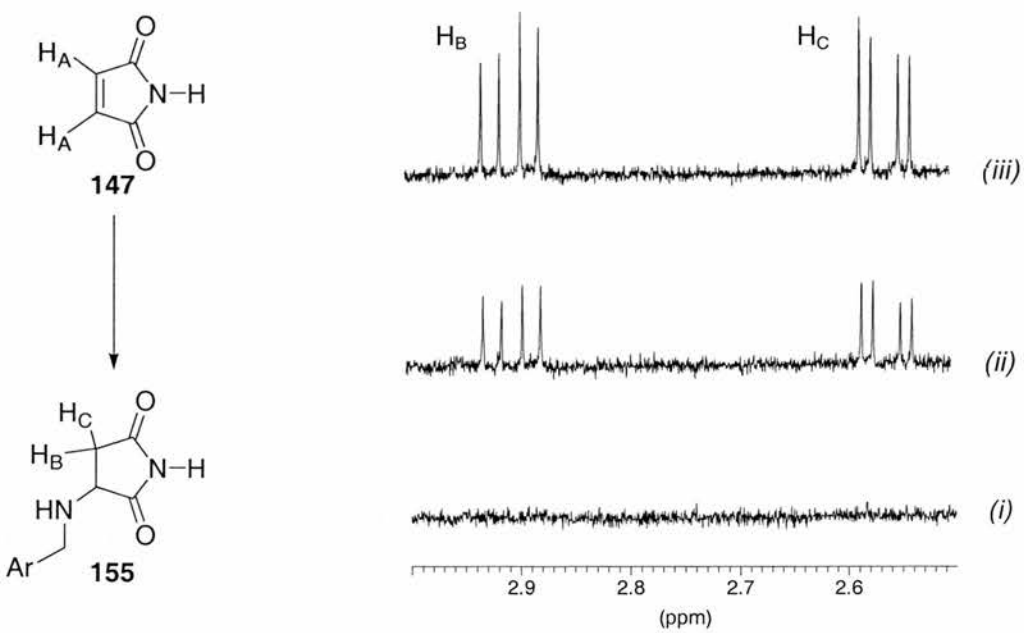

Figure 3.7.1.1 Partial 500MHz ^{1}H NMR spectra displaying the appearance of the conjugate adduct over *(i)* 0 mins, *(ii)* 510 mins and *(iii)* 990 mins. The resonances arise from the new methylene group created as a result of saturating the double bond.

The resulting data was plotted to produce a graph displaying the appearance of the conjugate adduct **155** against time.

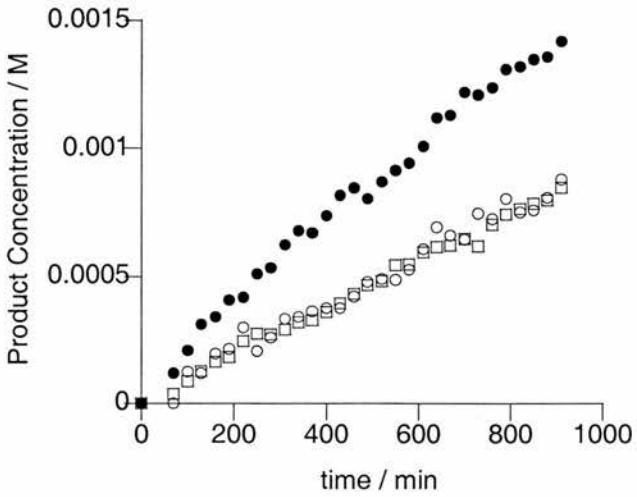

Figure 3.7.1.2 Kinetic data of the Michael addition reaction between maleimide and 4-fluorobenzylamine. Open circles represent the reaction in the presence of Monomethylated control **154**, open squares are the reaction in the absence of additives and closed circles represent the reaction in the presence of receptor **149**.

A simple comparison of estimates of the initial rates of reaction can be made from linear regression of the initial data points and subsequent extrapolation.

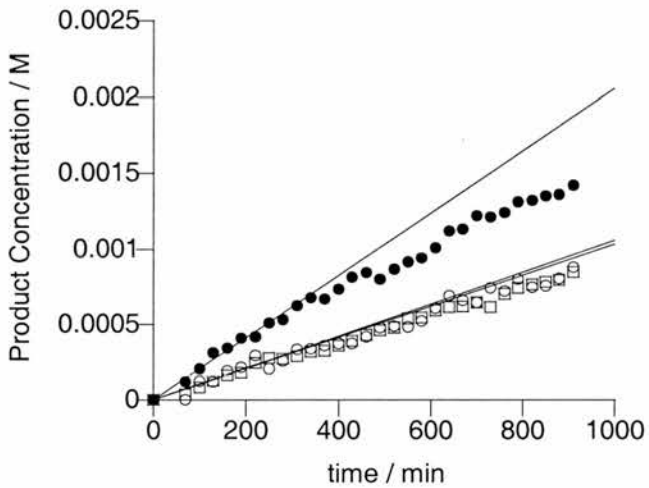

Figure 3.7.1.3 Graph displaying the projection of the initial rates of the Michael addition reaction between maleimide and 4-fluorobenzylamine as calculated by linear regression analysis of product concentration in the initial reaction.

Comparison of the estimated initial rate lines provides further confirmation that the partially methylated control compound **154** does not have any significant affect on the reactivity of maleimide with 4-fluorobenzylamine. The initial rate in the presence of the receptor, however, can be seen to be significantly higher and this will be investigated by systematic rate constant calculation in **Section 3.6.2**.

It is interesting to note however, that only the Michael addition product is observed and accelerated. This is in contrast to the previous polar additions in **Section 2.5.1** and may appear to be counterintuitive. The explanation lies in the breakdown of the tetrahedral intermediate.

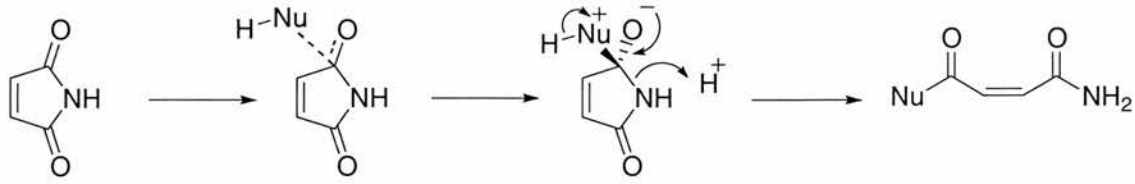

Figure 3.7.1.4 Reaction mechanism for the direct addition of a nucleophile to maleimide.

On the collapse of the tetrahedral intermediate, the carbon nitrogen bond must be broken. The leaving group in this example is a primary amide, rather than the secondary phenyl amide in the former example. The negative charge in the phenyl amide can be delocalised through the benzene ring improving the leaving group ability. So as addition to the maleimide carbonyl is reversible, the nucleophile is extruded rather than the amide.

It might be expected, however, that the receptor would still accelerate the direct addition in preference to the conjugate addition. As previously discussed in **Figure 2.5.1.6** the carbonyl group is more electrophilic than the alkene and is made even more so by binding to a hydrogen binding receptor. However, the design of this receptor in particular makes direct addition unlikely. As previously mentioned, the direct addition proceeds via a tetrahedral intermediate. The addition transition state is usually rate determining and so to effect acceleration, it is this species which needs to be bound and stabilised.

Addition of the nucleophile to maleimide would force the carbonyl group out of plane with the three hydrogen bonded array in the receptor. If the receptor reoriented to adjust to the conformational change in the guest, only a maximum of two of the three hydrogen bonds could be maintained.

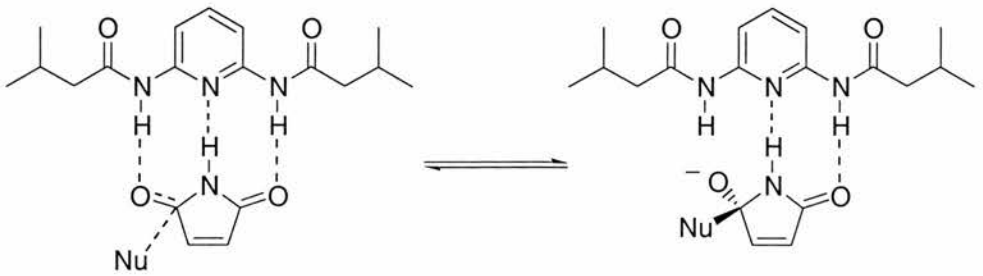

Figure 3.7.1.5 Representation of how direct nucleophilic addition would disrupt host – guest binding.

Conjugate addition provides all the benefits of charge-reinforced hydrogen bonding but without the disruption to the complex and so the less polar conjugate addition reaction is accelerated over direct addition.

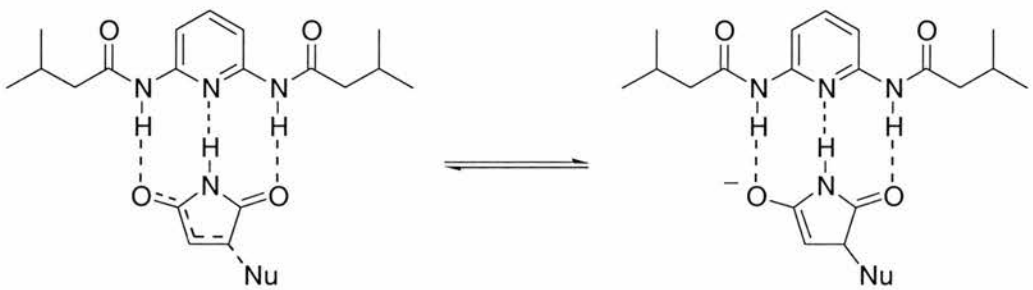

Figure 3.7.1.6 Conjugate addition to maleimide enables all three hydrogen bonds to be maintained.

If **Figure 3.7.1.5** and **Figure 3.7.1.6** are compared, it can be seen that only conjugate addition enables the conservation of all three hydrogen bonds. Charge reinforced hydrogen bonding in the transition state is also possible without conformational change.

3.7.2 Fitting the 4-Fluorobenzylamine Addition to Maleimide

The sets of kinetic data were fitted using a series of models developed in SimFit. All three reactions retain the binding characteristics present in the starting material in the product, as a result, the models developed for the reactions are very similar. As an example, the models written to represent the addition of 4-fluorobenzylamine to maleimide in the presence and absence of receptor are presented. The overall model for the background and accelerated reaction is presented in **Figure 3.6.2.1**.

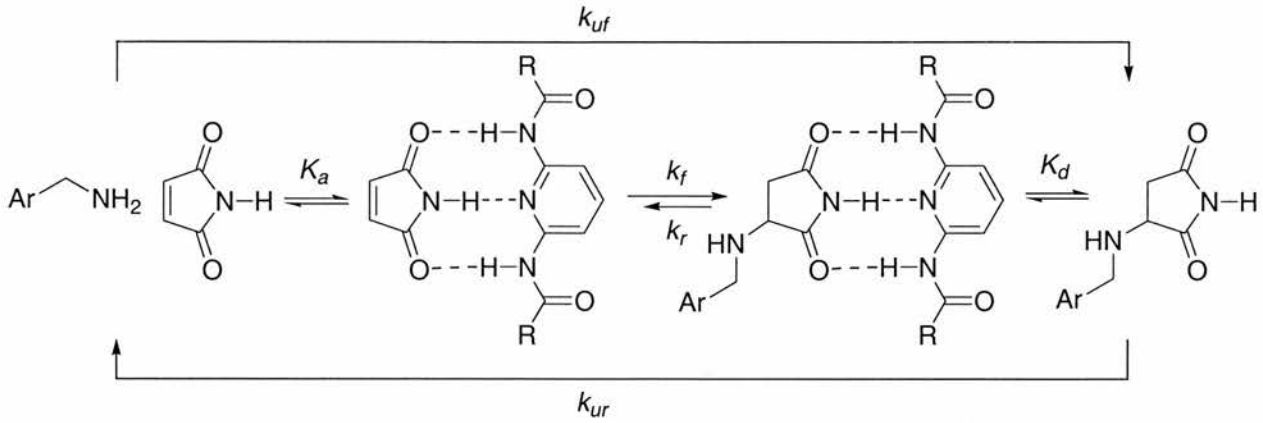

Figure 3.7.2.1 Representation of all the kinetic processes in the reaction between 4-fluorobenzylamine and maleimide in the presence and absence of receptor **149**. Ar = 4-fluorophenyl, R = $CH_2CH(CH_3)_2$, K_a = Association constant, k_f = forward rate constant, k_r = reverse rate constant, k_{uf} = forward background rate constant, k_{ur} reverse background rate constant

The background reaction consists of the addition of 4-fluorobenzylamine **119** to maleimide **147**. The reaction is assumed to be reversible and this reversibility was incorporated into the model shown in **Figure 3.6.2.1**. Therefore, for the background reaction the only process defined was the reversible reaction under consideration.

Figure 3.7.2.2 Model of the addition reaction between maleimide and 4-fluorobenzylamine. Amine represents 4-fluorobenzylamine and Adduct represents the conjugate adduct product.

The product formation against time was supplied to the model in the form of an input file and the initial concentrations of A and B were specified as 0.02 M. Approximations were made for the forward and reverse rate constants and the amount by which these rate constants could be varied was also specified. These values were refined after the initial calculation.

The addition of a receptor to the reaction increases the number of processes in the reaction mixture. Four equilibria can be identified, background reaction, association of host and guest, the reaction in the presence of the receptor and dissociation of the product from receptor. This series of equilibria is detailed in **Figure 3.7.2.3.**

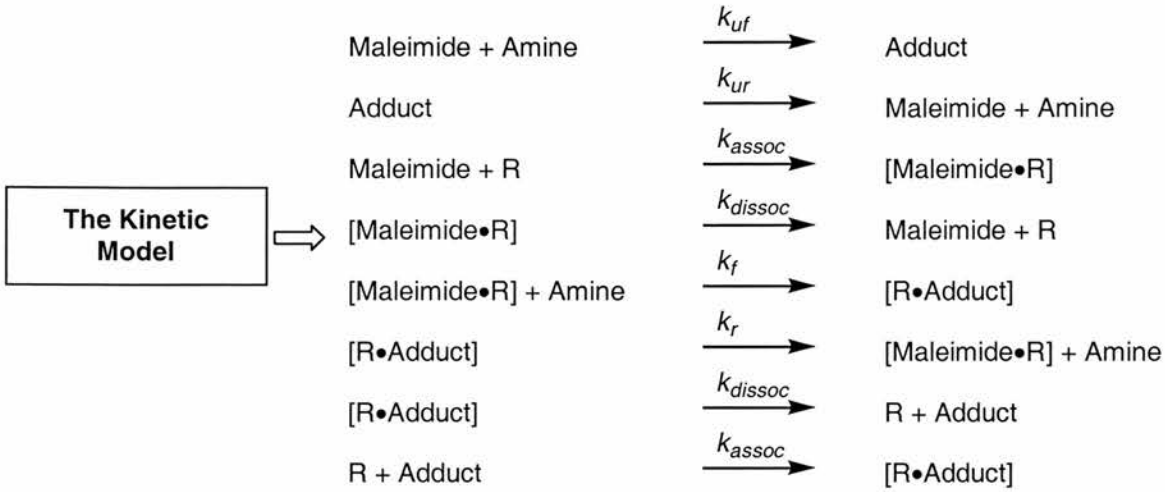

Figure 3.7.2.3 The four equilibria representing the reaction between maleimide and 4-fluorobenzylamine and the background reaction. Amine represents 4-fluorobenzylamine, Adduct represents the conjugate adduct product and Receptor represents receptor **149**.

The initial reaction rates had already been established by the previous model. The association constant between maleimide and receptor **149** had been previously calculated experimentally. It was previously noted that the rate of the equilibration of the reactive complex was extremely fast, faster than the NMR timescale. The rate constants for the association between **147** and **149** were set so that the forward rate was at the limit of diffusion control and was calculated so that $K_a = k_{assoc}/k_{dissoc}$. In this manner, the rate of formation of the complex would not be a limiting factor when calculating the unknown rate constants. The dissociation of product from receptor was assumed to be the same as the inverse of the association constant. This is a fair assumption because the site of modification of the substrate does not affect the hydrogen bonded array. Some extra complex stabilisation may be obtained by withdrawal of electron density from the double bond so the actual dissociation constant may be higher than the model represents, however, the difference is expected to be negligible.

The fitted data are displayed in **Figure 3.6.2.4** with the curve calculated to fit the raw experimental figures.

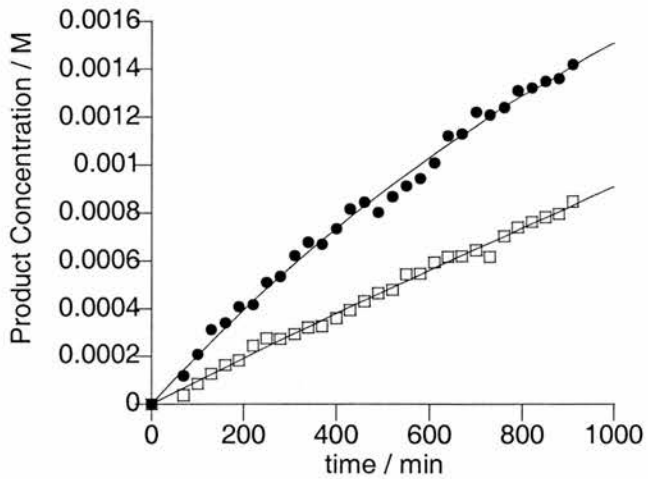

Figure 3.7.2.4 Kinetic data fitted to the reaction model for the Michael addition of 4-fluorobenzylamine to maleimide. Closed circles represent the reaction in the presence of the receptor **149**, open squares represent the background reaction.

The rate constants calculated by the fitting of the data were as follows.

Table 3.7.2.5 Rate constants calculated from the kinetic data collated for the Michael Addition between amine **119** and maleimide **147**.

Background Reaction		**With Receptor** 149	
k_{uf} / M^{-1} min^{-1}	k_{ur} / M^{-1} min^{-1}	k_f / M^{-1} min^{-1}	k_r / M^{-1} min^{-1}
4.08 (± 0.09) x 10^{-5}	8 (± 9) x 10^{-7}	4.4 (± 0.1) x 10^{-4}	4.5 (± 0.5) x 10^{-5}

The value observed for k_f/k_{uf} = 10.8 ± 0.5 (also termed k_{cat}/k_{uncat}) indicates that the reaction rate is accelerated in the presence of receptor **149**.

3.8 Assessing Cycloaddition Reactions

Maleimide was again subjected to reaction in the presence and absence of host **149** with one equivalent of a dipole or diene. **Table 3.8.1** details the results observed.

Table 3.8.1 Percentage completions observed for each reaction with maleimide. Measurements were taken by 300 MHz ^{1}H NMR spectrometry and assessed by deconvolution.

Nucleophile	Temperature °C	With Receptor % Completion	Without Receptor % Completion
	0	0	0
	50	0	0
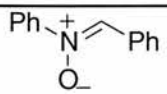	10	20	10
	40	8	6

Only dimerisation of cyclopentadiene was observed over the concentration and temperature range available so this diene was rejected.

3.8.1 Reaction of Maleimide with *N*-Benzylidene-aniline *N*-oxide[155]

The reaction between *N*-benzylidene-aniline *N*-oxide and maleimide was investigated in further detail. The receptor is not expected to induce diastereoselectivity and so the total product was recorded rather than the ratio of *endo* to *exo*.

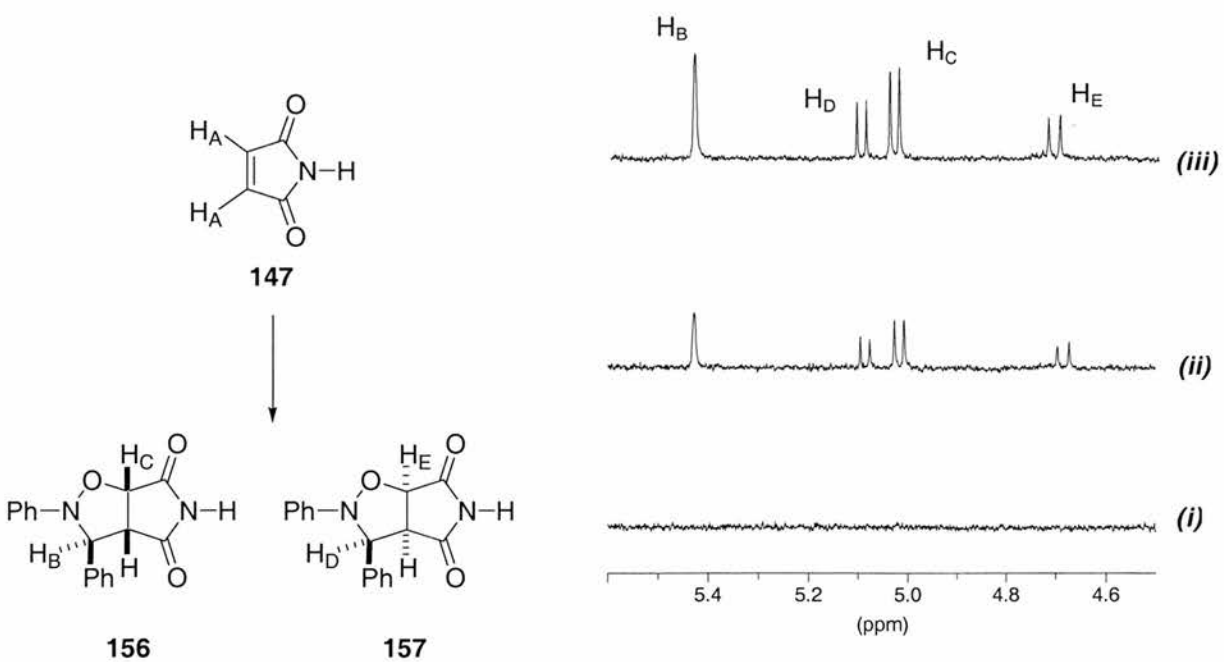

Figure 3.8.1.1 Appearance of the *endo* and *exo* products as observed by 500MHz ^{1}H NMR spectroscopy over *(i)* 0, *(ii)* 510 and *(iii)* 990 min.

Figure 3.8.1.1 displays the appearance of the two products as observed in the first, sixteenth and thirty-first spectra. These resonances were deconvoluted to establish the percentage completion.

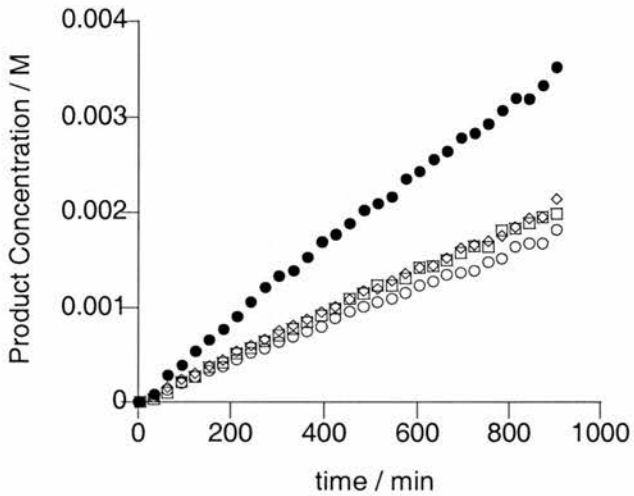

Figure 3.8.1.2 Kinetic data from the reaction between *N*-benzylidene-aniline *N*-oxide and maleimide. Open circles represent the reaction in the presence of Monomethylated control **154**, open squares are the reaction in the absence of additives and closed circles represent the reaction in the presence of receptor **149**.

Again the initial rates of reaction were superimposed on to the rate data.

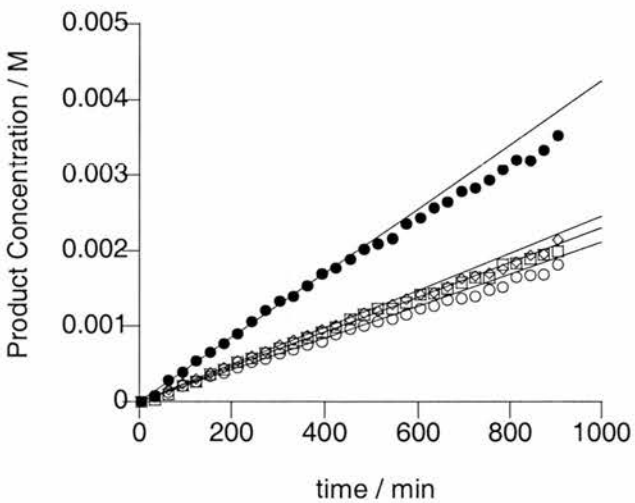

Figure 3.8.1.3 Graph displaying the projection of the initial rates of the cycloaddition between maleimide and *N*-benzylidene-aniline *N*-oxide as calculated by linear regression analysis of product concentration in the initial reaction.

As can be observed in **Figures 3.8.1.2** and **3.8.1.3** there appears to be a significant effect on the addition of receptor **149**. Comparison of the reaction data and the

estimated initial rate data also suggests that the background reaction and the two control reactions proceed at approximately the same rate.

3.8.2 Fitting of the Kinetic Data

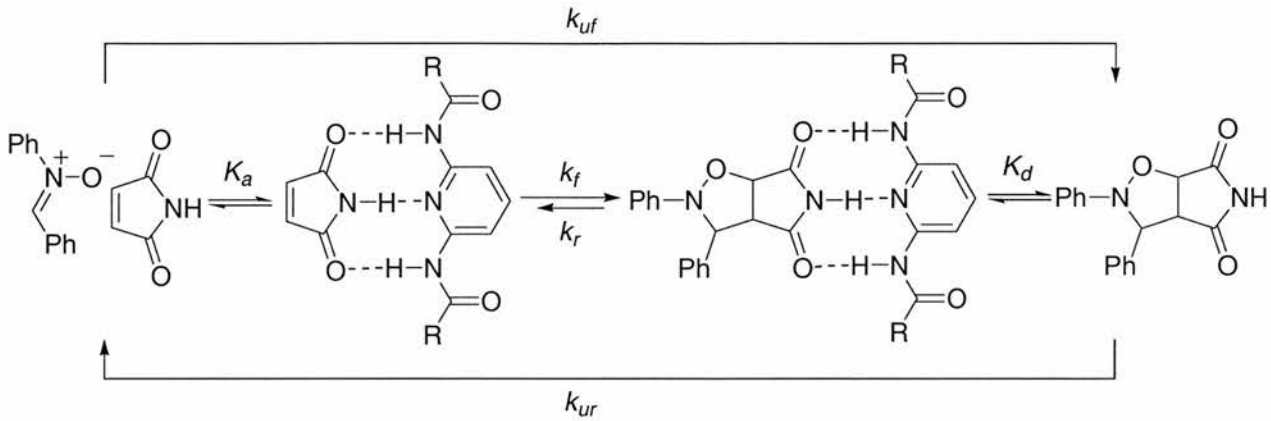

Figure 3.8.2.1 Representation of all the kinetic processes in the reaction between *N*-benzylidene-aniline *N*-oxide and maleimide in the presence and absence of receptor **149**. R = $CH_2CH(CH_3)_2$, K_a = Association constant, k_f = forward rate constant, k_r = reverse rate constant, k_{uf} = forward background rate constant, k_{ur} reverse background rate constant *Kd* = dissociation constant

As can be seen in **Figure 3.8.2.1** the control reactions all have a similar rate of reaction, whereas, the reaction in the presence of receptor **149** is significantly faster.

Figure 3.8.2.2 Model of the addition reaction between maleimide and *N*-benzylidene-aniline *N*-oxide. Dipole represents *N*-benzylidene-aniline *N*-oxide and Adduct represents the cycloadduct.

The *N*-benzylidene-aniline *N*-oxide maleimide cycloaddition was modelled according to **Figures 3.8.2.1** and **3.8.2.2** and a series of rate equations for the reaction mixture in the presence of the receptor **149** were evaluated in a similar manner to the 4-fluorobenzylamine maleimide addition as shown in **Figure 3.8.2.3**.

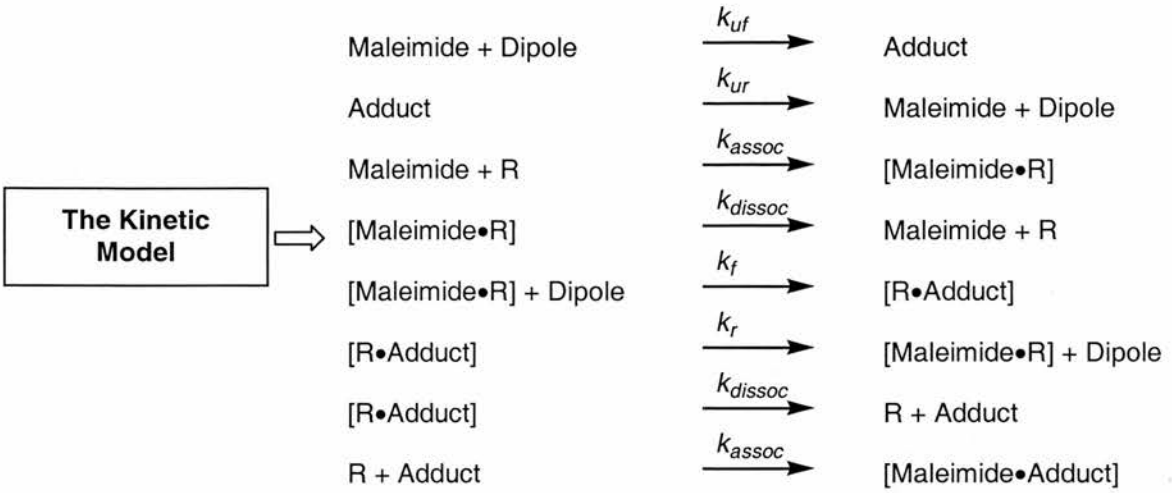

Figure 3.8.2.3 The four equilibria representing the reaction between maleimide and *N*-benzylidene-aniline *N*-oxide and the background reaction. Dipole represents *N*-benzylidene-aniline *N*-oxide, Adduct represents the cycloadduct product and Receptor represents receptor **149**.

From this kinetic model and previously established rates calculated from the background reaction and the binding equilibria, it was possible to evaluate the forward and reverse rates of the *N*-benzylidene-aniline *N*-oxide, maleimide equilibrium.

The experimental data with the calculated best fit are presented in **Figure 3.8.2.3**

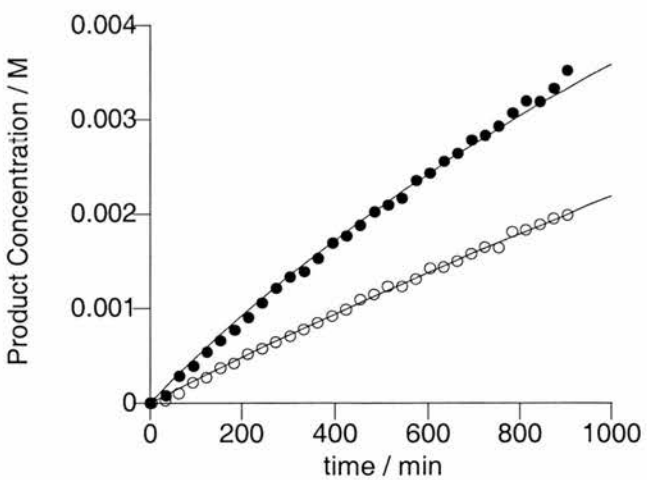

Figure 3.8.2.4 Kinetic data fitted to the reaction model for the cycloaddition of *N*-benzylidene-aniline *N*-oxide to maleimide. Closed circles represent the reaction in the presence of the receptor **149**, open squares represent the background reaction.

As can be observed in **Figure 3.8.2.5**, the experimental data and calculated curve are a good fit, indicating the validity of the kinetic model proposed in **Figure 3.8.2.3**.

Rate constants for the forward and reverse reactions were evaluated from the fit and are listed in **Table 3.8.2.5**.

Table 3.8.2.5 Kinetic parameters calculated for the [3+2] dipolar cycloaddition between Maleimide **147** and Diphenyl Nitrone.

Background Reaction		With Receptor 149	
k_{uf} / M^{-1} min^{-1}	k_{ur} / M^{-1} min^{-1}	k_f / M^{-1} min^{-1}	k_r / M^{-1} min^{-1}
1.03 (± 0.01) x 10^{-4}	2 (± 3) x 10^{-10}	7.30 (± 0.07) x 10^{-4}	7 (± 7) x 10^{-7}

The kinetic data provides a value of k_{cat}/k_{uncat} = 7.09 ± 0.14. This is slightly raised from the published value, but this is accounted for by the recalculation of binding constant.

3.8.3 Furan Maleimide Diels Alder Reaction

Furan was chosen as a less polar reactant to compare with the nitrone and amine additions. The reaction was followed in the same manner as previously described by ^{1}H NMR spectroscopy in the absence of receptors, in the presence of one equivalent of bisamide receptor **149** and with monomethylated control **154**.

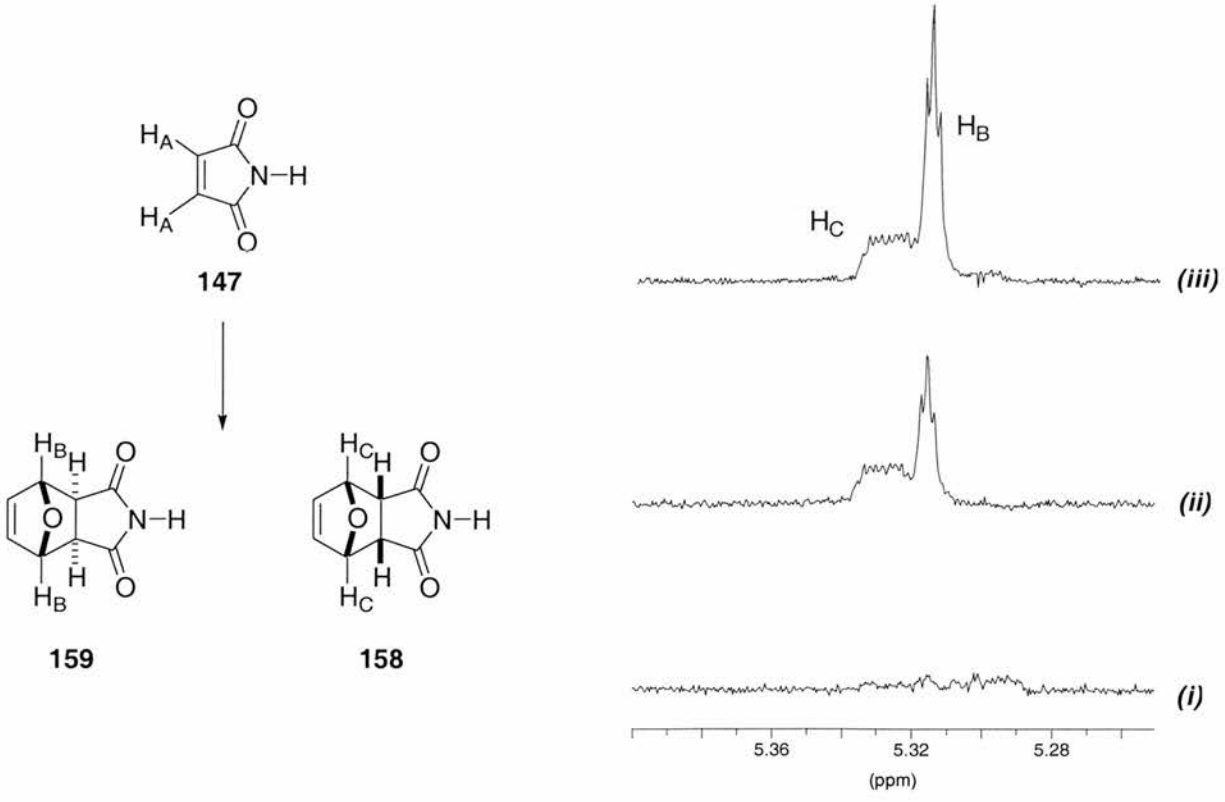

Figure 3.8.3.1 Partial 500MHz ^{1}H NMR spectra showing the appearance of resonances relating to the formation of the *endo* and *exo* adducts over the 15 hours of reaction, *(i)* 30 minutes, *(ii)* 480 minutes, *(iii)* 930 minutes.

The proton resonanaces attributed to the 6-5 fused ring system were deconvoluted. As these resonances were multiplets, several curves were used to model the resonance shape. The difference spectrum was used as a gauge to assess whether the deconvoluted peak shape was an accurate model for the actual spectrum. The errors in the collection of the reaction data will, however, be increased.

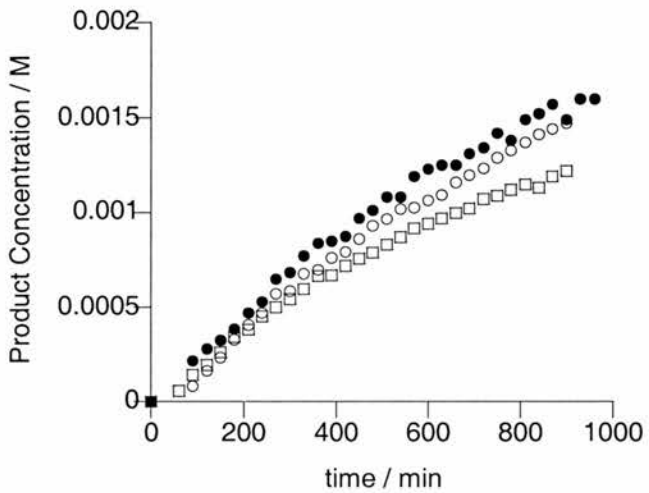

Figure 3.8.2.4 Kinetic data from the reaction between furan and maleimide. Open circles represent the reaction in the presence of Monomethylated control **154**, open squares are the reaction in the absence of additives and closed circles represent the reaction in the presence of receptor **149**.

Figure 3.8.2.4 shows a very small amount of acceleration is evident on the addition of receptor **149**.

As previously, initial rates were estimated, comparison of these initial rates however, is not informative, this may arise from poor initial deconvolution as a result of low product concentration. Importantly, the initial rates of the reaction in the presence of receptor **149**, control **154** and the background reaction do not appear to differ widely. This suggests that the Diels Alder reaction is not significantly accelerated, however, if correct, it will be apparent in the kinetic data calculated later.

3.8.4 Fitting of the Diels Alder reaction between Furan and Maleimide

A similar process was performed for the Diels Alder reaction. Fitting of the data was achieved according to the model presented in **Figure 3.8.3.1**

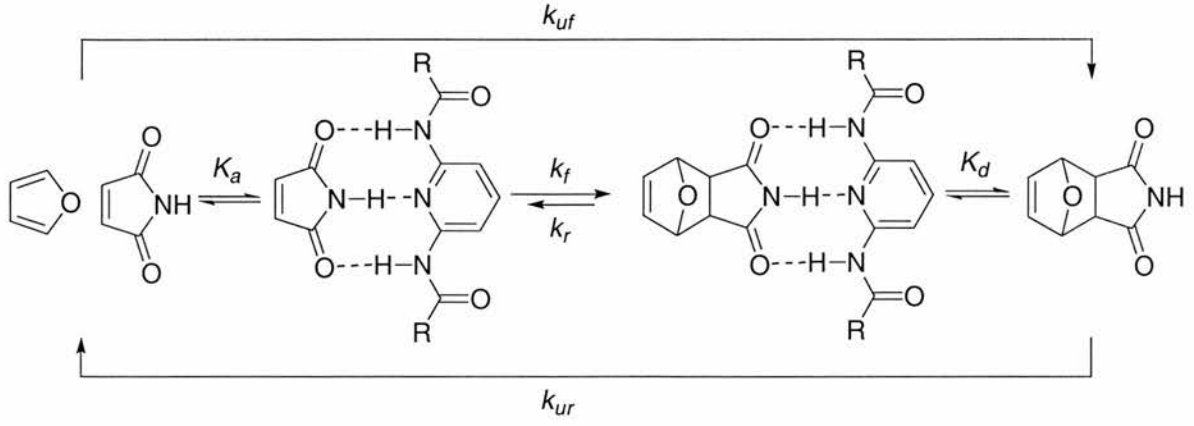

Figure 3.8.4.1 Representation of all the kinetic processes in the reaction between furan and maleimide in the presence and absence of receptor **149**. R = $CH_2CH(CH_3)_2$, K_a = Association constant, k_f = forward rate constant, k_r = reverse rate constant, k_{uf} = forward background rate constant, k_{ur} reverse background rate constant K_d = Dissociation constant of the product.

The reaction data fitted to the raw data points are presented in **Figure 3.8.3.2**. From this model, the background reaction was as follows.

The Background Kinetic Model

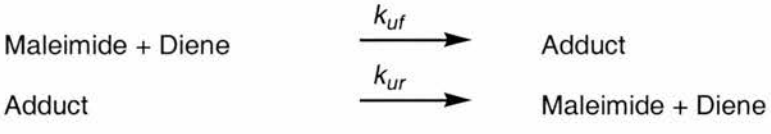

Figure 3.8.4.2 Model of the addition reaction between maleimide and Furan. Diene represents Furan and Adduct represents the cycloadduct.

The furan maleimide Diels Alder reaction was modelled according to **Figures 3.8.4.1** and **3.8.4.2** and a series of rate equations for the reaction mixture in the presence of the receptor **149** were evaluated in a similar manner to the other reactions as detailed in **Figure 3.8.4.3**.

The Kinetic Model

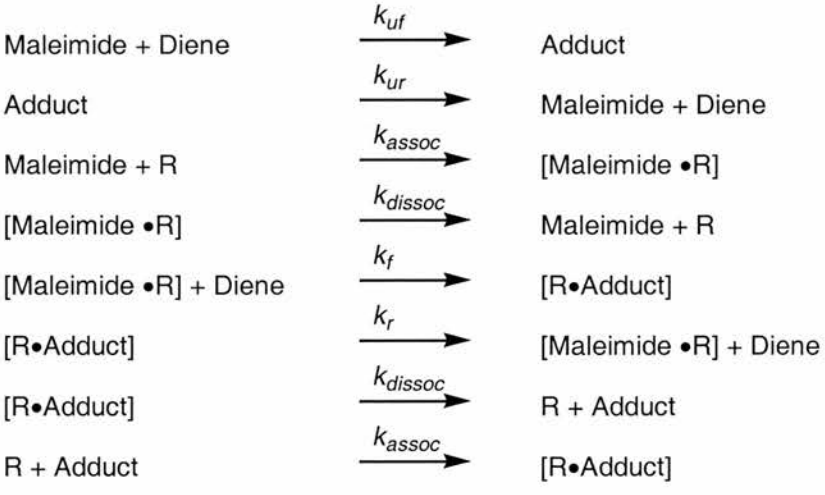

Figure 3.8.4.3 The four equilibria representing the reaction between maleimide and furan and the background reaction. Diene represents furan, adduct represents the cycloadduct product and Receptor represents receptor **149**.

The equations in **Figure 3.8.4.3** were modelled in SimFit. It was assumed that the background reaction would maintain the same forward and reverse rates. The rates of association and dissociation were set to be significantly faster than any of the reaction rates and so that $k_{assoc}/k_{dissoc} = K_a$. The product association constant was assumed to be the same as for the substrate.

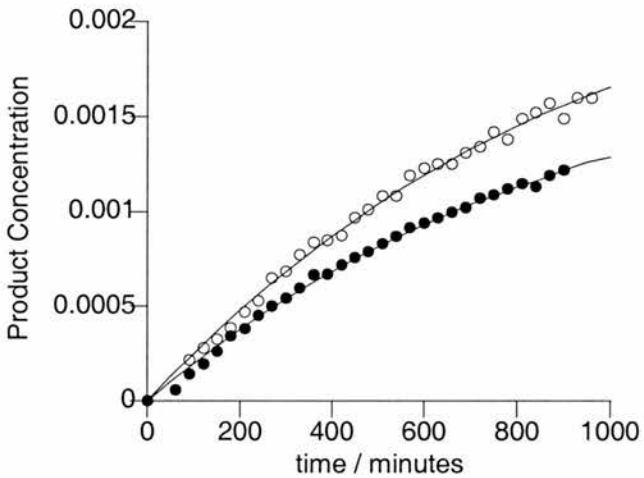

Figure 3.8.3.2 Kinetic data fitted to the reaction model for the cycloaddition of furan to maleimide. Closed circles represent the reaction in the presence of the receptor **149**, open squares represent the background reaction.

The calculated rate equations are listed below. The rate of the background reaction was assumed to be identical to the reaction in the absence of the receptor. The rate constants relating to the association constants were set so that the forward rate over the reverse was equal to the association constant and that the rate of equilibration was many of orders of magnitude faster than the other rates.

Table 3.8.3.3 Rate constants calculated from the kinetic data collated for the Diels Alder reaction between furan **146** and maleimide **147**.

Background Reaction		**With Receptor 149**	
k_{uf} / M^{-1} min^{-1}	k_{ur} / M^{-1} min^{-1}	k_f / M^{-1} min^{-1}	k_r / M^{-1} min^{-1}
8.8 (± 0.1) x 10^{-5}	1.43 (± 0.07) x 10^{-5}	3.66 (± 0.03) x 10^{-4}	8 (± 3) x 10^{-7}

Several interesting observations can be made from this data. Interestingly the value observed for k_f/k_{uf} = 4.16 ± 0.08 (also termed k_{cat}/k_{uncat}) indicating that the reaction rate is increased.

3.9 Conclusions

A receptor has been synthesised which clearly accelerates not only a Michael addition but also a [3+2] dipolar cycloaddition under the same reaction conditions. This has never been achieved before for a receptor operating *via* hydrogen bonding interactions alone. In traditional supramolecular catalyst design, highly specific binding and acceleration is often sought when broad spectrum acceleration as observed for this maleimide **147**, receptor **149** system may be more synthetically valuable. There is also no reason why other Michael additions or [3+2] dipolar cycloadditions to maleimide should not be accelerated by the bis-amide receptor **149**.

A summary of the rate accelerations attained by complexation of maleimide to bis-amide receptor **149** are detailed in **Table 3.8.1**.

Table 3.9.1 Summary of the k_{cat}/k_{uncat} values evaluated for the three reactions.

Michael Addition	[3+2] Dipolar Cycloaddition	Diels-Alder Reaction
10.8 ± 0.5	7.09 ± 0.14	4.16 ± 0.08

Observing the trends for the three reactions, it can be observed that all three reactions are accelerated by a significant amount. As expected, the most polar reaction investigated, the Michael addition, is accelerated by the greatest amount. The reaction possessing the least polar transition state, the Diels-Alder reaction, is accelerated by the least amount. Unfortunately acceleration of a direct addition reaction was not possible for the complex owing to the disruption of binding an reaction with a nucleophile **Figure 3.7.1.5**.

It is apparent that the design requires adaptation to allow more flexibility so that nucleophilic additions to the guest do not disturb the binding of the substrate to the receptor. It would also be desirable to increase the solubility of the guest and increase the association constant so that a more marked effect may be observed.

4. Changing the Receptor Design

4.1 Separation of Interactions

In **Section 3.7.1** the implications of combining the binding hydrogen bonding sites and the hydrogen bond donors designed to interact with the transition state were discussed. There are few reasons why these interactions need to be located in the same place. Indeed, this might be detrimental to the action of the catalyst. The bis-amide receptor **149** was incapable of accelerating a direct addition reaction because addition to the carbonyl carbon would pucker the maleimide ring preventing efficient binding to the receptor. The bis-amide and bis-sulfonamide complexes also suffered from poor ass ociation constants.

As a result, we adapted the design of the receptor separating the binding interactions from those capable of stabilising a transition state.

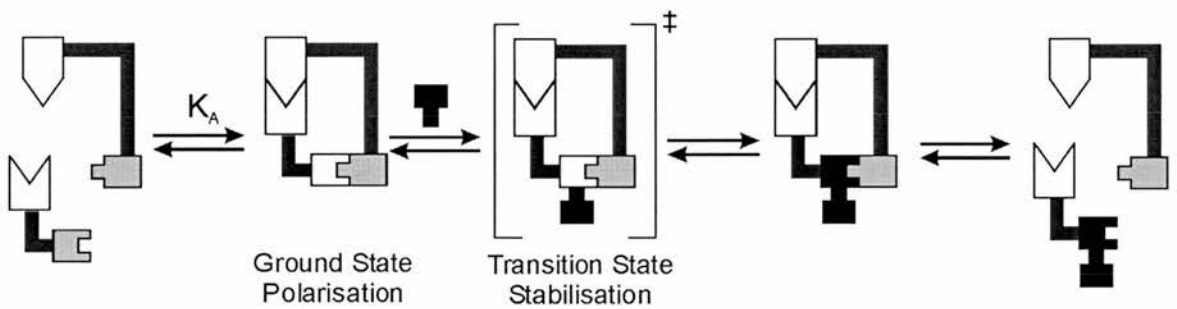

Figure 4.1.1 Schematic diagram representing a receptor with the binding sites and the sites capable of stabilising transition states separated.

The design enables greater steric and synthetic flexibility. Any binding conflicts can be resolved as a result of the improved conformational flexibility of the host and guest. Greater flexibility may result in reduced binding constant. However, we suggest this can be resolved by the incorporation of the two recognition sites.

It was previously proposed that the *N*-phenylmaleimide **117** bis-sulfonamide receptor **138** complex could exist in two different binding modes depending on the bite angle of the receptor and other stabilising interactions in the molecule (**Figure 2.1.9**).

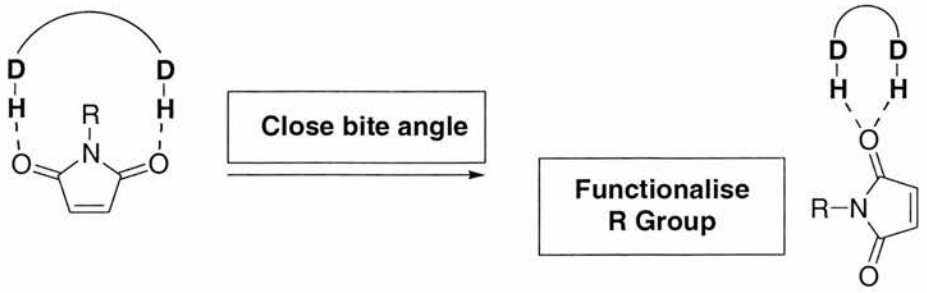

Figure 4.1.2 Closing the bite angle of the receptor enables binding to one of the carbonyl groups freeing the R group for further modification into a second binding interaction.

Closing the bite angle should promote the binding of the hydrogen bond donors to one of the carbonyl groups and enable the R group on the functionalised maleimide to become available for alternative binding modes.

(2,5-Dioxo-2,5-dihydro-pyrrol-1-yl)-acetic acid **92** was chosen as a suitable guest. Reactivity should be similar to maleimide and *N*-phenylmaleimide however; the carboxylic acid group should enable binding to the receptor without disturbing the transition state of a reaction.

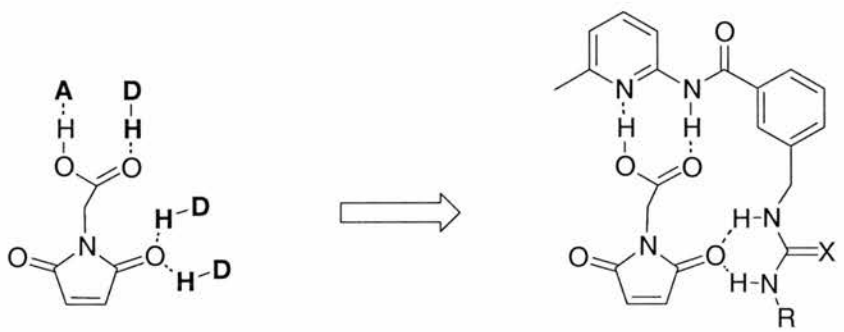

92

Figure 4.1.3 The (2,5-dioxo-2,5-dihydro-pyrrol-1-yl)-acetic acid **92** can be bound to a hydrogen bond donor acceptor array and a hydrogen bond donor donor array in two two point interactions

The donor acceptor recognition pattern of the carboxylic acid is a common motif for recognition by amides. The acceptor acceptor pattern of the lone pairs of the carbonyl group can be readily bound to a urea or thiourea. Incorporation of these motifs with a spacer should enable simultaneous binding of both moieties.

4.2 Synthesis

4.3.1 Synthesis of Receptors and Substrates

A threefold excess of 2-amino-6-methylpyridine was reacted with 3-chloromethylbenzoyl chloride to form quantitatively the amide **161**. The chloride was subsequently converted to the azide **162** in very high yield followed by selective reduction to the amine **163**, which was isolated from the crude mixture as its hydrochloride salt. The free amine was subsequently liberated be neutralisation and extraction in moderate overall yield. The amine was subsequently reacted with cyclohexyl isocyanate in near quantitative yield affording the urea **164**. Reaction with cyclohexylisothiocyanate to form the thiourea **165** however, did not proceed as smoothly and the yield of the corresponding thiourea was accordingly lower.

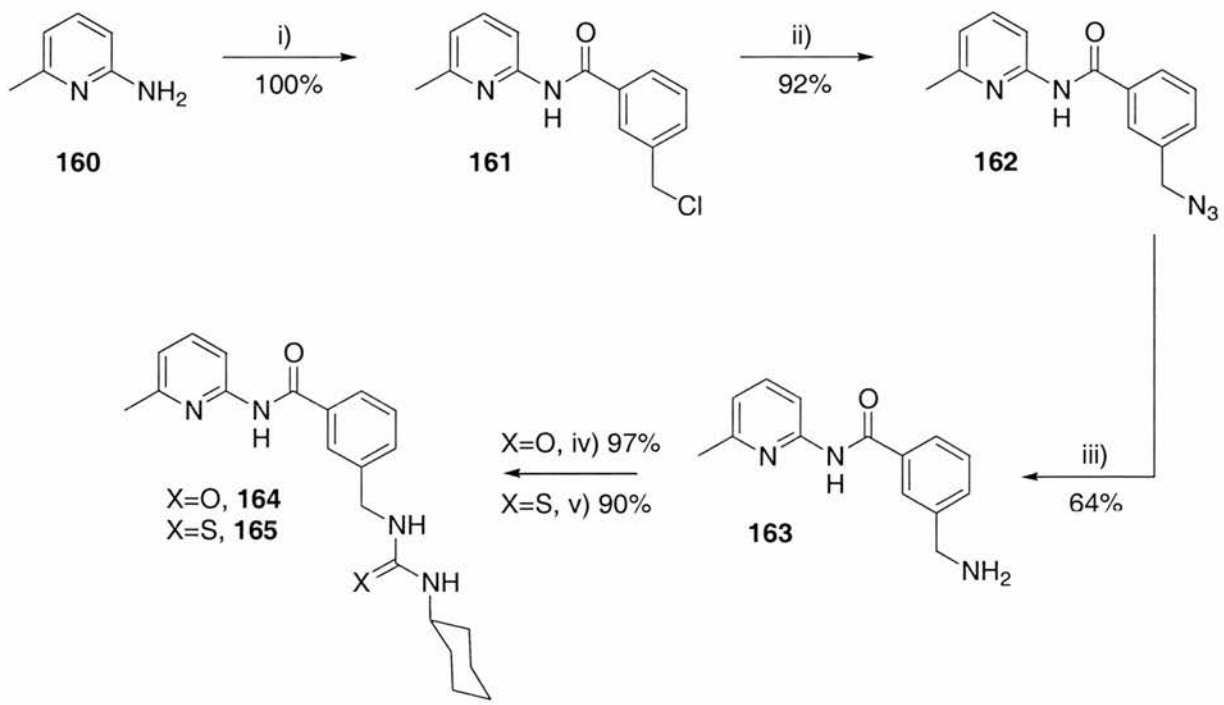

Scheme 4.3.1.1 Scheme showing the formation of the urea and thiourea receptors. i) 3-Chloromethylbenzoyl chloride, CH_2Cl_2, 15h, 0°C to r.t., ii) NaN_3, Acetone, 15h, reflux, iii) PPh_3, THF, H_2O, 15h, r.t, iv) Cyclohexylisocyanate, Et_2O, 1h, 0°C to r.t., v) Cyclohexylisothiocyanate, EtOAc, 1h, reflux

The functionalised maleimide guest, (2,5-dioxo-2,5-dihydro-pyrrol-1-yl)-acetic acid **92** was synthesised by reaction of maleic anhydride with glycine.

The reactants were stirred in acetic acid to form the insoluble intermediate **167** and then refluxed to cyclise the maleimide ring. The low yield of **92** over the two reaction

steps is attributable to the competing polymerisation rather than cyclisation reaction of the intermediate.

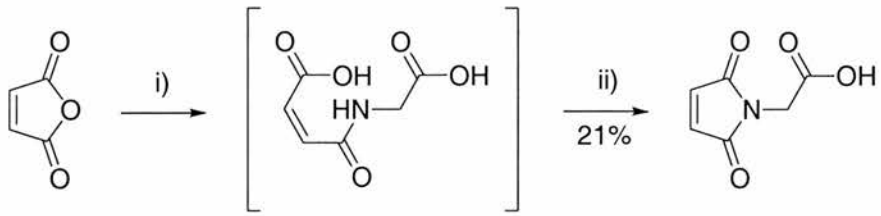

166 **167** **92**

Scheme 4.3.1.2 i) Glacial acetic acid, glycine, r.t. 16 hrs, ii) Reflux, 8 hrs

More simple receptors were designed and synthesised omitting the recognition features of the original design but retaining the potential polarising urea and thiourea hydrogen bond donors.

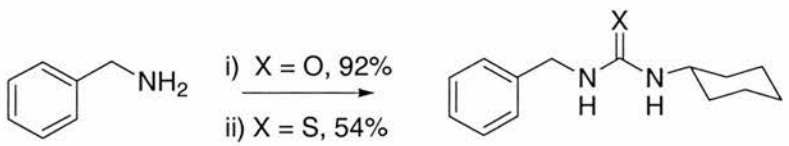

168

X=O, **169**
X=S, **170**

Scheme 4.3.1.3 i) cyclohexylisocyanate, Et_2O, 1h, 0°C to r.t., ii) cyclohexylisothiocyanate EtOAc, 1h, reflux

A receptor containing the amidopicoline recognition unit **171** was also synthesised in one step for comparison with the other receptors.

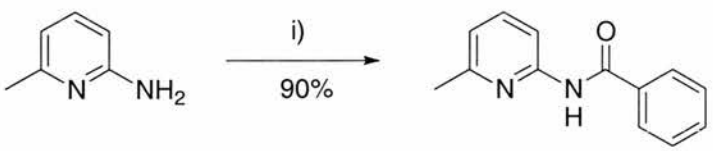

160 **171**

Scheme 4.3.1.4 i) Benzoyl chloride, CH_2Cl_2, 16hrs, 0°C to r.t.

4.3.2 Characterisation of Reaction Products

The products of the reactions under investigation were synthesised to assist with the identification of product resonances when following the reactions by ^1H NMR spectroscopy.

The reaction to produce the adduct arising from the Michael addition between heptane thiol and (2,5-dioxo-2,5-dihydro-pyrrol-1-yl)-acetic acid **92** was required to be

catalysed by triethylamine as the reaction was too slow unless a catalyst or an external base was utilised. This resulted in a moderate overall yield of 31%.

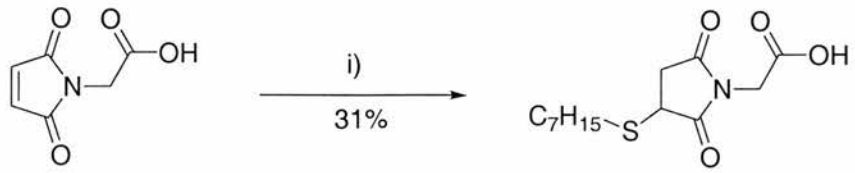

92 **172**

Scheme 4.3.2.3 i) Heptane thiol, CH_2Cl_2, Et_3N, r.t., 3 days

Stoichiometric quantities of *N*-benzylidene-aniline *N*-oxide and functionalised maleimide (2,5-Dioxo-2,5-dihydro-pyrrol-1-yl)-acetic acid **92** were reacted in poor overall yield to form the diastereoisomeric products **174** and **175**.

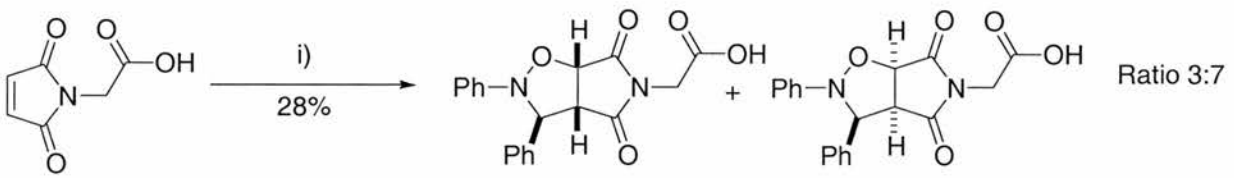

92 **173** **174**

Scheme 4.3.2.2 i) *N*-benzylidene-aniline *N*-oxide , CH_2Cl_2, r.t., 3 days

One equivalent of furan and one equivalent of the (2,5-dioxo-2,5-dihydro-pyrrol-1-yl)-acetic acid **92** were reacted in poor overall yield to form the diastereoisomeric products **175** and **176**.

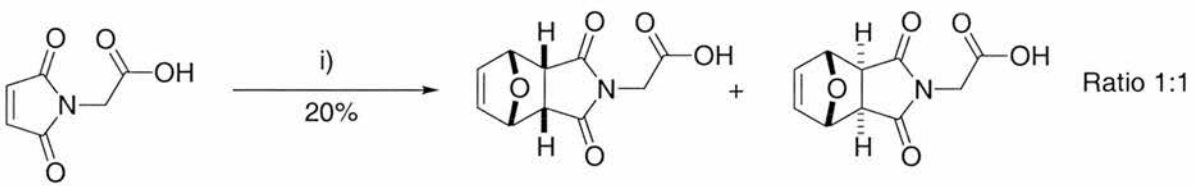

92 **175** **176**

Scheme 4.3.2.1 i) Furan, CH_2Cl_2, r.t., 5 days

4.3 Computational Investigations

4.3.1 Binding Geometry

Binding geometry was initially assessed by computational investigations. An initial set of host guest complexes were modelled using AMBER* forcefield modelled in chloroform solution.[145] Conformational searches were then performed on these minimised structures using the Monte-Carlo technique to find structures accessible in

solution. The lowest energy structure for [urea receptor **164** • maleimide **92**] complex is depicted in **Figure 4.3.1.1**

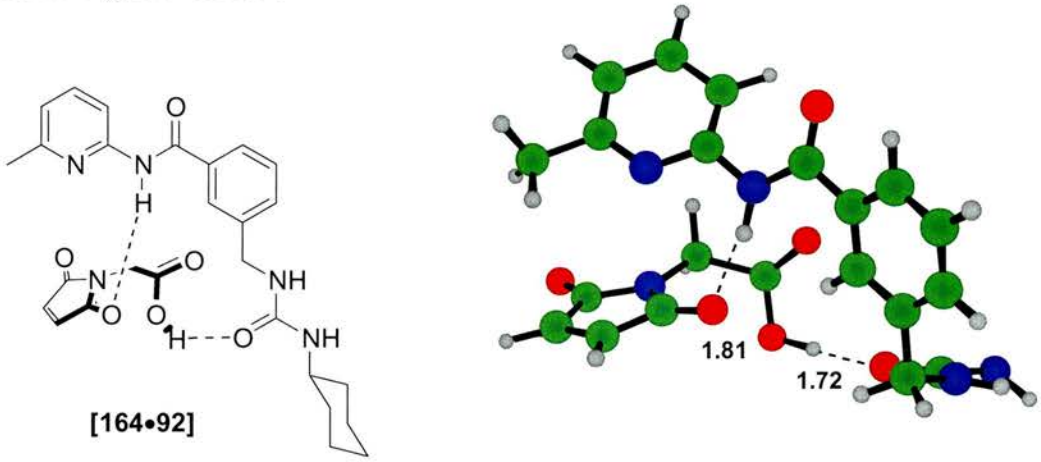

Figure 4.3.1.1 A diagram of the global minimum energy structure using the AMBER* forcefield modelled in chloroform using Monte-Carlo conformational search technique. All intermolecular distances are in Å. The modelling was performed in the presence of the cyclohexyl R group, however, this has been omitted for clarity in the three-dimensional structure depicted.

The lowest energy structure was not the one anticipated for this complex and included a strained (158°) hydrogen bond between the enone carbonyl and the amide NH. The results were assessed to evaluate the contribution from this and the predicted binding modes.

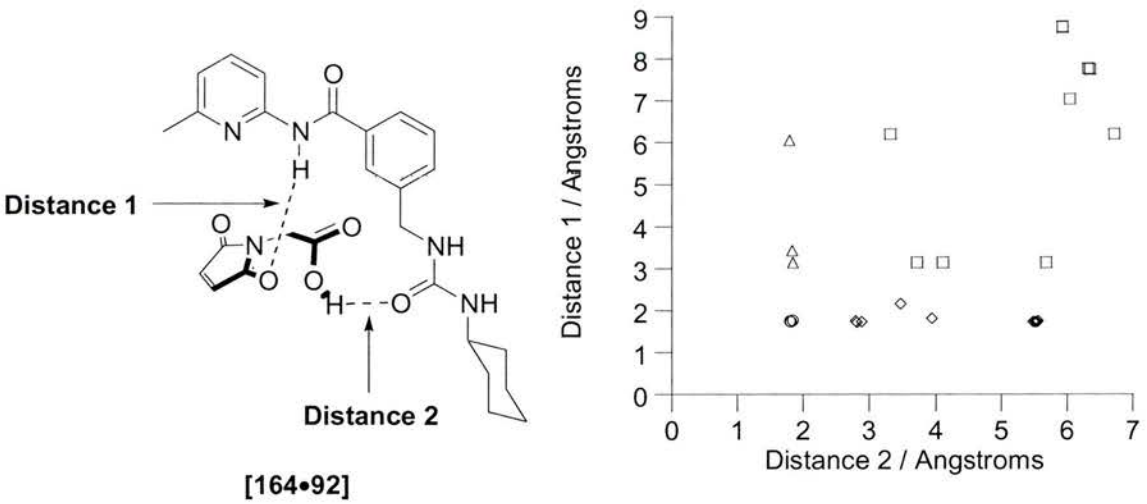

Figure 4.3.1.2 Scatter plot of the distances between the host and guest, implicated as hydrogen bonds in the lowest energy structure, in the structures with energies + 10kJ mol^{-1} relative to the Global minimum. Circles represent coconformations possessing both hydrogen bonds, triangles and diamonds possess one hydrogen bond and squares represent structures with no hydrogen bonding present.

The relative distances between the donors and acceptors can be extracted from the Monte-Carlo minimisation results and represented as scatter graphs. **Figure 4.3.1.2** shows the scatter plot of the distances between the carbonyl group and the amide and the acid and urea observed as hydrogen bonds in the coconformation of the complex global minimum. It is assumed that interatomic distances of less than 2.5 Å between potential hydrogen bond donors and atoms bearing lone pairs are probable hydrogen bonds. In this manner the contribution of different low energy structures to the solution binding mode can be evaluated.

From the scatter graph **Figure 4.3.1.2,** it is apparent that this structure is not exclusive. Some coconformations adopt similarly short contacts to one (triangles and diamonds), or both groups (circles) but a significant number fail to adopt these hydrogen-bonding motifs (squares).

The data was reanalysed to assess contact distances between the carbonyl groups on the maleimide and the urea protons. Data was collected for both carbonyl groups and additional data was assessed for the acid amido-picoline motif to assess the contribution to binding.

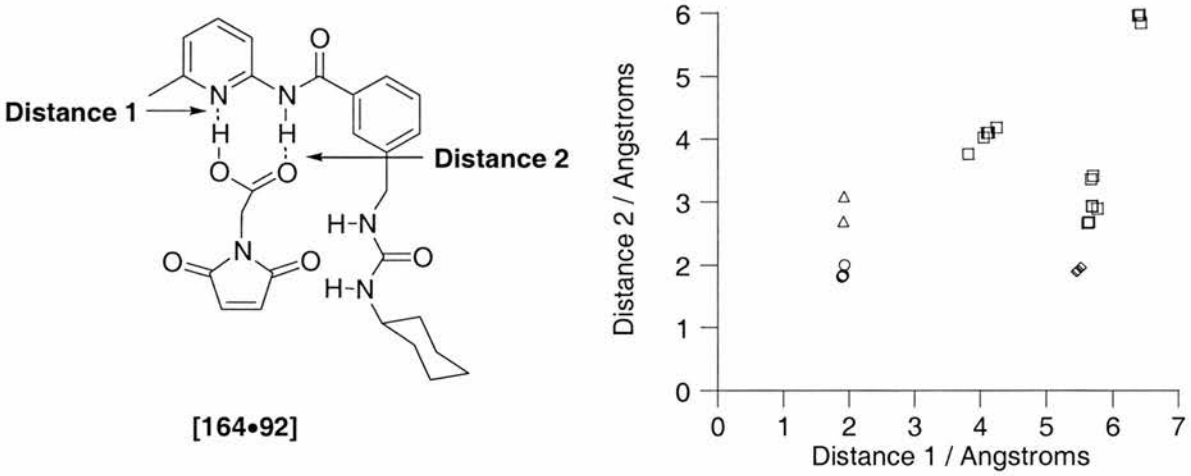

Figure 4.3.1.3 Scatter plot of the distances between the carboxylic acid group and amide in the structures with energies + 10 kJ mol^{-1} relative to the Global minimum. Circles represent coconformations possessing both hydrogen bonds, triangles and diamonds possess one hydrogen bond and squares represent structures with no hydrogen bonding present.

From **Figure 4.3.1.3,** it is apparent that there are several low energy coconformations possessing the amido-picoline carboxylic acid binding motif.

The distances between the urea protons and the maleimide carbonyls can be assessed (denoted distances 3 and 4). It is apparent from **Figure 4.3.1.4** that some low energy structures possess contacts short enough to be attributable to hydrogen bonds. Several coconformations indicate structures with two short contacts for distance 3 and 4, as the contact distances are around 2 Å, it is reasonable to assume that these distances represent hydrogen bonding interactions.

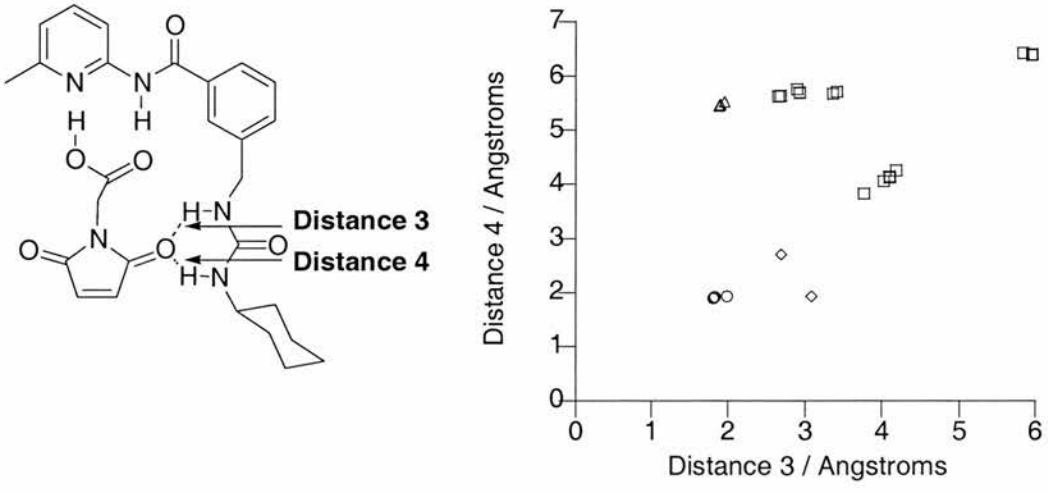

Figure 4.3.1.4 Scatter plot of the distances between the urea group and carbonyl in the structures with energies + 10 kJ mol^{-1} relative to the Global minimum. Circles represent coconformations possessing both hydrogen bonds, triangles and diamonds possess one hydrogen bond and squares represent structures with no hydrogen bonding present.

In conclusion, for the urea receptor **164**, the lowest energy coconformation was not that predicted for the system, however, the global minimum retains a strained hydrogen bond to the carbonyl carbon of the enone and other coconformations containing urea carbonyl hydrogen bonds are implicated. This data suggests that several productive coconformations may exist for this complex and it might be effective at accelerating reactions.

A similar assessment was performed on the thiourea receptor **165**. Initial structures were minimised in unison with an AMBER* forcefield in simulated chloroform.[145] This minimised structure was then subjected to a conformational search using the Monte-Carlo technique. The structure of the calculated global minimum coconformation between thiourea **165** and maleimide **92** is depicted in **Figure 4.3.1.5**.

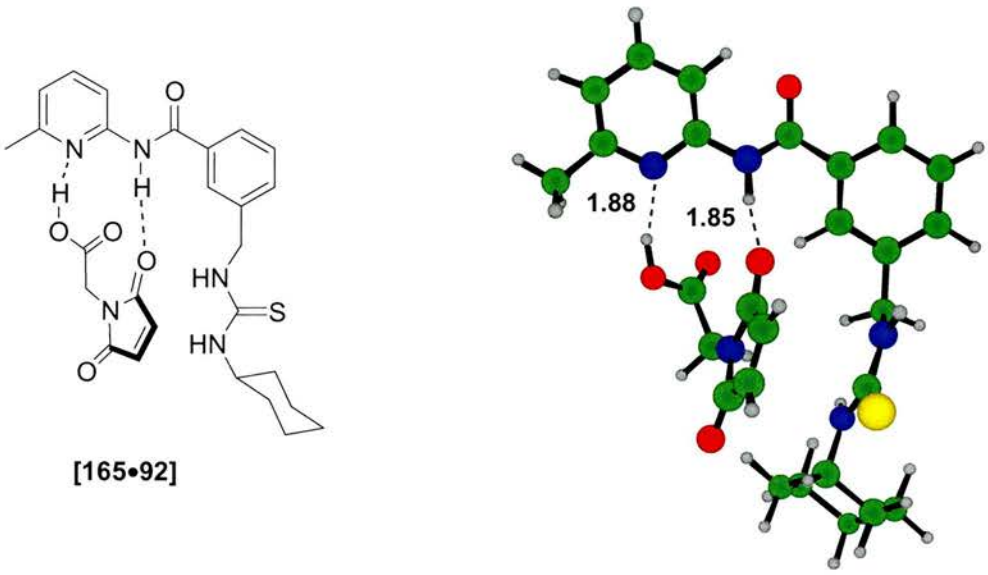

[165•92]

Figure 4.3.1.5 The coconformation of the global minimum structure for thiourea **165** represented in two dimensions as well as the calculated three-dimensional ball and stick model. All intermolecular distances are in Å.

The minimum energy coconformation is again not that predicted for the complex, however, a strained (160°) hydrogen bond between the guest carbonyl and host amide is retained which could have a similar effect on the electronics of the guest as binding the carbonyl moiety to the thiourea.

As previously, conformational searching yielded information about other low energy structures, which may be accessible under the reaction conditions. It is informative to consider these when taking into account complex coconformations accessible in solution. The complex will be highly dynamic within the complex and between the complex and other bound and unbound species. Providing that the equilibria between reactive complexes and unreactive complexes are faster than the reaction equilibrium, the Curtin Hammett Principle states that reaction can occur *via* the reactive complexes, irrespective of the relative concentration of precursor in solution.[156]

The recorded complexes were evaluated to establish the frequency of structures similar to the global minimum depicted in **Figure 4.3.1.6**.

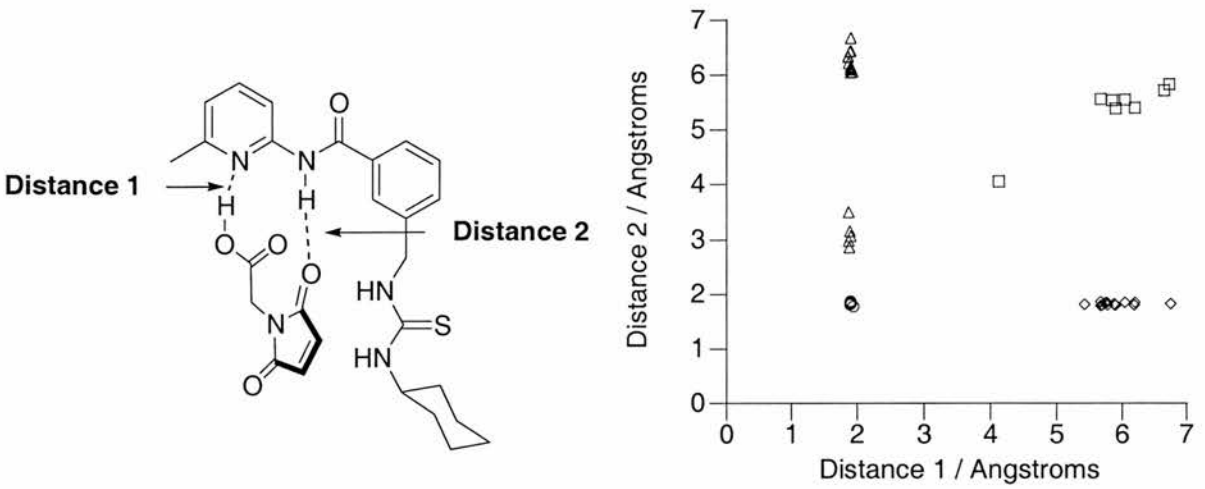

Figure 4.3.1.6 Scatter plot of the distances between the host and guest implicated as hydrogen bonds in the lowest energy coconformation in the structures with energies + 10 kJ mol^{-1} relative to the Global minimum. Circles represent coconformations possessing both hydrogen bonds, triangles and diamonds possess one hydrogen bond and squares represent structures with no hydrogen bonding present.

From **Figure 4.3.1.6** it is apparent that many of the coconformations adopted by the complex are dissimilar to the global minimum. Many of the structures conserve one of the observed hydrogen bonds (triangles and diamonds), a few conserve both (circles), however some structures possess neither of these hydrogen-bonding interactions (squares).

The data was re-examined to assess the proportion of low energy structures containing the amido picoline, carboxylic acid binding motif predicted for the complex.

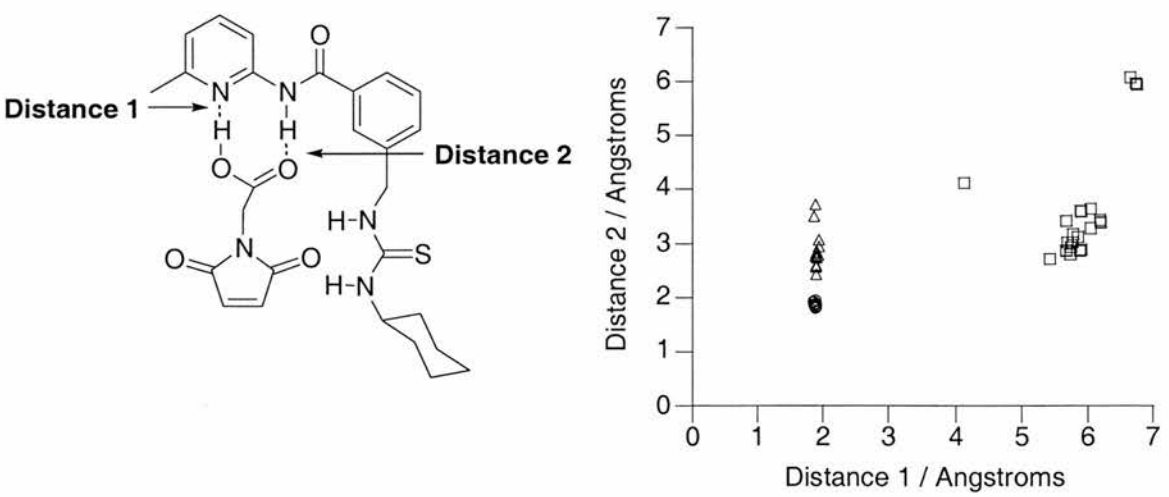

Figure 4.3.1.7 Scatter plot of the distances between the acid group and amido picoline in the structures with energies + 10 kJ mol^{-1} relative to the Global minimum. Circles represent coconformations possessing both hydrogen bonds, triangles possess one hydrogen bond and squares represent structures with no hydrogen bonding present.

Figure 4.3.1.7 shows the contact distances between the amido picoline and carboxylic acid groups. It is apparent that a significant number of low energy coconformations (<10 kJ mol^{-1} higher than the global minimum) possess this binding motif.

It is of greater interest to the action of the receptor to investigate whether the binding even between the thiourea and carbonyl group occurs. From **Figure 4.3.1.8,** it is apparent that some of the low energy structures may contain interactions, which are short enough to be weak hydrogen bonds (triangles and diamonds) but many fail to form hydrogen bonds between the thiourea and carbonyl of the maleimide moiety (squares).

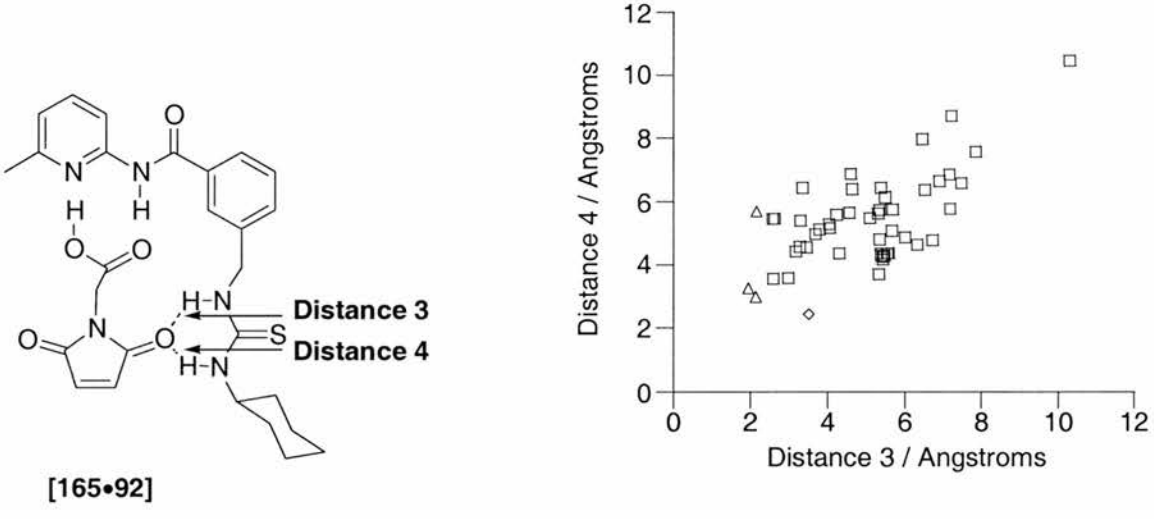

[165•92]

Figure 4.3.1.8 Scatter plot of the distances between the thiourea group and carbonyl in the structures with energies + 10 kJ mol^{-1} relative to the Global minimum. Triangles and diamonds possess one hydrogen bond and squares represent structures with no hydrogen bonding present.

If the data set is expanded to include structures of slightly higher energy, more short contacts are revealed, however, this indicates that the ground state binding interaction between thiourea **165** and maleimide **92** is less than ideal.

It is important to question, however, the validity of the computational modelling. **Figure 4.3.1.5** shows the calculated structure of the global minimum of the thiourea maleimide **92** complex. Interestingly, a cis arrangement is observed between the carbon sulfur and one of the nitrogen hydrogen bonds. Thioureas are normally represented as possessing a double bond between the carbon and sulfur atoms. This is potentially misleading. π-Bonding requires overlap of p orbitals and the

degree of overlap depends upon the relative energies of the p orbitals. As the p orbitals in sulfur are in the 3 shell rather than the 2, the relative energies of the p orbitals on carbon and sulfur are very different. Thioureas therefore, have a significant contribution to their molecular bonding from the zwitterionic resonance forms depicted in **Figure 4.3.1.8**.

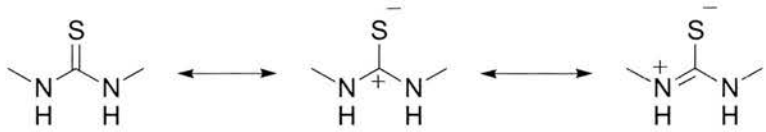

Figure 4.3.1.8 Some of the canonical forms of a simple thiourea.

The resulting negative charge on sulfur is readily delocalised into the empty 3d orbitals. The carbocation is resonance stabilised by the lone pairs on the nitrogen atoms. This has two overall effects; restricted rotation around the CN bonds and increased acidity of the thiourea nitrogen groups. The partial positive charge on the nitrogen atoms and their associated increased acidity will strengthen any observed hydrogen bonding. This effect is not accounted for in the AMBER* forcefield in Macromodel however, indeed the lowest energy structures calculated for simple ureas and thioureas using a Monte Carlo conformational search are different, as shown in **Figure 4.3.1.9**. Additionally, the carbon nitrogen bond lengths in the calculated urea structure are 0.1 Å shorter than in the thiourea example, indicating the CN bond order is greater in urea than thiourea, which is counter-intuitive.

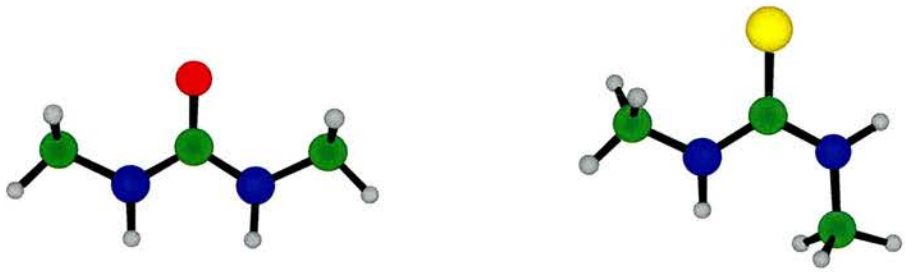

Figure 4.3.1.9 Conformations of a simple urea and thiourea as calculated using Macromodel with an AMBER* forcefield employing a Monte-Carlo conformational search algorithm. Carbon atoms are represented in green, nitrogen in blue, oxygen in red and sulfur in yellow.

From this simple calculation, it is apparent that no special electronic or torsion parameters are utilised to restrict motion around the CN bond when modelling thioureas and this may lead to inaccuracies in the computation of more complex

molecular conformations and result in the underestimation of the hydrogen bond donor ability of the group.

4.3.2 Electronic Effects

Semi-empirical computer modelling was employed to investigate the effect on the electronics of the guest on binding the (2,5-dioxo-2,5-dihydro-pyrrol-1-yl)-acetic acid **92** to the receptors **164** and **165**. To accelerate computation time, maleimide and urea or thiourea were used to model electron density changes using Spartan. All structures were calculated in a simulated vacuum.

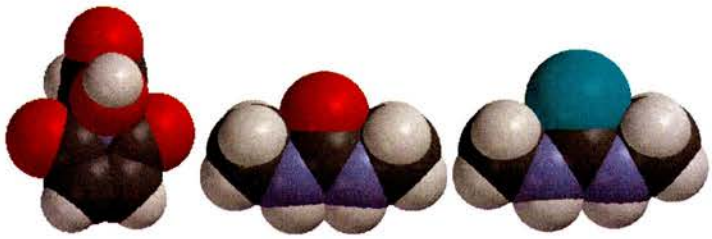

Figure 4.3.2.1 CPK or "space filling" models of maleimide **92**, a simple urea and thiourea. Carbon atoms are grey, hydrogen atoms are white, oxygen atoms are red, nitrogen atoms are blue and the sulphur atom is cyan.

As before the electrostatic potential surface is projected onto a van der Waals representation of the complex.

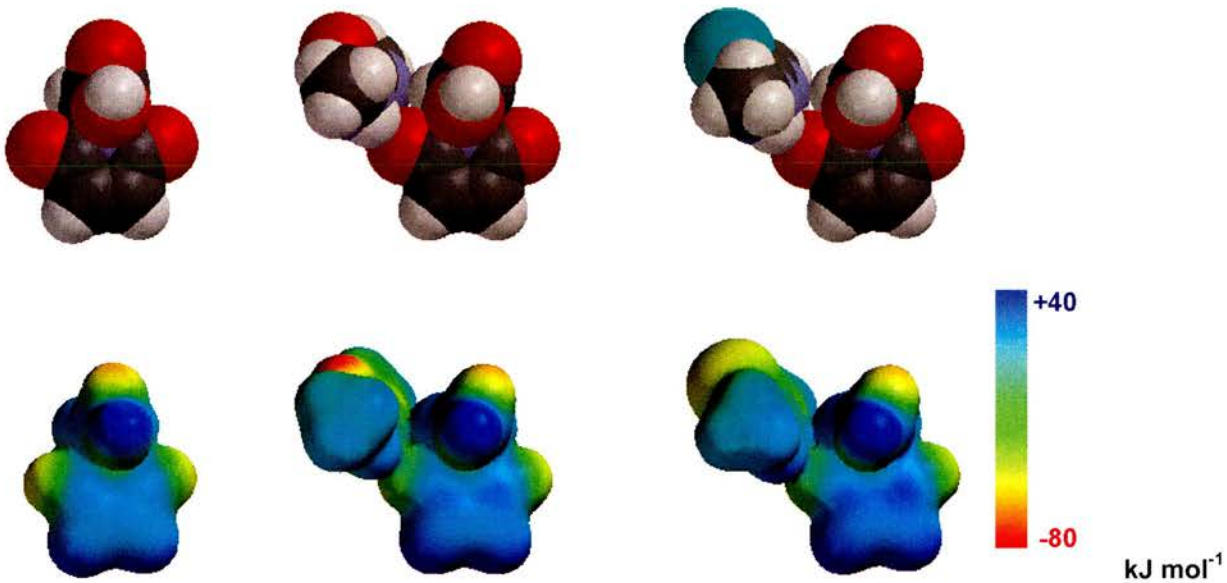

Figure 4.3.2.2 Electrostatic potential surface diagrams for maleimide **92** and urea and thiourea. Areas of positive charge are at the blue end of the spectrum; areas of negative charge are towards the red end of the spectrum.

Figure 4.3.2.2 demonstrates the electrostatic potential on the structures in the unbound maleimide **92** and bound to the urea and thiourea moieties. It can be observed from **Figure 4.3.2.2** that in both urea and thiourea binding, all alkene and carbonyl carbons adopt a darker blue colouration indicating the removal of electron density.

The lowest energy coconformations of the urea and thiourea complexes however, did not possess this interaction but were observed to include a hydrogen bond from the amide proton to the carbonyl of the (2,5-dioxo-2,5-dihydro-pyrrol-1-yl)-acetic acid **92**.

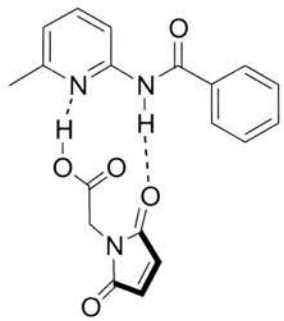

Figure 4.3.2.3 Interactions modelled to assess the effect of binding the (2,5-dioxo-2,5-dihydro-pyrrol-1-yl)-acetic acid **92** to the amidopicoline **171**.

Taking the thiourea low energy structure as a basis, a complex containing this hydrogen bond was modelled to investigate the effect on the electronics of the bound maleimide. For ease of computation time, only the amidopicoline and (2,5-dioxo-2,5-dihydro-pyrrol-1-yl)-acetic acid **92** were modelled.

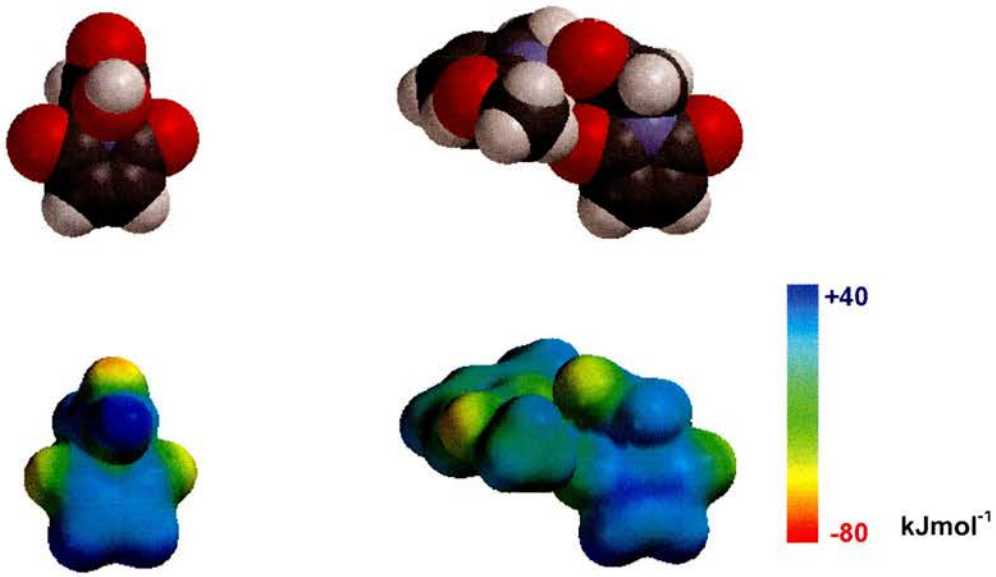

Figure 4.3.2.4 Electrostatic potential surface diagrams for maleimide **92** and amide **171**. Areas of positive charge are displayed in blue; areas of negative charge are displayed in red.

As previously, the interactions were calculated and mapped onto a space filling representation of the complex. The complexes are orientated to allow analysis of the changes to the electrostatic potential on the maleimide to be readily assessed.

As can be observed in **Figure 4.3.2.4** there is an effect on the electron density of the (2,5-dioxo-2,5-dihydro-pyrrol-1-yl)-acetic acid **92** on binding to the amido picoline unit, however, the electron withdrawal is mainly localised on the carbonyl carbons with a smaller reduction in electron density on the alkene carbons. This result however, justifies the inclusion of the amidopicoline receptor **171** as a control to assess the contribution from this binding motif to accelerating reactions.

4.4 Assessment of Binding

In the light of the computational investigations, it is apparent that the binding motif initially proposed for the complex is not exclusive and may have an effect upon the investigation of the binding constants. Indeed all of the binding motifs depicted in **Figure 4.4.1** were observed in addition to other coconformations.

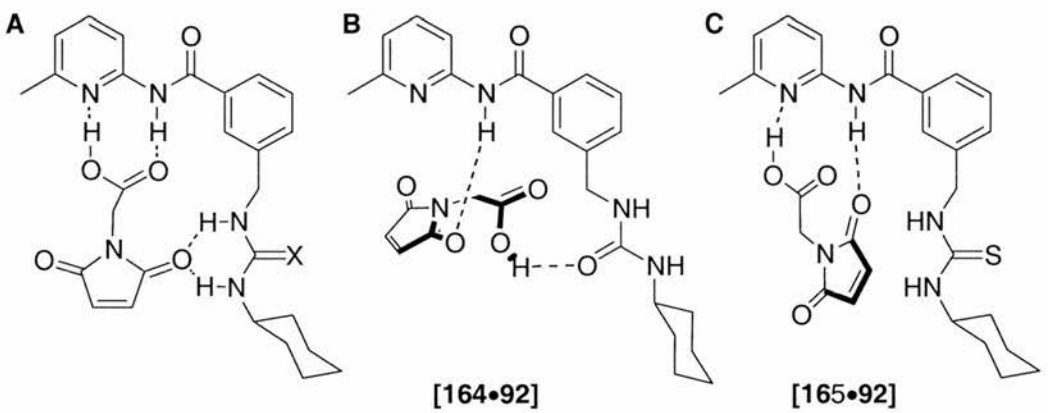

Figure 4.4.1 The predicted binding motif **A** alongside the two global minima **B** and **C** calculated using the AMBER* forcefield utilising a Monte Carlo conformational search technique in simulated chloroform using Macromodel.

Some of the binding coconformations observed in solution will be solely between the host and carboxylic acid group. Coconformations containing the acid amide recognition motif are common as observed in **Figures 4.3.1.3** and **4.3.1.7** and are more frequently observed than amide, urea or thiourea binding to the enone carbonyl. It is therefore imperative for the kinetic fitting that when we consider binding between the host and guest, as far as possible, we ignore the non-productive binding modes. One manner in which this may be achieved is by observing the

change in the CH alkene resonance only. Binding to either the acid moiety or the enone could potentially exhibit a change in chemical shift of the methylene group, however, only productive binding modes exhibiting hydrogen bonding to the enone will result in a change in chemical shift of the alkene CH.

Binding investigations were performed as previously using 500 MHz ^{1}H NMR spectroscopic titrations. Owing to the poor solubility of the guest and the considerations about non-productive binding, the host concentration was varied and the changes in chemical shifts of resonances arising from the functionalised maleimide **92** were followed.

The observed chemical shift changes in the alkene resonance of (2,5-dioxo-2,5-dihydro-pyrrol-1-yl)-acetic acid **92** were unfortunately much smaller than those arising in the hosts, $\Delta\delta_{MAX}$ = 0.05 ppm. Chemical shifts cannot be confidently reported to three decimal places as the error in measurement is generally considered to be ± 0.001 ppm. As the changes in chemical shift were on the limit of the accuracy of measurement, the errors in measuring the chemical shifts were accordingly large.

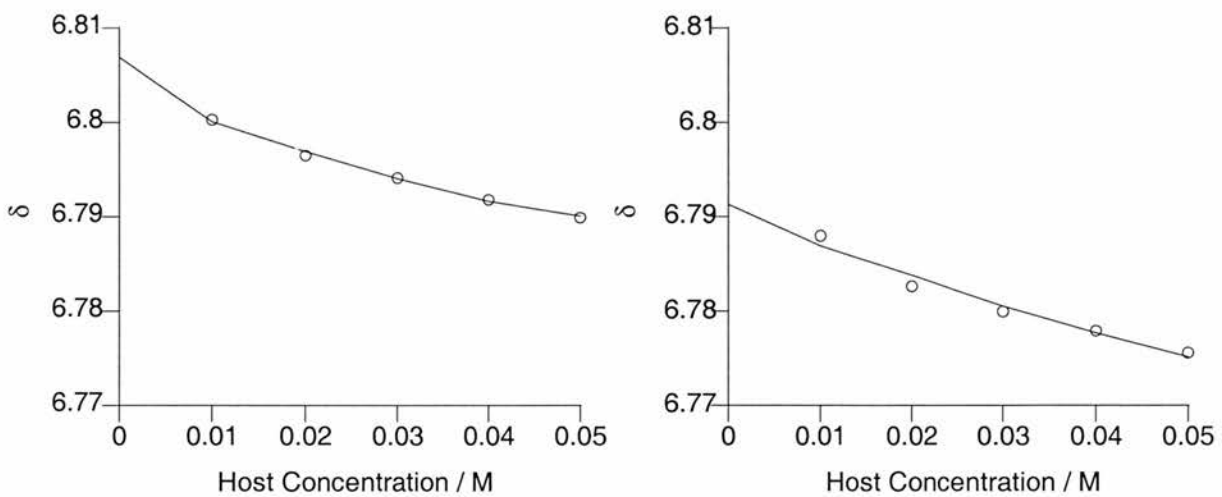

Figure 4.4.2 Experimental results of the dilution experiment attempted between urea receptor **164** and maleimide **92** at i) 283 K and ii) 313K alongside the calculated fit in each case. The associated errors with the calculated fits are large as a result of the small chemical shift change being observed and the maximum solubility of the host limiting the available concentration range.

Solutions were prepared with 10 mM of (2,5-dioxo-2,5-dihydro-pyrrol-1-yl)-acetic acid **92** and varying concentrations of urea **164** or thiourea host **165**. Curve fitting was performed by minimising errors in WineqNMR and assessing the best curve fit.

For the urea **164**, maleimide **92** complex, the association constant to the enone oxygen atoms was assessed to be 8 ± 8 M^{-1} and 2 ± 6 M^{-1} at 283 and 313 K respectively. The errors connected with the association constants are so large that the approximate magnitude of the chemical shifts is of greater importance than the exact result. The important factor is that productive association between the urea receptor **164** and the maleimide guest **92** enone moiety is weak and of the order 10^0 to 10^1 M^{-1}.

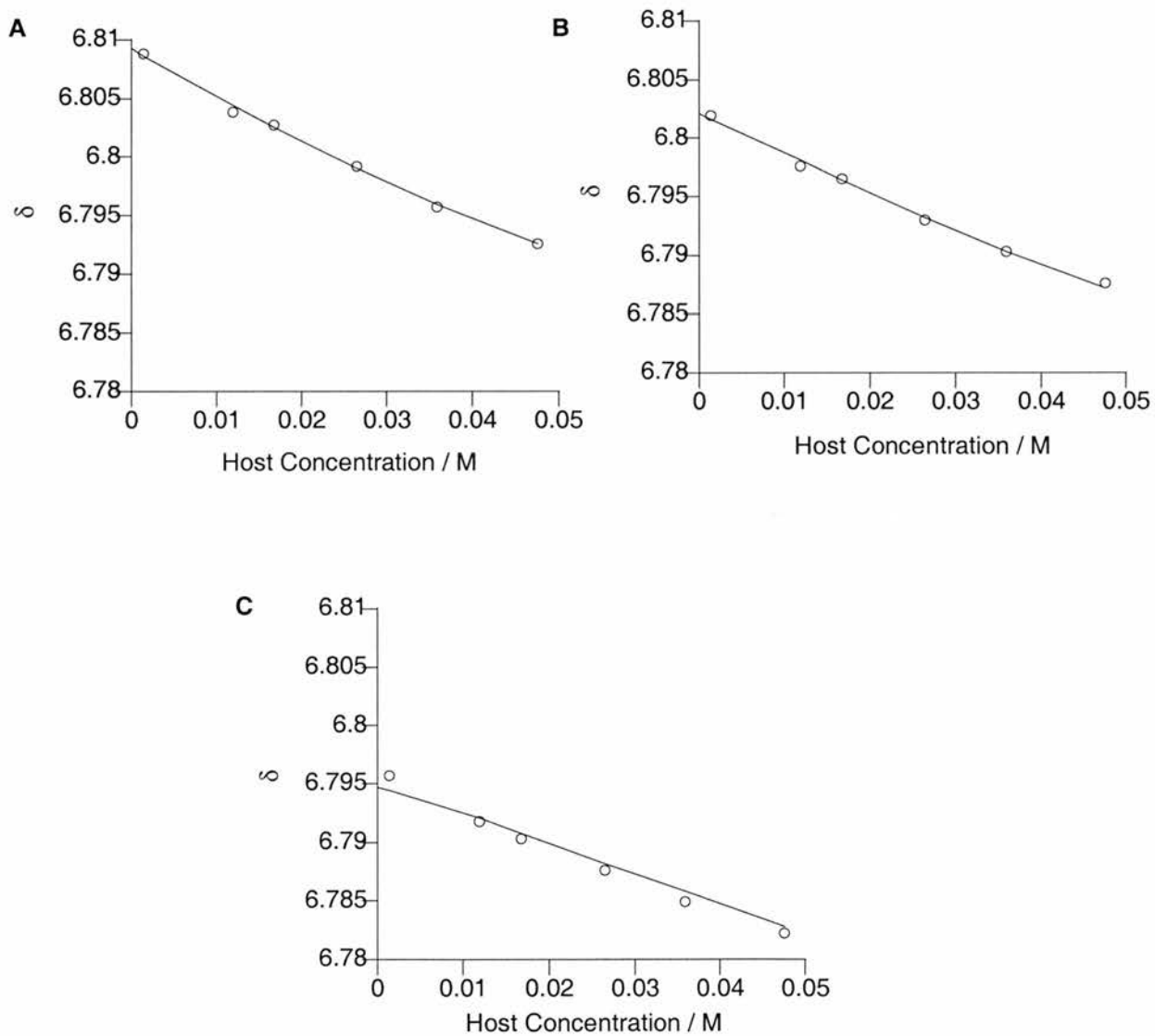

Figure 4.4.3 Graphs for the attempted titration of thiourea receptor **165** with maleimide 92 at A) 283, B) 300 and C) 423 K. Again, the observed errors were high as a result of small chemical shift changes and a poor available concentration range.

The same titration exercise was performed with the thiourea receptor **165**, the association constants calculated were 9 ± 2 M^{-1}, 6.8 ± 0.6 M^{-1}, 1 ± 1 M^{-1}. From **Figure 4.4.3**, it is apparent that although chemical shift changes were observed, they were approximately linear over the available concentration range. The associated errors were large and the association constants were of the same order of magnitude as the urea.

The results obtained for the association constant determination, although disappointing are informative. Over the available concentration ranges, the titration graphs were generally linear. Although this precludes accurate K_a determination, it does suggest that productive binding as indicated in **Figure 4.4.4** is weak.

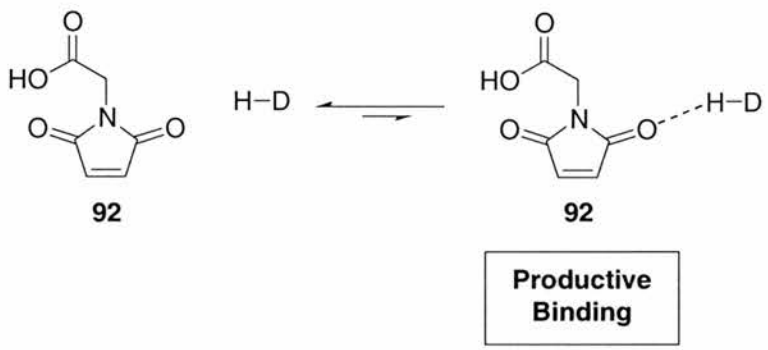

Figure 4.4.4 A diagrammatic representation of the weak productive co-ordination between maleimide **92** and guest hydrogen bond donors.

We can conclude that for these systems, productive ground state binding is poor, although investigation of potential capability to accelerate reactions is still valid. Transition state binding may differ widely from that observed between receptor and substrate ground state.

4.5 Nucleophilic Reactions

As with receptors **138** and **149**, interactions are present in the receptor molecules **164** and **165** to bind charged transition states. The only difference is that with this new generation of receptors a second recognition site is present for binding and orientation of the substrate.

Initial reactivity was assessed by performing a small-scale reaction in deuterated chloroform in the presence and absence of receptors **164** and **165**. The overall conversion to product was observed after a fixed period. Unfortunately, the guest precluded the choice of 4-fluorobenzylamine as a reactant due to the salting out of starting materials prior to reaction.

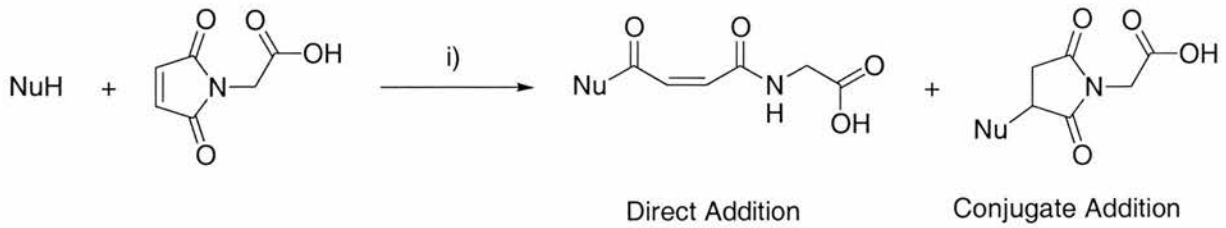

Scheme 4.5.1 The two possible products arising from nucleophilic addition to the (2,5-Dioxo-2,5-dihydro-pyrrol-1-yl)-acetic acid **92**. i) $CDCl_3$, NuH

Table 4.5.2 Preliminary results for the addition of various nucleophiles to maleimide **92**. Results are reported as percentage completion.

		% Completion with Urea Receptor **164**		% Completion with Thiourea Receptor **165**		Without Receptor	
Nucleophile	Temp	Direct	Michael	Direct	Michael	Direct	Michael
$H_{15}C_7$–SH	25	0	0	0	50	0	0
F–C$_6$H$_4$–CH$_2$–NH_2	0	Salting out of starting materials					

The preliminary results for the conjugate and Michael addition of nucleophiles to (2,5-dioxo-2,5-dihydro-pyrrol-1-yl)-acetic acid **92** are detailed in **Table 4.5.2**. Primary amines could not be used as a result of their basicity. Attempting the reaction in the presence of the amine and (2,5-dioxo-2,5-dihydro-pyrrol-1-yl)-acetic acid **92** resulted in the formation of a salt removing the reactants from solution.

4.5.1 Michael Addition

It was decided to study the Michael addition between heptane thiol and (2,5-dioxo-2,5-dihydro-pyrrol-1-yl)-acetic acid **92** in greater detail. Kinetic data were obtained for the Michael addition in the presence and absence of all the receptors and controls synthesised.

Unfortunately, as no reaction was observed in the absence of the thiourea receptor or control under the conditions employed, there was no means of comparison between the accelerated and background reactions.

The appearance of product resonances over the reaction in the presence of thiourea receptor **165** is depicted in **Figure 4.5.1.1**.

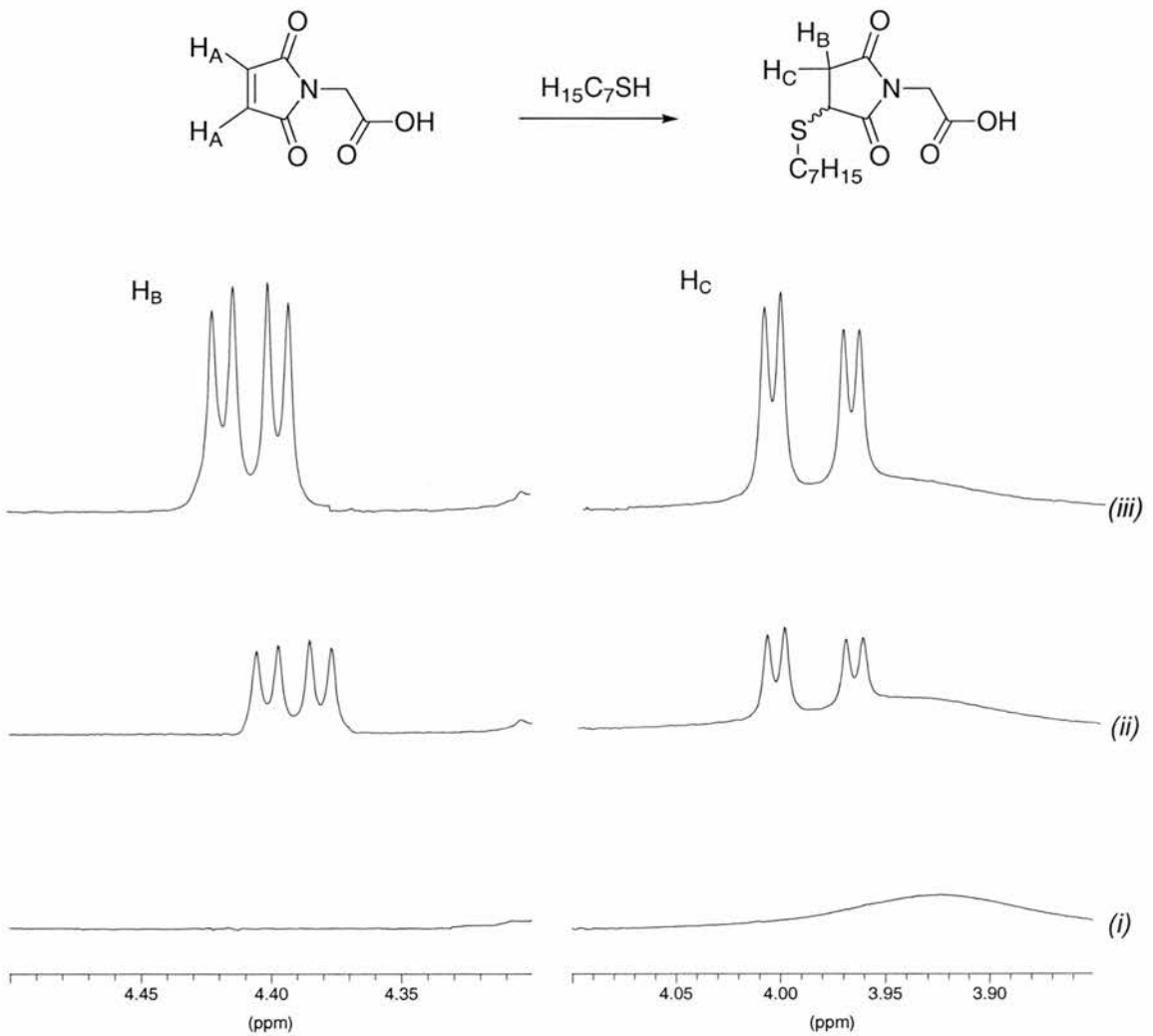

Figure 4.5.1.1 Partial 500 MHz ^{1}H NMR spectra displaying the formation of product resonances for the Michael addition of heptane thiol to (2,5-dioxo-2,5-dihydro-pyrrol-1-yl)-acetic acid **92** over i) 7, ii) 427 and 1027 minutes. In the absence of a background rate of reaction, the product formation in the presence of thiourea receptor **165** is presented here.

Unfortunately over the period of the reaction, some of the product resonances are coincident with a broad resonance arising from the receptor. To facilitate deconvolution, the baseline was corrected using WinNMR. **Figure 4.5.1.2** illustrates

the correction of the baseline to enable the percentage conversion to product to be calculated.

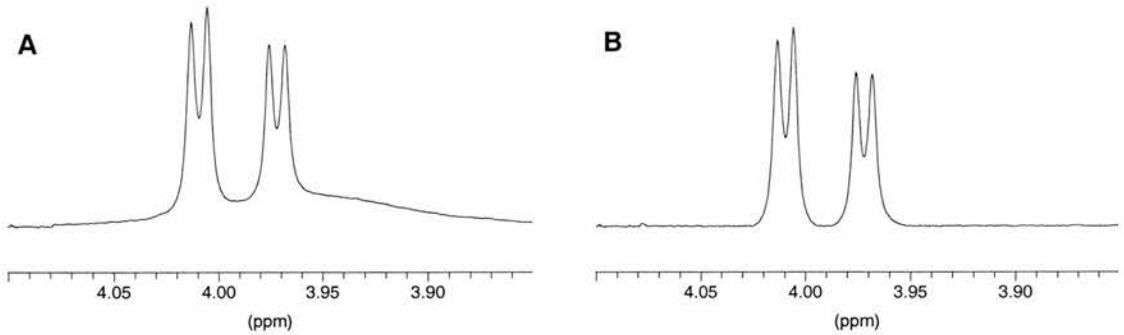

Figure 4.5.1.2 Partial 500 MHz ^{1}H NMR spectra showing the correction of the baseline to enable accurate deconvolution of the product resonances.

By making this correction, accurate deconvolution and comparisons could be made.

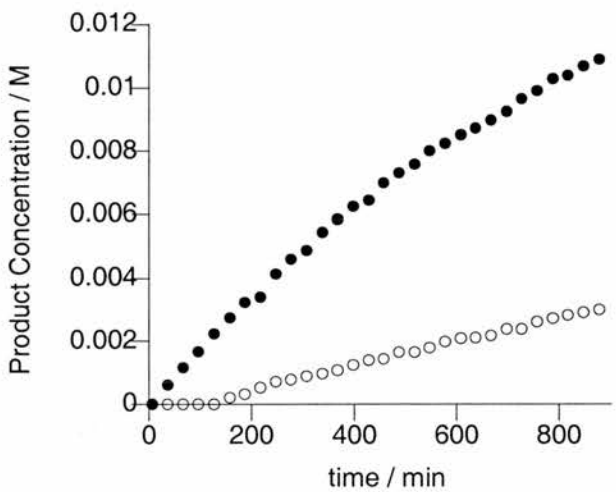

Figure 4.5.1.3 Kinetic data from the reaction between heptane thiol and (2,5-dioxo-2,5-dihydro-pyrrol-1-yl)-acetic acid **92**. Open circles represent the reaction in the presence of thiourea receptor **165**, open circles thiourea control **170**, there was no reaction in the presence of urea receptor **164**, urea control **169**, amide control **171** and there was no background reaction.

The Michael Addition between heptane thiol and the (2,5-dioxo-2,5-dihydro-pyrrol-1-yl)-acetic acid **92** was investigated by ^{1}H NMR spectroscopy. The conversion to product was evaluated by previously established deconvolution methodologies. As can be seen in **Figure 4.5.1.3**, in the absence of a receptor containing a thiourea moiety no conversion to product is observed. This is significant, yet it is important to rationalise this result alongside the knowledge that no product formation is observed in the background reaction.

A visualisation of the initial rate of reaction can be made by linear regression of the initial data points deconvoluted for the reaction. This method has been informative to illustrate the degree of acceleration in a qualitative manner.

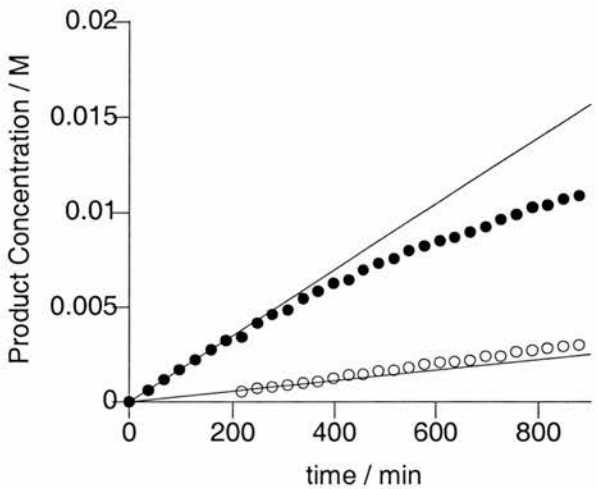

Figure 4.5.1.4 Graph displaying the projection of the initial rates of the Michael addition between functionalised maleimide **92** and heptane thiol as calculated by linear regression analysis of product concentration in the initial reaction.

In **Figure 4.5.1.4,** the initial rate of the reaction in the presence of thiourea receptor **165** is seen to be extremely fast. The initial rate in the presence of thiourea control **170** deviates from the expected line as a result of poor accuracy of the initial deconvolution results despite removing the results arising from the first 200 minutes of observations.

In response to questions raised about the level of acceleration achieved for the thiourea receptor **165**, a one to one reaction was performed between the 3-(2,5-dioxo-2,5-dihydro-pyrrol-1-yl)-propionic acid **62** and heptane thiol. Reactions were undertaken in the presence and absence of urea and thiourea receptors **164** and **165** under the same conditions adopted for the previous Michael addition. No reaction was observed in any of these experiments. It would not be expected that the reactivity of maleimides **62** and **92** would differ so dramatically unless the addition to one was accelerated by binding to the thiourea receptor. This, along with the data evaluated for the controls for the previous Michael addition proves unequivocally that the reaction is accelerated specifically by binding to thiourea receptor **165** and not because of any general acid or base catalysis by impurities or moieties present in the receptor structure.

Rationalisation for the observed acceleration in the presence of thiourea **165** but absence of reaction in the presence of urea **164** can be rationalised by a series of arguments. If the binding mode of the transition state is similar to that adopted in **Figure 4.1.3**, the difference can be readily explained.

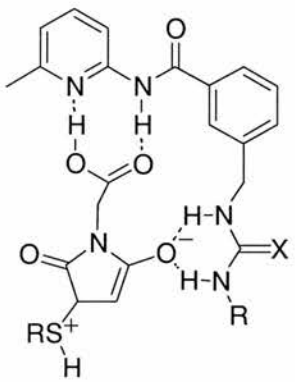

Figure 4.5.1.5 A representation of the charged intermediate of the Michael Addition reaction bound to the receptors in the initially supposed binding mode.

Thiourea and urea are very different structurally. A significant resonance contributor to the overall structure of thiourea is depicted in **Figure 4.5.1.6**. As discussed in **Section 4.3.1**, this is as a result of the increased energy gap between the C 2p and the S 3p orbitals, the energy difference prevents efficient overlap, carbon and sulphur atoms cannot therefore form a strong π bond.

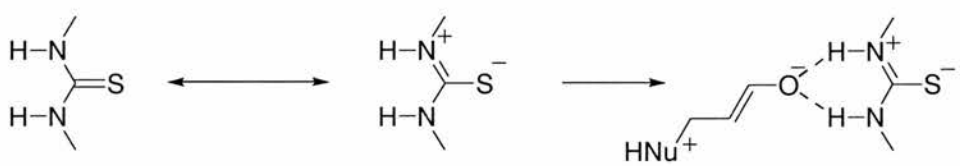

Figure 4.5.1.6 A resonance form of thiourea and how it assists binding to the intermediate if a Michael Addition.

The highly significant zwitterionic resonance form of thioureas enhances the hydrogen bonding capability of the moiety by increasing the acidity of the hydrogen bond donors and charge – reinforced hydrogen bonding.

It is important to recall however, that the binding mode depicted in **Figure 4.5.1.5** was not the lowest energy structure for the ground state complex predicted in a simulated chloroform solution with an AMBER* forcefield, however, modelling of

thioureas was found to be inaccurate and transition state binding may differ greatly from ground state recognition.

4.5.2 Fitting of Michael Addition

The raw kinetic data was fitted using SimFit. The initial model was as follows.

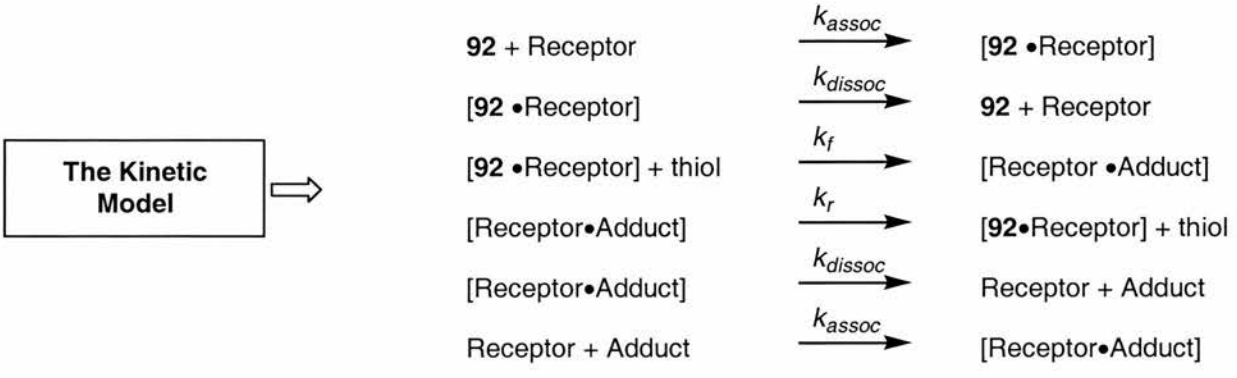

Figure 4.5.2.1 The three equilibria representing the reaction between (2,5-dioxo-2,5-dihydro-pyrrol-1-yl)-acetic acid **92** and heptane thiol in the presence of thiourea receptor **165**.

No background reaction was observed so this was not included in the model. The association constant was as calculated previously. $K_a=k_{assoc}/k_{dissoc}$. The forward association rate was set at the diffusion limit in solution so as not to be the limiting rate.

The choice of following solely productive binding in the complexes was justified by modelling all three sets of data with higher association constants, more typical for these type of complexes. It was found that the data could not be fitted using higher association constants. Although this does not prove that our method for assessing association constants was correct, it does confirm that the value for the association constant is of the correct order of magnitude.

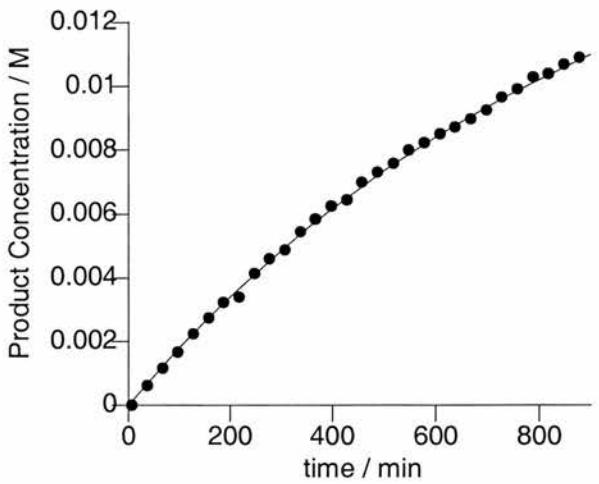

Figure 4.5.2.2 Kinetic data fitted to the reaction model for the Michael addition of heptane thiol to (2,5-dioxo-2,5-dihydro-pyrrol-1-yl)-acetic acid **92**. Closed circles represent the reaction in the presence of the thiourea receptor **165**.

As can be observed from **Figure 4.5.2.2**, an excellent fit between experimental data and the curve calculated experimentally was observed.

The calculated rate constants with the associated errors were as follows:

Table 4.5.2.3 Rate constants calculated for the Michael addition between heptane thiol and the (2,5-dioxo-2,5-dihydro-pyrrol-1-yl)-acetic acid **92**.

k_f / M^{-1} min^{-1}	k_r / M^{-1} min^{-1}
1.13 (± 0.01) x 10^{-4}	2.3 (± 0.3) x 10^{-5}

Unfortunately as the background rate was too slow to be measured over a fifteen-hour timescale, k_{cat} / k_{uncat} values cannot be calculated for this system.

4.6 Cycloaddition Reactions

As with previous receptors, the interactions between the urea and thiourea groups in receptors **164** and **165** can exert a polarising effect upon the conjugated enone similar to a Lewis acid. This can in turn accelerate the cycloaddition between the enone and a diene or dipole.

Table 4.6.1 Initial reaction results for the cycloaddition reaction of dienes or a dipole with (2,5-dioxo-2,5-dihydro-pyrrol-1-yl)-acetic acid **92**. All reactions were performed at 25 mM in $CDCl_3$ at the temperatures reported. Results are reported as percentage conversion to product.

Dipole or Diene	Temp	% Completion with Thiourea Receptor **165**	% Completion with Urea Receptor **164**	Without Receptor
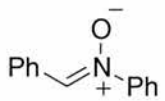	10	35	35	25
	50	0	0	0
	40	18	16	14

Only dimerisation was observed in the reaction between freshly cracked cyclopentadiene and (2,5-dioxo-2,5-dihydro-pyrrol-1-yl)-acetic acid **92** in the presence or absence of either receptors. Reaction was observed however, between *N*-benzylidene-aniline *N*-oxide **141** or furan and (2,5-dioxo-2,5-dihydro-pyrrol-1-yl)-acetic acid **92**. These [3+2] dipolar cycloaddition and Diels Alder reactions were investigated in more detail.

4.6.1 [3+2] Dipolar Cycloaddition

Reactions with the *N*-benzylidene-aniline *N*-oxide **141** and furan were shown to exhibit reactivity in both the presence and absence of the receptor and so these reactions were investigated in further detail using 500MHz ^{1}H NMR spectroscopy.

The nitrone cycloaddition with maleimide **92** was followed by observation of the appearance of four product resonances relating to the two diastereoisomeric products.

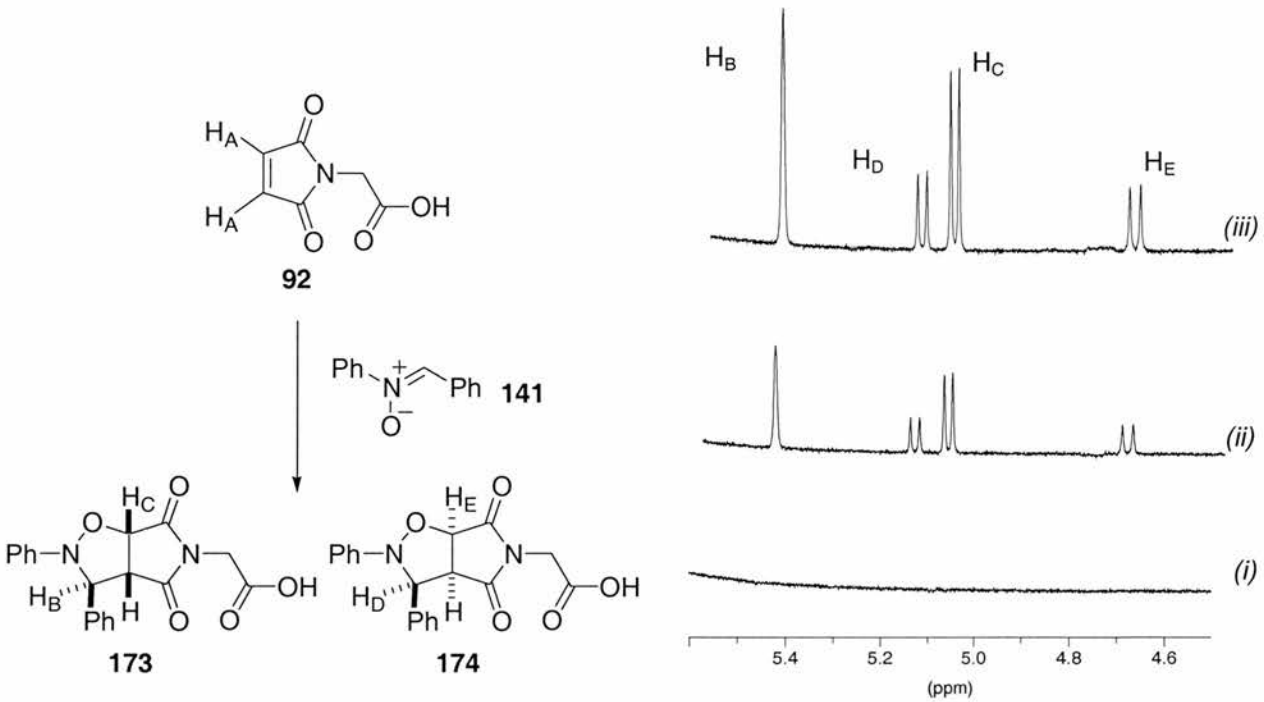

Figure 4.6.1.1 Partial 500 MHz ^{1}H NMR spectra showing the appearance of resonances attributable to the protons from the 5 5 fused *endo* and *exo* adducts, the spectra shown are recorded over *i)* 7, *ii)* 427 and *iii)* 907 minutes.

The percentage conversion to product was evaluated by deconvolution of the product resonances H_B to H_E against the starting material resonance H_A (**Figure 4.6.1.1**).

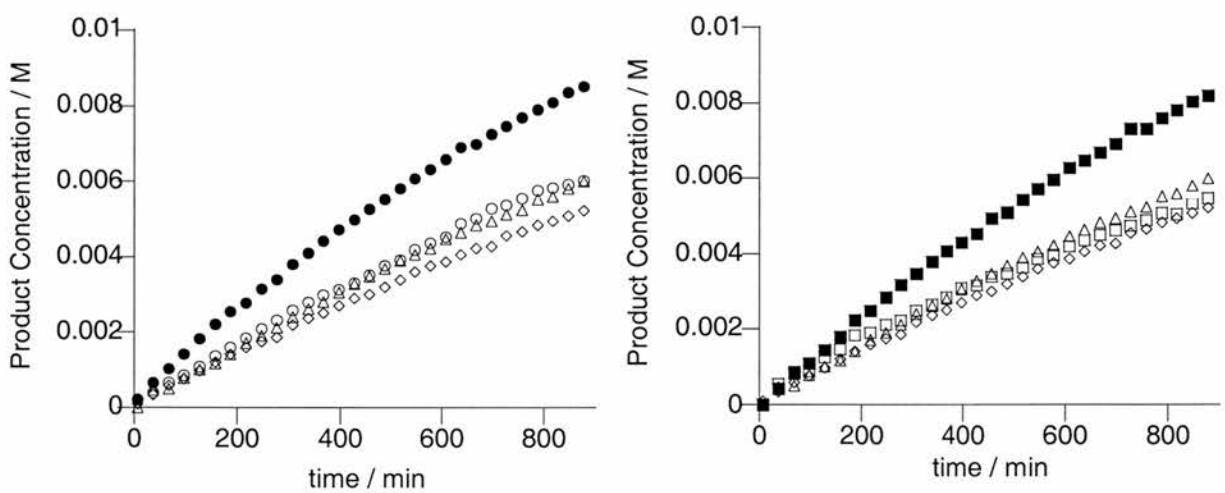

Figure 4.6.1.2 Kinetic data from the reaction between *N*-benzylidene-aniline *N*-oxide and (2,5-dioxo-2,5-dihydro-pyrrol-1-yl)-acetic acid **92**. Open circles represent the reaction in the presence of thiourea receptor **165**, filled squares urea receptor **164**, open circles thiourea control **170**, open squares urea control **169**, open triangles amide control **171**, open diamonds no receptors or controls.

As previously, initial rates were assessed diagrammatically for the reactions by drawing tangents to the initial reaction data. This method is often a more effective

manner in which to visualise reaction accelerations and ignores reaction data late in the reaction when competition for starting materials may obscure the results.

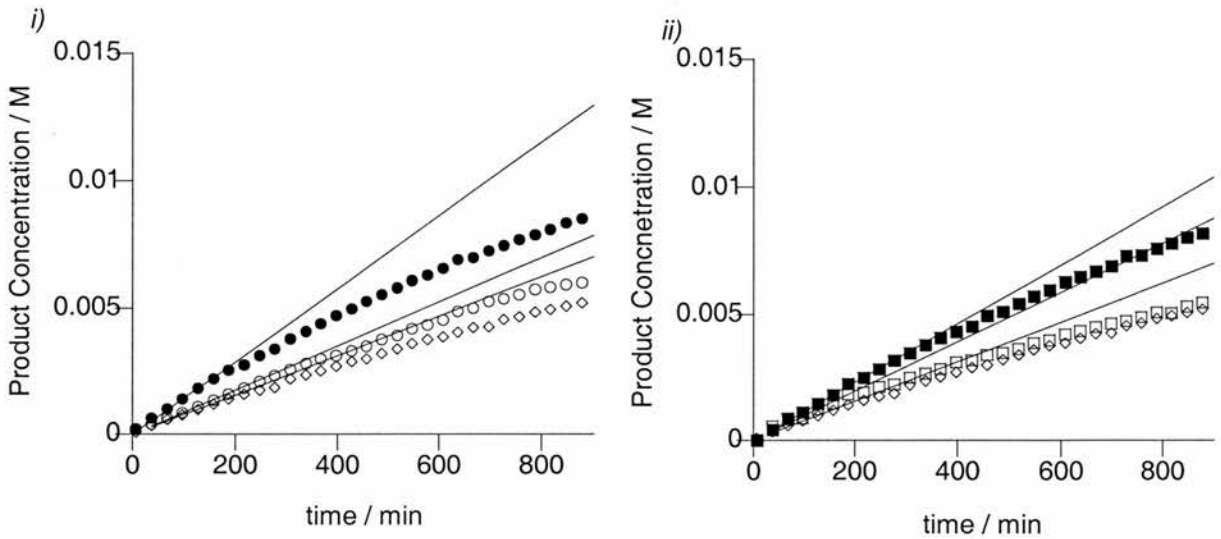

Figure 4.6.1.3 Graph displaying the projection of the initial rates of the cycloaddition between functionalised maleimide **92** and *N*-benzylidene-aniline *N*-oxide in the presence of *i)* thiourea receptor **165** (closed circles) or thiourea control **170** (open circles), *ii)* urea receptor **164** (closed squares) or urea control **169** (open squares) as calculated by linear regression analysis of product concentration in the initial reaction.

It can be observed in **Figures 4.6.1.2** and **4.6.1.3** that receptors **164** and **165** accelerate the formation of the nitrones and it appears that the thiourea receptor **165** accelerates the reaction to the greatest degree. Although the increase in rate is small, it is significant. In the absence of either of the receptors or the presence of the controls, the reaction proceeds at a much lower rate. The thiourea control **170** also accelerates the reaction to a small degree indicating some binding of a carbonyl group on the guest to the thiourea moiety.

4.6.2 Fitting of [3+2] Dipolar Cycloaddition

The cycloaddition between (2,5-dioxo-2,5-dihydro-pyrrol-1-yl)-acetic acid **92** and *N*-benzylidene-aniline *N*-oxide was modelled in a similar manner as before. As a background reaction is present in this example, the rate constants were evaluated from the data and then incorporated into the later model.

The rate constants for the background reaction were calculated using a simple bimolecular reaction model as follows.

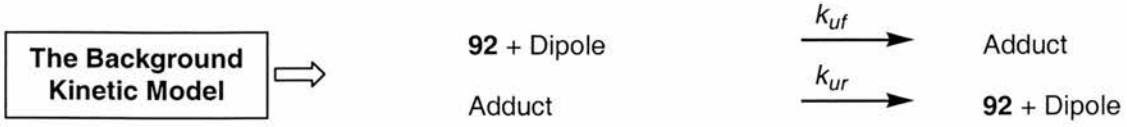

Figure 4.6.2.1 Kinetic model for the background reaction between *N*-benzylidene-aniline *N*-oxide and (2,5-dioxo-2,5-dihydro-pyrrol-1-yl)-acetic acid **92**.

From this kinetic model, the errors were minimised and a fit was obtained minimising the errors between the curve and the experimental data.

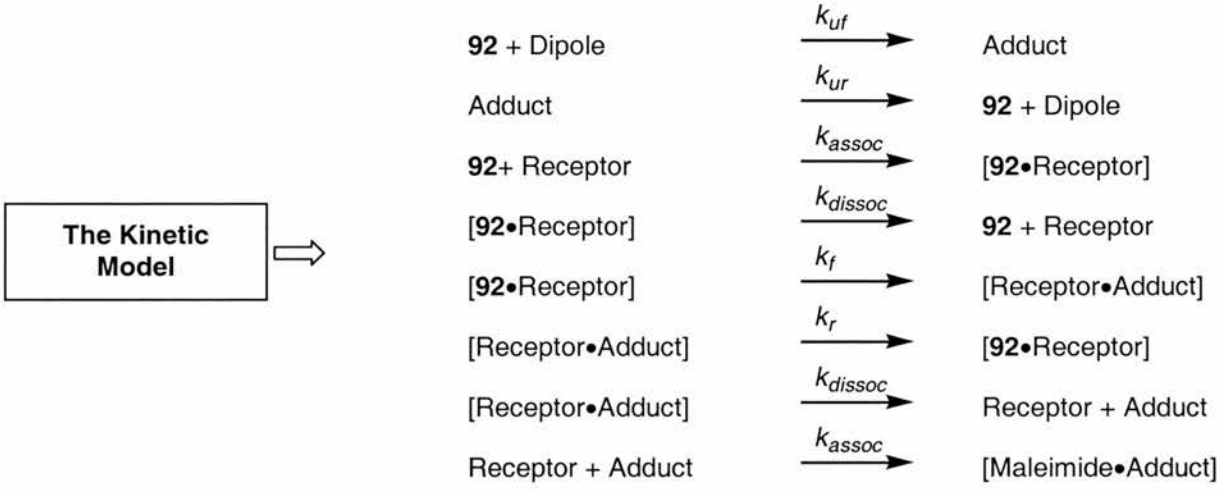

Figure 4.6.2.2 Kinetic model for the reaction of *N*-benzylidene-aniline *N*-oxide with functionalised maleimide 92. Maleimide represents maleimide **92**, dipole represents *N*-benzylidene-aniline *N*-oxide , adduct represents the cycloadduct, receptor represents thiourea **165** or urea **164** receptors.

The kinetic data was fitted to this model, including the previously calculated background rate constants and the weak association constant calculated previously. As before the forward association constant was set at a rate far in excess of the other rate constants to ensure that the rate of complex formation was not rate limiting. As previously, only very low association constants would enable the kinetic data to be fitted to the model, justifying the monitoring of the alkene resonance when calculating the association constant.

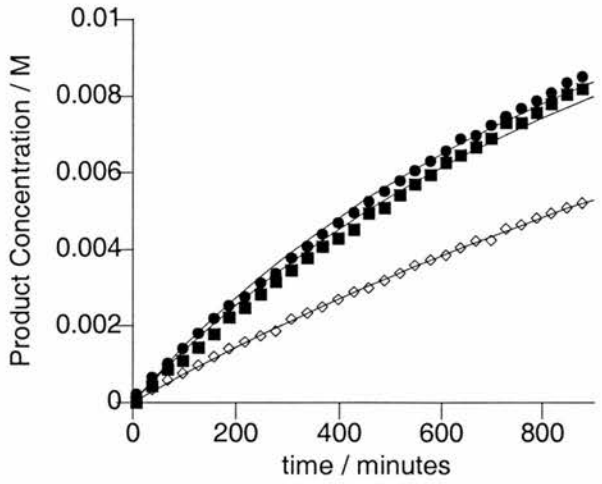

Figure 4.6.2.3 Kinetic data fitted to the reaction model for the cycloaddition of *N*-benzylidene-aniline *N*-oxide to (2,5-dioxo-2,5-dihydro-pyrrol-1-yl)-acetic acid **92**. As previously, filled circles and filled squares represent the reaction conducted in the presence of thiourea **165** and urea **164** receptors respectively. Open diamonds represent the experimental data observed in the absence of receptors.

The original data with the fitted curves are depicted in **Figure 4.6.2.3.**

Table 4.6.2.4 A summary of the rate constants calculated for the reaction of 92 with *N*-benzylidene-aniline *N*-oxide .

Background Reaction

k_{uf} / M^{-1} min^{-1}	k_{ur} / M^{-1} min^{-1}
$2.07 \pm 0.01 \times 10^{-4}$	$9 \pm 3 \times 10^{-7}$

Thiourea 165		Urea **164**	
k_{uf} / M^{-1} min^{-1}	k_{ur} / M^{-1} min^{-1}	k_f / M^{-1} min^{-1}	k_r / M^{-1} min^{-1}
$2.12 \pm 0.02 \times 10^{-3}$	$5 \pm 3 \times 10^{-10}$	$1.95 \pm 0.02 \times 10^{-3}$	$3 \pm 3 \times 10^{-10}$

Therefore, the values for k_{cat}/k_{uncat} for the urea and thiourea receptors are 10.2 ± 0.2 and 9.4 ± 0.2 respectively.

4.6.3 Diels Alder Reaction

Appearance of the two multiplets arising from the *meso endo* and *exo* adducts were followed by 500MHz ^{1}H NMR spectroscopy.

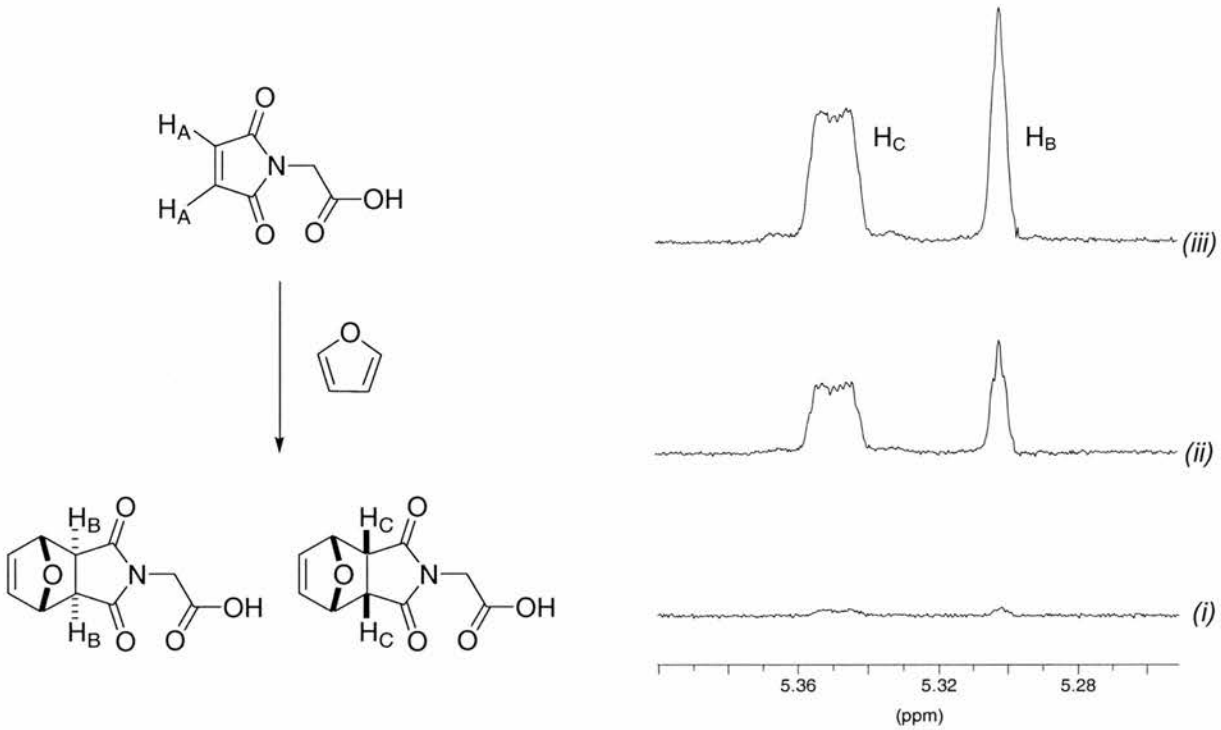

Figure 4.6.3.1 Partial 500 MHz ^{1}H NMR spectrum of the formation of resonances attributable to the endo and exo cycloadducts of the furan, maleimide **92** Diels Alder reaction. The spectra shown were recorded over *i)* 30, *ii)* 480 and *iii)* 930 minutes.

The product resonances arising from the 6 5 fused rings were multiplets as a result deconvolution was less accurate that previous examples. To ensure the deconvolution was accurate, the fit between the experimental data and the deconvolution curves was assessed by inspecting the difference spectra between the experimental and deconvoluted graphs. The deconvolution combined with low conversion to product will result in the errors for the assessment of the Diels Alder reaction being higher than for the other reactions investigated.

Figure 4.6.3.2 shows the kinetic data recorded for the cycloaddition between (2,5-Dioxo-2,5-dihydro-pyrrol-1-yl)-acetic acid **92** and furan.

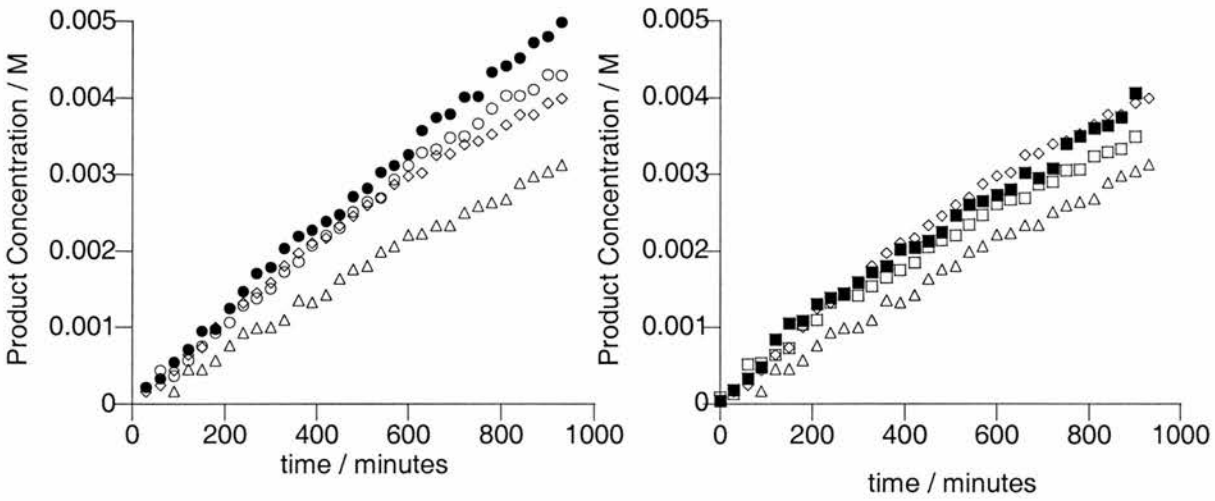

Figure 4.6.3.2 Kinetic data from the reaction between furan and (2,5-dioxo-2,5-dihydro-pyrrol-1-yl)-acetic acid **92**. Open circles represent the reaction in the presence of thiourea receptor **165**, filled squares urea receptor **164**, open circles thiourea control **170**, open squares urea control **169**, open triangles amide control **171**, open diamonds no receptors or controls.

Again, as an estimate of the initial rate acceleration, tangents to the rate data were drawn. In this manner, the results from the kinetic investigations could be more readily compared.

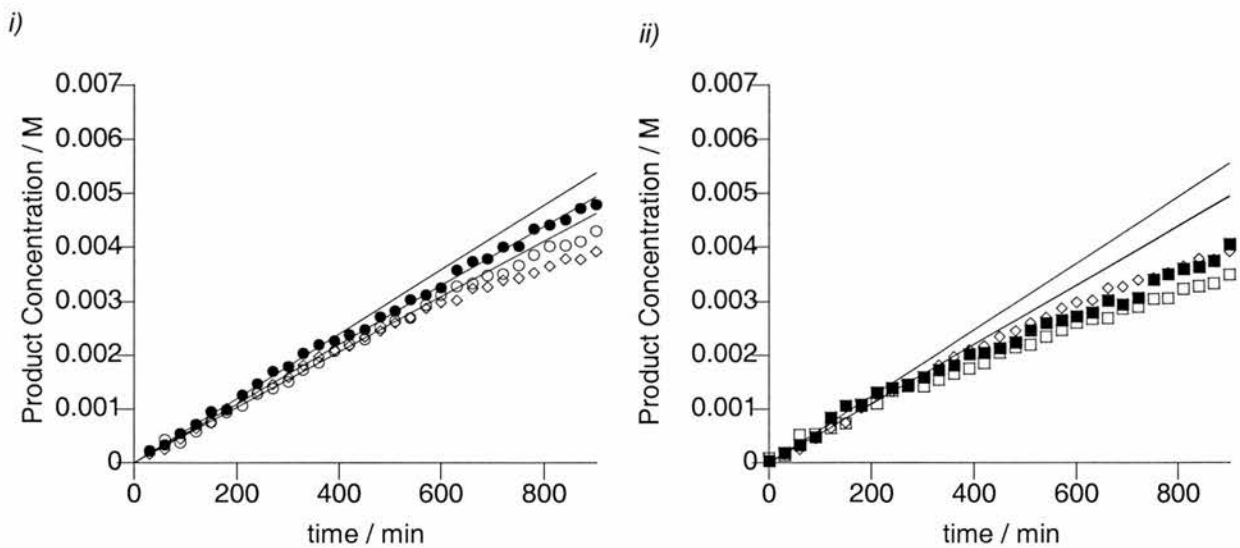

Figure 4.6.3.3 Graph displaying the projection of the initial rates of the cycloaddition between functionalised maleimide **92** and furan in the presence of i) thiourea receptor **165** (closed circles) or thiourea control **170** (open circles), ii) urea receptor **164** (closed squares) or urea control **169** (open squares) as calculated by linear regression analysis of product concentration in the initial reaction.

It is apparent from **Figures 4.6.3.2** and **4.6.3.3** that the addition of the receptors and controls has little effect on the rate of reaction, however, fitting the experimental data to a kinetic model will generate more quantitative assessments.

4.6.4 Fitting of Diels Alder Reaction

The data arising from the Diels Alder reaction between furan and (2,5-dioxo-2,5-dihydro-pyrrol-1-yl)-acetic acid **92** was fitted using non-linear curve fitting procedures according to the models presented.

The Background Kinetic Model ⇨

92 + Diene $\xrightarrow{k_{uf}}$ Adduct

Adduct $\xrightarrow{k_{ur}}$ **92**+ Diene

Figure 4.6.4.1 The reaction model used to calculate the background rate of reaction of the cycloaddition between **92** and furan. Diene represents furan, maleimide represents 92, and Adduct represents the Diels Alder product.

In the absence of any receptors, the reaction kinetics were calculated and then incorporated into the kinetic models in the presence of each receptor. In **Section 4.4**, we observed the thiourea association constant to be $1 \pm 1 M^{-1}$ at 313 K. As changes in chemical shift were observed, it is fair to assume that there is some association occurring in solution. Therefore, the upper limit of the association constant was taken for purposes of calculation of the rate constants of the reaction.

The Kinetic Model ⇨

92+ Diene $\xrightarrow{k_{uf}}$ Adduct

Adduct $\xrightarrow{k_{ur}}$ **92**+ Diene

92+ Receptor $\xrightarrow{k_{assoc}}$ [**92**•Receptor]

[**92**•Receptor] $\xrightarrow{k_{dissoc}}$ **92**+ Receptor

[**92**•Receptor] $\xrightarrow{k_f}$ [Receptor•Adduct]

[Receptor•Adduct] $\xrightarrow{k_r}$ [**92**•Receptor]

[Receptor•Adduct] $\xrightarrow{k_{dissoc}}$ Receptor + Adduct

Receptor + Adduct $\xrightarrow{k_{assoc}}$ [Receptor•Adduct]

Figure 4.6.4.2 Kinetic model for the reaction of *N*-benzylidene-aniline *N*-oxide with functionalised maleimide 92. Maleimide represents maleimide **92**, diene represents furan, adduct represents the cycloadduct, receptor represents thiourea **165** or urea **164** receptors. Prior to minimisation, only k_f and k_r were unknown.

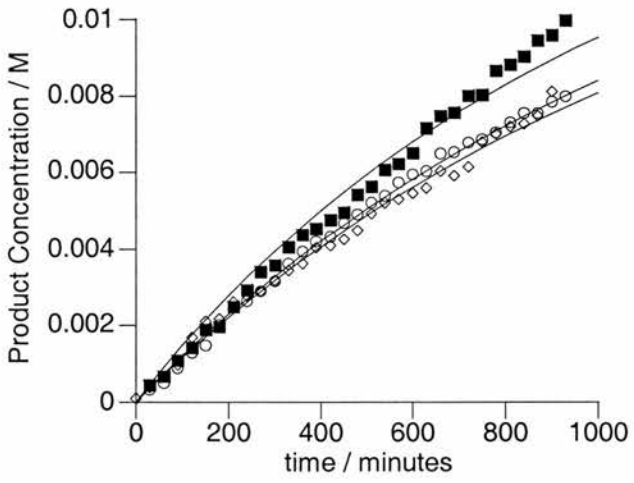

Figure 4.6.4.3 Kinetic data fitted to the reaction model for the cycloaddition of furan to (2,5-dioxo-2,5-dihydro-pyrrol-1-yl)-acetic acid **92**. As previously, filled circles and filled squares represent the reaction conducted in the presence of thiourea **165** and urea **164** receptors respectively. Open diamonds represent the experimental data observed in the absence of receptors. Some deviation from the experimental data is observed, however, it is assumed that the deviation arises from deconvolution errors resulting from the low product concentration and the requirement to deconvolute complex multiplets.

It can be seen that the errors for the rate constants are high and this is reflected by the unsatisfactory fit of the calculated curve to the experimental data. It is important to recall that the overall conversion to product in the reactions in the presence and absence of the receptors is significantly lower than seen previously for the nitrone cycloaddition or Michael Addition and so the associated errors in deconvolution will be significantly higher. The increased errors in the calculation of the forward rate constants in the presence of the receptors are seen in **Table 4.6.4.4**.

Table 4.6.4.4 Summary of the calculated rate constants for the reaction between 92 and furan.

Background Reaction

k_{uf} / M^{-1} min^{-1}	k_{ur} / M^{-1} min^{-1}
$3.41 \pm 0.04 \times 10^{-4}$	$2 \pm 44 \times 10^{-8}$

Thiourea 165		Urea 164	
k_f / M^{-1} min^{-1}	k_r / M^{-1} min^{-1}	k_f / M^{-1} min^{-1}	k_r / M^{-1} min^{-1}
$2.6 \pm 0.1 \times 10^{-3}$	$3 \pm 3 \times 10^{-10}$	$4.4 \pm 0.5 \times 10^{-4}$	$8 \pm 3 \times 10^{-7}$

Therefore, the values for k_{cat}/k_{uncat} for the thiourea and urea receptors are 7.6 ± 0.4 and 1.3 ± 0.1 respectively

4.7 Conclusions

Table 4.7.1 Summary of the kcat/kuncat values evaluated for the three reactions.

Michael Addition	[3+2] Dipolar Cycloaddition		Diels-Alder Reaction	
	Thiourea 165	Urea 164	Thiourea 165	Urea 164
Cannot be calculated	10.2 ± 0.2	9.4 ± 0.2	7.6 ± 0.4	1.3 ± 0.1

Although the value for k_{cat}/k_{uncat} cannot be calculated for the addition of heptane thiol to functionalised maleimide **92** in the presence of thiourea receptor **165**, as the background rate is too slow to measure over the time period, intuitively, the figure must be particularly large, much larger than the observed accelerations of the cycloaddition reactions. Although direct comparison of rate accelerations is not possible, this does confirm that the increase in the rate of reaction is amplified as the transition state polarity rises.

Rational design of synthetic catalysts is not simple. Unless a receptor is highly preorganised to a substrate, many non-productive binding modes may exist, binding modes which would not be possible for the more simple receptors **138** and **149**. Although some of the binding modes will assist with accelerating reactions, the relative contributions from the productive and non-productive binding modes is difficult to quantify experimentally when a system is in fast exchange.

Initially the validity of the measured association constants was doubted. If the expected complex was the major association observed, association constants of the order 10^2 M^{-1} would be anticipated. Modelling of the chemical reactions with association constants of this order was also attempted, however, no calculated fits for the experimental data could be obtained. Only considering productive binding in the kinetic models is a simplification, however, the approximation allows fitting of the kinetic data and is an improvement upon a kinetic model incorporating all binding present in solution.

Incorporation of a binding functionality into the N substituent of the maleimide also affected the solubility of the substrate in chloroform. A method to overcome this decrease in solubility also needs to be developed.

5. Developing the Receptor Design

5.1 Lengthening the Spacer Group

In **Section 4** the problems associated with the receptors **164** and **165** were discussed. Although soluble, the associated functionalised maleimide **92** had a maximum solubility of 25 mM in $CDCl_3$. The complexes were also found to be non-ideal fits by computational and experimental methods.

In **Section 4.3.1** it was calculated that not all structures in solution of the urea and thiourea receptors **164** and **165** adopted the anticipated coconformation. Changing the spacer may be able to improve the fit between host and guest. It was decided that to investigate the reactivity trends further and improve solubility, a longer spacer should be incorporated into the receptor. In this manner the solubility of the guest may be improved and the ether linkage allows greater potential variability in the structure of the molecule.

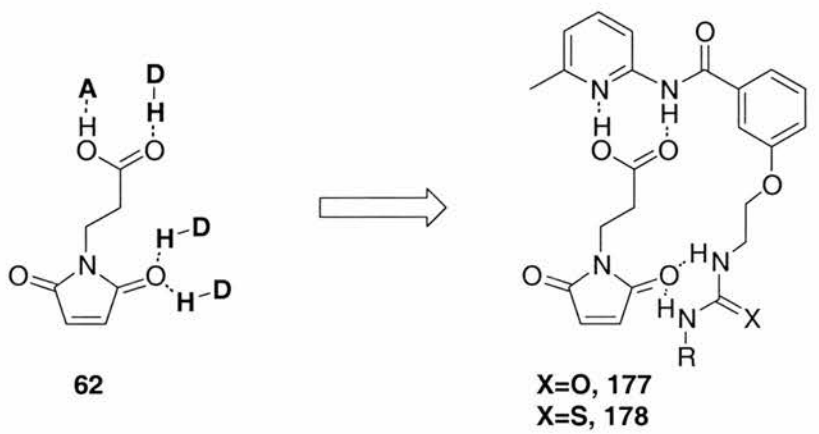

Figure 5.1.1 Incorporation of a longer spacer group enables design of a new receptor to expand the data set and enable greater solubility. X = O, S.

The resulting compound would then bind to a functionalised maleimide **62**, which has been previously synthesised and known to be more soluble than the maleimide possessing a shortened tether length **92**.

The receptors would adopt a similar mechanism for catalysis to **Figure 4.1.1**, possessing different binding and stabilising moieties. The carboxylic acid group is designed to bind with the amidopicoline and be undisturbed by any reaction processes occurring at the maleimide reaction centre. As previously, the urea or

thiourea moieties are intended to polarise the ground state of the molecule and stabilise any transition state negative charge.

5.2 Molecular Modelling

The design was assessed using a molecular modelling program, Macromodel in a similar manner to the previous receptor designs. Complexes were modelled using an AMBER* forcefield in simulated chloroform.[145] As before, structures were modelled separately, minimised and subsequently minimised together. The resulting local minimum coconformation was subjected to a Monte Carlo conformational search to find the global minimum. The structure calculated for the urea bound to the functionalised maleimide **62** is depicted in **Figure 5.2.1**.

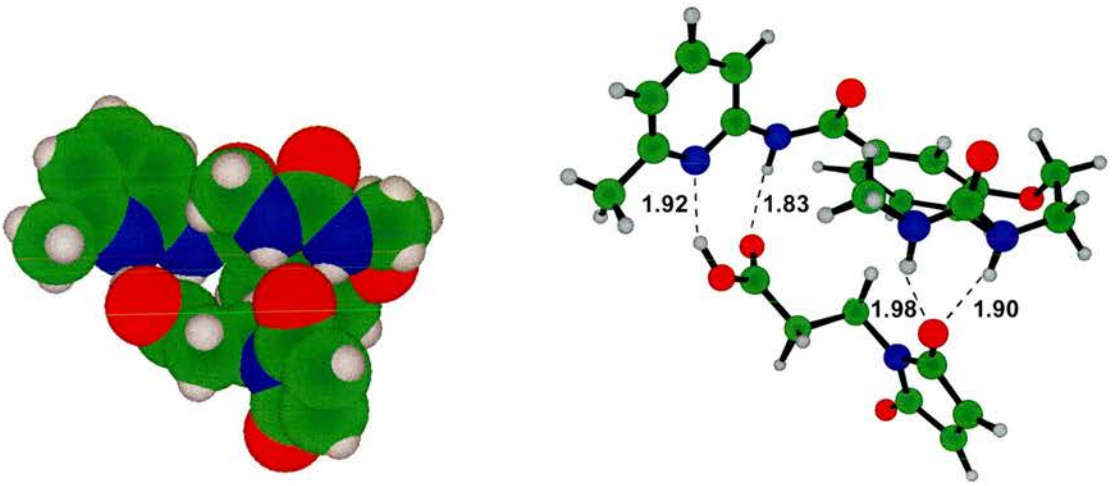

Figure 5.2.1 Space filling and ball and stick models of the calculated global minimum energy complex between receptor **177** and maleimide **62**. All intermolecular distances are in Å. The cyclohexyl group is omitted for clarity.

The receptor is seen to fold internally making two-dimensional representation difficult. All the anticipated hydrogen bonds are however, present in the calculated global minimum energy structure.

We previously observed that the global minimum energy structure is not exclusive and other structures may be accessible in solution in a dynamic system. As a result, it is often informative to examine the structures identified as low energy conformations.

The coconformations were analysed further to assess the number containing the expected recognition motifs. Analysing the structures higher in energy than the

global minimum revealed that very few structures were within 10 kJ mol^{-1} of the global minimum because of the very low relative energy of the global minimum. Expanding the data set to include more coconformations up to 20 kJ mol^{-1} higher in energy revealed the global minimum structure was not the only example of a coconformation with the depicted hydrogen bonds. Of the structures up to 20 kJ mol^{-1} higher in energy than the global minimum, 46% possessed the amide / carboxylic acid recognition motif. Analysing these coconformations further in **Figure 5.2.2** provides some information about the frequency of the occurrence of the coconformation.

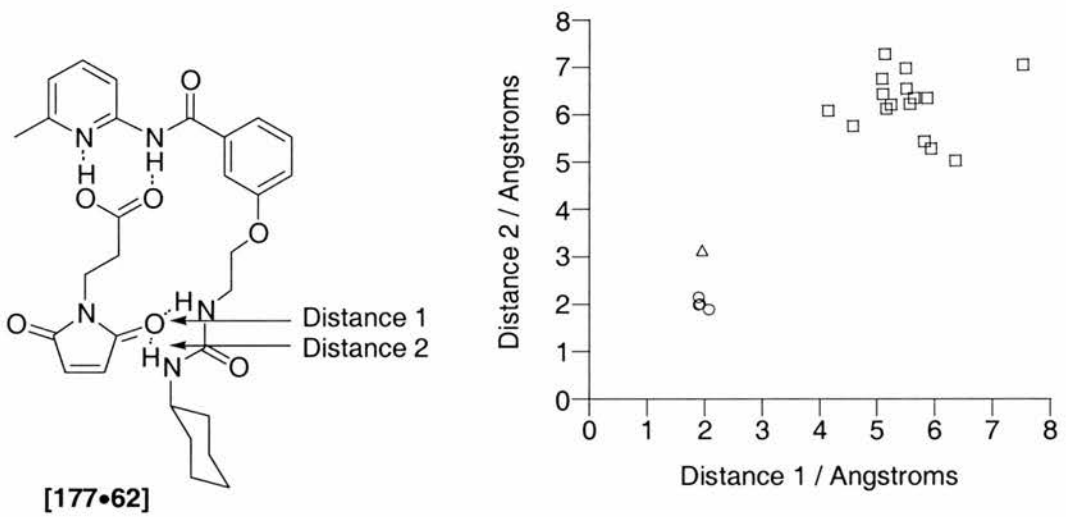

Figure 5.2.2 Scatter plot of the distances between the carbonyl groups and urea protons in the structures with energies + 20kJ mol^{-1} relative to the Global minimum. All the structures depicted possess the acid amidopicoline recognition unit. Circles represent coconformations possessing both hydrogen bonds to the urea moeity, triangles and diamonds possess one hydrogen bond and squares represent structures with no hydrogen bonding present.

Of all the structures less than 20 kJ mol^{-1} higher in energy, 9% contain all four hydrogen bonds, a further 7% contain hydrogen bonds to the enone moiety in the absence of amide carboxylic acid recognition. From this computational investigation, it is clear that the global minimum structure, which is particularly low in energy, possesses all the expected hydrogen bonds and other low energy coconformations in solution will also possess the expected interactions.

The conformational analysis was extended to the thiourea receptor **178**. It was previously observed that the conformational analysis of thioureas was possibly

inaccurate, however, it may be of interest to pursue the calculation and observe whether the expected recognition motif is present.

Modelling the complex yielded the global minimum structure depicted in **Figure 5.2.3** As can be observed, this was not the expected coconformation of the complex.

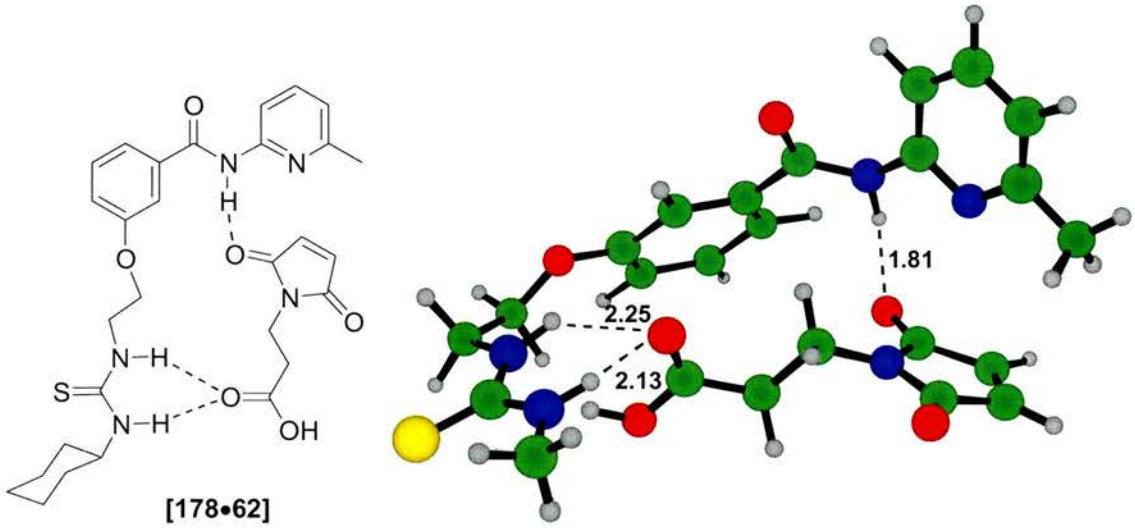

Figure 5.2.3 Global minimum energy structure of thiourea **178** with functionalised maleimide **62**. The structure was calculated in a simulated chloroform solution using a Monte-Carlo conformational search technique with an AMBER* forcefield. The structure was modelled in the presence of the cyclohexyl R group, however this is omitted for clarity in the coconformation shown.

Analysing the structures higher in energy than the global minimum revealed that only 5 coconformations were within 10 kJ mol^{-1} of the global minimum. Expanding the data set to include more coconformations up to 20 kJ mol^{-1} higher in energy revealed the global minimum structure was the only example of a coconformation with the depicted hydrogen bonds. It was therefore decided to analyse the data to assess the contribution from the expected coconformational motif to the binding in solution. The structures of appropriate energy were sorted to exclusively investigate those possessing the acid amido-picoline recognition motif. These were analysed further to assess the frequency of binding from the thiourea moiety to the carbonyl group of the enone.

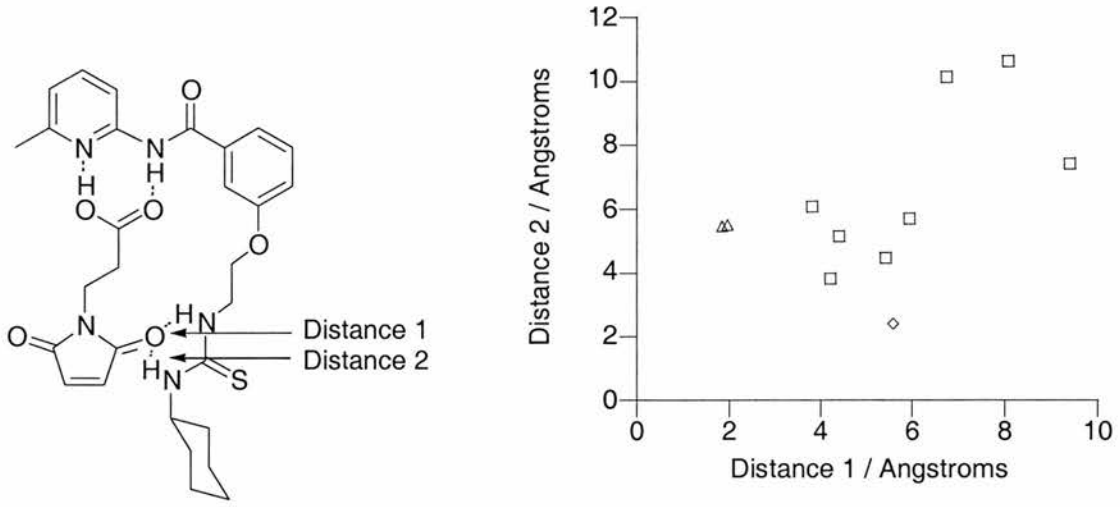

Figure 5.2.4 Scatter plot of the distances between the carbonyl groups and thiourea protons in the structures with energies + 20kJ mol^{-1} relative to the Global minimum. All the structures depicted possess the acid amidopicoline recognition unit. triangles and diamonds represent coconformations possessing one hydrogen bond to the thiourea moeity, and squares represent structures with no hydrogen bonding present.

As can be observed in **Figure 5.2.4**, only three coconformations (triangles and diamonds) possess structures containing hydrogen bonding to the thiourea and the amide carboxylic acid recognition motif. In these coconformations, only one hydrogen bond is observed. It was previously suggested however, that thioureas were not efficiently modelled in Macromodel and the hydrogen bond donor ability was underestimated.

5.3 Synthesis

Synthesis of the funtionalised maleimide 3-(2,5-dioxo-2,5-dihydro-pyrrol-1-yl)-propionic acid **62** was performed as described for compound **92**. The reaction yield was poor as a result of the competing polymerisation reaction of the intermediate **179**.

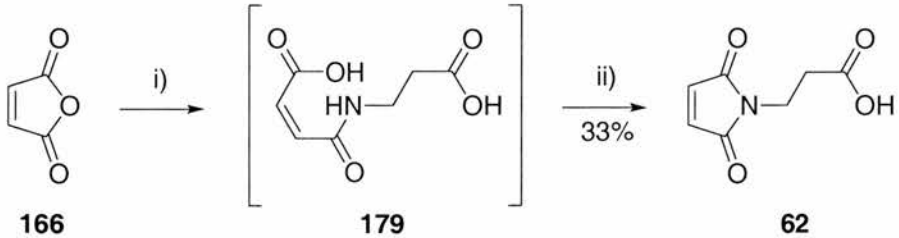

Scheme 5.3.1 i) Glacial acetic acid, β-alanine, r.t. 16 hrs, ii) Reflux, 8 hrs

Retrosynthetic analysis was employed on the proposed receptors to find a suitable synthetic strategy. The initially proposed route was a sequential synthesis of each receptor.

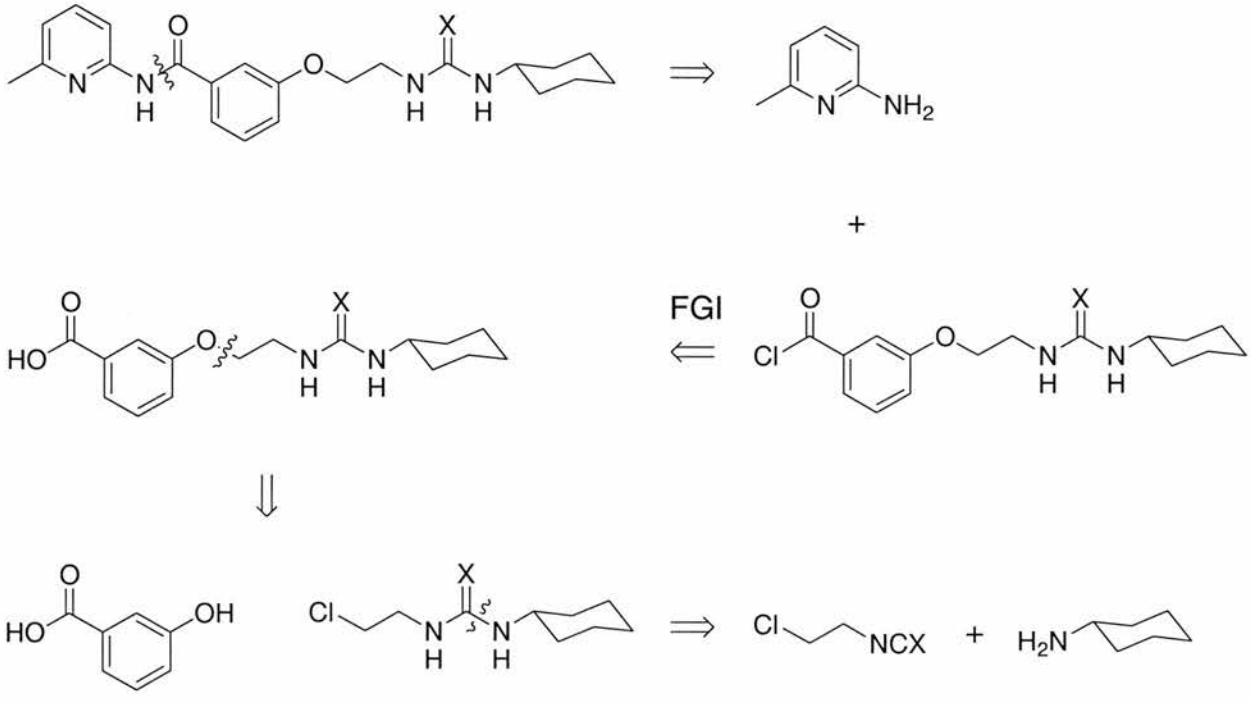

Scheme 5.3.2 Retrosynthetic analysis for the synthesis of receptors **177** and **178**.

The synthesis of the urea and thiourea chlorides **183** and **184** proceeded in high and moderate yield respectively.

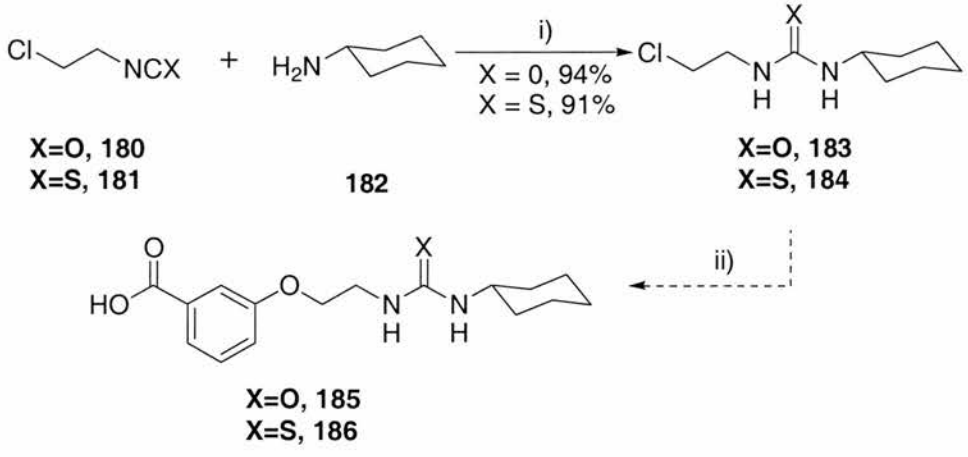

X=O, 180
X=S, 181

182

X=O, 183
X=S, 184

X=O, 185
X=S, 186

Scheme 5.3.3 Formation of the urea and thiourea chlorides **183** and **184** and subsequent failed coupling with 3-hydroxybenzoic acid. i) Et_2O, 0ºC – r.t, 1hr, ii) K_2CO_3, CH_3CN, 3-hydroxybenzoic acid, reflux 5 days.

The attempted coupling of the chlorides **183** and **184** to 3-hydroxybenzoic acid **190** however, was unsuccessful. It was hypothesised that the excess potassium carbonate would cause a double deprotonation of the 3-hydroxy benzoic acid causing precipitation of the starting material from the reaction solvent, reducing the nucleophilicity and preventing attack of the phenolate anion onto the chloride **183**.

An alternative route was proposed as depicted in **Scheme 5.3.4**.

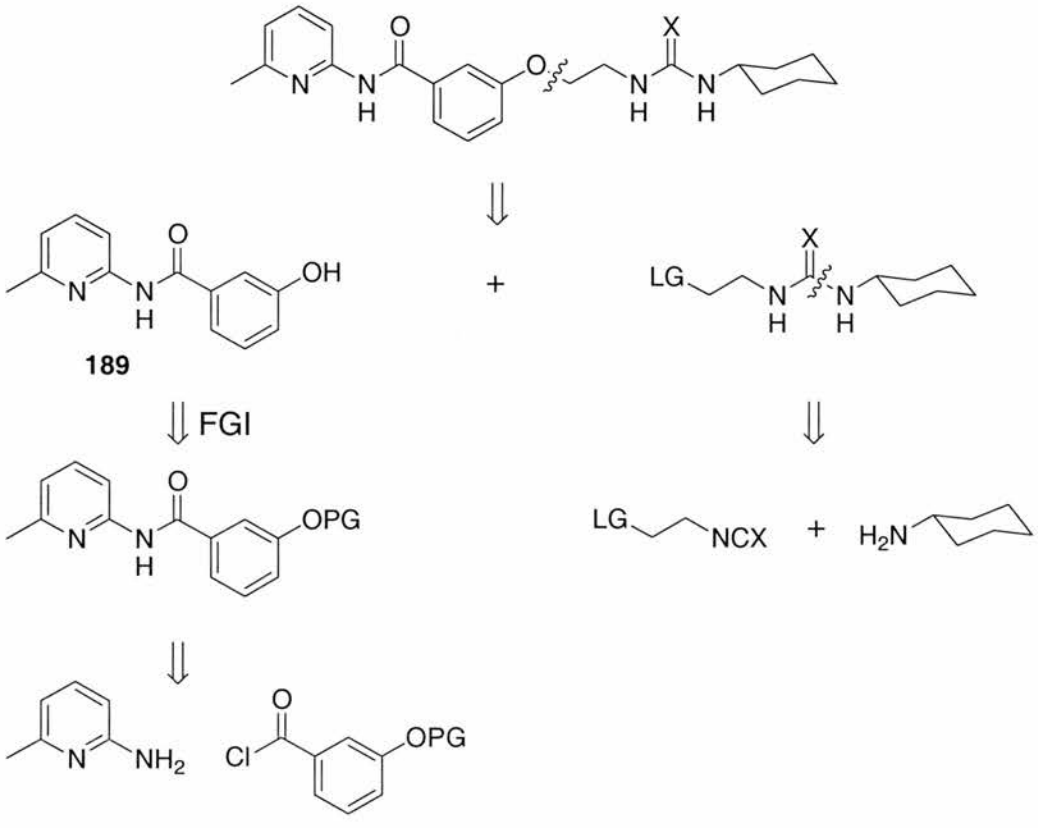

Scheme 5.3.4 Retrosynthetic analysis for the synthesis of receptors **177** and **178**.

The advantages to this alternative synthetic strategy are the simultaneous synthesis of both receptors *via* a key 3-hydroxy-*N*-(6-methyl-pyridin-2-yl)-benzamide **189** and the adoption of a parallel rather than sequential synthesis.

The initial synthesis of amide **189** was attempted *via* reaction of 3-methoxy benzoyl chloride 187 with 2-amino-6-methylpyridine and subsequent deprotection of the methoxy group.

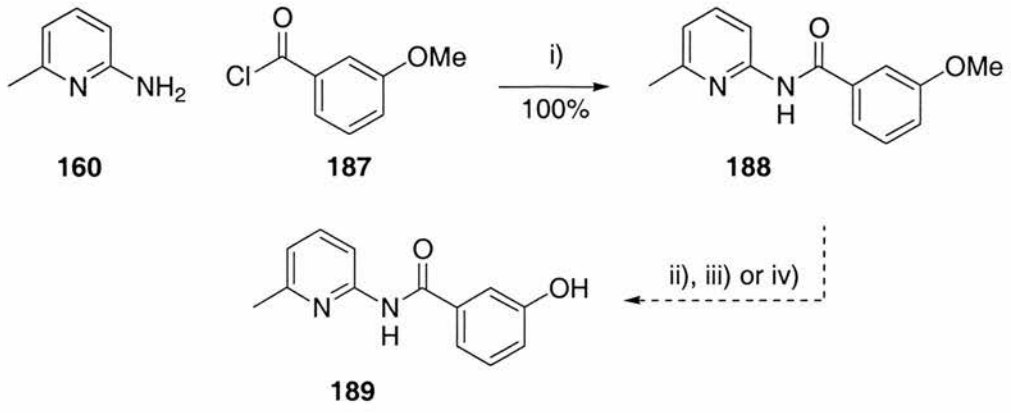

160 187 188 189

Scheme 5.3.5 i) CH_2Cl_2, 0°C – r.t. 16hrs, ii) BBr_3, CH_2Cl_2, 0°C 2 hrs iii) BBr_3, CH_2Cl_2, r.t. 16 hrs iv) BBr_3, CH_2Cl_2, reflux 2 hours.

The deprotection was attempted under increasingly aggressive conditions, however, only starting material was recovered from the reaction mixture.

An alternative strategy was adopted involving the simultaneous protection of the phenolic and carboxylic acid groups. The protected 3-hydroxybenzoic acid **191** was converted to the corresponding acid chloride **192**, 3-(*tert*-butyl-dimethyl-silanyloxy)-benzoyl chloride which was then reacted directly with a solution of 2-amino-6-methylpyridine **160** *in situ*. The 3-(*tert*-butyl-dimethyl-silanyloxy)-*N*-(6-methyl-pyridin-2-yl)-benzamide **193** was then purified *via* column chromatography and reverted to the 3-hydroxy-*N*-(6-methyl-pyridin-2-yl)-benzamide **189** using standard conditions.

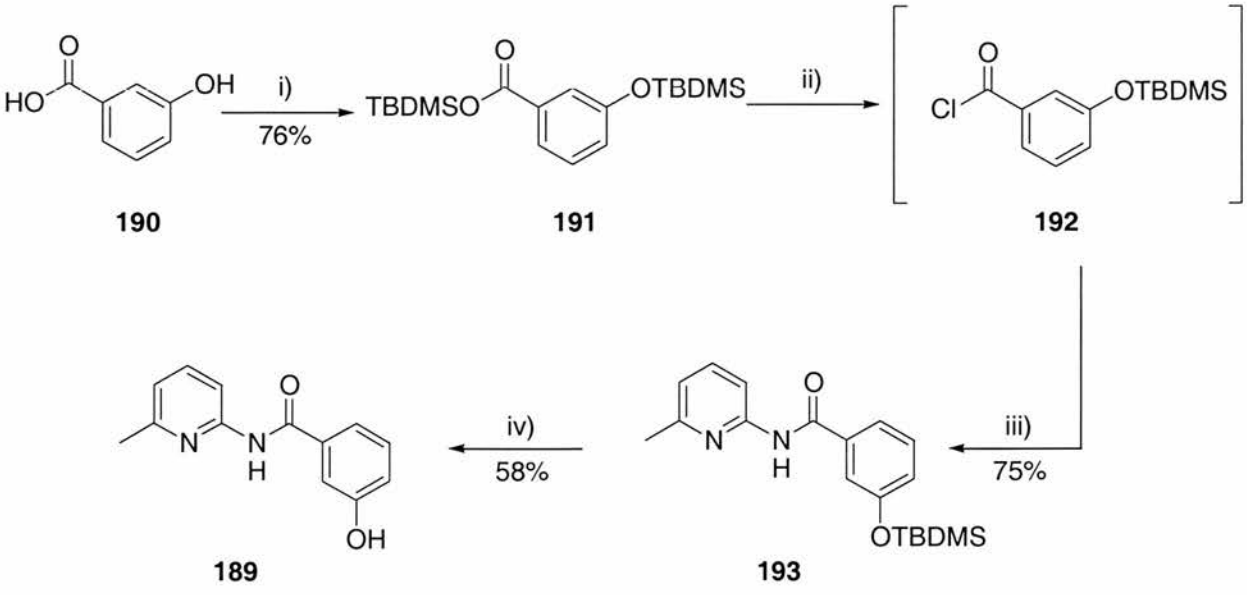

190 191 192 193 189

Scheme 5.3.6 i) TBDMSCl, imidazole, CH_2Cl_2, 0°C - r.t., 16hrs, ii) $(COCl)_2$, DMF, CH_2Cl_2, 40 hrs, r.t., iii) 2-Amino-6-methylpyridine **160**, CH_2Cl_2, 16hrs, r.t, iv) TBAF, 1M in THF, 1 hr, r.t

The one pot deprotection and activation step presents an interesting transformation. In one capacity the similarity between the reactivity of the phenol and carboxylic acid is displayed and yet in the deprotection and activation the carboxylic acid is specifically attacked.

The interesting deprotection, activation mechanism was partially proposed by the original authors for the production of esters *in situ*.[156] DMF **194** is vital in the reaction mixture and the transformation fails in its absence. The authors propose the formation of the intermediate **195**, normally termed the Vilsmeier reagent.[157]

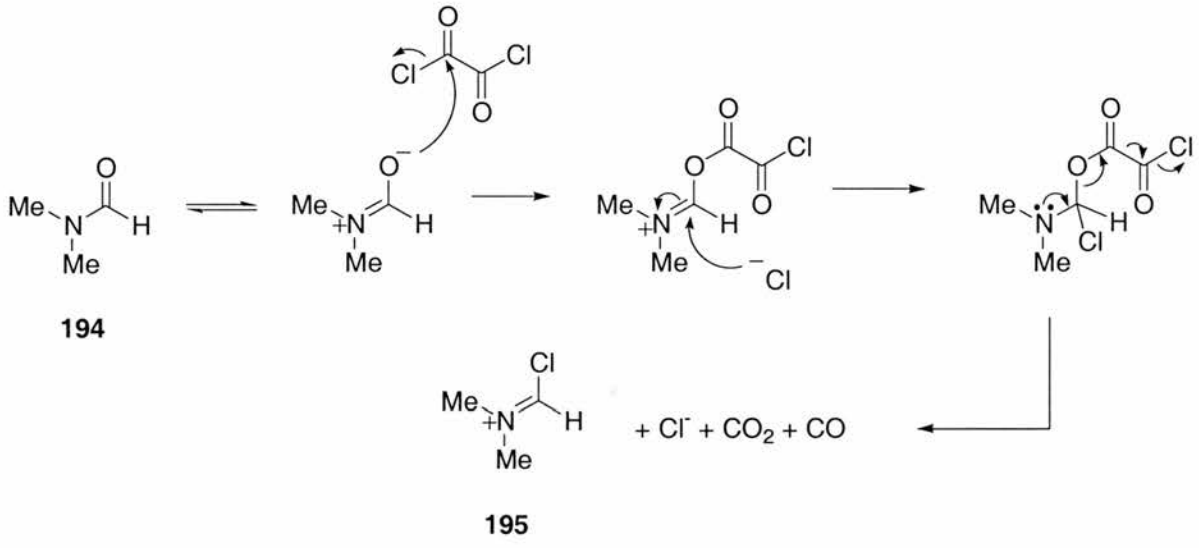

Figure 5.3.7 Formation of the Vilsmeier reagent **195** from reaction of DMF with oxalyl chloride.

Generation of the Vilsmeier reagent **195** is more commonly accomplished *in situ* using DMF and $POCl_3$, however use of oxalyl chloride enables the generation of a second equivalent of chloride anion which is vital in this particular transformation.

The Vilsmeier reagent **195** is more commonly used for converting aromatic derivatives to aryl aldehydes,[159] or cyclic ketones[160] however, in this example, attack of the chloride anion on the protected acid and subsequent attack of the carbonyl onto the Vilsmeier reagent **195** yields an intermediate capable of fragmentation.

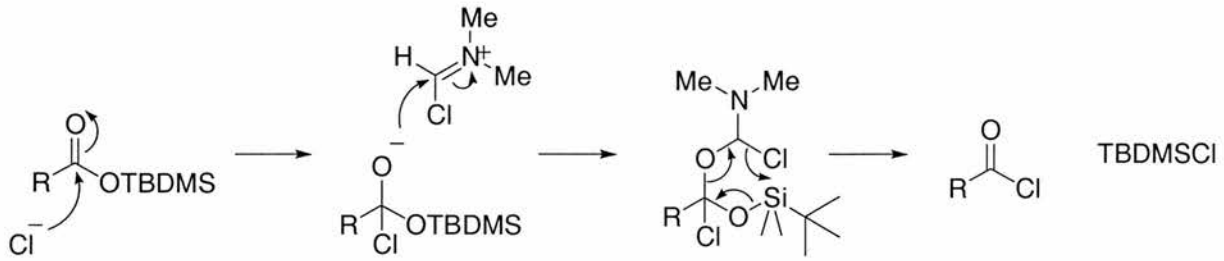

Figure 5.3.8 Attack of the protected carboxylate onto the Vilsmeier reagent and subsequent decomposition to the acid chloride.

This deprotection and activation is unusual because it is selective for the protected acid only and removal of the t-butyldimethylsilyl group must proceed *via* an intramolecular attack of a chloride rather than the more commonly observed fluoride; chloride reacting in an intermolecular sense is not commonly considered able to perform this transformation.

It was decided that optimisation of the ether formation reaction to afford 1-cyclohexyl-3-(2-phenoxy-ethyl)-urea **196** should be performed prior to conducting the synthesis with the 3-hydroxy-*N*-(6-methyl-pyridin-2-yl)-benzamide **189**. The initial method employed was the traditional phenolic ether formation using excess potassium carbonate. The yields observed however were low.

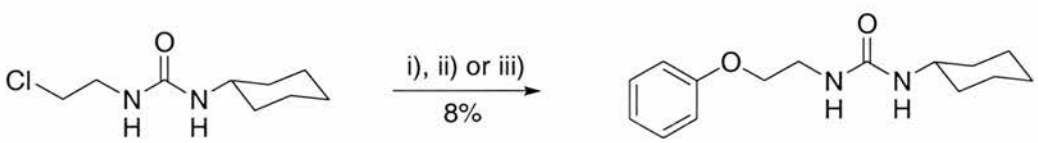

183 **196**

Scheme 5.3.9 i) K_2CO_3, CH_3CN, Phenol, reflux 5 days. ii) $CsCO_3$, CH_3CN, Phenol, reflux 5 days. iii) NaH, Phenol, THF. The yield reported is for method c.

A new reaction was attempted using sodium hydride stoichiometrically. However, the reaction suffered from similarly low yields.

In order to improve the yields, the leaving group ability of the urea was improved. Synthesis and subsequent coupling of toluene-4-sulfonic acid 2-(3-cyclohexyl-ureido)-ethyl ester **200** and toluene-4-sulfonic acid 2-(3-cyclohexyl-thioureido)-ethyl ester was attempted.

The yield of the tosylation of **198** was poor, however, tosylation or mesylation of urea containing compounds has not been widely reported in the literature.

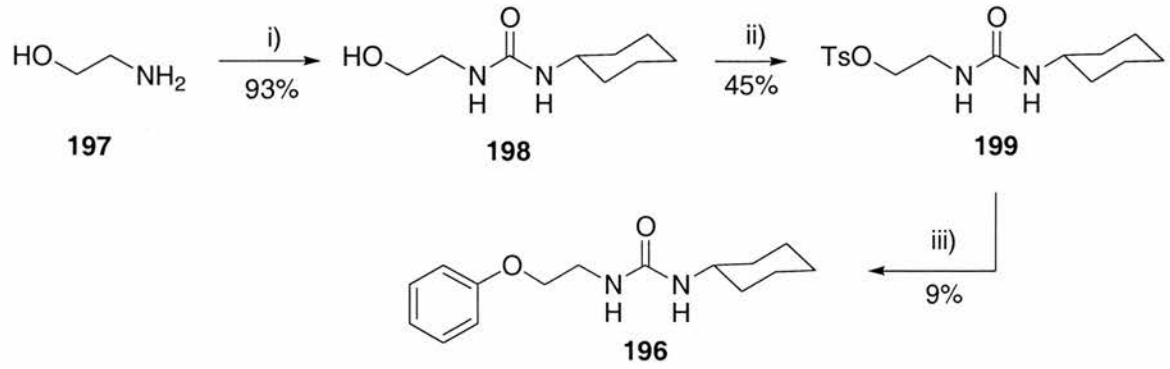

197 198 199 196

Scheme 5.3.10 i) Cyclohexyl isocyanate dry Et_2O, 0°C to r.t, ii) TsCl, Et_3N, CH_2Cl_2, r.t., 16 hrs. iii) Phenol, K_2CO_3, CH_3CN, reflux 5 days

It is hypothesised one of the reasons for the low yields observed for the addition of phenol to 1-(2-chloro-ethyl)-3-cyclohexyl-urea **183** or toluene-4-sulfonic acid 2-(3-cyclohexyl-ureido)-ethyl ester **199** were as a result of binding of the phenolate to the urea moiety. Binding of the phenolate ion would dramatically reduce the nucleophilicity of the reactant. It is not surprising that this occurred in solution, ureas were chosen in the receptor design for their ability to bind to carbonyl groups or the transition states of nucleophilic additions.

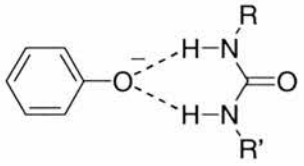

Figure 5.3.11 Representation of the stabilisation of the phenolic cation by the presence of a urea in a reaction mixture.

The reaction was repeated in using dimethylformamide as a solvent to help fragment the phenolate urea aggregates in solution. Although the product was formed, isolation was difficult as removal of the DMF solvent from the reaction mixture was problematic.

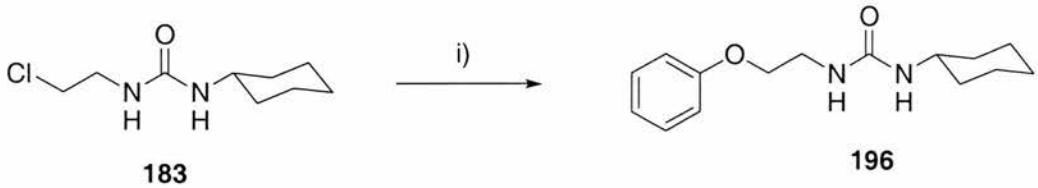

183 196

Scheme 5.3.12 i) NaH, Phenol, NaI, DMF

The zwitterionic resonance form of DMF, would be bound with a high association constant by the urea moieties present in solution. The remaining DMF in the reaction

mixture was too tightly bound to be extracted with water. As a result of the complexation of the dimethylformamide by the urea starting material and product, reproducible column chromatography conditions were unobtainable and in all occasions the urea was isolated containing DMF as a contaminant.

Figure 5.3.13 Binding of DMF with ureas, the zwitterionic resonance form is tightly bound by charge reinforced hydrogen bonding.

Ultimately, a Mitsunobu reaction was employed for direct coupling of the previously synthesised alcohols and phenol.[161]

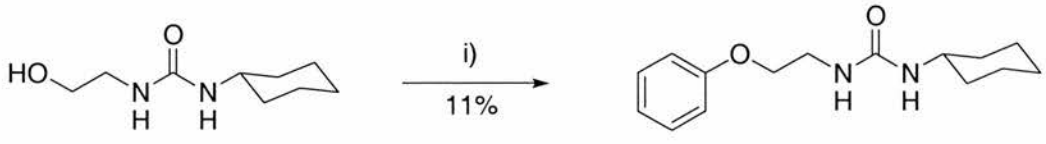

198 **196**

Scheme 5.3.14 The Mitsunobu reaction to couple an ether to phenol. i) DEAD, Phenol, PPh_3, CH_2Cl_2, 0°C – r.t. 72 hrs.

Although the overall yield was not greatly improved by the use of the Mitsunobu reaction, the number of side reactions was minimised making isolation of the product less challenging. This may have been due to milder reaction conditions.

The position of the leaving group in relation to the urea would enable an intramolecular cyclisation to occur, this type of intramolecular reaction has been previously observed in the literature.[162, 163] Although the cyclic product **200** was not isolated from the reaction mixtures, it is interesting to refer to the mass spectra of the tosylate **199** and the chlorides **183** and **184**. The spectra of compounds **199** and **183** contain significant proportions of the cyclic product **200** formed during the vapourisation of the sample. The mass spectrum of **184** indicates that the rearrangement the thiourea is highly favoured under the conditions employed for recording the mass spectrum. Qualitatively, this result would be anticipated, contribution to thiourea molecular bonding from the zwitterionic resonance forms possessing a negative charge on the sulfur atom was discussed in **Section 4.3**.

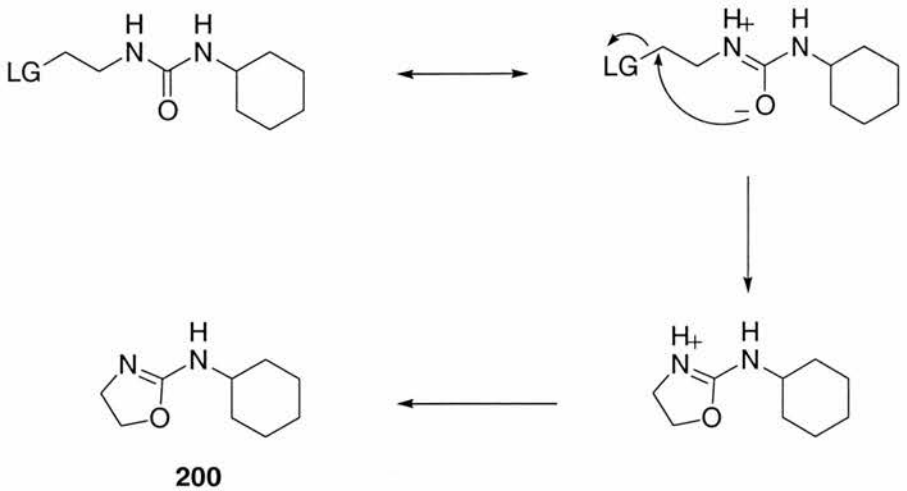

200

Scheme 5.3.15 A rationalisation for the poor yields observed in the reactions to form the urea 196 by the intramolecular cyclisation of the starting material. LG = OTs or Cl.

The Mitsunobu reaction also generates a phenolate anion as shown in **Scheme 5.3.16** so inhibition by urea binding may still be expected, however the more gentle reaction conditions employed by performing the reaction at room temperature, prevents some of the side reactions from occurring.

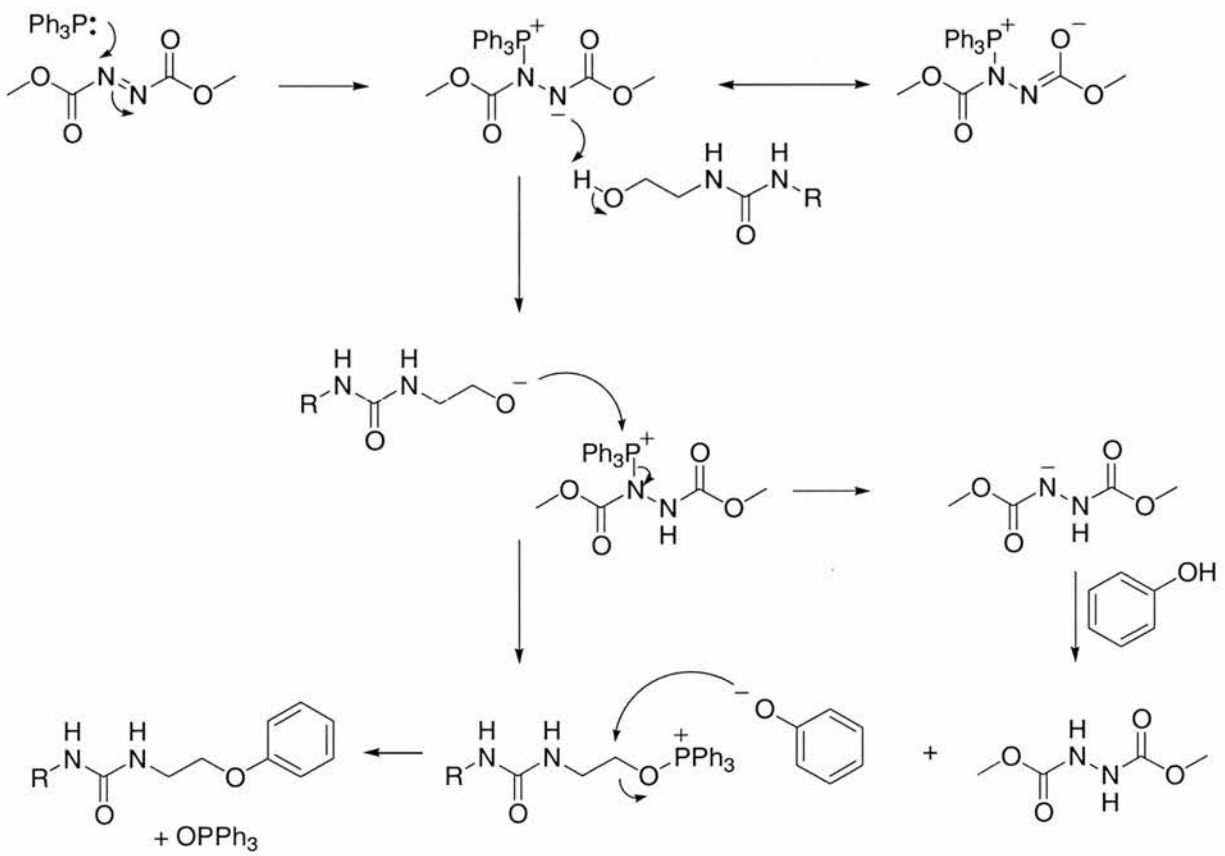

Scheme 5.3.16 The Mechanism of the Mitsunobu reaction as applied to the formation of 1-cyclohexyl-3-(2-phenoxy-ethyl)-urea **196**. R = cyclohexyl.

Synthesis of urea receptor **177** was also attempted utilising the Mitsonobu reaction. Unfortunately, owing to the low solubility of the urea product, it could not be isolated. However, the synthesis of the crude poorly soluble mixture proved that the extreme insolubility of the urea in deuterated chloroform rendered it unsuitable as a potential receptor.

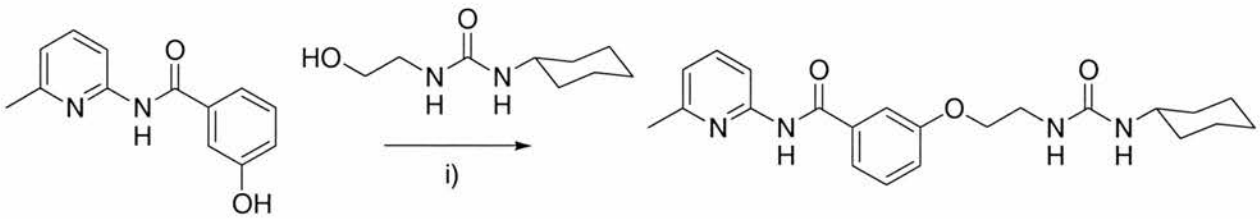

189 **177**

Scheme 5.3.17 Synthesis of receptor **177** *via* a Mitsunobu ether formation. i) DEAD, Phenol, PPh_3, CH_2Cl_2, 0°C – r.t. 72 hrs.

5.4 Increasing the Receptor Solubility

It was assessed that the receptors designed previously were synthetically challenging, had poor solubility and were a non-ideal fit for the guest. To assist synthesis, solubility and improve catalyst design, the urea and thiourea moieties of the receptor were abandoned in favour of a sulfonamide.

The altered design was adopted as shown in **Figure 5.4.1**. The previously synthesised 3-hydroxy-*N*-(6-methyl-pyridin-2-yl)-benzamide was chosen as a basis for the design.

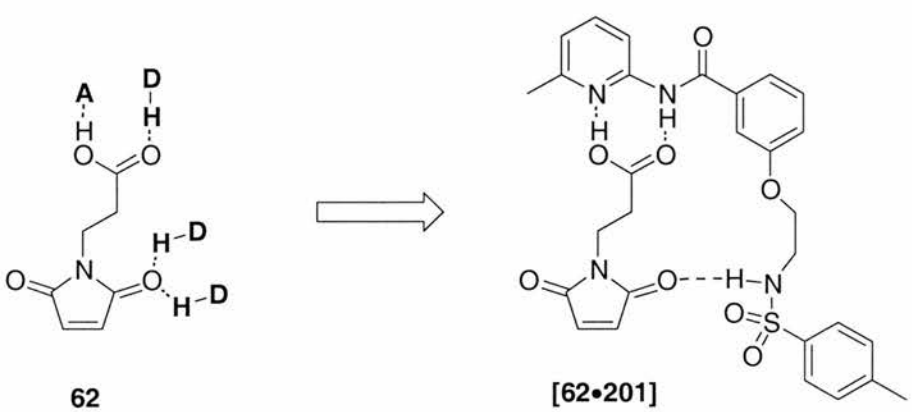

62 **[62•201]**

Figure 5.4.1 The adapted design for a receptor **202** to bind maleimide **62**.

Possessing one hydrogen bond donor rather than two may at first seem counterproductive, however, the modelling with thiourea and urea receptors **177** and **178** suggests that few low energy coconformations adopt both hydrogen bonds to the urea or thiourea.

Molecular modelling was employed to assist in the design of the new receptors. Structures were minimised in energy using the AMBER* forcefield in simulated chloroform. A Monte-Carlo conformational search algorithm was employed to establish low energy coconformations and minimise all coconformations up to 50 kJ mol^{-1} higher in energy than the global minimum.

The lowest energy structure for the tosylated ether was assessed to adopt the predicted amido-picoline recognition motif as well as a hydrogen bond between the sulfonamide and carbonyl groups.

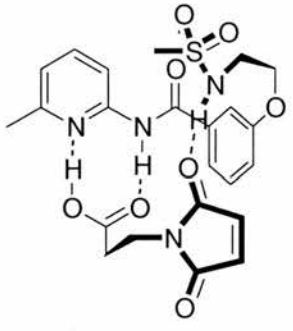

Figure 5.4.2 A two-dimensional representation of the lowest energy structure for the complex between maleimide **62** and receptor **201**. The p-toluene group is omitted for clarity.

The lowest energy structure is depicted two-dimensionally in **Figure 5.4.2** but is most readily visualised in a space filling model as shown in front and rear views in **Figure 5.4.3**.

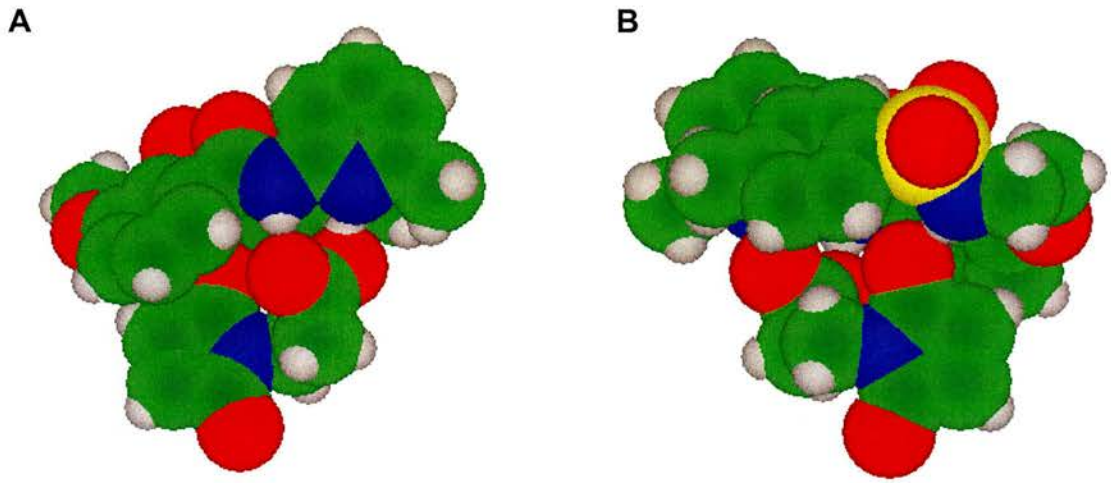

Figure 5.4.3 A space filling model of the lowest energy structures of the complex between functionalised maleimide **62** and tosylated receptor **201**. A) Front view displaying the carboxylic acid, amido picoline recognition motif. B) Rear view of the maleimide sulfonamide hydrogen bond.

The calculated low energy **[62•201]** complex appears to include an offset stack π-π system, explaining the tendency for the *N*-(6-Methyl-pyridin-2-yl)-3-[2-(toluene-4-sulfonylamino)-ethoxy]-benzamide **201** to fold in on itself.

The Mitsunobu reaction had been previously identified as the most efficient method of coupling the phenol to the urea side chain. As a result the Mitsunobu reaction was employed to react the *N*-(2-Hydroxy-ethyl)-4-methyl-benzenesulfonamide with the 3-hydroxy-*N*-(6-methyl-pyridin-2-yl)-benzamide **202** as seen in **Scheme 5.4.4**.

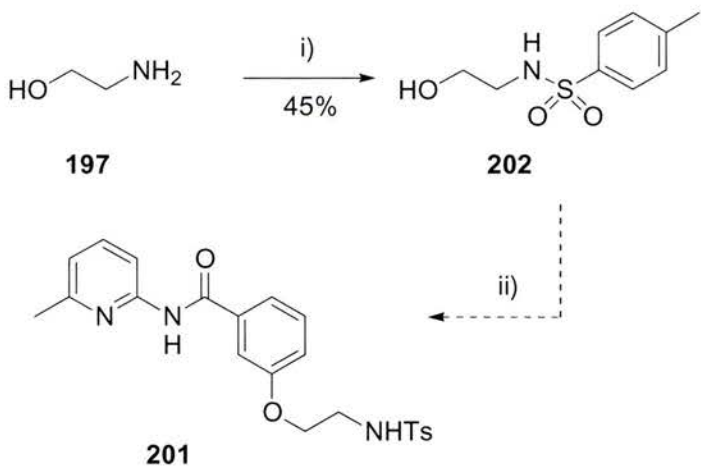

Scheme 5.4.4 The synthesis of sulfonamide **202** and attempted coupling with phenol to synthesise receptor **201**. i) TsCl, CH_2Cl_2, 0°C to r.t., ii) DEAD, Phenol, PPh_3, CH_2Cl_2, 0°C – r.t. 72 hrs.

Although some reaction was evident, only starting material could be recovered from the reaction mixture.

5.5 Conclusions and Future Directions

The synthesis of the urea **177**, thiourea **178** and sulfonamide **201** receptors was attempted, however the syntheses were unsuccessful as a result of the coupling step and insolubility of the products. The problems associated with the reduction in the nucleophilicity of phenol and the complexation of DMF (**Figures 5.3.11** and **5.3.13**) confirm the receptors ability to bind anions and justify the choice of the design.

The synthesis of the previously unsynthesised 3-hydroxy-*N*-(6-methyl-pyridin-2-yl)-benzamide **189** was completed in 33% over four synthetic steps. The methodology developed for this synthesis will enable other receptors similar in design in the future, based on this intermediate. Computational modelling suggested that receptors of this design are viable as potential receptors to accelerate different reactions.

Currently receptors similar to this design are being developed within our research group. The design is being developed further to include intramolecular hydrogen bonding to rigidify the structure and enhance the hydrogen bond donating ability without compromising solubility.

6. Conclusions

On reviewing the literature on synthetic catalysis, it is clear that a general assumption is that emulating enzymic efficiency would enable the creation of enzymes to catalyse any reaction. In Kirby's review[80] of enzyme mechanisms models and mimics he states:

"a proper understanding of how enzymes work holds out the promise of artificial catalysts more robust than proteins and available for practically any organic reaction of interest."

This approach adopted by supramolecular chemists fails to address the types of reactions enzymes perform which may significantly affect the outcome of any attempt to emulate their efficiency.

It would be informative at this stage to evaluate the k_{cat}/k_{uncat} values observed for each receptor. It was stated in **Section 1.10** that it would be of interest to compare k_{cat}/k_{uncat} and reaction polarity. One difficulty with achieving this task however, is the absence of an accurate method to calculate transition state polarity. A qualitative representation is presented in **Figure 6.1**.

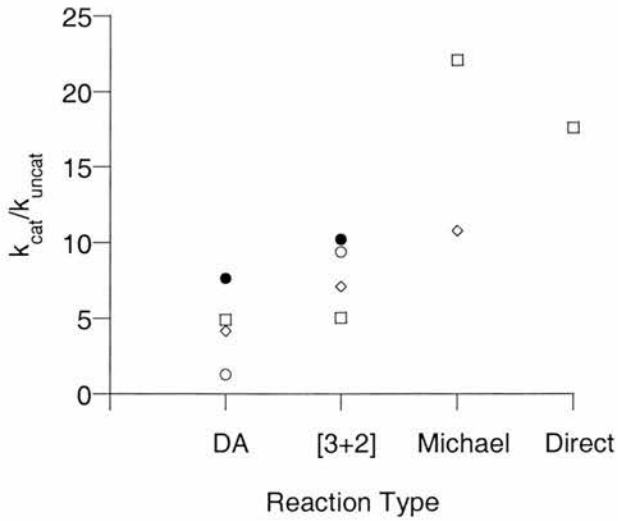

Figure 6.1 A comparison of the values obtained for k_{cat}/k_{uncat} with the type of reaction accelerated. Squares represent in the presence of receptor **138**, diamonds receptor **149**, open circles urea **164** closed circles, thiourea **165**.

Although the data set is small, there are obvious general trends from these results. Using hydrogen bond receptors to accelerate reactions without calling upon pseudointramolecularity, nucleophilic additions are more readily catalysed than less polar cycloaddition reactions.

This report provides indirect proof to support the theory postulated by Pauling that the majority of enzymic efficiency arises from stabilisation of a transition state. In the receptors discussed in this thesis, catalysis can only be induced by electron depletion of substrates and subsequent stabilisation of transition states. The differences observed not only go some way to explaining why enzymes catalyse polar reactions but demonstrate that transition state stabilisation must be an important factor in enzymic catalysis or further examples of Diels-Alderases would be observed.

The lack of observed enzymes catalysing non-polar reactions raises interesting evolutionary questions. Mock *et al* proposed[97] transition state stabilisation of a Diels-Alder reaction by Cucurbituril, however, the application of this method to biologically significant molecules would result in low specificity and product inhibition, as a generalised hydrophobic cavity would be open to all non-polar reactants.

It is important to realise, however, that it is possible for cycloaddition reactions to be catalysed by Lewis Acid catalysts; this method has been used to produce efficient chiral receptors capable of effecting large rate increases with a high level of enantioselectivity.[164-168] Some enzymes have evolved to contain Lewis acidic metal cofactors such as zinc in Thermolysin. If the potential for Lewis acid incorporation into enzymes is there, why hasn't enzyme acceleration of cycloadditions developed? One suggestion could be that enzymic catalysis arose from purely hydrogen bonded receptors. Polar reactions were catalysed because charges in the transition state enable selective charged reinforced hydrogen bonding of transition states with little product inhibition. As has been proved in this report, it is much more straightforward to effect rate acceleration for polar reactions than non-polar and so non-polar reactivity may have been rejected by primitive enzymes. Alternative synthetic routes would have had to be found to synthesise the natural products required by the organism. This hypothesis would suggest therefore that the predisposition for adopting polar reactivity in enzymes was adopted early in the development of

enzymes. If this is the case, development of efficient artificial Diels-Alderases is unlikely unless prosthetic groups are incorporated into the structure.

In order to investigate catalysis it has been necessary to develop broad-spectrum receptors capable of accelerating polar and non-polar reactions. Surprisingly this area has been neglected in the past. It could be envisaged that adoption of such broad spectrum catalysts may enable resins to be synthesised in the future containing simple receptors which would subsequently be able to bind to enones and catalyse a wide range of chemical transformations. It is predicted that the efficiency of these receptors will be increased by adopting a flow system or performing reactions with a large excess of reactant, as demonstrated by Kelly and co-workers Diels Alder catalyst.

This thesis also provides guidance for the supramolecular chemist when designing artificial catalysts. Accepting Pauling's principle on transition state stabilisation means we need to advance our ideas on catalysis. We cannot adopt a closed view that catalysis is only achieved through minimising transition state translational or rotational motion by rendering a process pseudointramolecular. If truly efficient catalysis is to be observed we need to incorporate the aspects of transition state stabilisation nature employs.

7 Experimental Section

7.1 General Procedures

Unless stated, all chemicals were purchased from Aldrich Chemical Co., Avocado, Apollo Scientific or Fisher Ltd. and were used as received. Tetrahydrofuran (THF) and diethyl ether (Et_2O) were distilled over sodium / benzophenone ketyl. Dichloromethane and acetonitrile were distilled over CaH_2. Dimethyl formamide was distilled over CaH_2 and stored over 4 Å molecular sieves. Pyridine and triethylamine (Et_3N) were both dried by distillation from potassium hydroxide pellets. Flash column chromatography was performed using Merck Kieselgel 60 (0.040-0.063mm, 230-400 mesh) or ICN EcoChrom Silica 32-63 μm, 60 Å. Thin layer chromatography (TLC) was performed on commercially prepared aluminium plates coated with a 0.2mm thickness of Merck or Riedel-de Haën silica gel 60 F254 and eluted plates were inspected under a UV lamp (366 nm). Where appropriate, TLC plates were developed in $KMnO_4$, PMA, iodine or ninhydrin to aid visualisation. Melting points were determined using an Electrothermal 9200 apparatus, reported to the nearest 0.5 °C, and are uncorrected. Infra-red (IR) Spectra were recorded as KBr discs, Nujol mulls or thin films using a Perkin Elmer Paragon 1000 spectrometer. ^1H Nuclear Magnetic Resonance (NMR) spectra were recorded using Bruker AC300 (300 MHz), Bruker AMX400 (400 MHz), Bruker DRX500 (500 MHz) Varian Gemini 2000 (300 MHz), Bruker Avance 300 (300 MHz) or Varian UnityPlus (500 MHz) instruments. ^{13}C NMR spectra were recorded using Bruker AC300 (75 MHz), or Bruker Avance 300 (75 MHz), instruments using the PENDANT pulse sequence. The deuterated solvent was used as the lock and the residual solvent as an internal reference in the recording of all ^1H and ^{13}C spectra. Unless stated, all spectra were recorded at 298 K, all ^1H coupling constants are quoted in Hz to one decimal place, all CF coupling constants are quoted in Hz to the nearest integer. The symbols s, d, t, q and m used in the assignment of ^1H NMR spectra denote singlet, doublet, triplet, quartet and multiplet resonances respectively. The precursor b is used to signify a broad resonance. Electron impact mass spectrometry (EIMS) and high-resolution mass spectrometry (HRMS) were carried out on either a VG PROSPEC or a VG AUTOSPEC mass spectrometer. Electrospray mass spectrometry (ESMS) was recorded on a VG PLATFORM mass spectrometer. Microanalyses (CHN) were carried out at the University of London, the University of Birmingham or the University of St. Andrews.

7.2 Computational Procedures

All calculations were performed on a Silicon Graphics 02 workstation. Semi-empirical (AM1) calculations were performed using SPARTAN (version 1.3, Wavefunction Inc., Irvine, USA). All molecular structure calculations were performed on Macromodel (version 7.1, Schrodinger Inc. Portland, USA, 2001) using an AMBER* forcefield together with the GB/SA solvation model for $CHCl_3$. Initially minimised complexes were further analysed using a Monte-Carlo conformational search technique minimizing up to 2000 structures using a maximum of 5000 iterations, all conformations generated within 50 $kJmol^{-1}$ of the global minimum were minimised. Global minima structures were exported and visualised using Chem3D. Data collected during the Monte-Carlo conformational search was exported into KaleidaGraph 3.51 to assess other low energy structures.

7.3 Initial Association Investigations

Initial binding investigations were performed by ^1H NMR spectroscopy in $CDCl_3$. Solutions were prepared with a 1:1 molar ratio of host to guest and spectra were recorded on a Bruker AC300 (300 MHz) spectrometer. The chemical shifts in the mixture were compared with solutions of the same concentration of the host and guest individually and any changes in chemical shift were noted. The convention used for quoting changes in chemical shift is as follows:

$$\Delta\delta = \delta_{\text{bound}} - \delta_{\text{unbound}}$$

Thus, a downfield shift would result in a positive value for $\Delta\delta$.

7.4 K_a Determination

Stability constants (K_a) were determined by the NMR titration method. A typical experiment was as follows, the stock solution of maleimide (0.02 M) was prepared in $CDCl_3$ and 0.5 ml of this solution was mixed with the appropriate quantity of 0.2 or 0.4 M *N,N'*-2,6-Pyridyl-bis-(3-methylbutyramide) **149** and made up to 1 ml with $CDCl_3$. Several solutions were prepared in a similar manner to give a series of molar

ratios from 0 : 1 to 20 : 1 host : maleimide. ^{1}H NMR spectra were recorded for each of these solutions and the change in chemical shift of the NH peak of maleimide was followed. The data was used to calculate the K_a and ΔG of association using the non-linear curve-fitting program, WinEQNMR,[152] according to the equations listed in **Appendix 1**.

7.5 Initial Investigations of Reaction Kinetics

All reactions were performed in $CDCl_3$. The experiment was performed with a 1:1:1 receptor reagent mixture with a 1:1 reagent mixture as a comparison. A typical experimental is as follows: A vial of 20 mM 1:1 mixture of diphenylnitrone and maleimide was prepared in $CDCl_3$ (1ml). 1:1:1 Diphenylnitrone, maleimide and *N,N'*-2,6-pyridyl-bis-(3-methylbutyramide) was dissolved in a vial in $CDCl_3$ (1ml) to make a 20 mM solution. These vials were then placed in a water bath at 50 °C and left for a period of 16 hours after which a ^{1}H NMR spectrum was taken of each experiment and the relative product concentration established by deconvolution.

7.6 Kinetic Measurements

All stock solutions were prepared by dissolving the appropriate amount of a given reagent in $CDCl_3$ using Volac 2 ml ± 0.015 ml or 5 ml ± 0.025 ml volumetric flasks. Reagents were measured using a 25 µl Hamilton gas tight syringe or mass was determined by a Sartorius BP 211D balance (± 0.01 mg) Subsequent experimental samples were obtained by mixing a fixed amount of appropriate stock solutions using a 1000 µl Hamilton gas tight syringe and filtering the solution into a Wilmad 528pp NMR tube, which was then fitted with a polyethylene pressure cap to minimise solvent evaporation over the course of the reaction. The reaction mixtures were monitored by 400 or 500 MHz ^{1}H NMR spectroscopy over 15 or 16 hours recording spectra at half hourly intervals. In each case the probe is pre-equilibrated at the appropriate temperature. The extent of reaction was determined using the deconvolution tool available in 1D WINNMR (version 6.2, Bruker Analytik, Germany 1998). Kinetic simulation and fitting of the resultant data to the appropriate kinetic models was accomplished using the SIMFIT-32 program. The rate of the reaction in the absence of any hosts was assumed to be identical to the background rate in the catalysed reaction.

7.7 Crystal Structure Determination

Single crystals of **149** were formed by slow vapour diffusion of hexane into a solution of **149** dissolved in CH_2Cl_2. X-ray diffraction data was recorded using MoKα radiation on a Rigaku R-Axis II diffractometer with rotating anode source and image plate detector. The data was processed using standard R-Axis II software and visualised in an Ortep representation of 50% thermal ellipsoids.

7.8 Synthetic Procedures

Benzene-1,3-disulfonic acid bis-butylamide 138

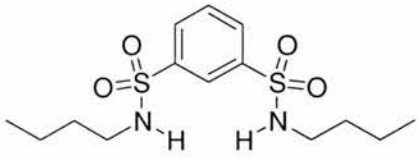

Butylamine (2.87 ml, 29.1 mmol) was added dropwise to a cooled (0°C) solution of 1,3 benzene disulfonyl chloride **137** (2.00g, 7.27 mmol) in dichloromethane (20 ml). The resulting solution was stirred at room temperature for 48 hours, the solvent was removed *in vacuo* and the residue was purified by flash column chromatography (SiO_2 : Et_2O) to yield **138** as a colourless solid (2.43 g, 91%); m.p. 99.0 – 99.5 °C (from Et_2O); E.A. $C_{14}H_{24}N_2O_4S_2$ requires C 48.25%, H 6.94%, N 8.04% found: C 48.51%, H 7.08%, N 7.97%,. ν_{max}(KBr disc)/cm^{-1} 3257 (NH), 2959, 2934, 2873 (CH), 1322, 1179 (SO_2N), δ_H (300 MHz; $CDCl_3$) 8.42 (1H, t, $^4J_{HH}$ = 1.8, CH, Ar), 8.06 (2H, dd, $^3J_{HH}$ = 7.7, $^3J_{HH}$ = 1.8, CH, Ar), 7.69 (1H, t, $^3J_{HH}$ = 7.7, CH, Ar), 5.12 (2H, t, $^3J_{HH}$ = 5.9, NH), 2.96 – 2.93 (4H, m, CH_2), 1.46 – 1.44 (4H, m, CH_2) 1.30 – 1.26 (4H, m, CH_2), 0.84 (6H, t, $^3J_{HH}$ = 7.1, CH_3); δ_C (75 MHz; $CDCl_3$), 141.6 (C, quat, Ar), 130.8 (CH, Ar), 129.9 (CH, Ar), 125.6 (CH, Ar), 43.1 (CH_2), 31.5 (CH_2), 19.6 (CH_2), 13.5 (CH_3) *m/z* (EI) 348 (M+, 23%), 305 (100), 293 (15), 276 (40). *m/z* (HRMS) found 348.1161 $[M]^+$, $C_{14}H_{24}N_2O_4S_2$ requires 348.1177.

β-Phenyl hydroxylamine 140[169]

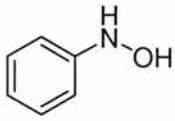

Zinc powder was added slowly to a solution of nitrobenzene **139** (10g, 80 mmol) and ammonium chloride (5g, 90 mmol) in H_2O (160 ml) as the reaction proceeded the temperature rose and was judged to have reached completion after 20 minutes. The reaction mixture was hot filtered and rinsed (hot H_2O, 30 ml). The filtrate was saturated with salt and cooled in an ice-salt bath for an hour to enable crystallisation of the product. The hydroxylamine / salt precipitate was filtered, the hydroxylamine was solubilised in Et_2O and dried ($MgSO_4$) to afford **140** as an unstable yellow solid (8.11 g, 46 %) which was used without further purification.

N-Benzylidene-aniline *N*-oxide 141[170]

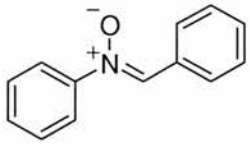

Benzaldehyde (2.61 ml, 25.6 mmol), was added to a solution of crude β-phenyl hydroxylamine **140** (2.80 g, 25.6 mmol) in ethanol (20 ml) and the resulting mixture was stoppered and left with the exclusion of light for 16 hours. The yellow crystals formed were filtered and recrystallised (EtOH) to afford **141** as a colourless solid (10.05g, 70 %); m.p. 111.2 – 111.9 °C from EtOH; ν_{max}(KBr disc)/cm^{-1} 3060 (Ar CH), 1548 (Ar), 771 (Ar), 750 (Ar); δ_H (300 MHz; $CDCl_3$) 8.41 – 8.39 (2H, m, CH, Ar), 7.92 (1H, s, CH), 7.78 – 7.75 (2H, m, CH, Ar) 7.48 – 7.45 (6H, m, CH, Ar); δ_C (75 MHz; $CDCl_3$) 149.1 (C, quat, Ar), 134.7 (CH), 131.0 (CH, Ar), 130.7 (C, quat, Ar), 130.0 (CH, Ar), 129.2 (2 CH, Ar), 129.1(2 CH, Ar), 128.7 (2 CH, Ar), 121.8 (2 CH, Ar); *m/z* (EI) 197 (M+, 37%), 180 (25), 91 (100).

3-Methyl-*N*-[6-(3-methyl-butyrylamino)-pyridin-2-yl]-butyramide 149

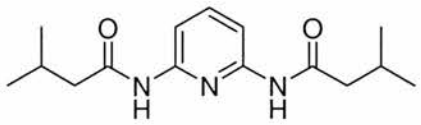

A solution of isovaleryl chloride (4.82 g, 40 mmol) in dry THF (100 ml) was added dropwise to a solution of 2,6-diaminopyridine **148** (2.18 g, 20 mmol) and Et_3N (5.60 ml, 40 mmol) in dry THF (100 ml). The mixture was stirred for 15 hours at room temperature under a positive pressure of nitrogen. The reaction mixture was filtered to remove the HCl salt and the solvent removed *in vacuo.* The resulting orange-brown oil was purified *via* column chromatography (SiO_2: 1:1 Hexane : EtOAc) to produce a beige solid which was further purified by recrystallisation (EtOAc / Hexane) to yield cream crystals of **149** (3.80 g, 69%); m.p. 120.2 – 121.2 °C from EtOAc / Hexane; E.A. $C_{15}H_{23}N_3O_2$ requires C 64.96%, H 8.36%, N 15.15% found: C 65.01%, H 8.51%, N 14.92%; ν_{max}(KBr disc)/cm^{-1} 3407 (NH), 2958, 2871 (CH), 1682 (CO), δ_H (300 MHz; $CDCl_3$) 7.89 (2H, d, $^3J_{HH}$ = 7.9, CH, Ar), 7.70 (1H, t, $^3J_{HH}$ = 7.9, CH, Ar), 7.62 (2H, br s, NH), 2.23 – 2.19 (4H, m, CH_2), 2.20 – 2.18 (2H, m, CH), 0.99 (12H, d, $^3J_{HH}$ = 6.3, CH); δ_C (75 MHz; $CDCl_3$), 171.2 (C, quat, CO), 149.5 (C, quat, Ar), 141.0 (CH, Ar), 109.6 (CH, Ar), 47.2 (CH_2), 26.3 (CH), 22.6 (CH_3) *m/z* (EI) 277 (M+, 70%), 262 (45), 220 (20), 193 (85).

N,N'-Dimethyl-pyridine-2,6-diamine 150

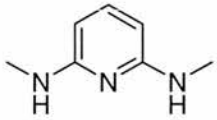

2,6-Diaminopyridine **148** was added to a solution of sodium (4.60 g, 200 mmol) in MeOH (60 ml). A solution of paraformaldehyde (1.68 g, 56 mmol) in MeOH (40 ml) was added to the reaction mixture and the resulting brown solution was stirred for 15 hours at room temperature. The solution was refluxed for 1 hour then allowed to cool after which time $NaBH_4$ (1.40g, 40 mmol) was added and the mixture was refluxed for 1 hour. Aqueous KOH (1M, 80 ml) was added to the hot solution, the reaction mixture was stirred overnight at room temperature and then extracted directly (EtOAc, 3 x 40 ml), dried ($MgSO_4$) and the solvent removed *in vacuo.* Column chromatography (SiO_2 : Et_2O) afforded a brown solid **150** (0.80 g, 29%). m.p.

71.5 - 72.0 °C from Et_2O; ν_{max}(KBr disc)/cm^{-1} 3300 (NH), 2995 (CH), 2935 (CH), δ_H (300 MHz; $CDCl_3$) 7.28 (1H, t, $^3J_{HH}$ = 8.0, CH, Ar), 5.72 (2H, d, $^3J_{HH}$ = 8.0, CH, Ar), 4.32 (2H, s, NH), 2.84 (6H, d, $^3J_{HH}$ = 5.5, CH_3); δ_C (75 MHz; $CDCl_3$) 159.1 (C, quat, Ar), 139.0 (CH, Ar), 94.2 (CH, Ar), 29.3 (CH_3); *m/z* (EI) 137 (M+, 100%), 107 (32), 81 (53); *m/z* (HRMS) found 137.0958 $[M]^+$, $C_7H_{11}N_3$ requires 137.0953.

3-*N*-Dimethyl-*N*-{6-[methyl-(3-methyl-butyryl)-amino]-pyridin-2-yl}-butyramide 151

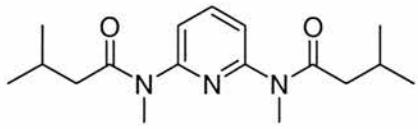

Isovaleryl chloride (0.73 ml, 6 mmol) dissolved in dry CH_2Cl_2 (10 ml) was added dropwise to *N,N'*-dmethyl-pyridine-2,6-diamine **150** (0.42 g, 3 mmol) dissolved in dry CH_2Cl_2 (20 ml) and dry Et_3N (1.25 ml, 9mmol). After 15 hours, the reaction was filtered to remove the $Et_3N.HCl$ and the solvents removed *in vacuo*. The product was purified *via* column chromatography (SiO_2 : 4:1 : CH_2Cl_2 : Hexane) to yield **151** as a brown crystalline solid (3.60 mg, 40%). m.p. 52.0 – 53.0 °C; ν_{max}(Nujol mull)/cm^{-1} 1653 (CO); δ_H (300 MHz; $CDCl_3$) 7.75 (1H, t, $^3J_{HH}$ = 7.7, CH, Ar), 7.21 (2H, d, $^3J_{HH}$ = 7.7, CH, Ar), 3.35 (6H, s, NCH_3), 2.21 – 2.17 (6H, m, CH, CH_2), 0.89 (12H, d, $^3J_{HH}$ = 6.3, CH_3), δ_C (75 MHz; $CDCl_3$), 173.3 (C, quat, CO), 155.3 (C, quat, Ar), 140.0 (CH, Ar), 118.2 (CH, Ar), 44.3 (CH_2), 35.7 (CH_3), 26.1 (CH), 23.0 (CH_3); *m/z* (ES) 328.2 (MNa^+, 100%), 306.2 (M+, 8), *m/z* (HRMS) found 328.2007 $[M + Na]^+$, $C_{17}H_{27}N_3O_2Na$ requires 328.2001.

***N*-(6-Amino-pyridin-2-yl)-3-methyl-butyramide 152**

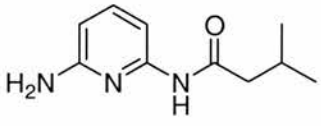

A solution of isovaleryl chloride (1.84 ml, 15.2 mmol) in dry THF (100 ml) was added dropwise over 2 hours to a solution of 2,6 diaminopyridine **148** (5.00 g, 46 mmol) in dry THF (200 ml). The mixture was stirred under nitrogen for 15 hours at room temperature. The reaction mixture was filtered, and the solvent removed *in vacuo.* The resulting solid was purified *via* column chromatography (SiO_2 : 1:1 EtOAc : Hexane) to yield the product **152** as a colourless solid (2.80 g, 95%). m.p. 110.5 - 113 °C from EtOAc / Hexane; ν_{max}(KBr disc)/cm^{-1} 3445 (NH), 3353 (NH),

2960 (CH), 1680 (CO); δ_H (300 MHz; $CDCl_3$) 7.79 (1H, s, NH), 7.54 (1H, d, $^3J_{HH}$ = 8.1, CH, Ar), 7.43 (1H, dd, $^3J_{HH}$ = 8.1, $^3J_{HH}$ = 8.1, CH, Ar), 6.23 (1H, d, $^3J_{HH}$ = 8.1, CH, Ar), 4.33 (2H, s, NH_2), 2.19 – 2.15 (3H, m, CH_2, CH) 0.96 (6H, d, $^3J_{HH}$ = 6.3, CH_3); δ_C (75 MHz; $CDCl_3$) 171.5 (C, quat, CO), 157.4 (C, quat, Ar), 150.2 (C, quat, Ar), 140.6 (CH, Ar), 104.6 (CH, Ar), 103.7 (CH, Ar), 47.4 (CH_2), 26.5 (CH), 22.9 (CH_3); *m/z* (EI) 193 (M+, 23%), 109 (100), 82 (14).

3-Methyl-*N*-(6-methylamino-pyridin-2-yl)-butyramide 153

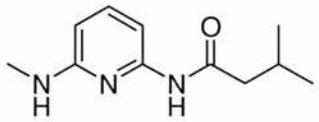

N-(6-Amino-pyridin-2-yl)-3-methyl-butyramide **152** (1.73 g, 9.0 mmol) was added to a solution of sodium (1.03 g, 45 mmol) in MeOH (20 ml). Paraformaldehyde (0.38 g, 12.6 mmol) in MeOH (10 ml) was added to the reaction mixture and the resulting solution was stirred for 15 hours at room temperature. The solution was refluxed for 1 hour then cooled after which time $NaBH_4$ (0.34 g, 9.0 mmol) was added and the mixture was refluxed for 1 hour. Aqueous KOH (1M, 20 ml) was added to the hot solution and the reaction mixture was stirred overnight at room temperature. The reaction was extracted directly (EtOAc, 3 x 40 ml), dried ($MgSO_4$) and the solvent removed *in vacuo*. Column chromatography (SiO_2 : 9:1 CH_2Cl_2 : EtOAc) afforded **153** (1.10 g, 59%) as a colourless oil. ν_{max}(thin film)/cm^{-1} 3374 (NH), 2958 (CH), 1682 (CO); δ_H (300 MHz; $CDCl_3$) 7.70 (1H, s, CONH), 7.45 – 7.43 (2H, m, CH, Ar), 6.13 (1H, d, $^3J_{HH}$ = 8.5, CH, Ar) 4.37 (1H, s, $NHCH_3$), 2.86 (3H, d, $^3J_{HH}$ = 5.2, $NHCH_3$), 2.20 – 2.15 (3H, m, CH, CH_2) , 0.97 (6H, d, $^3J_{HH}$ = 6.6 , CH_3); δ_C (75 MHz; $CDCl_3$), 171.1 (C, quat, CO), 158.5 (C, quat, Ar), 150.0 (C, quat, Ar), 139.9 (CH, Ar), 102.1 (CH, Ar), 102.0 (CH, Ar), 47.3 (CH_2), 29.1 (CH_3), 26.3 (CH), 22.6 (CH_3); *m/z* (CI) 208 (MH+, 100%), 192 (4), *m/z* (HRMS) found 230.1263 $[M + Na]^+$, $C_{11}H_{17}N_3ONa$ requires 230.1269.

3-Methyl-*N*-{6-[methyl-(3-methyl-butyryl)-amino]-pyridin-2-yl}-butyramide 154

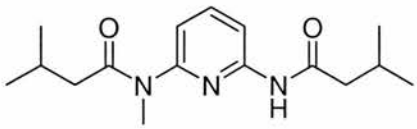

A solution of isovaleryl chloride (4.82 g, 40 mmol) in dry THF (50 ml) was added dropwise to a solution of 3-methyl-*N*-(6-methylamino-pyridin-2-yl)-butyramide **153** (0.80 g, 3.9 mmol) and Et_3N (0.39 ml, 3.9 mmol) in dry THF (50 ml). A suspension was formed after 10 minutes at room temperature, which was then stirred for 15 hours under a positive pressure of nitrogen. The light yellow, cloudy reaction mixture was filtered to remove the $Et_3N.HCl$ salt and the solvent removed *in vacuo.* The resulting crude product was recrystallised (EtOAc / Hexane) to afford **154** as a colourless solid (1.08 g, 95%). m.p. 121.5 – 122.0 °C; ν_{max}(KBr disc)/cm^{-1} 3250 (NH), 2959, 2870 (CH), 1698 (CO) 1640 (CO); δ_H (300 MHz; $CDCl_3$) 8.18 – 8.15 (2H, m, NH, CH, Ar), 7.75 (1H, dd, $^3J_{HH}$ = 8.1, $^3J_{HH}$ = 7.7 , CH, Ar), 6.92 (1H, d, $^3J_{HH}$ = 7.7 , Ar), 3.28 (3H, s, NCH_3), 2.22 – 2.18 (6H, m, CH, CH_2), 1.02 (6H, d, $^3J_{HH}$ = 6.3, CH_3), 0.85 (6H, d, $^3J_{HH}$ = 6.6, CH_3); δ_C (75 MHz; $CDCl_3$), 173.1 (C, quat, CO), 175.1 (C, quat, CO), 154.4 (C, quat, Ar), 151.3 (C, quat, Ar), 140.5 (CH, Ar), 116.1 (CH, Ar), 112.2 (CH, Ar), 46.6 (CH_2), 43.4 (CH_2), 35.5 (CH_3), 26.1 (CH), 25.8 (CH), 22.6 (CH_3), 22.5 (CH_3), *m/z* (ES) 314.2 ([M + Na]$^+$, 100%), 292 ([M+H]+, 80), *m/z* (HRMS) found 314.1840 [M + Na]$^+$, $C_{16}H_{25}N_3O_2Na$ requires 314.1844.

3-Chloromethyl-*N*-(6-methyl-pyridin-2-yl)-benzamide 161[170-172]

3-(Chloromethyl)benzyl chloride (14.1 mmol, 2 ml) was added dropwise to a solution of 2-amino-6-picoline (42.2 mmol, 4.56 g) in dry dichloromethane (60 ml) at 0°C. The solution was stirred and allowed to warm to room temperature overnight. The hydrochloride salt was removed by filtration and the filtrate was concentrated *in vacuo*. The amide was purified *via* flash column chromatography (SiO_2 : CH_2Cl_2) to yield **161** as a colourless solid (3.67 g , 100%). m.p. 89.0 – 90.0 °C from CH_2Cl_2

(Lit[170-172] 89.2 – 90.4 °C from CH_2Cl_2); ν_{max}(KBr disc)/cm^{-1} 3264 (NH), 1658 (CO), 1532 (CN Py); δ_H (300 MHz; $CDCl_3$) 8.60 (1H, s, NH), 8.18 (1H, d, $^3J_{HH}$ = 8.1, CH, Ar), 7.94 (1H, s, CH, Ar), 7.87 (1H, s, CH, Ar), 7.65 (1H, dd, $^3J_{HH}$ = 8.1, $^3J_{HH}$ = 7.7, CH, Ar), 7.58 (1H, d, $^3J_{HH}$ = 7.7, CH, Ar), 7.48 (1H, dd, $^3J_{HH}$ = 7.7, $^3J_{HH}$ = 7.7, CH, Ar), 6.93 (1H, d, $^3J_{HH}$ = 7.7, CH, Ar), 4.63 (2H, s, CH_2), 2.46 (3H, s, CH_3); δ_C (75 MHz; $CDCl_3$) 165.5 (C, quat, CO), 157.3 (C, quat, Ar), 151.1 (C, quat, Ar), 139.3 (CH, Ar), 138.7 (C, quat, Ar),135.3 (C, quat, Ar), 132.6 (CH, Ar), 129.6 (CH, Ar), 127.8 (CH, Ar), 127.5 (CH, Ar), 120.0 (CH, Ar), 111.5 (CH, Ar), 45.8 (CH_2), 24.3 (CH_3); *m/z* (ES) 285 ([M + Na]$^+$, 20%), 283 ([M + Na]$^+$, 100%), 263 (13), 261 (62)

3-Azidomethyl-N-(6-methyl-pyridin-2-yl)-benzamide 162[171,172]

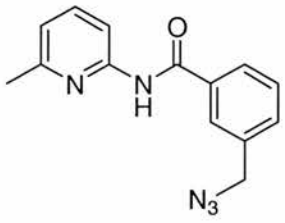

Sodium azide (2.77 g, 42.6 mmol) was added slowly to a solution of 3-chloromethyl-*N*-(6-methyl-pyridin-2-yl)-benzamide **161** (3.67 g, 14.2 mmol) in acetone. After 16 hours under reflux, the NaCl salt was removed by filtration and the acetone was removed *in vacuo*. The residue was redissolved (CH_2Cl_2, 60 ml) and washed (2 x 80ml water). The organic fraction was dried ($MgSO_4$) and the solvent removed *in vacuo* to produce 3-azidomethyl-*N*-(6-methyl-pyridin-2-yl)-benzamide **162** as a colourless oil (3.48 g, 92 %); ν_{max}(film)/cm^{-1} 3400 (NH), 2100 (N_3), 1671 (CO); δ_H (300 MHz; $CDCl_3$) 8.99 – 8.95 (1H, bs, NH), 8.18 (1H, d, $^3J_{HH}$ = 8.5, CH, Ar), 7.86 – 7.83 (2H, m, CH, Ar), 7.63 (1H, dd, $^3J_{HH}$ = 8.5, $^3J_{HH}$ = 7.4, CH, Ar), 7.48 – 7.45 (2H, m, CH, Ar) 6.89 (1H, d, $^3J_{HH}$ = 7.4, CH, Ar) 4.37 (2H, s, CH_2), 2.36 (3H, s, CH_3); δ_C (75 MHz; $CDCl_3$) 165.4 (C, quat, CO), 157.0 (C, quat, Ar), 150.9 (C, quat, Ar), 138.8 (CH, Ar) 136.3 (C, quat, Ar), 135.1 (C, quat, Ar), 131.6 (CH, Ar), 129.3 (CH, Ar), 127.1 (CH, Ar), 127.1 (CH, Ar), 119.6 (CH, Ar), 111.2 (CH, Ar) 54.3 (CH_2), 23.8 (CH_3); *m/z* (EI) 267 (M+, 35%), 238 (88), 225 (15), 210 (48); *m/z* (HRMS) found 267.1107 [M]$^+$, $C_{14}H_{13}N_5O$ requires 267.1120.

3-Aminomethyl-*N*-(6-methyl-pyridin-2-yl)-benzamide 163

Triphenylphosphine (2.16 g, 8.23 mmol), was added to a solution of 3-azidomethyl-N-(6-methyl-pyridin-2-yl)-benzamide **162** dissolved in THF (70 ml) and H_2O (1.35 ml, 74.8 mmol). The reaction was stirred at room temperature for 24 h and the solvent was removed *in vacuo*. The residue was dissolved in EtOH (20 ml) and concentrated HCl solution (38%, *ca.* 7 ml) was added dropwise until the product hydrochloride salt began to precipitate. The salt was left to precipitate over one hour then isolated by filtration and conversion to the free-base form *via* dissolution in aqueous KOH (4 M, 40 ml) and extraction (EtOAc, 2 x 50 ml). The organic fractions were combined, dried ($MgSO_4$) and the solvent removed *in vacuo* to yield 3-aminomethyl-*N*-(6-methyl-pyridin-2-yl)-benzamide **163** as a colourless solid (1.16 g, 64%). m.p. 98.0 – 100.0 °C; ν_{max}(KBr disc)/cm^{-1} 3354 (NH), 2918 (CH), 1669 (CO); δ_H (300 MHz; $CDCl_3$) 8.59 (1H, s, NH), 8.18 (1H, d, $^3J_{HH}$ = 8.1, CH, Ar), 7.89 (1H, s, CH, Ar), 7.79 (1H, d, $^3J_{HH}$ =7.7, CH, Ar), 7.64 (1H, dd, $^3J_{HH}$ = 8.1, $^3J_{HH}$ = 7.7, CH, Ar), 7.51 (1H, d, $^3J_{HH}$ =7.7, CH, Ar), 7.44 (1H, dd, $^3J_{HH}$ = 7.7, $^3J_{HH}$ =7.7, CH, Ar), 6.92 (1H, d, $^3J_{HH}$ = 7.7, CH, Ar), 3.95 (2H, s, CH_2), 2.46 (3H, s, CH_3); δ_C (75 MHz; $CDCl_3$) 165.7 (C, quat, CO), 156.9 (C, quat, Ar), 150.9 (C, quat, Ar), 143.9 (C, quat, Ar), 138.7 (CH, Ar), 134.6 (C, quat, Ar), 130.9 (CH, Ar), 128.9 (CH, Ar), 125.9 (CH, Ar), 125.7 (CH, Ar), 119.4 (CH, Ar), 111.0 (CH, Ar), 46.1 (CH_2), 23.9 (CH_3); *m/z* (CI) 242 (MH+, 100%), 57 (61); *m/z* (HRMS) found 242,1284 $[MH]^+$, $C_{14}H_{16}N_3O$ requires 242.1293.

3-[(3-Cyclohexyl-ureido)-methyl]-*N*-(6-methyl-pyridin-2-yl)-benzamide 164

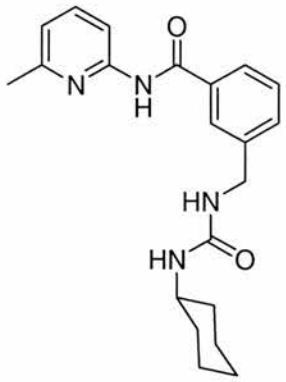

Cyclohexyl isocyanate (0.40 ml, 3.1 mmol) was added dropwise at 0 °C to a solution of 3-aminomethyl-N-(6-methyl-pyridin-2-yl)-benzamide **163** in dried Et_2O (20 ml). The reaction was allowed to warm to room temperature under an atmosphere of dry nitrogen whereupon a precipitate was formed. The product was isolated from the reaction mixture by filtration to yield **164** as a colourless solid (1.10 g, 97%). m.p. 165.0 – 165.5 (from Et_2O); ν_{max}(KBr disc)/cm^{-1} 3352 (NH), 3304 (NH), 2929 (CH), 2854 (CH), 1690 (CO), 1627 (CO); δ_H (300 MHz; $CDCl_3$) 8.74 (1H, s, NH amide), 8.14 (1H, d, $^3J_{HH}$ = 8.1, CH, Ar), 7.75 – 7.73 (2H, m, CH, Ar), 7.63 (1H, dd, $^3J_{HH}$ = 8.1, $^3J_{HH}$ = 7.4, CH, Ar), 7.43 (1H, d, $^3J_{HH}$ = 7.7, CH, Ar), 7.39 – 7.35 (1H, m, CH, Ar), 6.92 (1H, d, $^3J_{HH}$ = 7.4, CH, Ar), 5.27 (1H, s, NH urea), 4.86 (1H, s, NH urea), 4.35 (2H, d, $^3J_{HH}$ = 5.9, CH_2), 3.52 – 3.49 (1H, m, CH), 1.90 – 1.80 (2H, m, cyclohexyl), 1.70 – 1.51 (3H, m, cyclohexyl), 1.36 – 1.04 (5H, m, cyclohexyl); δ_C (75 MHz; $CDCl_3$) 165.8 (C, quat, CO), 157.8 (C, quat, Ar), 156.8 (C, quat, Ar), 150.7 (C, quat, Ar), 140.6 (C, quat, Ar), 138.8 (CH, Ar), 134.4 (C, quat, Ar), 131.2 (CH, Ar), 128.9 (CH, Ar), 125.9 (CH, Ar), 125.8 (CH, Ar), 119.5 (CH, Ar), 111.1 (CH, Ar), 48.9 (CH), 43.7 (CH_2), ; *m/z* (CI) 367 (MH+, 92%), 284 (45), 268 (55), 195 (55), 100 (60), 58 (100); *m/z* (HRMS) found 367.2126 $[M]^+$, $C_{21}H_{27}N_4O_2$ requires 367.2134.

3-[(3-Cyclohexyl-thioureido)-methyl]-*N*-(6-methyl-pyridin-2-yl)-benzamide 165

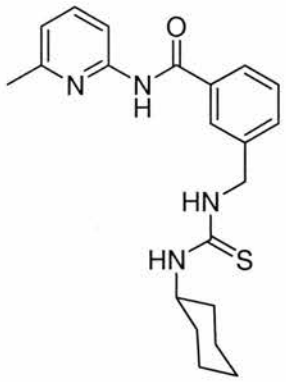

Cyclohexyl isothiocyanate (0.71 ml, 5 mmol) was added dropwise to a solution of 3-aminomethyl-N-(6-methyl-pyridin-2-yl)-benzamide **163** in dried EtOAc (20 ml). The reaction was refluxed for one hour under an atmosphere of dry nitrogen. The solvent was removed *in vacuo* and the residual solid was purified *via* flash column chromatography (SiO_2 3:1 CH_2Cl_2:Et_2O) to yield **165** as a pale yellow solid (1.71 g, 90%). m.p. 83 – 85 °C (from CH_2Cl_2 / Et_2O); ν_{max}(KBr disc)/cm^{-1} 3281 br s (NH), 2929 (CH), 2853 (CH), 1674 (CS), 1603 (CO); δ_H (300 MHz; $CDCl_3$) 8.66 – 8.62 (1H, bs, NH amide), 8.11 (1H, d, $^3J_{HH}$ = 8.5, CH, Ar), 7.78 – 7.75 (3H, m, CH, Ar), 7.64 (1H, dd, $^3J_{HH}$ = 8.5, $^3J_{HH}$ = 7.5, CH, Ar), 7.53 (1H, d, $^3J_{HH}$ = 7.7, Ar), 7.43 – 7.41 (1H, m, CH, Ar), 6.93 (1H, d, $^3J_{HH}$ = 7.5, CH, Ar), 6.35 – 6.31 (1H, bs, NH thiourea), 6.06 – 6.01 (1H, m, NH thiourea), 4.75 (1H, d, $^3J_{HH}$ = 4.8, CH_2), 3.87 (1H, s, CH), 2.00 – 1.88 (2H, m, cyclohexyl), 1.70 – 1.52 (3H, m, cyclohexyl), 1.35 - 1.11 (5H, m, CH_2); δ_C (75 MHz; $CDCl_3$) 181.1 (C, quat, CS), 166.0 (C, quat, CO), 157.0 (C, quat, Ar), 150.6 (C, quat, Ar), 139.0 (C, quat, Ar), 139.0 (CH, Ar), 134.5 (C, quat, Ar), 131.7 (CH, Ar), 129.1 (CH, Ar), 126.3 (CH, Ar), 119.8 (CH, Ar), 111.3 (CH, Ar), 53.0 (CH), 47.9 (CH_2), 32.8 (CH_2), 32.7 (CH_2), 25.4 (CH_2), 24.7 (CH_2), 23.9 (CH_3); *m/z* (ES) 406.2 (M + Na^+ + H, 32%), 405.2 (100); *m/z* (HRMS) found 405.1734 $[MNa]^+$, $C_{21}H_{26}N_4ONaS$ requires 405.1755.

Functionalised Malemides, General Procedure[170-172]

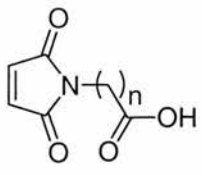

Maleic anhydride and the appropriate amino acid were dissolved in acetic acid and stirred for 8 hours, during this time a precipitate of the insoluble intermediate formed. The reaction mixture was refluxed for 16 hours, subsequently, the acetic acid was removed *in vacuo*.

n=1, (2,5-Dioxo-2,5-dihydro-pyrrol-1-yl)-acetic acid 92

(2,5-Dioxo-2,5-dihydro-pyrrol-1-yl)-acetic acid was prepared as above starting from maleic anhydride (15.0g, 153 mmol), glycine (11.5g, 153mmol) and acetic acid (500 ml). The crude maleimide was purified *via* flash column chromatography (SiO_2 : 1:19 AcOH, CH_2Cl_2) and subsequent crystallisation from CH_2Cl_2 to yield large colourless crystals of **92** (5.02g, 21%). m.p. 114 – 115.5 °C from CH_2Cl_2 Lit.[171] 113 – 113.5 °C from CH_2Cl_2; ν_{max}(KBr disc)/cm^{-1} 3102 (OH), 1700 (CO), 1694 (CO); δ_H (300 MHz; $CDCl_3$) 6.80 (2H, s, CH), 6.49 (1H, s, OH), 4.32 (2H, s, CH_2); δ_C (75 MHz; $CDCl_3$) 175.7 (C, quat, CO), 169.7 (C, quat, CO), 134.6 (CH), 38.1 (CH_2); *m/z* (EI) 155 (M+, 5%), 110 (100), 82 (47)

n=2, 3-(2,5-Dioxo-2,5-dihydro-pyrrol-1-yl)-propionic acid 62

(2,5-Dioxo-2,5-dihydro-pyrrol-1-yl)-propionic acid was prepared as above starting from maleic anhydride (5.50g, 56.1 mmol) and β-alanine (5.00, 56.1 mmol) in acetic acid (190 ml). The crude maleimide was purified *via* flash column chromatography (SiO_2 : 1:19 AcOH, CH_2Cl_2) to yield **62** as a colourless solid (3.09 g, 33%). m.p. 101 - 102 °C from CH_2Cl_2 Lit.[171] 105 – 105.5 °C from CH_2Cl_2; ν_{max}(KBr disc)/cm^{-1} 3398 (OH), 1701 (CO); δ_H (300 MHz; $CDCl_3$) 8.41 (1H, s, OH), 6.71 (2H, s, CH), 3.82 (2H, t, $^3J_{HH}$ = 7.3, CH_2), 2.69 (2H, t, $^3J_{HH}$ = 7.3, CH_2); δ_C (75 MHz; CD_3CN) 175.0 (C, quat, CO), 175.6 (C, quat, CO), 135.9 (CH), 35.1 (CH_2), 33.9 (CH_2); *m/z* (EI) 169 (M+, 15%), 151 (45), 123 (100), 110 (98); *m/z* (HRMS) found 169.0381 $[M]^+$, $C_7H_7NO_4$ requires 169.0375.

1-Benzyl-3-cyclohexyl-urea 169[173]

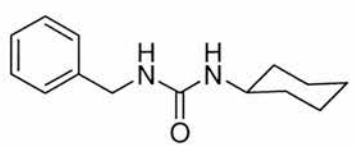

Cyclohexyl isocyanate (1.28 ml, 10 mmol) was added dropwise at 0 °C to a solution of benzyl amine **168** (1.28 ml, 10 mmol) in dried Et_2O (30 ml). The reaction was

allowed to warm to room temperature under an atmosphere of dry nitrogen whereupon a precipitate was formed. The product was isolated from the reaction mixture by filtration to yield **169** as a colourless solid (2.05 g, 92 %). m.p. 150.5 - 153 °C from Et_2O. Lit[173] 150 – 153.5 (from $CHCl_3$/MeOH); ν_{max}(KBr disc)/cm^{-1} 3318 (NH), 2931 (CH), 2849 (CH), 1620 (CO); δ_H (300 MHz; $CDCl_3$) 7.32 - 7.20 (5H, m, CH, Ar), 4.96 (1H, s, NH), 4.58 (1H, d, $^3J_{HH}$ = 7.7), 4.30 (2H, d, $^3J_{HH}$ = 5.5), 3.55 – 3.43 (1H, m, CH), 1.90 – 1.85 (2H, m, cyclohexyl), 1.68 – 1.53 (3H, m, cyclohexyl), 1.36 – 1.22 (2H, m, cyclohexyl), 1.16 – 0.98 (3H, m, cyclohexyl); δ_C (75 MHz; $(CD_3)_2SO$) 157.7 (C, quat, CO), 141.3 (C, quat, Ar), 128.5 (CH, Ar), 127.3 (CH, Ar), 126.9 (CH, Ar), 48.2 (CH), 43.1 (CH_2), 33.6 (CH_2), 25.6 (CH_2), 24.8 (CH_2); *m/z* (EI) 232 (M^+, 90%), 151 (26), 133 (27), 106 (80), 91 (92), 56 (100).

1-Benzyl-3-cyclohexyl-thiourea 170[174]

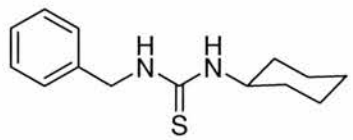

Cyclohexyl isothiocyanate (2.56 ml, 18 mmol) was added dropwise to a solution of benzyl amine **168** in EtOAc (60 ml). The reaction was refluxed for 1 hour under an atmosphere of dry nitrogen. The crude thiourea was purified *via* column chromatography (SiO_2 : CH_2Cl_2) to yield **170** as a colourless solid (2.40 g, 54 %). m.p. 90 – 92 °C from CH_2Cl_2. Lit[174] 91 – 92 °C from EtOH; ν_{max}(KBr disc)/cm^{-1} 3312 (NH), 3241 (NH), 2931 (CH), 2854 (CH), 1558 (CS); δ_H (300 MHz; $CDCl_3$) 7.36 – 7.30 (5H, m, Ar), 6.19 (1H, s, NH), 5.81 (1H, s, NH), 4.61 (2H, s, CH_2), 3.83 (1H, s, CH), 1.94 – 1.91 (2H, m, cyclohexyl), 1.69 – 1.55 (3H, m, cyclohexyl), 1.38 – 1.25 (2H, m, cyclohexyl), 1.18 - 1.07 (3H, m, cyclohexyl); δ_C (75 MHz; $CDCl_3$) 180.9 (CS), 137.4 (C, Ar), 129.3 (CH, Ar), 128.3 (CH, Ar), 127.9 (CH, Ar), 53.4 (CH), 48.7 (CH_2), 33.1 (CH_2), 25.7 (CH_2), 24.9 (CH_2); *m/z* (CI) 249 (MH+, 100%), 159 (30).

N-(6-Methyl-pyridin-2-yl)-benzamide 171

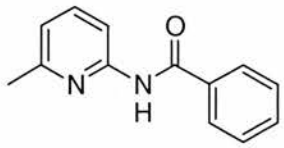

Benzoyl chloride (1.07 ml, 9.3 mmol) was added dropwise to a solution of 2-amino-6-picoline (3.00 g, 27.7 mmol) in dry dichloromethane (60 ml) at 0°C. The solution was stirred and allowed to warm to room temperature overnight. The hydrochloride salt was removed by filtration and the filtrate was concentrated *in vacuo*. The amide was purified *via* flash column chromatography (SiO_2 : CH_2Cl_2) to yield *N*-(6-methyl-pyridin-2-yl)-benzamide **171** as a colourless solid (1.78 g, 90 %) m.p. 88.5 – 89 °C (from CH_2Cl_2).; ν_{max}(Nujol mull)/cm^{-1} 3425 (NH), 1653 (CO); δ_H (300 MHz; $CDCl_3$) 8.68 – 8.59 (1H, bs, NH), 8.21 (1H, d, $^3J_{HH}$ = 8.3, CH, Ar), 7.97 – 7.92 (2H, m, CH, Ar), 7.68 (1H, dd, $^3J_{HH}$ = 8.3, $^3J_{HH}$ = 7.5, CH Ar), 7.61 – 7.47 (3H, m, CH Ar), 6.95 (1H, d, $^3J_{HH}$ = 7.5, CH, Ar); δ_C (75 MHz; $CDCl_3$) 165.8 (C, quat, CO), 156.9 (C, quat, Ar), 150.9 (C, quat, Ar), 138.8 (CH, Ar), 134.4 (C, quat, Ar), 134.4 (CH, Ar), 132.2 (CH, Ar), 128.8 (CH, Ar), 127.3 (CH, Ar),119.5 (CH, Ar), 111.1 (CH, Ar), 23.9 (CH_3); *m/z* (ES) 235 ([M + Na]$^+$, 100%), 213 (20).

1-(2-Chloro-ethyl)-3-cyclohexyl-urea 183[175]

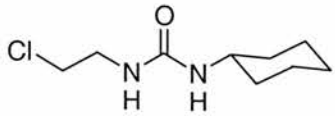

2-Chlororethyl isocyanate (5.00 ml, 58.6 mmol) was added dropwise at 0 °C to a solution of cyclohexylamine **182** in dried Et_2O (180 ml). The reaction was allowed to warm to room temperature under an atmosphere of dry nitrogen whereupon a precipitate was formed. The product was isolated from the reaction mixture by filtration to yield **183** as a colourless solid (11.31 g, 94 %): m.p. 130.0 – 131.0 °C (from Et_2O) Lit.[175] 130-132 °C from H_2O; ν_{max}(KBr disc)/cm^{-1} 3344 (NH), 3304 (NH), 1628 (C, quat, CO); δ_H (300 MHz; CD_3OD) 3.57 (2H, t, $^3J_{HH}$ = 6.0, CH_2), 3.50 – 3.48 (1H, m, CH), 3.41 (2H, t, $^3J_{HH}$ = 6.0, CH_2), 1.88 – 1.83 (2H, m, NH urea), 1.75 – 1.70 (3H, m, cyclohexyl) 1.62 – 1.58 (2H, m, cyclohexyl), 1.42 – 1.12 (5H, m, cyclohexyl); δ_C (75 MHz; $CDCl_3$) 160.7 (C, quat, CO), 50.5 (CH), 45.6 (CH_2), 43.6 (CH_2), 35.3

(CH_2), 27.3 (CH_2), 26.7 (CH_2); *m/z* (EI) 204 (M+, 12%), 169 (11), 161 (12), 123 (25) 56 (100)

1-(2-Chloro-ethyl)-3-cyclohexyl-thiourea 184

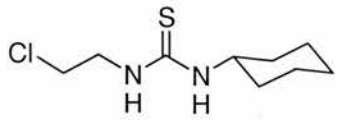

2-Chlororethyl isothiocyanate (3.95ml, 41.1 mmol) was added dropwise at 0 °C to a solution of cyclohexylamine **182** (4.70 ml, 41.1 mmol) in dried Et_2O (140 ml). The reaction was allowed to warm to room temperature under an atmosphere of dry nitrogen whereupon a precipitate was formed. The product was isolated from the reaction mixture by filtration to yield **184** as a colourless solid (3.65 g, 40 %). m.p. 201.0 – 202.5 °C (from Et_2O); ν_{max}(Nujol mull)/cm^{-1} 1559 (CS), 720 (CH_2); δ_H (300 MHz; $CDCl_3$) 10.56 – 10.42 (1H, bs, NH), 10.20 – 10.09 (1H, bs, NH), 3.98 (2H, t, $^3J_{HH}$ = 7.6, CH_2), 3.49 (2H, t, $^3J_{HH}$ = 7.6, CH_2), 2.17 – 2.10 (2H, m, cyclohexyl), 1.98 – 1.72 (3H, m, cyclohexyl), 1.62 – 1.48 (2H, m, cyclohexyl), 1.41 – 1.20 (3H, m, cyclohexyl); δ_C (75 MHz; $CDCl_3$) 160.7 (C, quat, CS), 50.5 (CH), 45.6 (CH_2), 43.6 (CH_2), 35.3 (CH_2), 27.3 (CH_2), 26.7 (CH_2); *m/z* (EI) 184 ([M – HCl]+, 75%), 103 (100), 56 (95); *m/z* (CI) 185 ([M – Cl]$^+$, 100%), 100 (15), 75 (5).

3-Methoxy-*N*-(6-methyl-pyridin-2-yl)-benzamide 188[171]

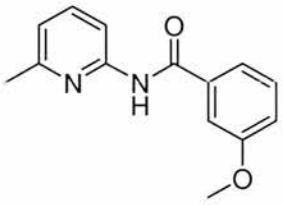

3-Methoxybenzoyl chloride (8.8 mmol, 1.24 ml) was added dropwise to a solution of 2-amino-6-picoline (26.4 mmol, 2.84 g) in dry dichloromethane (50 ml) at 0°C. The solution was stirred and allowed to warm to room temperature overnight. The reaction mixture was concentrated *in vacuo* and purified *via* flash column chromatography (SiO_2 : 1:1:1 Et_2O, Hexane, CH_2Cl_2) to yield **188** as a colourless oil 2.13g, 100%; ν_{max}(KBr disc)/cm^{-1} 3004 (NH), 1682 (CO), 1592 (CN Py); δ_H (300 MHz; $CDCl_3$) 8.58 (1H, bs, NH), 8.20 (1H, d $^3J_{HH}$ = 8.3, CH, Ar), 7.67 (1H, dd, $^3J_{HH}$ = 8.3, $^3J_{HH}$ = 7.3, CH, Ar), 7.51 – 7.44 (2H, m, CH, Ar), 7.43 – 7.38 (1H, m, CH, Ar), 7.10 (1H, ddd, $^3J_{HH}$ = 8.1, $^4J_{HH}$ = 2.6, $^4J_{HH}$ = 1.3, CH, Ar), 6.95 (1H, d, $^3J_{HH}$ = 7.3, CH, Ar),

3.71 (3H, s, CH_3), 2.31 (3H, s, CH_3); δ_C (75 MHz; $CDCl_3$) 160.4 (C, quat, CO), 157.2 (C, quat, Ar), 153.0 (C, quat, Ar), 151.1 (C, quat, Ar),139.3 (CH, Ar), 136.2 (C, quat, Ar), 130.2 (CH, Ar), 119.8 (CH, Ar), 119.4 (CH, Ar), 119.0 (CH, Ar), 112.7 (CH, Ar), 111.4 (CH, Ar), 55.9 (CH_3), 24.3 (CH_3); *m/z* (EI) 242 (M^+, 32%), 213 (55), 135 (100).

tert-butyldimethylsilyl 3-((_tert_-butyldimethylsilyl)oxy)benzoate 191

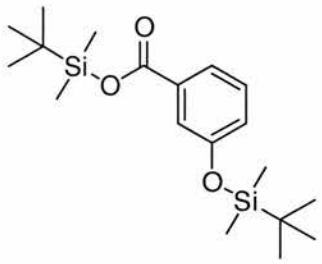

Imidazole (1.48g, 21.7 mmol) was added in one portion to a solution of 3-hydroxybenzoic acid **190** (1g, 7.2 mmol) in dry CH_2Cl_2 (20 ml) at 0°C. *t*Butyldimethylsilyl chloride was added portionwise over 5 minutes and the reaction mixture was stirred overnight at room temperature. The reaction mixture was washed with water (20 ml) and saturated $NaHCO_3$ (aq) solution (20 ml). The aqueous layers were combined and extracted with Et_2O (2 x 20 ml). The organic fractions were combined, dried ($MgSO_4$) and the solvent was removed *in vacuo* to yield **191** as a colourless oil (2.01 g, 76%), which was used without further purification.

3-(_tert_-Butyl-dimethyl-silanyloxy)-_N_-(6-methyl-pyridin-2-yl)-benzamide 193

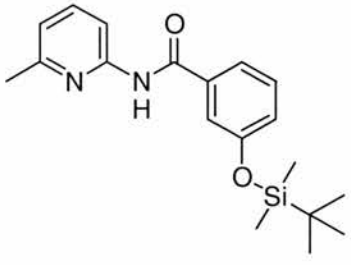

Oxalyl chloride (0.90g, 7.1mmol) was added slowly to a solution of *tert*-butyldimethylsilyl 3-((*tert*-butyldimethylsilyl)oxy)benzoate **191** (1.85g, 5mmol) in CH_2Cl_2 (5 ml) and DMF (0.1 ml) and the resulting solution was stirred for 40 hours. The reaction was quenched with a solution of 2-amino-6-picoline (1.63g, 15.2 mmol) in CH_2Cl_2 (25 ml) and stirred overnight at room temperature. The mixture was filtered to remove the amine hydrochloride salt and purified *via* column chromatography

(SiO_2: 9:1 40-60°C Petroleum Ether : EtOAc) to yield **193** as a colourless oil (1.30g, 75%) . ν_{max}(thin film)/cm^{-1} 3300 (NH), 1682 (CO), 1580 (Ar), 1287 (SiC); δ_H (300 MHz; $CDCl_3$) 8.63 – 8.58 (1H, bs, NH), 8.20 (1H, d, $^3J_{HH}$ = 8.3, CH, Ar), 7.66 (1H, dd, $^3J_{HH}$ = 8.3, $^3J_{HH}$ = 7.4), 7.48 (1H, ddd, $^3J_{HH}$ = 7.8, $^4J_{HH}$ = 1.7, $^4J_{HH}$ = 1.0, CH, Ar), 7.42 (1H, dd, $^4J_{HH}$ = 1.7, $^4J_{HH}$ = 2.5, CH, Ar), 7.34 (1H, $^3J_{HH}$ = 7.8, $^3J_{HH}$ = 8.1, CH, Ar), 7.02 (1H, ddd, $^3J_{HH}$ = 8.1, $^4J_{HH}$ = 2.5, $^4J_{HH}$ = 1.0, CH, Ar), 6.93 (1H, d, $^3J_{HH}$ = 7.36, CH, Ar); δ_C (75 MHz; $CDCl_3$) 165.1 (C, quat, CO), 157.1 (C, quat, Ar), 156.2 (C, quat, Ar), 150.2 (C, quat, Ar), 139.4 (CH, Ar), 136.7 (CH, Ar), 130.0 (CH, Ar), 124.3 (CH, Ar), 120.2 (CH, Ar), 119.8 (CH, Ar), 119.7 (CH, Ar), 26.1 (CH_3), 26.0 (CH_3), 24.1 (CH_3), 16.4 (C); *m/z* (EI) 342 ([M]+, 16%), 313 (10), 285 (46) 75 (100); *m/z* (HRMS) found 342.1755 $[M]^+$, $C_{19}H_{26}N_2O_2Si$ requires 342.1764.

3-Hydroxy-*N*-(6-methyl-pyridin-2-yl)-benzamide 189

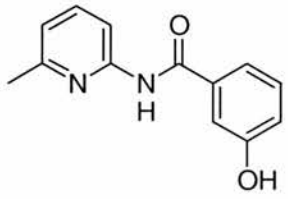

3-(*tert*-Butyl-dimethyl-silanyloxy)-*N*-(6-methyl-pyridin-2-yl)-benzamide **193** (1.3g, 3.8 mmol) was dissolved in a solution of TBAF in THF (1M, 3.9 ml, 3.9 mmol) and THF (15 ml) and stirred for one hour after which time the reaction mixture was poured onto EtOAc (40 ml), washed (H_2O, 2 x 20 ml), dried ($MgSO_4$) and the solvent removed *in vacuo*. The crude solid was purified by recrystallisation (Et_2O / MeOH / hexane) to yield **189** as colourless crystals (0.87 g, 58%). m.p. 178.5 – 179.0 ºC (from Et_2O / MeOH / hexane); ν_{max}(Nujol mull)/cm^{-1} 1691 (CO), 1587 (Ar), 1543 (Ar); δ_H (300 MHz; $CDCl_3$) 9.27 (1H, s, NH), 8.29 (1H, d, $^3J_{HH}$=8.2, CH Ar), 7.72 (1H, dd, $^3J_{HH}$=8.2, $^3J_{HH}$=7.2, CH Ar), 7.66 – 7.62 (1H, m, CH Ar), 7.57 – 7.54 (1H, m, CH, Ar), 7.36 – 7.33 (1H, m, CH, Ar), 7.09 – 7.05 (1H, m, CH, Ar), 7.00 – 6.98 (1H, m, CH, Ar), 2.62 (3H, s, CH_3); δ_C (75 MHz; $(CD_3)_2SO$) 166.3 (C, quat, CO), 157.7 (C, quat, Ar), 156.9 (C, quat, Ar), 151.8 (C, quat, Ar), 138.6 (CH, Ar), 135.9 (C, quat, Ar), 129.7 (CH, Ar), 119.3 (CH, Ar),119.2 (CH, Ar),118.8 (CH, Ar), 115.2 (CH, Ar),112.0 (CH, Ar), 23.9 (CH_3); *m/z* (EI) 228 ([M]+, 40%), 199 (65), 121 (100); *m/z* (HRMS) 228.0905 $[M]^+$, $C_{13}H_{12}N_2O_2$ requires 228.0898.

1-Cyclohexyl-3-(2-phenoxy-ethyl)-urea 196

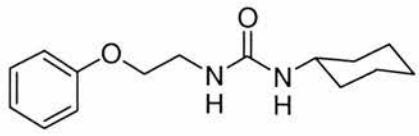

Method A: A solution of phenol (0.92 g, 9.8 mmol) and K_2CO_3 (4.01 g, 29.3 mmol), was prepared in CH_3CN (20 ml). The reaction mixture was refluxed for 3 hours, cooled and a solution of 1-(2-chloro-ethyl)-3-cyclohexyl-urea **183** (2.00 g, 9.8 mmol) in CH_3CN (20 ml) was added. The reaction mixture was refluxed for 5 days. The reaction mixture was cooled, filtered, the solid washed (2 x 10 ml CH_2Cl_2) and the solvent removed *in vacuo*. The residue was diluted with CH_2Cl_2 (20 ml) and washed with HCl (1M, 2 x 15 ml) followed by H_2O (20 ml). The organic layer was separated, dried ($MgSO_4$) and the solvent removed *in vacuo*. The residue was purified by column chromatography (SiO_2 : CH_2Cl_2) to yield the product **196** (0.42 g, 16 % crude) which could not be purified further.

Method B: A solution of phenol (0.46 g, 4.9 mmol), $CsCO_3$ (1.92 g, 5.9 mmol), and NaI (0.73, 4.9 mmol) was prepared in CH_3CN (25 ml). The reaction mixture was refluxed for 3 hours, cooled and a solution of 1-(2-chloro-ethyl)-3-cyclohexyl-urea **183** (1.00 g, 4.9 mmol) in CH_3CN (25 ml) was added. The reaction mixture was refluxed for 5 days after which time only side product formation was observed by TLC.

Method C: A solution of phenol (0.46g, 4.9 mmol) in THF (50 ml) was added dropwise at 0 °C in a dry nitrogen atmosphere to sodium hydride (60% on mineral oil, 0.20g, 4.9 mmol) in THF (20 ml). 1-(2-Chloro-ethyl)-3-cyclohexyl-urea **183** (1.00 g, 4.9 mmol) dissolved in THF (50 ml) was added dropwise at room temperature and the reaction was refluxed for 4 hours. The solvent was removed in vacuo, the residue redissolved in CH_2Cl_2, washed with H_2O and dried ($MgSO_4$). The product was isolated by column chromatography (SiO_2 : CH_2Cl_2) to yield **196** as a colourless solid (100 mg, 8%).

Method D: A solution of phenol (1.38g, 14.7 mmol) in DMF (20 ml) was added dropwise at 0 °C in a dry nitrogen atmosphere to sodium hydride (60% in mineral oil, 0.59 g, 14.7 mmol) in DMF (10 ml). 1-(2-Chloro-ethyl)-3-cyclohexyl-urea **183** (2.00g,

14.7 mmol) and sodium iodide (0.44 g, 2.9 mmol) dissolved in DMF (10 ml) was added dropwise at room temperature and the reaction was stirred at 90 °C for 22 hours. The reaction mixture was poured onto H_2O (100 ml) and extracted with CH_2Cl_2 (2 x 50 ml), the organic layer was isolated, dried ($MgSO_4$) and the solvent removed in vacuo. Residual traces of DMF were difficult to remove and prevented isolation of the product in its pure form.

Method E: Phenol (1.87g, 19.9 mmol), and K_2CO_3 (8.17g, 59.7 mmol), were refluxed in CH_3CN (40 ml) for 3 hours. The reaction mixture was cooled and a solution of toluene-4-sulfonic acid 2-(3-cyclohexyl-ureido)-ethyl ester **199** (6.58g, 19.9 mmol) in CH_3CN (40 ml) was added dropwise and the resulting reaction mixture was refluxed for 5 days. The reaction mixture was cooled, filtered, the solid washed (2 x 10 ml CH_2Cl_2) and the solvent removed *in vacuo*. The residue was diluted with CH_2Cl_2 (20 ml) and washed with HCl (1M, 2 x 15 ml) followed by H_2O (20 ml). The organic layer was separated, dried ($MgSO_4$) and the solvent removed *in vacuo*. The residue was purified by column chromatography (SiO_2 : CH_2Cl_2) to yield the product as a colourless solid **196** (50 mg, 9 %)

Method F: DEAD (0.64 ml, 4 mmol), was added at 0 °C to a solution of Phenol (0.38 g, 4 mmol), triphenylphosphine (1.06 g, 4 mmol) and 1-cyclohexyl-3-(2-hydroxy-ethyl)-urea **198** (0.75 g, 4 mmol) in CH_2Cl_2 (10 ml). After 0.5 hours, the reaction mixture was warmed to r.t. and stirred for 72 hours. The reaction mixture was poured onto H_2O (25 ml) and extracted with CH_2Cl_2 (2 x 20 ml). The product was isolated by column chromatography (SiO_2 : CH_2Cl_2) to yield **196** as a colourless solid (120 mg, 11%)

m.p. 127.0 - 127.5 °C (from CH_2Cl_2); ν_{max}(Nujol mull)/cm^{-1} 3311 (NH), 1622 (CO), 1576 (Ar), 753 (Ar); δ_H (300 MHz; $(CD_3)_2SO$) 7.31 – 7.25 (2H, m, CH, Ar), 6.95 – 6.90 (3H, m, CH, Ar), 5.96 – 5.88 (2H, m, CH_2), 3.92 (2H, t, 3JHH = 5.7, CH_2), 1.74 – 1.49 (6H, m, CH_2, NH), 1.03 – 0.99 (7H, m, CH_2, NH); δ_C (75 MHz; $CDCl_3$) 162.8 (C, quat, CO), 158.9 (C, quat, Ar), 130.0 (CH, Ar), 121.5 (CH, Ar), 114.8 (CH, Ar), 68.0 (CH_2), 49.7 (CH), 40.5 (CH_2), 34.2 (CH_2), 25.9 (CH_2), 25.3 (CH_2); *m/z* (CI) 263 ($[MH]^+$, 50%), 169 (10), 58 (100); *m/z* (HRMS) found 263.1772 $[MH]^+$, $C_{15}H_{23}N_2O_2$ requires 263.1760.

1-Cyclohexyl-3-(2-hydroxy-ethyl)-urea 198[176]

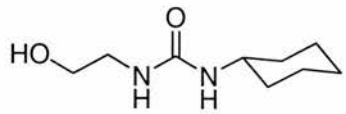

Cyclohexylisocyanate (3.18 ml, 24.9 mmol) was added dropwise at 0 °C to a solution of ethanolamine (1.50 ml, 24.9 mmol) **197** in dried Et_2O (50 ml). The reaction was allowed to warm to room temperature under an atmosphere of dry nitrogen whereupon a precipitate was formed. After one hour, the product was isolated from the reaction mixture by filtration to yield **198** as a colourless solid (4.31 g, 93 %) 90 - 90.5 °C Lit[176] 90 – 91 °C (from acetone / Et_2O); ν_{max}(Nujol mull)/cm^{-1} 3333 (OH), 1622 (CO); δ_H (300 MHz; $CDCl_3$) 4.95 – 4.85 (1H, bs, NH), 4.77 – 4.67 (1H, bs, NH), 3.32 – 3.14 (3H, m, CH_2, CH), 2.99 – 2.90 (2H, m, CH_2), 1.66 – 0.83 (10H, m, CH_2 cyclohexyl); δ_C (75 MHz; $CDCl_3$) 158.2 (C, quat, CO), 117.0 (CH_2), 62.0 (CH_2), 48.3 (CH), 42.3 (CH_2), 33.0 (CH_2), 25.1 (CH_2), 24.4 (CH_2); *m/z* (EI) 186 ($[M]^+$, 78%), 171 (25), 156 (100).

Toluene-4-sulfonic acid 2-(3-cyclohexyl-ureido)-ethyl ester 199

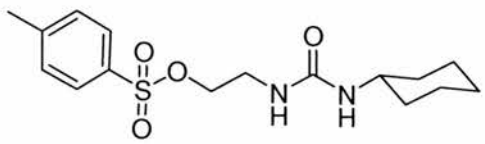

*p*Toluenesulfonyl chloride (2.06 g, 10.8 mmol) was dissolved in CH_2Cl_2 (25 ml), filtered and added dropwise at 0°C to a solution of 1-Cyclohexyl-3-(2-hydroxy-ethyl)-urea **198** (1.00 g, 5.4 mmol) dissolved in CH_2Cl_2 (25 ml) and Et_3N (1.50 ml, 10.8 mmol). After stirring at room temperature overnight the reaction was washed with HCl (aq) (2 M, 2 x 30ml), dried ($MgSO_4$) and purified *via* column chromatography (SiO_2: 3:1 Hexane : CH_2Cl_2 to 2:1 Hexane : CH_2Cl_2) to yield the product **199** as a colourless solid (0.80g, 45%): m.p. 76.0 – 77.0 °C (from Hexane / CH_2Cl_2); ν_{max}(Nujol mull)/cm^{-1} 3381 (NH), 1678 (CO), 1420 (SO); δ_H (300 MHz; $CDCl_3$) 7.69 (2H, d, $^3J_{HH}$ = 8.5), 7.34 (2H d, $^3J_{HH}$ = 8.5), 3.92 (2H, t, $^3J_{HH}$ = 7.2), 3.63 (2H, t, $^3J_{HH}$ = 7.2), 2.43 (3H, s), 1.89 – 1.21 (11H, CH_2, CH); δ_C (75 MHz; $CDCl_3$) 151.4 (C, quat, CO), 145.6 (C, quat, Ar), 136.0 (C, quat, Ar), 130.5 (CH, Ar), 127.2 (CH, Ar), 50.4 (CH), 46.9 (CH_2), 42.1 (CH_2), 33.2 (CH_2), 25.8 (CH_2), 25.0 (CH_2), 22.0 (CH_3); *m/z* (CI) 359 ($[MH + H_2O]^+$, 100%), 169 (32), 157 (30).

N-(2-Hydroxy-ethyl)-4-methyl-benzenesulfonamide 202[177]

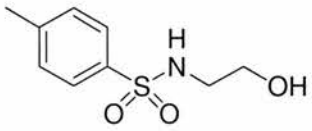

p-Toluene sulfonyl chloride (1.00 g, 5.25 mmol) was added to a solution of ethanolamine **197** (1.60 ml, 26.2 mmol) at 0 °C in CH_2Cl_2 and stirred for 48 hours at room temperature. The solution was filtered and the filtrate was purified *via* column chromatography by gradient elution (SiO_2 : CH_2Cl_2 to Et_2O) to yield **202** as a colourless oil. ν_{max}(thin film)/cm^{-1} 3487 (OH), 2928, 2885 (CH_2), 1598 (Ar), 1323 (SO); δ_H (300 MHz; $CDCl_3$) 7.76 (2H, d, $^3J_{HH}$ = 8.1, CH, Ar), 7.32 (2H, d, $^3J_{HH}$ = 8.1), 4.86 – 4.76 (1H, bs, NH), 3.72 – 3.68 (2H, m, CH_2), 3.12 – 3.07 (2H, m, CH_2), 2.43 (3H, s, CH_3); δ_C (75 MHz; $CDCl_3$) 144.0 (C, quat, Ar), 136.9 (C, quat, Ar), 130.2 (CH, Ar), 127.5 (CH, Ar), 61.6 (CH_2), 45.6 (CH_2), 21.9 (CH_3); *m/z* (EI) 215 ([M]$^+$, 7%), 184 (82), 155 (88), 91 (100).

7.9 Characterisation of Reaction Products

General Procedure

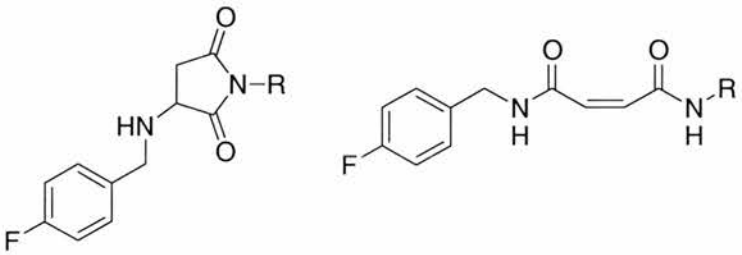

4-fluorobenzylamine was added to one equivalent of the appropriate maleimide in CH_2Cl_2 and the resulting solution was stirred at room temperature for 72 hrs.

R = H, 3-(4-Fluoro-benzylamino)-pyrrolidine-2,5-dione 155

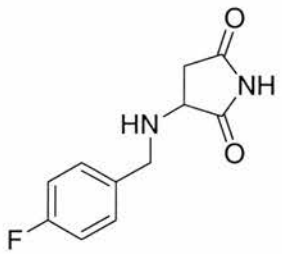

Only the Michael addition product was formed which was isolated by column chromatography (SiO_2 : Et_2O) to yield the product as a yellow solid (150 mg, 17%)

m.p. 105.0 – 106.5 °C (from Et_2O); ν_{max}(Nujol mull)/cm^{-1} 1705 (CO); δ_H (300 MHz; $CDCl_3$) 8.14 – 7.92 (1H, bs, NH succinimide), 7.34 – 7.28 (2H, m, CH, Ar), 7.08 – 7.00 (2H, m, CH, Ar), 3.86 – 3.81 (3H, m, CH, CH_2), 2.58 (1H, dd, $^2J_{HH}$ = 18.1, $^3J_{HH}$ = 8.4, CH_2 succinimide), (1H, dd, $^2J_{HH}$ = 18.1, $^3J_{HH}$ = 5.3, CH_2 succinimide); δ_C (75 MHz; $CDCl_3$) 178.6 (C, quat, CO), 175.7 (C, quat, CO), 162.6 (d, $^1J_{CF}$=244, C, quat, CF, Ar), 134.7 (C, quat, Ar), 130.3 (d, $^3J_{CF}$=8, CH, Ar), 115.9 (d, $^2J_{CF}$=21, CH, Ar) 57.0 (CH), 51.4 (CH_2), 37.7 (CH_2); *m/z* (CI) 223 ([MH]+, 60%), 156 (100), 56 (95); *m/z* (HRMS) 223.0889 $[MH]^+$ $C_{11}H_{12}N_2O_2F$ requires 223.0883

R=Ph

The adducts were prepared as above using *N*-phenylmaleimide (1.00 g, 5.8 mmol) and 4-fluorobenzylamine (0.66 ml, 5.8 mmol). After reaction, the solvent was removed in vacuo and the resulting mixture was purified by gradient elution column chromatography (SiO_2 : CH_2Cl_2 to 1:1 CH_2Cl_2 : EtOAc) to yield the direct adduct, but-2-enedioic acid 4-fluoro-benzylamide phenylamide **121** (0.44 g , 27%) and the conjugate adduct 3-(4-fluoro-benzylamino)-pyrrolidine-2,5-dione **120** (130 mg, 8%) as colourless solids.

But-2-enedioic acid 4-fluoro-benzylamide phenylamide 121[178]

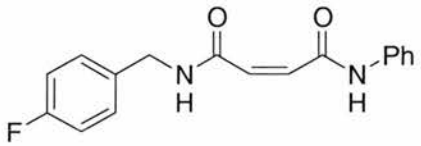

m.p. 73.5 – 75.0 °C from CH_2Cl_2 (Lit[178] 73.8 – 74.9 °C from $CHCl_3$); ν_{max}(Nujol mull)/cm^{-1} 1636 (CO), 825 (Ar); δ_H (300 MHz; $CDCl_3$) 11.42 – 11.35 (1H, bs, NH), 7.60 – 7.21 (6H, m, NH and CH, Ar), 7.16 – 6.76 (4H, m, CH, Ar), 6.18 (1H, d, $^3J_{HH}$ = 13.4, CH alkene), 6.05 (1H, d, $^3J_{HH}$ = 13.4, CH alkene), 4.43 (2H, d, $^3J_{HH}$ = 5.8, CH_2); δ_C (75 MHz; $CDCl_3$) 165.6 (C, quat, CO), 163.1, (C, quat, CO), 162.6 (d, $^1J_{CF}$ = 244, C, quat, CF, Ar), 138.2 (C, quat, Ar), 135.9 (CH, alkene), 133.2 (C, quat, Ar), 131.4 (CH, alkene), 130.4 (d, $^3J_{CF}$ = 8, CH, Ar), 129.4 (CH, Ar), 125.2 (CH, Ar), 120.8 (CH, Ar), 115.9 (d, $^2J_{CF}$ = 21, CH, Ar), 43.6 (CH_2); *m/z* (CI) 299 ($[MH]^+$, 100%), 206 (23), 94 (21).

3-(4-Fluoro-benzylamino)-pyrrolidine-2,5-dione 120[178]

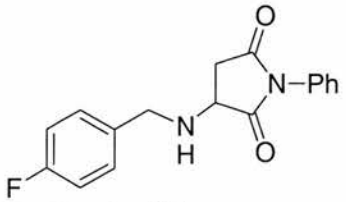

m.p. 121.5 – 122.5 °C from CH_2Cl_2 (Lit[178] 121.4 – 122.0 °C from $CHCl_3$); ν_{max}(Nujol mull)/cm^{-1} 1701 (CO); δ_H (300 MHz; $CDCl_3$) 7.51 – 7.02 (9H, m, CH Ar), 3.97 – 3.93 (3H, m, CH_2, CH), 3.06 (1H, dd, $^2J_{HH}$ = 18.0, $^3J_{HH}$, 8.4), 2.71 (1H, dd, $^2J_{HH}$ = 18.0, $^3J_{HH}$, 5.1); δ_C (75 MHz; $CDCl_3$) 178.2 (C, quat, CO), 174.5 (C, quat, CO), 162.6 (d, $^2J_{CF}$=244, CF), 136.1 (C, quat, Ar), 131.9 (C, quat, Ar), 130.3 (d, $^4J_{CF}$=8, CH, Ar), 129.6 (CH, Ar), 129.2 (CH, Ar), 126.7 (CH, Ar), 115.9 (d, $^3J_{CF}$=21, CH, Ar) 56.0 (CH), 51.6 (CH_2), 37.0 (CH_2); *m/z* (CI) 299 ([MH]$^+$, 100%), 271 (5), 124 (15).

(3-Heptylsulfanyl-2,5-dioxo-pyrrolidin-1-yl)-acetic acid 172

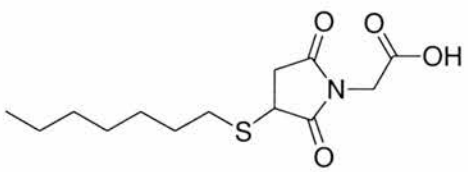

Heptane thiol (0.50 ml, 3.2 mmol) was added to one equivalent of the maleimide **92** (0.50 g, 3.2 mmol) dissolved in CH_2Cl_2 (20 ml) and Et_3N (0.5 ml). The resulting solution was stirred for 48 hrs. The reaction mixture was subsequently washed with 1M HCl (2 x 25 ml), dried ($MgSO_4$) and the solvent removed *in vacuo*. The product **172** was isolated as a colourless oil (0.29g, 31%); ν_{max}(thin film)/cm^{-1} 3165 (OH), 1714 (CO), 1698 (CO); δ_H (300 MHz; $CDCl_3$) 4.33 (2H, s, CH_2), 3.82 (1H, dd, $^3J_{HH}$ = 9.2, $^3J_{HH}$ = 3.8, CH succinimide), 3.25 (1H, dd, $^2J_{HH}$ = 18.9, $^3J_{HH}$ = 9.2, CH succinimide), 2.93 – 2.71 (2H, m, CH_2), 2.64 (1H, dd, $^2J_{HH}$ = 18.9, $^3J_{HH}$ = 3.8, CH succinimide), 1.72 – 1.56 (2H, m, CH_2), 1.42 – 1.22 (8H, m, CH_2), 0.91 – 0.87 (3H, m, CH_3); δ_C (75 MHz; $CDCl_3$) 176.1 (C, quat, CO), 174.4 (C, quat, CO), 171.9 (C, quat, CO), 39.8 (CH_2), 39.6 (CH), 36.6 (CH_2), 32.0 (CH_2), 31.9 (CH_2), 29.3 (CH_2), 29.2 (CH_2), 29.1 (CH_2), 23.0 (CH_2),14.5 (CH_3); *m/z* (CI) 288 ([MH]$^+$, 100), 189 (8), 158 (30), 133 (15), 57 (15); *m/z* (HRMS) found 288.1283 [MH]$^+$, $C_{13}H_{22}NO_4S$ requires 288.1270.

General Procedure

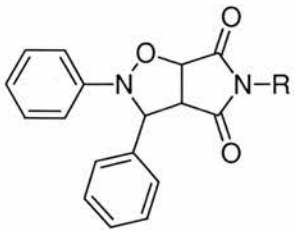

One equivalent of *N*-benzylidene-aniline *N*-oxide **141** and one equivalent of the appropriate maleimide, dissolved in a suitable solvent were stirred at room temperature for 5 days. The solvent was removed *in vacuo* and the residue was purified as detailed below.

R = Ph 2,3,5-Triphenyl-tetrahydro-pyrrolo[3,4-d]isoxazole-4,6-dione 142 and 143[179]

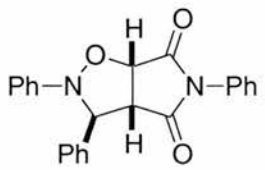

142

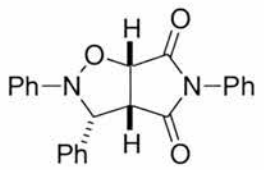

143

Ratio 7:3

The reaction was performed as in the general procedure above using *N*-phenylmaleimide (1.00g, 5.77 mmol) and *N*-benzylidene-aniline *N*-oxide (1.14g, 5.77 mmol). The yellow solid was purified *via* recrystallisation (CH_2Cl_2 / Hexane) to yield **142** and **143** as a colourless powder in a 7:3 diastereoisomeric ratio (0.85g, 40%): m.p. 155.0 – 160 °C (from CH_2Cl_2 / hexane); ν_{max}(Nujol mull)/cm^{-1} 1719 (CO), 1596 (Ar); δ_H (300 MHz; $CDCl_3$) 7.61 – 6.97 (30H, m, CH, Ar **142** and **143**), 6.64 – 6.61(2H, m, CH, Ar, **142** and **143**), 5.78 (1H, s, CH, **142**), 5.31 (1H, d, CH, $^3J_{HH}$ = 7.9, **143**), 5.13 (1H, dd, CH, $^3J_{HH}$ = 7.5, $^4J_{HH}$ = 0.5, CH **142**), 4.96 (1H, d, CH, $^3J_{HH}$ = 9.2, CH **143**), 4.12 – 4.09 (1H, m, CH, **143**), 4.06 – 4.03 (1H, m, CH, **142**); δ_C (75 MHz; $CDCl_3$) 174.6 (C, quat, CO, **143**), 173.9 (C, quat, CO, **142**), 173.0 (C, quat, CO, **143**), 171.8 (C, quat, CO, **142**), 149.2 (C, quat, Ar, **143**), 147.8 (C, quat, Ar, **142**), 139.0 (C, quat, Ar, **143**), 134.9 (C, quat, Ar, **142**), 131.5 (C, quat, Ar, **142**), 131.3 (C, quat, Ar, **143**), 129.8, 129.6, 129.5, 129.4, 129.3, 129.3, 129.2, 129.1, 129.0, 128.6, 127.9, 126.9, 126.5, 126.4, 125.2, 123.3, 119.2, 114.8 (CH, Ar, **142** and **143**), 77.7 (CH, **143**), 77.3 (CH, **142**), 71.8 (CH, **142**), 70.4 (CH **143**), 57.7 (CH **143**), 55.0 (CH **142**); *m/z* (CI), 371 ($[MH]^+$, 100%), 198 (65), 182 (35), 174 (42).

R = H, 2,3-Diphenyl-tetrahydro-pyrrolo[3,4-*d*]isoxazole-4,6-dione

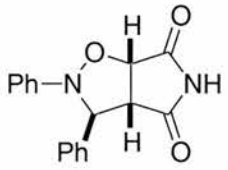

156

The procedure was followed as above using *N*-Benzylidene-aniline *N*-oxide **141** (0.99 g, 5.0 mmol) and maleimide **147** (0.49 g, 5.0 mmol) dissolved in $CHCl_3$ (250 ml). The yellow solid was purified *via* column chromatography (SiO_2: gradient elution 1:1 Et_2O : Hexane to Et_2O) to yield the two diastereoisomers, **156** as a yellow solid, (0.62 g, 42%,) m.p. 140ºC (dec); ν_{max}(KBr disc)/cm^{-1} 3162 (NH), 3074 (CH), 1786 (C, quat, CO), 1709 (C, quat, CO); δ_H (300 MHz; $CDCl_3$) 8.05 (1H, s, NH), 7.42 – 6.91 (10H, m, Ar), 5.43 (1H, s, CH), 5.03 (1H, d, $^3J_{HH}$ = 7.4, CH), 3.87 (1H, dd, $^3J_{HH}$ = 7.4, $^3J_{HH}$ = 1.3, CH); δ_C (75 MHz; $CDCl_3$) 175.8 (C, quat, CO), 173.8 (C, quat, CO), 147.9 (C, quat, Ar), 138.2 (C, quat, Ar), 135.5 (CH, Ar), 129.3 (CH, Ar), 128.6 (CH, Ar), 127.3 (CH, Ar), 123.3 (CH, Ar), 115.8 (CH, Ar), 77.9 (CH), 70.2 (CH), 58.8 (CH); *m/z* (CI) 295 ([MH]+, 100%), 198 (60), 182 (90); *m/z* (HRMS) 295.1094 $[MH]^+$ $C_{17}H_{15}N_2O_3$ requires 295.1083.

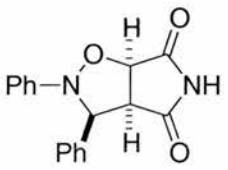

157

157, as a colourless solid, (0.35 g, 24%) m.p. 170ºC (dec); ν_{max}(KBr disc)/cm^{-1} 3188 (NH), 3063 (CH); δ_H (300 MHz; $CDCl_3$) 8.24 (1H, s, NH), 7.37 – 7.06 (10H, m, Ar), 5.09 (1H, d, $^3J_{HH}$ = 7.7, CH), 4.71 (1H, d, $^3J_{HH}$ = 9.2, CH), 3.87 (1H, dd, $^3J_{HH}$ = 7.7, $^3J_{HH}$ = 9.2, CH); δ_C (75 MHz; $CDCl_3$) 175.8 (C, quat, CO), 173.8 (C, quat, CO), 149.9 (C, quat, Ar), 134.4 (C, quat, Ar), 129.4 (CH, Ar), 129.3 (CH, Ar), 129.1 (CH, Ar), 127.8 (CH, Ar), 125.6 (CH, Ar), 120.3 (CH, Ar), 77.8 (CH), 71.6 (CH), 56.4 (CH); *m/z* (CI) 295 ([MH]+, 100%), 198 (60), 182 (90); *m/z* (HRMS) 295.1094 $[MH]^+$ $C_{17}H_{15}N_2O_3$ requires 295.1083.

R=CH_2COOH (4,6-Dioxo-2,3-diphenyl-hexahydro-pyrrolo[3,4-d]isoxazol-5-yl)-acetic acid 173 and 174[170]

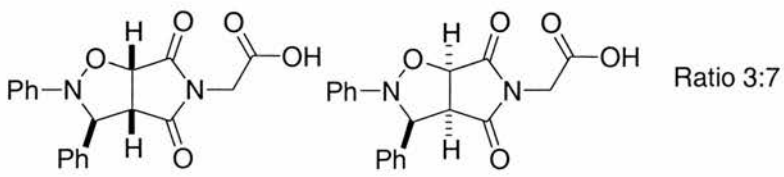

173 **174**

The reaction was performed as described above using *N*-Benzylidene-aniline *N*-oxide **141** (0.40 g, 2.0 mmol) and (2,5-dioxo-2,5-dihydro-pyrrol-1-yl)-acetic acid **92** (0.31, 2.0 mmol) in CH_2Cl_2. The crude yellow solid was purified *via* recrystallisation (CH_2Cl_2 / Hexane) to yield **173** and **174** as a colourless powder in a 7:3 diastereoisomeric ratio (0.20 g, 28%); m.p. > 150 °C (dec) (Lit > 150 °C (dec)); ν_{max}(Nujol mull)/cm^{-1} 3001 (OH), 1718 (CO); δ_H (300 MHz; $CDCl_3$) 7.50 – 7.28 (10H, m, CH, Ar, **173** and **174**), 7.25 – 6.85 (10H, m, CH, Ar, **173** and **174**), 5.47 (1H, s, CH, **173**), 5.18 (1H, d, $^3J_{HH}$ = 7.6, CH, **174**) 5.12 (1H, d, $^3J_{HH}$ = 7.4, **174**), 4.74 (1H, s, $^3J_{HH}$ = 9.0, **173**), 4.44 – 3.92 (6H, m, CH_2, CH, **173** and **174**); δ_C (75 MHz; $CDCl_3$) 177.1 (C, quat, CO, **174**), 176.6 (C, quat, CO, **173**), 174.7 (C, quat, CO, **173**), 174.6 (C, quat, CO, **174**), 164.2 (C, quat, CO, **173**), 163.9 (C, quat, CO, **174**), 149.0 (C, quat, Ar, **173**), 144.8 (C, quat, Ar, **174**), 140.5 (C, quat, Ar, **174**), 136.3 (C, quat, Ar, **173**), 130.3, 130.1, 130.0, 129.9, 129.8, 129.5, 129.0, 126.8, 124.2, 122.2, 117.2, 117.1 (CH, Ar, **173** and **174**), 78.7 (CH, **174**), 78.6 (CH, **173**), 73.6 (CH, **174**), 71.6 (CH, **173**), 58.7 (CH, **173**), 56.6 (CH, **174**), 40.8 (CH_2, **173** and **174**); *m/z* (CI) 353 ([MH]+, 27%), 337 (10%), 198 (30), 182 (100).

General procedure

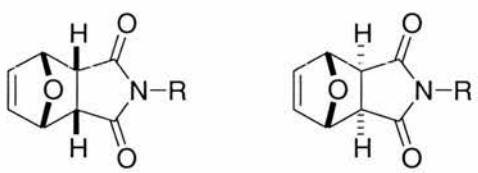

A solution of the appropriate maleimide and furan was stirred at room temperature in CH_2Cl_2 or EtOAc for 5 days until reaction was judged to have reached maximum completion. The solvent was removed *in vacuo* and the cycloadducts were purified as described below.

R=Ph 4-Phenyl-10-oxa-4-aza-tricyclo[5.2.1.02,6]dec-8-ene-3,5-dione *exo* isomer 145

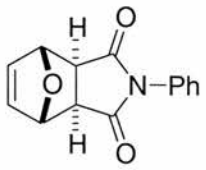

The procedure was performed as above using *N*-phenylmaleimide (1.00g, 5.77 mmol), and furan (0.42 ml, 5.77 mmol) in CH_2Cl_2 (50 ml). The solvent was removed *in vacuo* and the resulting residue was recrystallised (CH_2Cl_2 / Hexane) to yield the *exo* adduct **145** as a colourless crystalline solid (0.35g, 25%). m.p. 154.5 – 155.0 °C (from CH_2Cl_2 / Hexane) Lit[180] 167 - 169 °C (mixture of diastereoisomers, from Et_2O); ν_{max}(Nujol mull)/cm^{-1} 1709 (CO), 1593 (Ar); δ_H (300 MHz; $CDCl_3$) 7.50 – 7.37 (m, 3H, CH, Ar), 7.29 – 7.26 (m, 2H, CH, Ar), 6.57 (s, 2H, alkene), 5.40 (s, 2H, CH), 3.02 (s, 2H, CH); δ_C (75 MHz; $CDCl_3$) 175.8 (C, quat, CO), 137.1 (CH alkene), 133.1 (C, quat, Ar), 129.6 (CH, Ar), 129.2 (CH, Ar), 127.0 (CH, Ar), 81.8 (CH), 47.9 (CH).

R=H 10-Oxa-4-aza-tricyclo[5.2.1.02,6]dec-8-ene-3,5-dione diastereoisomeric mixture 158 and 159

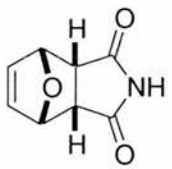

158

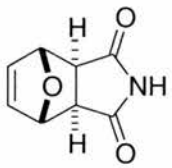

159

Ratio 6:4

Maleimide **147** (1.32 g, 13.7 mmol) was reacted with furan (1.00 ml, 13.7 mmol) in CH_2Cl_2 (50 ml) as above. The resulting crude adducts were purified by column chromatography by serial dilution (SiO2, 1:1 to 1:4 Hexane : Et_2O) to yield **158** and **159** as a colourless crystalline solid (0.44 g, 19%) comprising a mixture of *endo* **158** and *exo* **159** stereoisomers in a 6:4 ratio respectively. m.p. 128 – 131 °C (from Hexane / Et_2O) ν_{max}(Nujol mull)/cm^{-1} 1706 (CO); δ_H (300 MHz; $CDCl_3$) 8.53 – 8.39 (1H, bs, NH, **159**), 8.13 – 7.94 (1H, bs, NH, **158**), 6.53 (2H, t, $^3J_{HH}$ = 0.9, CH alkene, **158**), 6.51 (2H, t, $^3J_{HH}$ = 1.0, CH alkene, **159**), 5.35 – 5.32 (2H, m, CH **158**), 5.31 (2H, t, $^3J_{HH}$ = 1.0, CH, **159**), 3.60 – 3.54 (2H, m, CH, **158**), 2.89 (2H, s, CH, **159**); δ_C (75 MHz; $CDCl_3$) 176.7 (C, quat, CO, **159**), 175.3 (C, quat, CO, **158**), 137.0 (CH, alkene, **159**), 135.0 (CH, alkene, **158**), 81.4 (CH, **159**), 79.8 (CH, **158**), 49.1 (CH, **159**), 47.8 (CH, **158**); *m/z* (CI) 166 ([MH]+, 77%), 98 (50), 69 (100).

R=CH_2COOH 10-Oxa-4-aza-tricyclo[5.2.1.02,6]dec-8-ene-3,5-dione diastereoisomeric mixture 175 and 176

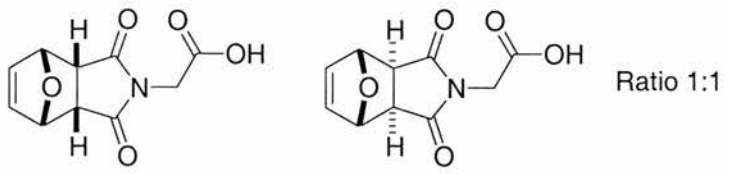

175 **176**

(2,5-Dioxo-2,5-dihydro-pyrrol-1-yl)-acetic acid **92** (0.80 g, 5.2 mmol) and an excess of furan (2.00 ml, 27.3 mmol) were dissolved in EtOAc (50 ml) and reacted as described above. The solvent was removed *in vacuo* and the resulting residue was purified by column chromatography (SiO_2 : 1 : 19 AcOH : CH_2Cl_2) to yield **175** and **176** as a colourless viscous oil comprising a mixture of *endo* and *exo* stereoisomers in a ratio of 1:1: ν_{max}(thin film)/cm^{-1} 2982 (OH), 1775 (CO), 1713 (CO); δ_H (300 MHz; $CDCl_3$) 6.81 (2H, s, CH alkene **175**), 6.42 (2H, t, $^3J_{HH}$ = 0.8, CH alkene **176**), 5.40 – 5.33 (2H, m, CH, **176**), 4.34 (2H, s, CH, **175**) 4.13 (2H, s, CH, **176**), 3.66 – 3.59 (2H, m, CH, **176**), 2.11 (CH_2, **175** and **176**), δ_C (75 MHz; $CDCl_3$) 177.6 (C, quat, CO, **176**), 174.2 (C, quat, CO, **175**), 172.7 (C, quat, CO, **176**), 171.8 (C, quat, CO, **175**), 135.0, (CH, alkene, **175**), 134.9 (CH, alkene, **176**), 79.9 (CH, **175** and **176**), 46.6 (CH, **175** and **176**), 39.3 (CH_2, **175**), 38.7 (CH_2, **176**).

(1) K. N. Houk, D. J. Tantillo *Stimulating Concepts in Chemistry*; Wiley-VCH:, **2000**.

(2) R. B. Silverman, *The Organic Chemistry of Enzyme Catalysed Reactions*; Academic Press: San Diego, **2000**.

(3) J. McMurray *Organic Chemistry*; Third Edition ed.; Brooks / Cole:, **1992**.

(4) R. G. Pearson *J. Am. Chem. Soc.* **1963**, *85*, 3533 - 3539.

(5) J. Songstad, R. G. Pearson *J. Am. Chem. Soc.* **1967**, *89*, 1827 - 1836.

(6) O. Eisenstein, J. Bottin, C. Minot, N. T. Anh *Tetrahedron Lett.* **1972**, *30*, 3015 - 3017.

(7) R. Huisgen, *J. Org. Chem.* **1976**, *41*, 403 - 419.

(8) M. Freccero, C. D. Valetin, R. Gandolfi, A. Rastelli *J. Org. Chem.* **2000**, *65*, 6112 - 6120.

(9) I. Fleming, *Fontier Orbitals and Organic Chemical Reactions*; John Wiley & Sons: Bristol, **1976**.

(10) K. Alder, O. Diels *Justus Liebigs Ann. Chem.* **1928**, *460*, 98 - 122.

(11) M. B Smith *Organic Synthesis* McGraw-Hill:, **1994**.

(12) S. Laschat *Angew. Chem. Int. Ed. Engl.* **1996**, *35*, 289 - 291.

(13) A. Datta, G. M. Blackburn, H. Denham, P. Wentworth Jr *Adv. Phys. Org. Chem* **1998**, *31*, 249 - 392.

(14) J. M. Jackman, J. M. Edwards *Aust. J. Chem.* **1965**, *18*, 1227.

(15) M. Asif-Ullah, P Kast, D Hilvert *Tetrahedron Lett.* **1996**, *37*, 2691 - 2694.

(16) P. Mattei, D J Gustin, P. Kast, O. Wiest, L. Lee, W W Cleland, D Hilvert *J. Am. Chem. Soc.* **1999**, *121*, 1756 - 1757.

(17) C. Gristomi, P. Kast, I. A. Chen, S. Li, U. Krengel, Y. Xue, D. Hilvert *J. Biol. Chem.* **2000**, *275*, 36832 - 36838.

(18) J. Andres, S. Marti, V. Moliner, E. Silla, I. Tunon, J. Bertran, M. J. Field *J. Am. Chem. Soc.* **2001**, *123*, 1709 - 1712.

(19) A. A. Bell, R. D. Stipanovic, D. H. O'Brien, M. J. Lukefahr *Tetrahedron Lett.* **1977**, *6*, 567 - 570.

(20) T. Glinka, J. F. Sanz-Cervera, R. M. Williams *J. Am. Chem. Soc.* **1993**, *115*, 347-348.

(21) J. F. Sanz-Cervera, R. M. Williams, F. Sancenon, J. A. Marco, K. Halligan *J. Am. Chem. Soc.* **1998**, *120*, 1090 - 1091.

(22) T. Yokota, H. Oikawa, A. Ichihara, S. Sakamura *J. Chem. Soc., Chem. Commun.* **1989**, 1284 - 1285.

(23) K. Katayama, H. Oikawa, Y. Suzuki, A. Ichihara *J. Chem. Soc., Chem. Commun.* **1995**, 1321 - 1322.

(24) T. Kobayashi, K. Katayama, H. Oikawa, M. Honma, A. Ichihara *Biochim. Biophys. Acta* **1998**, *1384*, 387 - 395.

(25) T. Kobayashi, H. Oikawa, Y. Suzuki, A. Ichihara *J. Org. Chem.* **1998**, *63*, 8748 - 8756.

(26) Y. Suzuki, H. Oikawa, K. Katayama, A. Naya, C. Sakano, A. Ichihara *J. Chem. Soc., Perkin Trans. 1* **1999**, 1225 - 1232.

(27) Y. Murakami, H. Oikawa, A. Ichihara *J. Chem. Soc., Perkin Trans. 1* **1992**, 2955 - 2959.

(28) W. Tan, D. E. Cane, W. R. Ott *J. Am. Chem. Soc.* **1993**, *115*, 527 - 535.

(29) D. J. Witter, Y. Yushizawa, Y. Liu, J. C. Vereras *J. Am. Chem. Soc.* **1994**, *116*, 2693 - 2694.

(30) A. Sutherland, K. Auclair, J. Kennedy, D. J. Witter, J. P. Van der Heever, A. R. Hutchinson, J. C. Verderas *J. Am. Chem. Soc.* **2000**, *122*, 11519 - 11520.

(31) T. Mie, K. Watanabe, A. Ichihara, H. Oikawa, M. Honma *J. Biol. Chem.* **2000**, *275*, 38393 - 38401.

(32) K. P. C. Vollhardt, R. L. Funk *J. Am. Chem. Soc.* **1977**, *99*, 5483 - 5484.

(33) N. M. Weishenker, E. J. Corey, T. K. Schaaf, W. Huber *J. Am. Chem. Soc.* **1969**, *91*, 5675 - 5677.

(34) A. Ichihara *Synthesis* **1987**, 207 - 222.

(35) C. N. Zimmerman, M. E. Jung, G. T. Lowen, S. I. Khan *Tetrahedron Lett.* **1993**, *34*, 4453 - 4456.

(36) V. P. Sandanayaka, E. A. Curtis, A. Padwa *Tetrahedron Lett.* **1995**, *36*, 1989 - 1992.

(37) Y. M. Choi, M. E. Jung *J. Org. Chem.* **1991**, *56*, 6729 - 6730.

(38) A. V. W. Mayweg, J. E. Baldwin, K Neumann, G J Pritchard *Org. Lett.* **1999**, *1*, 1933 - 1935.

(39) E. D. Lollar, P. N. Confalone, G. Pizzolate, M. R. Uskokovic *J. Am. Chem. Soc.* **1978**, *100*, 6291 - 6292.

(40) R. J. Sciotti, W. R. Roush *J. Am. Chem. Soc.* **1998**, *120*, 7411 - 7419.

(41) C. J. Moody, N. Bushby, D. A. Riddick, I. R. Waldron *J. Chem. Soc., Perkin Trans. 1* **2001**, 2183 - 2193.

(42) G. Cravotto, G. Appendino, A. Minassi, G. Palmisano *Eur. J. Org. Chem.* **2001**, 3711 - 3717.

(43) N. J. Patmore, C. Hague, C. G. Frost, M. F. Mahon, A. S. Weller *J. Chem. Soc., Chem. Commun.* **2001**, 2286 - 2287.

(44) L. Toupet, A. Guillam, J. Maddaluno *J. Org. Chem.* **1999**, *64*, 9348 - 9357.

(45) S. J. Benkovich, and R. A. Lerner K. D. Janda *Science* **1988**, *241*, 1188.

(46) M. C. Tedford, C. J. Suckling, L. M. Bence, J. I. Irvine, W. H. Stimson *J. Chem. Soc., Perkin Trans. 1* **1993**, 1925 - 1929.

(47) K. W. Hill, D. Hilvert, K. D. Nared, M. T. M. Auditor *J. Am. Chem. Soc.* **1989**, *111*, 9261 - 9262.

(48) D. Hilvert, *Acc. Chem. Res.* **1993**, *26*, 552 - 558.

(49) D. Hilvert, J. A. Shin *Bioorg. Med. Chem. Lett.* **1994**, *4*, 2945 - 2948.

(50) E. Mundorff, H. D. Ulrich, B. D. Santarsiero, E. M. Driggers, R. C. Stevens, P. G. Schultz *Nature* **1997**, *389*, 271 - 275.

(51) M. A. Hanson, E. C. Mundorff, A. Varvak, H. Ulrich, P. G. Schultz, R. C. Stevens *Biochemistry* **2000**, *39*, 627 - 632.

(52) H. S. Cho, E. M. Driggers, C. W. Liu, C. P. Katzka, A. C. Braisted, H. D. Ulrich, D. E. Wemmer, P. G. Schultz *J. Am. Chem. Soc.* **1998**, *120*, 1945 - 1958.

(53) D. Hilvert *Annu. Rev. Biochem.* **2000**, *67*, 751 - 793.

(54) L. Pauling *Nature* **1948**, *161*, 707 - 709.

(55) A. Jaschke, C. Frauendorf *Angew. Chem. Int. Ed. Engl.* **1998**, *37*, 1378 - 1381.

(56) R. C. Janssen, T. W. Wiegland, B. E. Eaton *Chem. Biol.* **1997**, *4*, 675 - 683.

(57) S. L. Tarasow, T. M. Tarasow, B. E. Eaton *Nature* **1997**, *389*, 54 - 57.

(58) S. L. Tarasow, T. M. Tarasow, C. Tu, E. Kellogg, B. E. Eaton *J. Am. Chem. Soc.* **1999**, *121*, 3614 - 3617.

(59) S. L. Tarasow, T. M. Tarasow, B. E. Eaton *J. Am. Chem. Soc.* **2000**, *122*, 1015 - 1021.

(60) A. Jaschke, B. Seelig *Chem. Biol.* **1999**, *6*, 167 - 176.

(61) M. A. Gilmore, D. Spivak, K. J. Shea *J. Am. Chem. Soc.* **1997**, *119*, 4388 - 4393.

(62) R. N. Karmalkar, B. Sellergren, K. J. Shea *J. Org. Chem.* **2000**, *65*, 4009 - 4027.

(63) A. O. Larsen, B. P. Santora, M. R. Gagne *Organometallics* **1998**, *17*, 3138 - 3140.

(64) K. A. Jorgensen, K. B. Simonsen, Q. S. Hu, L. Pu *J. Chem. Soc., Chem. Commun.* **1999**, 811 - 812.

(65) D. Philp, L. M. Greig *Chem. Soc. Rev.* **2001**, *30*, 287 - 302.

(66) K. A. Taskinen, D. C. Sherrington *Chem. Soc. Rev.* **2001**, *30*, 83 - 93.

(67) T. J. Malefetse, G. F. Swiegers *Chem. Rev.* **2000**, *100*, 3483 - 3537.

(68) J. Rebek Jr, M. M. Conn *Chem. Rev.* **1997**, *97*, 1647 - 1668.

(69) J. F. Stoddart, M. C. T. Fyfe *Acc. Chem. Res.* **1997**, *30*, 393 - 401.

(70) B. Askew, J. Rebek Jr, N. Islam, M. Killoran, D. Nemeth, R. Wolak *J. Am. Chem. Soc.* **1985**, *107*, 6736 - 6738.

(71) H. Wirtz, T. Merz, F. Vogtle *Angew. Chem. Int. Ed. Engl.* **1986**, *25*, 567 - 569.

(72) W. Wu, S. C. Zimmerman, Z. Zeng *J. Am. Chem. Soc.* **1991**, *113*, 196 - 201.

(73) S. Gonzalez, M. Fe de la Torre, E. G. Campos, M. L. Mussons, J. R. Moran, M. C. Caballero *Tetrahedron Lett.* **1997**, *38*, 8591 - 8594.

(74) D. Van Engen, S. K. Chang, E. Fan, A. D. Hamilton *J. Am. Chem. Soc.* **1991**, *113*, 7640 - 7645.

(75) N. Perez, C. Raposo, M. Almarez, M. L. Mussons, M. C. Caballero, J. R. Moran *Tetrahedron Lett.* **1995**, *36*, 3255 - 3258.

(76) A. Yatsimirsky, H. J. Schneider *Principles and Methods in Supramolecular Chemistry*; John Wiley & Sons: Chichester, **2000**.

(77) M. Almarez, C. Raposo, M. Martin, V. Weinrich, M. L. Mussons, V. Alcazar, M. C. Caballero, J. R. Moran *Chem. Lett.* **1995**, 759 - 760.

(78) D. Nemeth, J. Rebek *J. Am. Chem. Soc.* **1986**, *108*, 5637 - 5638.

(79) S. Goswami, F. Garcia-Tellado, S. K. Chang, S. J. Geib, A. D. Hamilton *J. Am. Chem. Soc.* **1990**, *112*, 7393 - 7394.

(80) A. J. Kirby *Angew. Chem. Int. Ed. Engl.* **1996**, *35*, 707 - 724.

(81) A. D. Hamilton, P. Tecilla *J. Chem. Soc., Chem. Commun.* **1990**, 1232 - 1234.

(82) V. Jubian, P. Tecilla, A D Hamilton *Tetrahedron* **1995**, *51*, 435 - 448.

(83) D. Philp, R. M. Bennes, N Spencer *Org. Lett.* **1999**, *1*, 1087 - 1090.

(84) D. Philp, C. A. Booth *Tetrahedron Lett.* **1998**, *38*, 6987 - 6990.

(85) A. Robertson, D. Philp *J. Chem. Soc., Chem. Commun.* **1998**, 879 - 880.

(86) D. Philp, A. Robertson, N. Spencer *Tetrahedron* **1999**, *55*, 11365 - 11384.

(87) M. S. Babiloni, R. Bennes, W. Hayes, D. Philp *Tetrahedron Lett.* **2001**, *42*, 2377 - 2380.

(88) N. Spencer, S. J. Howell, D. Philp *Tetrahedron* **2001**, *57*, 4945 - 4954.

(89) J. M. Lehn, M. W. Hosseini, M. P. Mertes *Helv. Chim. Acta* **1983**, *66*, 2454 - 2466.

(90) J. M. Lehn, M. W. Hosseini *Helv. Chim. Acta* **1987**, *70*, 1312 - 1319.

(91) J. M. Lehn, M. W. Hosseini, L. Maggiora, K. B. Mertes, M. P. Mertes *J. Am. Chem. Soc.* **1987**, *109*, 537 - 544.

(92) J. M. Lehn, M. W. Hosseini, K. C. Jones, K. E. Plute, K. B. Mertes, M. P. Mertes *J. Am. Chem. Soc.* **1989**, *111*, 6330 - 6335.

(93) D. G. Lynn, J. T. Goodwin *J. Am. Chem. Soc.* **1992**, *114*, 9197 - 9198.

(94) C. Zhao, T. R. Kelly, G. J. Bridger *J. Am. Chem. Soc.* **1989**, *111*, 3744 - 3745.

(95) G. J. Bridger T. R. Kelly, C. Zhao *J. Am. Chem. Soc.* **1990**, *112*, 8024 - 8034.

(96) P. R. Spencer, S. J. Howell, N. Spencer, D. Philp *Org. Lett.* **2001**, *3*, 353 - 356.

(97) T. A. Irra, W. L. Mock, J. P. Wepsiec, M. Adhya *J. Org. Chem.* **1989**, *54*, 5302 - 5308.

(98) A. Vidal-Ferran, Z. Clyde-Watson, L. J. Twyman, C. J. Walter, D. W. J. McCallien, S. Fanni, N. Bampos, R. S. Wylie, J. K. M. Sanders *New J. Chem.* **1998**, 493 - 502.

(99) A. J. Sinclair, A. Robertson, D. Philp *Chem. Soc. Rev.* **2000**, *29*, 141-152.

(100) B. Wlotzka, G. von Kiederwski, J. Helbing, M. Matzen, S. Jordan *Angew. Chem. Int. Ed. Engl.* **1991**, *30*, 423 - 426.

(101) P. Ballester T. Tjivikua, J. Rebek Jr *J. Am. Chem. Soc.* **1990**, *112*, 1249 -1250.

(102) Q. Feng, J. S. Nowick, T. Tjivikua, P. Ballester, J. Rebek Jr *J. Am. Chem. Soc.* **1991**, *113*, 8831 - 8839.

(103) E. A. Wintner, M. M. Conn, J. Rebek Jr *J. Am. Chem. Soc.* **1994**, *116*, 8823 - 8824.

(104) J. I. Hong, V. Rotello, J. Rebek Jr *J. Am. Chem. Soc.* **1991**, *113*, 9422 - 9423.

(105) M. M. Conn, E. A. Wintner, J. Rebek Jr *Acc. Chem. Res.* **1994**, *27*, 198 - 203.

(106) A. V. Eliseev, F. M. Menger, N. A. Khanjin *J. Am. Chem. Soc.* **1994**, *116*, 3613 - 3614.

(107) A. V. Eliseev, F. M. Menger, N. A. Khanjin, M. J. Sherrod *J. Org. Chem.* **1995**, *60*, 2870 - 2878.

(108) D. M. Rudkevich, D. N. Reinhoudt, F. de Jong *J. Am. Chem. Soc.* **1996**, *118*, 6880.

(109) M. M. Conn E. A. Wintner, J. Rebek Jr *J. Am. Chem. Soc.* **1994**, *116*, 8877 - 8884.

(110) I. O. Sutherland, B. Wang *J. Chem. Soc., Chem. Commun.* **1997**, 1495 - 1496.

(111) D. Philp, V. C. Allen, N. Spencer *Org. Lett.* **2001**, *5*, 777 - 780.

(112) J. Rebek Jr *Sci. Am.* **1994**, *271*, 34 - 40.

(113) J. Rebek Jr, *Chem. Ind.* **1992**, 171 - 174.

(114) S. Hoffman *Angew. Chem. Int. Ed. Engl.* **1992**, *31*, 1013 - 1016.

(115) Q. Feng, T. K. Park, J Rebek Jr *J. Am. Chem. Soc.* **1992**, *114*, 4529 - 4532.

(116) F. Diederich *Angew. Chem. Int. Ed. Engl.* **1988**, *27*, 362 - 386.

(117) E. M. Seward, S. B. Ferguson, F. Diederich, E. M. Sanford, A. Chou, P. Inocencio-Szweda, C. B. Knobler *J. Org. Chem.* **1988**, *53*, 5593 - 5595.

(118) H. J. Schneider *Angew. Chem. Int. Ed. Engl.* **1991**, *30*, 1417 - 1436.

(119) A. L. Thakkar, P. V. Demarco *J. Chem. Soc., Chem. Commun.* **1970**, 2 - 4.

(120) W. Saenger *Angew. Chem. Int. Ed. Engl.* **1980**, *19*, 344 - 362.

(121) Y. Kiyosuke, I. Tabushi, T. Sugimoto, K. Yamamura *J. Am. Chem. Soc.* **1978**, *100*, 916 - 919.

(122) R. Breslow, D. C. Rideout *J. Am. Chem. Soc.* **1980**, *102*, 7816 - 7817.

(123) H. J. Schneider, N. K. Sangwan *J. Chem. Soc., Perkin Trans. 2* **1989**, 1223 - 1227.

(124) C. J. Easton, A. G. Meyer, S. F. Lincoln, G. W. Simpson *J. Chem. Soc., Chem. Commun.* **1997**, 1517 - 1518.

(125) C. W. Rautenstrauch H Hopff *Chem. Abs.* **1942**, *36*, 1046.

(126) F. Schuster, R. Braun, J. Sauer *Tetrahedron Lett.* **1986**, *27*, 1285 - 1288.

(127) P. Garner P. A. Grieco, Z. M. He *Tetrahedron Lett.* **1983**, *24*, 1897 - 1900.

(128) U. Maitra, R. Breslow, D. Rideout *Tetrahedron Lett.* **1983**, *24*, 1901 - 1904.

(129) J. R. Moran V. Alcazar, J. de Mendoza *Tetrahedron Lett.* **1995**, *36*, 3941 - 3944.

(130) M. Almarez, C. Raposo, M. Crego, M. L. Mussons, N. Perez, M. C. Caballero, J. R. Moran *Tetrahedron Lett.* **1994**, *38*, 7065 - 7068.

(131) M. Almarez, C. Raposo, M. Martin, M. C. Caballero, J. R. Moran *Tetrahedron Lett.* **1996**, *37*, 6947 - 6950.

(132) M. Almarez, C. Raposo, M. Martin, V. Alcazar, M. C. Caballero, J. R. Moran *Chem. Lett.* **1997**, 173 - 174.

(133) A. Luengo C. Raposo, M. Almarez, M. L. Mussons, M. C. Caballero, J. R. Moran *Tetrahedron* **1996**, *52*, 12323 - 12332.

(134) M. W. Gobel M. S. Muche *Angew. Chem. Int. Ed. Engl.* **1996**, *35*, 2126 - 2129.

(135) A. Veronese V. Jubian, R. P. Dixon, A. D. Hamilton *Angew. Chem. Int. Ed. Engl.* **1995**, *34*, 1237 -1238.

(136) K. Konishi, M. Tominaga, T. Aida *J. Am. Chem. Soc.* **1999**, *121*, 7704 - 7705.

(137) J. W. Gould, K. N. Rankin, R. J. Boyd *J. Am. Chem. Soc.* **2001**, *123*, 2047 - 2052.

(138) P. Calcagno, P. R. Ashton, N. Spencer, D. Philp *Org. Lett.* **2000**, *2*, 1365 - 1368.

(139) P. Meghani, T. R. Kelly, V. S. Ekkundi *Tetrahedron Lett.* **1990**, *31*, 3381 - 3384.

(140) K. D. M. Harris, B. M. Kariuki, D. Philp, J. M. A. Robinson *J. Am. Chem. Soc.* **1997**, *119*, 12679 - 12680.

(141) M. Kurz, T. Schuster, M. W. Gobel *J. Org. Chem.* **2000**, *65*, 1697 - 1701.

(142) I. Fleming *Frontier Orbitals and Organic Chemical Reactions*; John Wiley & Sons: Bristol, **1976**.

(143) R. Huisgen, In *1, 3-Dipolar Cycloaddition Chemistry*; A. Padwa, Ed.; John Wiley & Sons: Chichester, **1984**; Vol. 1.

(144) R Schubert, R. Sustmann *Angew. Chem. internat. Edit.* **1972**, *11*, 840 - 840.

(145) A. Tempczyk, W. C. Still, R. C. Hawley, T. Hendrickson *J. Am. Chem. Soc.* **1990**, *112*, 6127 - 6129.

(146) J. K. M. Sanders C. A. Hunter *J. Am. Chem. Soc.* **1990**, *112*, 5525 - 5534.

(147) O. Kennard, R. Taylor *Acc. Chem. Res.* **1984**, *17*, 320 - 326.

(148) C. S. Wilcox, *Frontiers in Supramolecular Organic Chemistry and Photochemistry*; VCH: Cambridge, **1991**.

(149) R. W. Strozier, K. N. Houk *J. Am. Chem. Soc.* **1973**, *95*, 4094 - 4096.

(150) R. H. Crabtree, K. Kavallieratos *J. Chem. Soc., Chem. Commun.* **1999**, 2109 - 2110.

(151) C. M. Bertao, K. Kavallieratos, R. H. Crabtree *J. Org. Chem.* **1999**, *64*, 1675 - 1683.

(152) M. J. Hynes *J. Chem. Soc. Dalton Trans.* **1993**, 311 - 312.

(153) S. G. Wierschke, J. Pranata, W. L. Jorgensen *J. Am. Chem. Soc.* **1991**, *113*, 2810 - 2819.

(154) S. C. Zimmerman, T. J. Murray *J. Am. Chem. Soc.* **1992**, *114*, 4010 - 4011.

(155) N. Spencer, H.L. Rowe, D. Philp *Tetrahedron Lett.* **2000**, *41*, 4475 - 4479.

(156) J. I. Seeman *J. Chem. Educ.* **1986**, *63*, 42 - 48.

(157) C. V. Grudzinskas, A. Wissner *J. Am. Chem. Soc.* **1978**, *43*, 3972 - 3974.

(158) A Haack A Vilsmeier *Ber.* **1927**, *60*, 119 - 122.

(159) M R de Maheas *Bull. Soc. Chim. Fr.* **1962**, 1989 - 1999.

(160) D R Williams, D T Witiak, S V Kakodkar *J. Org. Chem.* **1974**, *39*, 1242 - 1247.

(161) O. Mitsunobu *Synthesis* **1981**, 1 - 28.

(162) H. Medzihradszky-Schweiger, H. S. Vargha, F. Ruff, K. Medzihradszky *Tetrahedron* **1983**, *39*, 2255 - 2258.

(163) P. Chabrier, H. Najer, R. Giudicelli *Bull. Soc. Chim. Fr.* **1959**.

(164) S. Yao, M. Johannsen, K. A. Jorgensen *J. Chem. Soc., Chem. Commun.* **1997**, 2169 - 2170.

(165) G. Boccaletti, S. Otto, J. B. F. N. Engberts *J. Am. Chem. Soc.* **1998**, *120*, 4238 - 4239.

(166) E. S. Anderson, V. K. Aggarwal, D. E. Jones, K. B. Obierey, R. Giles *J. Chem. Soc., Chem. Commun.* **1998**, 1985 - 1986.

(167) T. Rovis, D. A. Evans, J. S. Johnson *Pure Appl. Chem.* **1999**, *71*, 1407 - 1415.

(168) K. A. Jorgensen, K. V. Gothelf *J. Chem. Soc., Chem. Commun.* **2000**, 1449-1458.

(169) *Organic Synthesis, Coll. Vol. 1*; John Wiley & Sons: New York, **1930**.

(170) V. Allen, University of Birmingham, **2000**.

(171) A. Sinclair, University of Birmingham, **2000**.

(172) C. Booth, University of Birmingham, **1999**.

(173) H. L. Rose, C. A. Ramsden *J. Chem. Soc., Perkin Trans. 1* **1997**, 2319 - 2327.

(174) S. Dhar, P. K. Mohanta, S. K. Samal, H. Ila, H. Junjappa *Tetrahedron* **2000**, *56*, 629 - 637.

(175) D. B. Rosen *Chem. Abstr.* **1963**, *59*, 7533.

(176) S. Chauhan, W. J. Lown *J. Med. Chem.* **1981**, *24*, 270 - 279.

(177) M. W. Hosseini, B. Dietrich, J. M. Lehn, R. B. Sessions *Helv. Chim. Acta* **1983**, *66*, 1262 - 1278.

(178) P. Calcagno, University of Birmingham, **2001**.

(179) T. Hisano, K. Harano, T. Marsuoka, S. Watanabe, T. Matsuzaki *Chem. Pharm. Bull.* **1989**, *37*, 907 - 911

(180) A. S. Milowsky, W. K. Anderson *J. Org. Chem.* **1984**, *50*, 5423 - 5424.

Appendix 1

Derivation of titration equation

The equations are reproduced and derived from C Wilcox, "Design Synthesis and Evaluation of an Efficacious Functional Group Dyad. Methods and Limitations in the use of NMR for Measuring Host-Guest Interactions." from "Frontiers in Supramolecular Organic Chemistry and Photochemistry."

The NMR titration method:

Simple binding equilibrium, RH is receptor, S is substrate.

1 $RH + S \rightleftharpoons RH::S$

2 $$K_d = \frac{[RH][S]}{[RH :: S]} = \frac{1}{K_a}$$

In a system in fast exchange, the observed chemical shift will be an average of the chemical shift as a result of the portion bound to the receptor and the chemical shift due to the portion of the substrate unbound in solution.

Therefore:

3 $$\delta_{obs} = \frac{S_0 - [RH :: S]}{S_0}.\delta_S + \frac{[RH :: S]}{S_0}.\delta_{RH :: S}$$

Where S_0 is the initial substrate concentration.

A value can be assigned to describe the difference between the chemical shift of the bound and unbound protons.

4 $\Delta\delta = \delta_{RH :: S} - \delta_S$

Rearrangement and insertion into **Equation 3** gives:

5 $$\delta_{obs} = \delta_S - \frac{[RH :: S]}{S_0} + \frac{[RH :: S]}{S_0} + \frac{[RH :: S]}{S_0}\Delta\delta$$

Therefore:

6 $$\delta_{obs} = \delta_S + \frac{[RH :: S]}{S_0}\Delta\delta$$

Using the initial concentrations of the receptor and substrate, **Equation 2** can be rewritten.

7 $$K_d = \frac{(R_0 - [RH :: S])(S_0 - [RH :: S])}{[RH :: S]}$$

8 $$K_d = \frac{R_0S_0 - R_0[RH :: S] - S_0[RH :: S] + [RH :: S]^2}{[RH :: S]}$$

9 $$K_d[RH :: S] = R_0S_0 - R_0[RH :: S] - S_0[RH :: S] + [RH :: S]^2$$

10 $$0 = R_0S_0 - R_0[RH :: S] - S_0[RH :: S] + [RH :: S]^2 - K_d[RH :: S]$$

This is now in the form of a quadratic equation:

11 $$[RH :: S] = \frac{-(-R_0 - S_0 - K_d) \pm \sqrt{(-R_0 - S_0 - K_d)^2 - 4R_0S_0}}{2}$$

Simplification and reinsertion into equation 6 gives

12 $$\delta_{obs} = \delta_S + \frac{\Delta\delta}{2S_0}\left[R_0 + S_0 + K_d) - \sqrt{(R_0 + S_0 + K_d)^2 - 4R_0S_0}\right]$$

Only the minus term is adopted in the equation as the other solution for [RH::S] would give a negative result that is counter-intuitive.

The data is fitted to a curve using a least squares method of calculating the best fit.

Errors are calculated from the standard deviation in the observed chemical shifts and substitution of this result into the equation above.

Appendix 2

Crystal Data and Details of the Structure Determination for **149**

Crystal Data

Formula	$C_{15}\ H_{23}\ N_3\ O_2$
Formula Weight	277.36
Crystal System	Orthorhombic
Space group	Aba2 (No. 41)
a, b, c [Angstrom]	a = 36.613(8)
	b = 18.900(4)
	c = 10.041(2)
Volume [Ang^3]	6948(3)
Z	16
d(calc) [g/cm^3]	1.061
Mu(MoKα) [mm^{-1}]	0.072
F(000)	2400
Crystal Size [mm]	0.10 x 0.10 x 0.50

Data Collection

Temperature (K)		293
Radiation [Angstrom]	MoKα	0.71069
Theta Min-Max		1.1º to 20.0º
Index Ranges		$-34 \leq h \leq 35$, $-17 \leq k \leq 18$, $-9 \leq l \leq 9$
Total reflections / unique reflections		6828 / 2474, [R_{int} = 0.074]
Observed data [I > 2.0 sigma(I)]		2296

Refinement

Nref, Npar	2474, 365
R, wR2, S	0.1081, 0.2984, 1.13
Max. and Av. Shift/Error	0.00, 0.01
Flack x	0.00(6)
Min. and Max. Resd. Dens. [e/Ang^3]	-0.25, 0.26